THE UNIVERSITY
of EDINBURGH

Design, development, and assessment of novel 3-dimensional co-culture systems to model musculoskeletal interfaces

Hamad Mohammed H. Alsaykhan (MBBS), MRes

PhD Thesis

2019

THE UNIVERSITY *of* EDINBURGH

Supervised by Dr Jennifer Z. Paxton

Anatomy@Edinburgh, Biomedical Sciences,

Edinburgh Medical School

Abstract

The interface between fibrous tissues (ligaments, tendons, cartilages and joint capsules) and bones is known as the enthesis. It has a unique anatomical structure transitioning from pure fibrous tissue to pure bone tissue. This unique structure gives the enthesis its ability to smoothly transfer mechanical power. However, when the enthesis is injured (e.g. in sports, automobile, or falls accidents), this unique structure is replaced by a weak scar tissue that is prone to re-injury and can cause chronic pain. The current gold standard management for enthesis repair is to re-attach the avulsed tendon directly to the bone, which results in the loss of the unique enthesis structure.

To explore alternative treatments for enthesis repair, it is important to understand the normal development of the enthesis and its natural healing process. Therefore, developing a reproducible and standardised enthesis model is of great importance.

The aim of this study was to design, develop and assess novel 3-dimensional (3D) co-culture systems to model the enthesis *in vitro*. Assessments of the 3D co-culture were intended to study two aspects: system suitability for cell culture and the effect of co-culture on extracellular matrix (ECM) formation. System suitability was determined by proving interface formation, cell viability and structural integrity using chick tendon fibroblasts (CTF) and mouse osteoblasts (MC3T3). The effect of co-culture on ECM formation was assessed by measuring the content of collagen and glycosaminoglycans (GAGs) using rat tendon fibroblasts (RTF) and bone cells (dROb).

Two 3D interface co-culture methods were designed and developed: a hydrogel-based scaffold-dependent method and a scaffold-less method. The scaffold-dependent 3D co-culture system was used to create an artificial 3D interface by encapsulating two populations of cells in agarose, gellan, fibrin and collagen hydrogels. A confocal fluorescent microscope was used to assess the interface presence and integrity over time. Moreover, cell viability was assessed by live-dead fluorescent staining and DNA quantification. These investigations were performed to assess hydrogel suitability for the system, which resulted in choosing fibrin hydrogel as the most suitable candidate to assess co-culture effect on ECM formation. ECM formation was assessed for bone and tendon cells encapsulated in fibrin hydrogel separately, then the summation of their results was compared to the co-culture of

both. The results showed no significant effect of co-culture on ECM formation. This was followed by comparison of ECM formation in separately cultured bone and tendon cells when cultured in 3D cell-encapsulated hydrogels in standard 2D culture. Surprisingly, the ECM formation assays were significantly greater in 2D culture than 3D.

Spheroids of tendon and bone cells were used as a second method of 3D co-culture interface. The interface formation between bone and tendon spheroids was observed by confocal fluorescent microscopy (CFM) and light microscopy, showing successful spheroid formation and integrity over time. ECM formation studies showed a decrease in collagen and GAGs due to co-culture.

In summary, this study has evaluated two novel methodologies to create 3D tissue interfaces *in vitro.* These techniques will be valuable for future work to further enhance these models to study ECM formation, cell-cell interactions and responses at the enthesis as well as a number of other interfacial tissue sites (e.g., muscle-tendon, cartilage-bone, nerve-muscle).

Lay summary

The enthesis is the junction between hard bone and soft tissue, such as tendon and ligament. It is a specialised area that has unique structure and function. It helps transfer power from muscles to bones smoothly. Young, active people involved in sports and those who suffer automobile accidents or falls are prone to injuries at these entheses. The injury could result in severe pain, disability, and loss of movement at nearby joints. While treatment usually involves surgery to the junction site, the unique features of the enthesis make treating injuries challenging. Also, existing treatments are not free of complications such as chronic pain or even re-injury. In fact, little is known about how the enthesis normally develops or how it endures after injury. Therefore, developing a reliable 3-dimensional (3D) artificial model of the enthesis in the laboratory will help uncover how these junction sites develop and repair after injury.

The aim of this project was to use the science of tissue engineering, the field which connects engineering sciences with biology, to design artificial 3D enthesis models by growing bone and tendon cells together in the laboratory. These models were to mimic the connection of bone cells to tendon cells found at the normal enthesis site in the body. Once designed, the models' support for cell health and the effect of bone and tendon cells coexisting together were evaluated.

Two models were designed and developed. The first model involved embedding tendon and bone cells in gels to grow them side by side in a culture plate. Agarose, gellan (natural gels produced by bacteria), fibrin and collagen gels (natural materials found in the body) were chosen to be assessed in the system. The gels were tested for their support for cell attachment, cell health, and ability to form a clear junction between the bone and tendon gels to decide a suitable material. Accordingly, fibrin gel was chosen as the best candidate. Following this decision, the effect of bone and tendon cells artificially coexisting was studied by assessing protein production. The protein production study revealed no difference in protein production caused by coexistence of bone and tendon cells in 3D, compared to when bone and tendon cells were grown separately in 3D. Moreover, growing tendon and bone cells in 3D by embedding them in a gel decreased their protein production compared to normal 2D culture.

The second 3D enthesis model was achieved by creating small clusters of cells, called spheroids, of both tendon and bone cells. Once formed, a bone spheroid and a tendon spheroid were placed together in one culture well to join together and make a junction between them. Protein production was measured to evaluate the effect of the bone and tendon spheroids coexisting and revealed less protein formed by the coexisting bone and tendon spheroids compared to bone and tendon spheroids cultured separately. Additionally, growing tendon and bone cells in 3D decreased their protein production compared to 2D culture.

In summary, this study has evaluated two original methodologies to create 3D tissue junction sites in the laboratory. Cell health was used as a deciding factor for the suitability of systems to be used. Protein production was used to study the effect of bone and tendon cells coexisting in 3D, which revealed a decrease in protein production due to coexistence of bone and tendon cells in 3D compared to production when grown separately. Moreover, it showed a decrease in protein production when using the 3D systems compared to 2D. These models will be valuable for future work to further improve the models and use them to study the formation or repair of the enthesis in the laboratory. They could also be adapted to model one of the many other tissue junction sites in the human body e.g. muscle-tendon, cartilage-bone, and ligament-bone.

Contents

List of figures

List of tables

Nomenclature

2D	2-Dimensional
3D	3-Dimensional
AB	G418 antibiotic
ABAM	antibiotic/antimycotic
ACL	Anterior cruciate ligament
AJ	Adherens junctions
ALP	Alkaline phosphatase
ANOVA	Analysis of variance
BMP	Bone morphogenetic proteins
BMSCs	Bone marrow stem cells
CFM	Confocal fluorescent microscopy
COMP	Cartilage oligomeric matrix protein
CSA	Cross-sectional surface area
CTF	Chick tendon fibroblasts
CTF-GFP	Chick tendon fibroblasts with green fluorescent protein
Col10α1	Type X collagen α1
Col2α1	Type II collagen α1
DMEM	Dulbecco's modified eagle's medium
DMSO	Dimethyl sulfoxide
DNA	Deoxyribonucleic acid
DPF	Dog primary tendon fibroblasts
dROb	Differentiated rat osteoblasts
dsDNA	Double stranded DNA
DSLR	Digital single-lens reflex camera
ECACC	European collection of authenticated cell cultures
ECM	Extracellular matrix
EDTA	Ethylenediaminetetraacetic acid
G-CSF	Granulocyte colony-stimulating factor
GAGs	Glycosaminoglycans

GFP	Green fluorescent protein
HEPES	4-(hydroxyethyl)-1-piperazineethanesulfonic acid
Ihh	Indian hedgehog
LMP	Low melting point
LST	Liquid surface tension
MC3T3	Mouse osteoblasts cell line
micro-CT	Micro computed tomography
MSCs	Mesenchymal stem cells
Max-coculture	Maximum contact co-culture
Mini-coculture	Minimum contact co-culture
NASA	National aeronautics and space administration
ns	Non significant
PBS	Phosphate buffer saline
PDMS	Polydimethylsiloxane
PI	Propidium iodide
PTHrPR	Parathyroid hormone-related peptide receptor
RFP	Red fluorescent protein
RNA	Ribonucleic acid
ROb	Rat osteoblast
RT-PCR	Reverse transcription polymerase chain reaction
RTF	Rat tendon fibroblasts
sDMEM	Supplemented dulbecco’s modified eagle’s medium
Scx	Scleraxis
Sox9	SRY-Box 9
TE	Tissue engineering
TGF-ß	Transforming growth factor beta
TNMD	Tenomodulin

Acknowledgements

I would like to take this opportunity to express appreciation and gratitude to the following people:

To my parents, Mohammed Alsaykhan and Badriyah Alfuhaid, for raising me to be the man I am now! For the continuous support throughout my education, and for their unconditional love and prayers.

To my beloved wife, **Nada Albassam**, for the unending support and love that pushed me further toward achieving my dreams. Never complaining about long working hours and late nights in the lab.

To our wee man! Mohammed, for being the source of happiness whenever I am heading back home after a long day!

To my hero and wonderful supervisor, **Dr Jennifer Z. Paxton**, for the time she dedicated and the wisdom of her advice and guidance throughout my time as a PhD student. I will forever be indebted to her and hope that I can repay her kindness and unlimited support.

To my second supervisor **Prof Jamie Davies** and committee chair **Dr Andrew Hall**, for their helpful comments and advice during annual reviews and meetings.

To my splendid friend, **Dr Jeremy Mortimer**, for the chats, the laughs, and being the best lab and office mate someone could ever hope for.

To our Master's student **Mario Macía**, for his contribution with caring for the cells and conducting collagen assay on the 2D monocultures.

To **Dr Anisha Kubasik Thayil**, for her training on using confocal fluorescent microscopy and 3D imaging software.

I would also want to thank my brilliant office mates, Natalie Courtney, Alannah Mole, Alison Thomson, Roxanna Munir, Rachel Kline, and Laura Comley for the wonderful chats, dinners, birthday cards (and winter-time cards 😉), and laughs. I am truly lucky to have been amongst you for the past few years. It is the kind of friendship that was forged to last.

The thanks also extend to all the students who I was honoured to have supervised, trained, helped, and became their friend: Johanna Kumhnemundt, Dominika Vojtasova, Aiste Marcinkute, Natalie Arandia, Miriam Graute, Peter Bruce-Wootton, Steve Buddle, Callum Muirhead, Calum Davie, Yousef Almajed, Alice Pearsons, Judith Fuentes, Jan Spende, Vicky Fassoula, Beinn Mackay, Amy Hall, Nika Vonk, Anna Steel, Hafiz El-Shazali, Rena Taher, Leandros Rapteas, and Kristy Asare.

Also, all the people from the Gillingwater and Murray groups who we share lab 222 with.

Finally, I cannot forget the fantastic job done by the staff of the Hugh Robson Building who facilitated our work without worrying about non-scientific logistics. On top of the list comes the ever so helpful **Carol Wollaston**, followed by **James Griffiths**, **Andrew Dinse-Harrower**, **Morag Laidlaw**, **Kerry Moore**, and **Deborah Allen**.

Signed Declaration

I declare that this thesis was submitted for the final examination in the award of Doctor of Philosophy and was written and composed by me. It details the results of a project carried out between June 2015 and May 2019 at The University of Edinburgh under the supervision of Dr Jennifer Z. Paxton (University of Edinburgh).

Unless otherwise stated, all the laboratory work for this project was carried out by me except the collagen assay conducted for 2D monocultures of tendon and bone cells, which was carried out by Mario Macía, a visiting Erasmus Master's student for summer placement training. The work carried out by Mario was under my direct supervision.

For a list of publications, and conference presentations and posters, see appendix A.

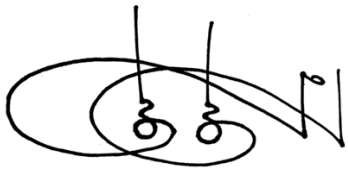

Hamad Mohammed H. Alsaykhan Date: 29th of May 2019

Chapter 1. Introduction

1.1 The enthesis: a musculoskeletal interface anchoring soft tissues to bone

The musculoskeletal system maintains structure and facilitates movement of the body. Despite it being formed by multiple tissue types, these different tissues are connected through specialised interfaces. These interfaces maintain function and efficient power transfer of mechanical force: generators (muscles), conductors (tendons), receivers (bones), shock absorbers (cartilages), and stabilisers (ligaments and joint capsules) (Parvizi and Kim 2010; Benjamin *et al.* 2002; Paxton, Baar, and Grover 2012). These tissues with different mechanical characteristics are interconnected by musculoskeletal interfaces. These interfaces include muscle-tendon, tendon-bone, ligament-bone, cartilage-bone, and capsule-bone. These interfaces represent the intra-musculoskeletal system interfaces, which are different from other interfaces that connect the musculoskeletal system with other systems such as the interfaces with nerves, blood vessels, and lymphatics tissues (C. R. Slater 2017; R Edwards *et al.* 2008; Dingle *et al.* 2018).

1.1.1 Focusing on the enthesis

Injuries to fibrous tissue in the musculoskeletal system have a poor healing outcome (Benjamin *et al.*, 2006; Mothersill *et al.*, 2007; Paxton *et al.* 2012). One of the commonly affected structures is the enthesis, which is the specialised tissue that anchors fibrous tissues (tendons, ligaments, cartilages and joint capsules) to bone. There are two types of enthesis, fibrous and fibrocartilaginous (Apostolakos *et al.* 2014; Benjamin *et al.* 2006). The fibrous type is formed by the insertion of collagen fibres directly from the fibrous tissue to the bone. These connecting collagen fibres are known as Sharpey's fibres (Woo *et al.* 2006). On the other hand, the fibrocartilaginous variety of enthesis, which is more common in the human body, has a unique anatomical structure consisting of four transitional zones: fibrous, fibrocartilaginous, mineralised fibrocartilaginous, and pure bone tissue (Apostolakos *et al.* 2014; Benjamin et al. 2006; Paxton et al. 2012). The focus of this study is on the fibrocartilaginous variant of enthesis that connects tendons to bones, hence, all following mentions of enthesis are directed to the fibrocartilaginous type.

The enthesis connects two mechanically and functionally different tissues. The bones are of weight bearing and rigid structure, while tendons are tensile and stretch resisting tissues. The enthesis smoothly transfers the mechanical power generated by muscles from tendons to the bones to move or stabilise an adjacent joint (Paxton

et al. 2012; Benjamin *et al.* 2006). A crucial factor for this efficient transfer of power is the gradient exhibition of tissue structure, cellular presence, ECM composition and mineralisation. However, due to the relatively smaller surface area of the interface connecting bone and muscle tendon compared to the mechanical load they transfer, the enthesis is prone to injury (Benjamin *et al.*, 2006; Mothersill *et al.*, 2007; Paxton *et al.* 2012).

A review of the field of enthesis research is described in the following sections, including ECM composition, cell population, normal development, injury and healing.

1.1.2 ECM content and cell population of the enthesis

As the enthesis has four transitional layers, each layer has its own ECM components and cell population. This gradient of tissue layers gives the enthesis its ability to smoothly transfer power from tendons/ligaments to bones. Therefore, each layer will be discussed separately.

1.1.2.1 Fibrous tissue layer

This fibrous tissue layer has a similar composition to the normal end of tendon/ligament; therefore, it is populated by fibroblasts (H. H. Lu and Thomopoulos 2013). The fibroblasts are arranged in groups of parallel columns that are found between longitudinally arranged type I collagen fibres, which are the most abundant ECM component of this layer. Low amounts of type III collagen, elastin, and proteoglycans are other ECM components that are mainly present surrounding the cells (Wrana *et al.* 1994; Laiho, Weis, and Massague 1990) (**Figure 1.1**). This arrangement of ECM composition and cells gives this layer of the enthesis similar mechanical properties to normal pure fibrous tissues (Angeline and Rodeo 2012). The parallel collagen fibres of this layer insert into the next layer of uncalcified fibrocartilage (P. J. Yang and Temenoff 2009).

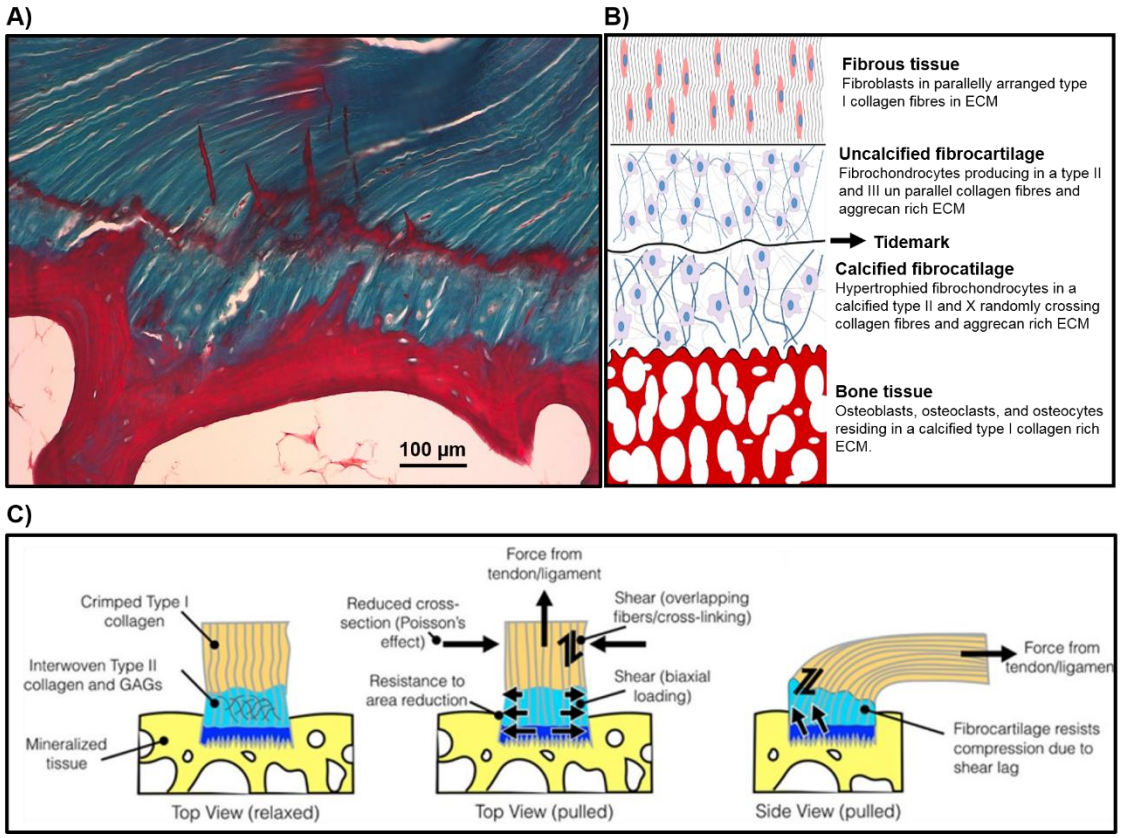

Figure 1.1: A) Modified Masson's trichrome staining showing the gradual regional transition from fibrous tissue to bone through 4 transitional zones (Alsaykhan and Fogg, 2014). *B) A diagram of the 4 enthesis zones depicting key cell populations and ECM components of each zone. C) A diagram depicting the mechanical forces that the enthesis is exposed to (Locke et al. 2017).*

1.1.2.2 Uncalcified fibrocartilage layer

This unique layer of the enthesis supports its ability to dissipate stress created by angled insertion of fibrous tissues from the tendon into the bone (Benjamin and Ralphs 2001). While the cartilage template for bone formation in foetal life was mineralised, mineralisation is stopped at the attachment site and part of the hyaline cartilage remains as part of the enthesis (Stavros Thomopoulos *et al.* 2003; I. E. Wang *et al.* 2006; Hiroyuki Fujioka *et al.* 1997; Stavros Thomopoulos *et al.* 2007). It is an avascular layer populated by fibrochondrocytes, round cells arranged in columnar groups similar to fibroblasts in the fibrous tissue layer, representing their phenotypic transformation caused by heterotypic fibroblast interaction during development (Benjamin and McGonagle 2001) (**Figure 1.1**). Thus, the main difference between these cells and the fibroblasts of the fibrous tissue is that they mainly secrete type II collagen in addition to high levels of type III collagen in the pericellular region and proteoglycans with its associated glycosaminoglycans (GAGs) (**Figure 1.1**). The specific composition of this layer highly represents the hyaline cartilage (Shaw and Benjamin 2007; Smith *et al.* 2012) in which the ECM is mainly composed of type II collagen. The collagen fibres are less parallel in this layer and they are larger than the ones in the fibrous tissue layer (Shaw and Benjamin 2007; P. J. Yang and Temenoff 2009) (**Figure 1.1**). It is also this specific structure and arrangement of collagen fibres that gives this part of the enthesis its ability to dissipate stress and force caused by the angled insertion of the tendon into the bone.

1.1.2.3 Tidemark

The tidemark is a basophilic line demarcating the mechanical margin separating the soft tissue from the hard tissue (Derwin *et al.* 2018) (**Figure 1.1**). The soft tissue refers to the uncalcified fibrocartilage while the hard tissue refers to the calcified fibrocartilage.

1.1.2.4 Calcified fibrocartilage layer

The calcified fibrocartilage layer is an avascular zone. It serves as the true barrier between bone and fibrous tissue as it creates a boundary with the subchondral bone (Benjamin and Ralphs 2001). The calcified layer of the enthesis is populated with a hypertrophied phenotype of fibrochondrocytes, which reside in a type II collagen-rich ECM with significant levels of collagen types X and I and GAGs (**Figure 1.1**) (H. H. Lu and Thomopoulos 2013; Benjamin and Ralphs 2001; Padulo *et al.* 2016; Angeline and Rodeo 2012; Laiho, Weis, and Massague 1990; Wrana *et al.* 1994; Scott *et al.*

2007; Juneja and Veillette 2013). GAGs content of the fibrocartilaginous layer of the enthesis is significantly higher than in the fibrous tissue of the tendon or ligament (Vogel *et al.* 1993, 1994; Koob and Vogel 1987).

Collagen fibres of this layer are bigger and less organised as they cross over other fibres to insert into the bone layer, which gives the attachment of fibrous tissue to bone its strength (P. J. Yang and Temenoff 2009; Benjamin and Ralphs 2001) (**Figure 1.1**). This layer exhibits a highly irregular attachment surface to the next layer of bone tissue, believed to serve as an increase in attachment surface area to enhance the strength of the fibrous tissue attachment to bone (P. J. Yang and Temenoff 2009).

1.1.2.5 Bone tissue layer

This layer has similar ECM composition and cell population to bone proper, a typical nanocomposite compound formed from organic and inorganic parts. Its ECM is rich with type I collagen as the main organic compound, aligned with hydroxyapatite as the main inorganic part that gives the bone its standard high calcium content (Derwin *et al.* 2018). The bone tissue is populated with osteoblasts, osteoclasts and osteocytes (**Figure 1.1**) (Benjamin and Ralphs 2001; Smith *et al.* 2012; P. J. Yang and Temenoff 2009; H. H. Lu and Thomopoulos 2013; Apostolakos *et al.* 2014b).

1.1.3 Development of the enthesis

The skeletal system in early foetal life is formed by cartilages. Bone formation occurs through endochondral ossification of these cartilages in the advanced stages of pregnancy (Oegema *et al.* 1997). Nonetheless, a transient mineralisation connection forms at the junction of the bone with soft tissues connecting ligaments, tendons, cartilages and capsules, which results in a fibrocartilaginous gradient structure: the enthesis. Chondrocytes from the original cartilaginous tissue are replaced by osteoclasts, osteoblasts, and osteocytes in the bone, while chondrocytes in the proximal (to bone) enthesis hypertrophy and start expressing type II and X collagen. Further up the arrangement of the enthesis are cells that exhibit a similar columnar arrangement to fibroblasts in the fibrous tissue, reflecting their phenotypic transformation from chondrocytes to fibrochondrocytes (Benjamin and McGonagle 2001). This heterotypic cell-cell communication in early foetal life is hypothesised to be the triggering factor for enthesis development (Smith *et al.* 2012; Sahoo, Toh, and Goh 2010).

The formation of cartilage (including bone forming cartilages), ligaments and tendons comes from a specific pool of progenitor cells in the limb bud during development

(Brent, Schweitzer, and Tabin 2003; Cserjesi *et al.* 1995; Schweitzer *et al.* 2001). These specific progenitor cells express Scleraxis (Scx) and/or Sox9 genetic markers (Sugimoto *et al.* 2013). Tendon-forming progenitor cells (tenogenitors, $Scx^{+}/Sox9^{-}$) maintain expression of Scx (Kraus *et al.* 2018; Cserjesi *et al.* 1995) (**Figure 1.2**). In contrast, chondrocyte-forming progenitor cells (chondrogenitors, $Scx^{-}/Sox9^{+}$) are progenitor cells expressing Sox9 (Sugimoto *et al.* 2013) (**Figure 1.2**). Furthermore, the progenitor cells in between tenogenitors and chondrogenitors, that eventually form the enthesis (enthesiogenitors, $Scx^{+}/ Sox9^{+}$), have a transient expression of both markers, with higher expression of Sox9 towards the chondrogenitor attachment and of Scx toward the tenogenitor attachment (Sugimoto *et al.* 2013) (**Figure 1.2**).

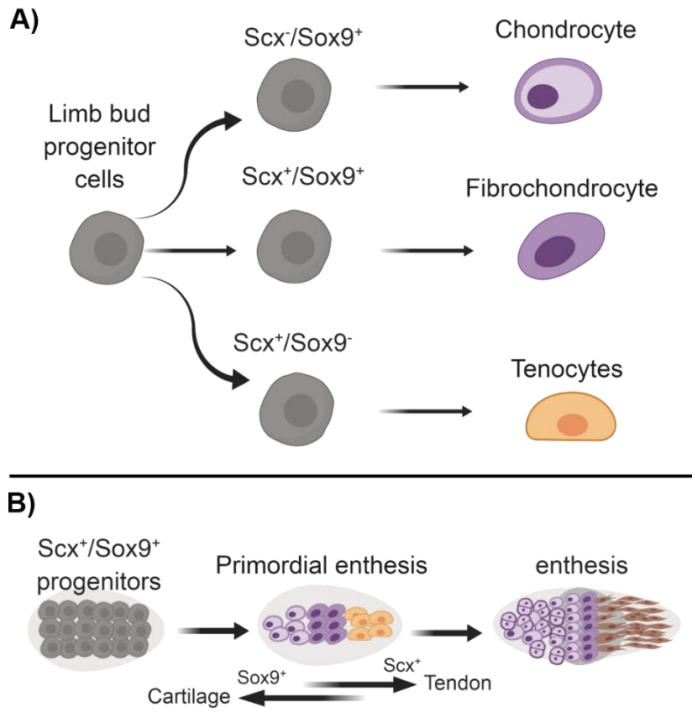

Figure 1.2: self-drawn diagram of embryonic differentiation of the enthesis, adapted from Sugimoto et al. (2013). *A) Scx and Sox9 expression determine cellular fate of a certain group of progenitor cells of the limb bud resulting in chondrocytes, fibrochondrocytes and tenocytes. B) Arrangement of progenitor cells' expression of Scx and Sox9 in a gradient with higher expression of Sox9 towards the bone-forming cartilage and higher expression of Scx towards the tendon end. This results in the differentiation of progenitor cells into interface relevant cells.*

The complexity of cellular phenotype and ECM in the relatively small structure of the enthesis makes the molecular mechanisms underlying its development and maintenance equally complex (Kronenberg 2003). Known signalling genes expressed in the enthesis include the Indian hedgehog (Ihh), parathyroid hormone-related peptide receptor (PTHrPR), type II collagen α1 (Col2α1) and type X collagen α1 (Col10α1) (Stavros Thomopoulos *et al.* 2003). These genes are similar to markers

expressed in the growth plate of bone (Kronenberg 2003). It has been established that Ihh protein secretion from the hypertrophic chondrocytes of the growth plate upregulates the PTHrPR expression of proliferating chondrocytes. This signalling pathway inhibit chondrocyte differentiation to the hypertrophic phenotype (Kronenberg 2003). Thomopoulos *et al*. (2010) discussed that there are accumulating indications that a similar signalling pathway is evident in the enthesis.

Normal biomechanical loading exerted on the enthesis structure is essential for enthesis maturation and development. This was expected, as all the cells in the enthesis are mechanoresponsive (H. H. Lu and Thomopoulos 2013). This was reported in studies that describe how paralysis of muscle groups in one side of an experimental animal, compared to opposite functional muscular groups, showed a significant difference in the size of fibrocartilage formation (Shaw and Benjamin 2007; Waggett *et al.* 1998; H. H. Lu and Thomopoulos 2013; Schwartz *et al.* 2013). They concluded that the mechanical loading from muscles on the enthesis influences the amount of fibrocartilage formed. Although entheses in the body have a consistent presence of the four transitional zones, variability in mechanical loading between different muscles, tendons, ligaments and cartilages results in an inconsistent size of layers; i.e., entheses are not identical structures (Hems and Tillmann, 2000; Benjamin et al., 2002). Thus, differences in enthesis layers vary noticeably between different muscles in the same body, from individual to individual, and between species.

To conclude, the development of the enthesis can be attributed to two factors: heterotypic cellular interaction and mechanical loading. The former is essential in the early phenotypic differentiation of enthesis cells, while mechanical stimuli are essential for enthesis maturation and growth post-partum (Zelzer and Blitz 2010; Stavros Thomopoulos *et al.* 2007; S Thomopoulos, Genin, and Galatz 2010).

1.1.4 Enthesis injury

Injuries to the enthesis are common in sports injuries such as anterior cruciate ligament (ACL) injuries (Gianotti *et al.* 2009), tennis elbow, jumper's knee, rotator cuff tendon tear and calcaneal tendon avulsion (Benjamin *et al.* 2006; B. S. Kim *et al.* 2014; Benjamin *et al.* 2002; Apostolakos *et al.* 2014b). For example, ACL injuries affect ~ 37 persons per one hundred thousand people and 65% of those injuries are caused by sports related activity (Gianotti *et al.* 2009). The fibrocartilaginous enthesis is prone to overuse injuries, as seen in rotator cuff and Achilles tendon injuries, due to the relatively small area of the enthesis compared to the mechanical load it

transfers (H. H. Lu and Thomopoulos 2013; Benjamin *et al.* 2002). Other causes of enthesis injury include entheseopathy diseases, spondyloarthropathy diseases, falls and automobile accidents (Benjamin and McGonagle 2001; Benjamin *et al.* 2002).

1.1.5 Enthesis normal healing and therapeutic management

Healing of the injured enthesis occurs through the formation of a fibrovascular scar tissue, which does not remodel into the normal anatomical structure of the enthesis (H. H. Lu and Thomopoulos 2013; Angeline and Rodeo 2012; Juneja and Veillette 2013; Rodeo *et al.* 1993; Aoki *et al.* 2001b; H Fujioka *et al.* 1998). Therefore, the mechanical stress on that affected region will pass through a mechanically weaker scar tissue instead of the normal smooth transition through the natural enthesis. This makes the newly formed scar tissue more prone to injury and treatment failure (Rodeo *et al.* 1993; Juneja and Veillette 2013; H Fujioka *et al.* 1998; Aoki *et al.* 2001a). Examples of commonly affected entheses include the anterior cruciate ligament (ACL), Achilles tendon, and tears to one of the tendons of the rotator cuff (Rodeo *et al.* 1993; Smietana *et al.* 2017). Treatment plans for such injuries require surgical reconstruction of the ligament/tendon attachment with autologous graft using expendable muscle tendons (Mothersill *et al.* 2007). The treatment procedure involves tunnelling the bone to fix the ligament/tendon directly to the bone, which does not restore the normal anatomy of the fibrocartilaginous enthesis. This procedure has a low and variable success rate, combined with multiple local morbidity and persistent pain (Paxton *et al.* 2012; Lim & Temenoff 2009; Friedman *et al.* 1985). Although the initial results of surgical intervention are usually successful, long term follow up shows high failure rates, signifying the difficulty in managing these cases (Tetsumura *et al.* 2006; Robertson, Daniel, and Biden 1986; Benjamin and McGonagle 2009). Moreover, almost fifty percent of patients with ACL reconstruction procedures have unresolved pain after one year of undergoing surgery (H. H. Lu and Thomopoulos 2013; Maffulli 1998; Fenwick *et al.* 2001; Beitzel *et al.* 2013; Lafosse *et al.* 2008). Therefore, an optimal gold standard treatment that recovers the normal anatomical structure and function of the enthesis has not yet been achieved. Interestingly, after ACL reconstruction surgery, an observation was documented that described the formation of random areas of fibrocartilage in the area of attachment of the tendon graft to bone, suggesting an important role of heterotypic cell communication on fibrocartilage formation (Rodeo *et al.* 1993; Eriksson, Kindblom, and Wredmark 2000; Blickenstaff, Grana, and Egle 1997; Yoshiya *et al.* 2000).

Improving treatment methods is limited by the current knowledge gap in enthesis development and healing processes. Understanding the developmental process of the enthesis will help in determining factors to consider when researching therapeutic options or engineering an enthesis *in vitro*. Indeed, understanding the healing processes occurring at the enthesis after injury and their limitations will help determine better intervention time points and methods. Nonetheless, as entheses are affected by repeated daily life activity and the stress exerted on them, they wildly differ from one person to another in terms of size and composition (Apostolakos *et al.* 2014). A successful gold standard treatment should restore the patient's quality of life and the normal function of the enthesis with a full range of movement of relevant adjacent joints for the rest of their life, i.e. restore the normal functioning enthesis.

1.1.6 Knowledge gap in enthesis biology and research

Structure-function relationship, particularly the increased fibrocartilaginous layer of the enthesis in muscles with higher load, remains imprecisely understood. Moreover, better understanding of how specific molecular, cellular and tissue structure contributes to natural function of the enthesis is required. Biochemical and biomechanical stimuli are evidently involved in enthesis development, however, knowledge about specific stimuli, their signalling pathways, and how they affect enthesis development remain unelucidated. There is a wealth of information regarding the phenotypic lineage of tendon, ligament, cartilage, and bone cells. However, fibrochondrocytes and their hypertrophic variant remain incompletely categorised. The intra-enthesis cell-cell interactions and their effect on normal development and function are also not understood. This could be due to the difficulty of isolating these specific cells individually; both occupy a microscale area and do not have a straight boundary of simple division. Additionally, growth factor roles and their interaction with different cellular components of the enthesis remain unclear.

Key points of this section:

- Enthesis injury prevalence is high in sports, automobiles, and falls accidents.
- Quality of life is not restored in a significant percentage of cases after enthesis repair.
- Poor understanding of normal enthesis development and healing processes hinder research of better treatment options.

- ECM of the enthesis has high levels of GAGs due to the presence of fibrocartilage.
- Collagen II is specifically expressed and produced in the fibrocartilaginous layer of the enthesis.
- Heterotypic cellular interaction in foetal life has an important role in triggering enthesis formation.

1.2 Tissue engineering

Tissue engineering (TE) knowledge and technologies are integral in the research to advance health care. The aim of tissue engineering is to combine engineering science applications and biological sciences. This facilitated understanding of physical and structural properties of tissues is for the purpose of improving, repairing or replacing damaged tissues and/or organs (Shafiee and Atala 2017; Lanza 2013). Consequently, an attempt to recreate these properties *in vitro* could be investigated in order to design new treatment options (O'Brien 2011; Langer 1993). Tissue Engineering is a multidisciplinary field; mechanical engineers, material scientists, stem cell scientists, developmental biologists, anatomists and biochemists are examples of disciplines involved in TE. 3D culture techniques are essential for the TE field. There are two types of 3D culture, either scaffold-dependent or scaffold-less (Fang and Eglen 2017; Shafiee and Atala 2017; J. Bin Kim 2005; Ravialy *et al.* 2015).

1.2.1 2D vs 3D culture

Two-dimensional (2D) tissue cultures have been used for decades in research in all disciplines involved in tissue cultures; for example, drug discovery, cell biology, stem cell biology, cancer research, tissue engineering, genetics and many other scientific fields. A 2D tissue culture is made by a monolayer of a single type of cells that are differentiated and anchored to the surface of a dish (**Figure 1.3** A). The idea of three-dimensional (3D) culture is to create a more natural structure by adding depth to the tissue culture. Accordingly, the cells have a more realistic structure and environment. This perspective in tissue culture has opened up new possibilities to test. Consequently, an increasing number of laboratories around the world are taking steps to adopt this technology into their research.

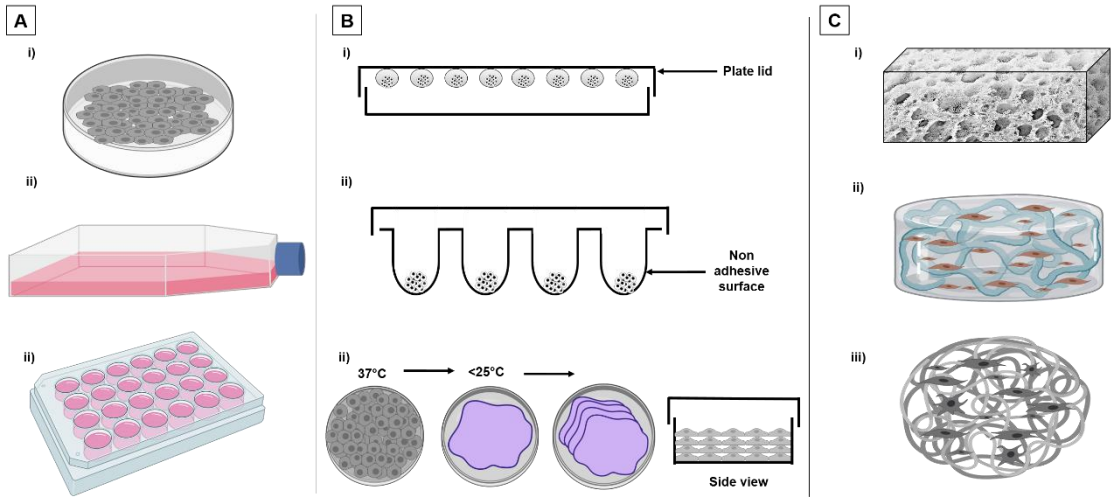

Figure 1.3: Different types of cell culture methods. *A) 2D culture method on a cell culture dish (i), in a flask (ii), or on culture well-plate (iii). B) 3D scaffold-less culture using spheroids generated by hanging-drop method (i), ultra-non-adhesive culture surface (ii), or stacking monolayers of cell sheets into a 3D layered construct. C) 3D scaffold-dependent cell culture using porous scaffolds (i), cell encapsulated hydrogels (ii), or cells cultured in nanofiber scaffold (iii).*

Advantages of 3D culture over 2D culture

There are many advantages of using 3D culture over 2D culture. An especially important advantage is the more realistic structure and environment. The fact that 2D cultures do not represent normal structure or environment in any way could give false positive or false negative results (Fang and Eglen 2017; Lv *et al.* 2017; Edmondson *et al.* 2014; Breslin and O'Driscoll 2013; Laschke and Menger 2017). Consequently, it is not surprising that almost ninety per cent of cancer drugs failed to produce the same result on 2D tissue culture of the same cells cultured in 3D (Ashworth *et al.* 2008). The unnatural environment of cells in 2D tissue culture could explain this conflict of results. In 2D monolayer culture, the cells are evenly distributed with direct access to nutrients, oxygen, metabolites and signalling molecules (**Figure 1.3** A), in contrast to cells in native tissues with different levels of access or exposure. (Kinney *et al.* 2014). In 3D tissue cultures, the cells are formed in a multilayer structure that is a step closer to representing the normal structure in forming a thick construct of tissue (**Figure 1.3** B and C, **Figure 1.4**). Accordingly, 3D culture provides better cell-cell interaction, proliferation and function, and a microenvironment that closely represents the microenvironment *in vivo* (Tibbitt and Anseth 2012). Moreover, cellular morphology is more natural in 3D than in 2D tissue culture (Lee *et al.* 2013). Cell morphology closely represents function, which means normal cell morphology would increase the chances of also having normal cell function. Additionally, cell viability is

higher in 3D cell tissue culture compared to 2D (Luca *et al.* 2013). Furthermore, differentiation of cells in 3D culture has been shown to be more prominent and includes expression of specific proteins and genes, lost in 2D tissue cultured cells (Luca *et al.* 2013; Lee *et al.* 2013).

Successful drug resistance studies on cancer cells in 2D culture produced very poor results when these drugs were used in animal models (van der Worp *et al.* 2010). Adapting 3D tissue culture in cancer research revealed increased drug resistance of the 3D culture compared to 2D in pancreatic cancer, as the 3D cultured cancer cells showed more similar characteristics to the in vivo microenvironment compared to 2D (Longati *et al.* 2013).

Limitations of 3D culture

3D culture presents an attractive solution to the limitations of 2D culture. However, it has its own limitations and challenges. 3D culture requires special expertise and materials that need more time and effort to acquire compared to 2D. Moreover, the cost of 3D culture materials for experiments and maintenance are higher than 2D culture. 3D culture can be achieved using a large number of materials, methodologies or combination of both. This creates a large variability between 3D culture outcomes. Accordingly, results acquired by an experiment using a certain 3D culture material and method does not represent 3D culture in general, as it only represents the use of this certain material and method of 3D culture. Compared to 2D culture, 3D culture results in the literature can only be compared to other results produced using the same material and method, whereas 2D culture results can be generalised to all 2D cultures. Furthermore, analysis of 2D culture has been extensively researched, resulting in the development of a broad spectrum of standardised investigative assays. These assays result in comparable results across the wider field of 2D culture. In contrast, 3D culture presents serious challenges to adapt similar assays and techniques. This is combined with the limitation of comparison and applicability to the certain material and method of 3D culture used. Consequently, switching from 2D to 3D culture requires considerable planning and preparation.

1.2.2 Scaffold-dependent 3D culture

Scaffolds are the mainstay of any 3D scaffold-dependent tissue-engineered product. A scaffold in 3D tissue engineering acts as an artificial extracellular matrix (ECM) to mimic the biological and mechanical properties of normal tissue (B. Kim, Baez, and Atala 2000). The natural ECM provides the tissue with structural integrity and

mechanical properties like stretching, resistance and weight bearing. It is also the ECM that stores different growth factors and potentiates their action (Chan and Leong 2008). Therefore, developing tissue-specific scaffolds that could function as an artificial ECM of that tissue is of great importance to 3D tissue engineering. Accordingly, the science of developing scaffolds requires the cooperation of many disciplines in engineering, chemistry, biochemistry and biomedical sciences to design a scaffold that mimics the natural ECM function of a particular tissue. Moreover, most mammalian cells are anchorage-dependent to live (Merten 2015; Ruoslahti and Reed 1994; Ahmad Khalili and Ahmad 2015); therefore, scaffolds should provide an attachment surface for cells in 3D tissue culture. Furthermore, scaffolds should support cell proliferation, growth, behaviour, migration and differentiation (Road 2003).

When choosing a scaffold for tissue engineering there are many requirements to be considered. These requirements include architectural design, material biocompatibility, biodegradability and manufacturing technologies. Accordingly, choosing the right scaffold requires rigorous testing and validation. Depending on the use of a scaffold, a suitable material and manufacturing technology should be chosen (Ramakrishna *et al.* 2001). Materials used to build scaffolds for 3D tissue engineering can be classified into three major types: 1) naturally occurring materials, 2) degradable synthetic materials, and 3) non-degradable synthetic materials (Dhandayuthapani *et al.* 2011). Manufacturing technologies include porous scaffolds, hydrogel encapsulation, fibrous scaffolds, acellular scaffolds and cell-sheets with self-excreted ECM.

1.2.2.1 Porous scaffolds

Highly interconnected porous structures that facilitate homogenous cellular growth are an integral part of tissue engineering (Zhang and Ma 1998). Pore size of the scaffold is an important factor that is dependent on the type of tissue intended for engineering (S. Yang *et al.* 2001). Nonetheless, consensus on an optimal pore size has not been achieved. For example, bone regeneration studies state a pore size ranging from 50 to 710 µm (Karande, Ong, and Agrawal 2004; S. Yang *et al.* 2001; Agrawal and Ray 2001). In contrast, fibrocartilaginous tissue engineering studies recommended the use of pores ranging between 200 to 300 µm (Elema *et al.* 1990). Another important factor to consider when choosing an appropriate porous scaffold is

surface chemistry (cell attachment support), biodegradability and mechanical properties (Kramschuster and Turng 2013).

The porous nature of this type of scaffold theoretically facilitates migration, attachment and nutrient diffusion (**Figure 1.3** Ci). A porosity of more than 90% of the scaffold structure was previously considered essential for tissue engineering applications (Freed *et al.* 1994). However, scaffold porosity ranging from 55% to 74% has been used for engineering bone tissue to improve mechanical loading capacity (Whang *et al.* 1999; Sherwood *et al.* 2002; Shao *et al.* 2006).

1.2.2.2 Encapsulation of cells in hydrogel scaffolds

Entrapment of cells in a hydrogel scaffold is one of the very promising applications in clinical and tissue engineering research (Drury and Mooney 2003) (**Figure 1.3** Cii). There are several types of polymers that can be used as hydrogels from synthetic and natural sources. Examples of these polymers used for scaffold-dependent tissue engineering are listed in **Table 1.1** and **Table 1.2,** respectively. Polymers used in hydrogel scaffolds have different properties and features (Drury and Mooney 2003). Synthetic polymers are cheaper, more controllable and reproducible, while natural polymers are more compatible and less toxic to cells (Alberts *et al.* 1994). Additionally, it is important to choose a polymer that does not damage cells during its preparation and setting conditions (Alberts *et al.* 1994). One especially important feature of encapsulation is that the biomaterials used are usually in a free liquid form that can be manipulated to desired shapes or structures, then cured to a solid state usually by pH, temperature or ionic activities. To list a few examples, alginate solidifies when its monomer solution is exposed to divalent ion solutions such as calcium chloride, where the calcium ion crosslinks the alginate; collagen monomers polymerise when they are switched from an acidic pH and low temperature to a neutral pH and body temperature. This important feature combines cell seeding and scaffold construction into one simple procedure. Accordingly, cells can be seeded into liquid hydrogel, then the liquid hydrogel can be cured to the desired shape and application. Using this approach ensures homogenous cell distribution through the construct and provides a simple one step procedure. Moreover, using this approach gives new possibilities for injectable applications, allowing curing after the injected hydrogel takes the target shape (Hoyer *et al.* 2015; Burg, Porter, and Kellam 2000). Consequently, this approach could be performed in minimally invasive techniques, producing less morbidity. Additionally, the fact that these encapsulated hydrogels are in free form means that they could be used in filling irregularly shaped defects. Nevertheless,

hydrogels have poor mechanical properties, which makes them unfeasible for weight bearing applications (Chan and Leong 2008).

Table 1.1: Examples of synthetic polymers used as scaffolds for tissue engineering.

Synthetic polymers	Tissue target	References
Poly(ethylene glycol)	Bone	Hasegawa *et al.* 2007; N. Y. C. Yu *et al.* 2010; Carletti *et al.* 2011
Polyhydroxyalkanoates	Bone, tendon, cartilage, skin	Ahmed *et al.* 2010; Jiong Liu *et al.* 2010; Rathbone *et al.* 2010; Hsu and Tseng 2004
Polyglycolide	Bone, tendon, cartilage, tooth	Knecht *et al.* 2007; Erggelet *et al.* 2007; Pihlajamaki *et al.* 2007; Ohara *et al.* 2010
Polylactide	Bone, tendon, cartilage, vascular	Francois *et al.* 2009; Inui *et al.* 2010; Ju *et al.* 2008; Chang *et al.* 2007
Poly(lactide-co-glycolide)	Bone, tendon, cartilage, liver	West *et al.* 2007; Spalazzi *et al.* 2008; Li *et al.* 2006; Tanaka *et al.* 2010
Polycaprolactone	Bone, ligament, cartilage, nerve	Pankajakshan *et al.* 2008; Mountziaris *et al.* 2010; Vaquette *et al.* 2010; Guarino and Ambrosio 2008

Table 1.2: Examples of natural polymers used as scaffolds for tissue engineering.

Natural polymers	Tissue target	References
Agarose	Nerve, cartilage, bone	X. Yu, Dillon, and Bellamkonda 1999; Leddy, Awad, and Guilak 2004; Suzawa *et al.* 2010
Alginate	Bone, cartilage, cornea, pancreas	Qi *et al.* 2009; Liang *et al.* 2011; X. Y. Liu *et al.* 2010
Fibrin	ligament, cartilage, heart valve	Paxton *et al.* 2010; Jockenhoevel *et al.* 2001; Dragoo *et al.* 2007
Collagen	Bone, cartilage, tendon, ligament	Zeugolis at al. 2009; Kuo and Tuan 2008; Mimura *et al.* 2008
Hyaluronic acid	Trachea, articular cartilage, nasal cartilage	Temiz *et al.* 2010; Grigolo *et al.* 2009; Wolf *et al.* 2008
Elastin	Vascular grafts	Kurane, Simionescu, and Vyavahare 2007

1.2.2.3 Nanofibrous scaffolds

Fibrous scaffolds are produced by controllable nano-scale fabrication methods. The generated scaffold pores better mimic the normal ECM (Yoshimoto *et al.* 2003)

(**Figure 1.3** Ciii). Examples of methods to produce nanofibers that are used in these scaffolds include electrospinning, self-assembly and phase separation (Dhandayuthapani *et al.* 2011). Electrospinning is the method of producing nanofibers by discharging a jet of electricity on a droplet of polymer. The jet will cause the polymer to realign, producing a nanofiber and solidification (Yoshimoto *et al.* 2003; Kumar and Dek 2010). Self-assembly is the organisation of polymeric molecules spontaneously to form the desired scaffold. This organisation of molecules is derived by many factors, including geometrical (dimension, shape, size, etc.), physiochemical (surface properties, charge, polarity, mass, etc.) and structural (anisotropy, heterogeneity, etc.) (L. Yang 2015). Phase separation is the creation of a foam structure from a polymer by separating the single solid phase of the polymer into a two-phase form. One of these phases has the polymer material while the other phase is an empty space. This method involves different techniques to achieve the desired effect including thermally induced phase separation, air-casting of a polymer solution, and immersion precipitation (van de Witte *et al.* 1996; Dhandayuthapani *et al.* 2011; Nam and Park 1999).

1.2.2.4 Acellular scaffolds

Acellular scaffolds are made by stimulating allogeneic or xenogeneic cells to produce their ECM (Knight *et al.* 2008; Borschel *et al.* 2005; J. H. Ingram *et al.* 2007; Hall 1997). The products are then decellularised by either physical treatment (such as freeze-thaw cycles) or chemical treatment (such as hypo or hypertonic solutions) (Gilbert, Sellaro, and Badylak 2006; Badylak 2004). Then the remaining biological antigens are removed by trypsin/EDTA (ethylenediaminetetraacetic acid) and detergent treatment to leave the ECM without immunity-stimulating antigens. This procedure makes these scaffolds antigen-free, therefore not triggering a response by the immune system when implanted (Chan and Leong 2008). Accordingly, these structures provide an excellent scaffold approximating nature that can be used in tissue engineering.

1.2.2.5 3D printing technology to create cell-encapsulated scaffolds

The use of 3D cell printing technology has opened up new possibilities for the tissue engineering field in general, and interface research specifically. The ability to control structure, shape, cell composition and faster production have brought exciting new possibilities and research opportunities (Sachs *et al.* 1992). 3D printing was initially used to produce acellular scaffolds from biocompatible material (Hutmacher 2000).

However, these types of 3D printed scaffolds were limited by the cellular ability to infiltrate the scaffold and exchange of nutrients, gas and waste (Hutmacher 2000). Meanwhile, with the recent advances in 3D cell printing technologies, cells encapsulated in a bio compatible hydrogel have been 3D printed and used for tissue engineering (O'Connell, Garcia, and Amir 2017). The flexibility of the new technology allowed production of a dependable and reproducible tissue engineered co-culture system of a muscle-tendon interface (Laternser *et al.* 2018) and a multicellular module as described in Ede *et al.* (2018).

1.2.3 Scaffold-less 3D culture

The concept of scaffold-less 3D culture depends on aggregating the cells in a 3D structure without the use of a scaffold. This method of 3D culture provides the cells with a higher degree of interaction and better tissue biomimicry (Ozbolat 2015). A description of the two main methods of producing scaffold-free 3D culture is discussed below:

1.2.3.1 Cell sheets with self-secreted ECM

Cell culture surfaces coated with polymers that offer a weak cell attachment allow cells to attach and proliferate to confluency. When the force of cell-cell attachment reaches a certain threshold, a full dissociation of the monolayer from the surface occurs, creating a cell sheet (H.-F. Lu *et al.* 2003; Du *et al.* 2007; Tzanakakis, Hansen, and Hu 2001). Moreover, thermo-responsive polymers like poly (N - isopropylacrylamide) can be used by thermally regulating the hydrophobicity of the polymer in order to detach a confluent monolayer of cells as a sheet (**Figure 1.3** Biii) (Okano *et al.* 2006). Accordingly, sheets of cells can be generated and stacked as a 3D structure (**Figure 1.3** Biii). This type of scaffolding technique is ideal for use in epithelium and endothelium tissue engineering studies. One very important advantage of this scaffold formation approach is to allow neo-vascularisation into the tissue, which is difficult to achieve in large and thick constructs of cell-seeded scaffolds (Chan and Leong 2008). However, the sheets are still very thin for use in thicker types of tissue. Additionally, it is still not possible to control the cell-to-ECM ratio, which is important when trying to engineer ECM rich tissues required for weight bearing purposes, for example.

1.2.3.2 Spheroid culture

An aggregate of cells which makes a 100-500 µm spheroid-like structure are named in the literature as mamospheres (Klopp *et al.* 2010), micromass (Greco *et al.* 2011),

spheroids (Rivron *et al.* 2012) or microfabricated tissues (Rivron *et al.* 2009). The concept of spheroid generation is to allow cells to self-organise into a 3D structure by using their anchorage-dependence and eliminating the presence of any other attachment surface. Therefore, cells are forced to attach to each other to form a 3D structure of aggregated cells that in this thesis will be named a spheroid.

1.2.3.2.1 Microenvironment in spheroids

Spheroid formation depends on cell attachment, mediated by adherens junctions (AJ). An important role for AJs is to support the physical connection between cells. The AJs connect the microtubules and actin filaments of neighbouring cells' cytoskeletons (Meng and Takeichi 2009). The distribution and location of adherence have tissue specific patterns (Takeichi 1988). In a flat 2D monolayer culture the cells are forced to attach to other cells only horizontally, which is not the natural arrangement of these cells in native tissue. However, spheroid culture provides a relatively normal cell attachment arrangement that mimics natural tissues (Lin and Chang 2008).

In 2D monolayer culture, the cells are evenly distributed with direct access to nutrients, oxygen, metabolites and signalling molecules. In contrast, cells in native tissues have different levels of exposure to nutrients, oxygen, metabolites and signalling molecules (Kinney *et al.* 2014). However, spheroid culture mimics these physiological conditions via their arrangement of cells from the periphery to the core of the spheroid. The cells at the periphery of the spheroid are exposed to higher concentrations of oxygen, nutrients, metabolites and signalling molecules (**Figure 1.4**). However, depending on the ability of each of these molecules to diffuse, different cell layers of the spheroid are exposed to their varying concentrations (Curcio *et al.* 2007; Jiang *et al.* 2005; Hu and Li 2007). Ultimately, this results in better cell viability, stable morphology, cell polarisation and increased proliferative and metabolic activity (Anton *et al.* 2015). Therefore, the use of spheroids has been adapted for various applications in the biomedical science field.

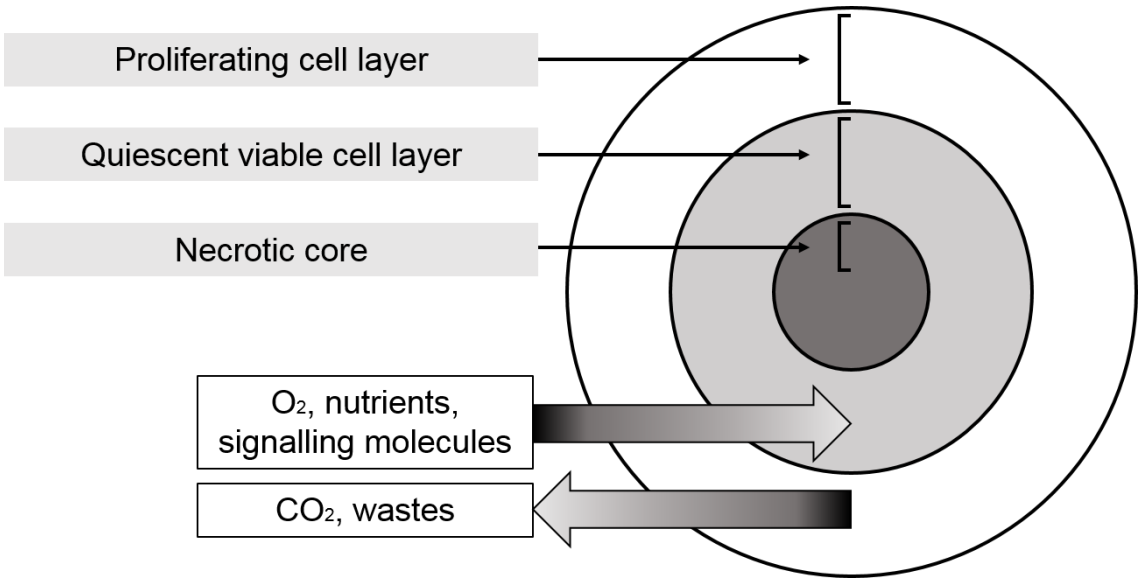

Figure 1.4: An illustration of the microenvironment of a spheroid depicting the different regions and the dynamic of nutrients and gas exchange.

1.2.3.2.2 Uses of spheroids

Spheroid culture has been used extensively as an avascular tumour model. This is not surprising, as the physiological properties of the spheroid microenvironment are like those of avascular tumours regarding their oxygen, nutrients and signalling molecule diffusion (Lin and Chang 2008). Spheroids and avascular tumours share the same layer composition of proliferative, quiescent and necrotic core (**Figure 1.4**). Moreover, a comparison between monolayer culture and spheroid culture of the same tumour cells revealed higher chemo- and radiotherapy resistance in the spheroid culture over the monolayer culture, mimicking the original tumour (Kunz-Schughart *et al.* 2004; Desoize, Gimonet, and Jardiller 1998; Dubessy *et al.* 2000). Accordingly, spheroid culture has provided an important tool for cancer research, drug discovery and development fields.

Studying gene function has also been an important application of spheroid culture thorough the use of specific blocking antibodies, short-interference RNA and signalling inhibitors (Laschke and Menger 2017). The combination of spheroid culture model and these gene-blocking methodologies has facilitated the study of gene function in cell migration, invasion and apoptosis of various cell types. For instance, the effect of interleukin-6 on triggering malignant features in normal mammary gland has been investigated through the use of spheroid culture (Sansone *et al.* 2007). Furthermore, use of spheroids has been documented in the research of caspase

(Gdynia *et al.* 2007), E-cadherin (Haga *et al.* 2008) and urokinase-type plasminogen activator (Gondi *et al.* 2007).

The natural complex tissue structure can be relatively represented by generating a spheroid with multiple cell types (Laschke and Menger 2017). Co-culture of spheroids, in which two or more cell types are used to generate spheroids, has been used in the literature to study cell-cell interaction. The effect of co-culture ranges from improved viability, protein secretions and ECM formation in pancreatic tissues (Shin *et al.* 2015; Wittig *et al.* 2013), to spheroid neovascularisation (Alajati *et al.* 2008; Walser *et al.* 2013; Road 2003; Beger *et al.* 1998). Therefore, the possibilities to explore the effects of co-culture on different cell type combinations are endless. Additionally, preconditioning the culture with biochemical or/and physical stimuli adds another dimension for research.

Spheroids can be used as building units for tissue engineering purposes. Designing a mould with a desired shape to be filled with spheroids can be used as an implantation construct (Fennema *et al.* 2013). This combines the classical implantation technique to fill tissue defects with the advantage of spheroid culture. Examples of this technique to fabricate replacement tissue constructs include cartilage (G. S. Huang *et al.* 2013), skin (Furukawa *et al.* 2001), myocardium (Chimenti *et al.* 2011) and ligament (Hoyer *et al.* 2015). Interestingly, co-culture of smooth muscle myoblasts and endothelial spheroids were used to create a single lumen structure. In addition, these spheroids can be arranged and lined up to form a single lumen with straight or even branching structure, which could be used as a delivery system for nutrients and oxygen in complex structures (Mironov *et al.* 2009). An interesting thought would be the use of different tissue spheroids stacked into a sophisticated tissue construct. For example, stacking osteoblast spheroid layers, divided with the previously described angiogenic layers, might form a sophisticated bone tissue construct that is efficiently perfused with nutrients and oxygen.

1.2.3.2.3 Generation of spheroids

Generation of spheroids requires specialised materials and techniques. Choosing a spheroid generation method is dependent on experimental needs, availability of funding, specialised materials, expertise and laboratory equipment. Therefore, a review of available spheroid generation methodologies and their advantages and disadvantages are described below.

Hanging-drop cultures

Spheroids can be formed when small amounts of cell suspension (approximately 15-30 µl) are deposited as drops on the back of a culture plate lid, which is then placed back on the plate and the drops on the lid kept hanging. The drops remain in place when the lid is placed back in position by the force generated from liquid surface tension (LST). The cells aggregate at the bottom of the drop by the action of gravity (**Figure 1.5** A). Cell numbers ranging from 100 to 3000 cells can be used to form spheroids using this method, depending on cell size and the force of cell-cell adhesion of different cell types. This methodology of spheroid generation has been enhanced with commercially available kits, providing a high-throughput technique to generate highly reproducible spheroids (Tung *et al.* 2011). Advantages of using the hanging-drop method to produce spheroids include cost effectiveness, simplicity of use, controllable spheroid size, fast spheroid formation and ability to make co-cultures (Lin and Chang 2008).

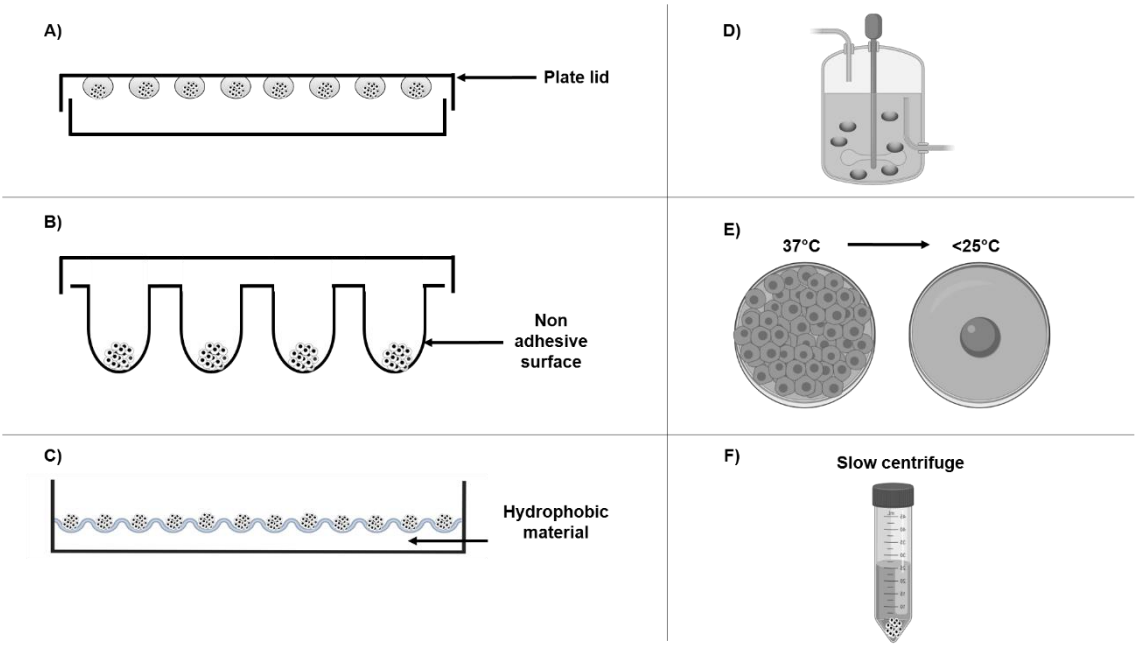

Figure 1.5: Different methods to generate spheroids include A) hanging-drop technique, B) use of non-adhesive surfaces, C) microfabricated wells on a hydrophobic material, D) rotary bioreactors, E) thermally detaching cell sheets, and F) forced aggregation of spheroids by slow centrifugation.

Non-adhesive culture ware surfaces

Standard plastic ware used for bacteriological culture have non-adhesive surfaces. These culture plates can be used to generate spheroids by directly adding a cell suspension to the plate (**Figure 1.5** B). Moreover, regular cell culture plate surfaces

can be transformed into non-adhesive surfaces by coating them with a thin layer of agarose (Yuhas *et al.* 1977) or hydrophobic polymers (Landry *et al.* 1985). Disadvantages of these methods include yielding variable shapes, sizes and cell numbers for spheroids (G. A. Hamilton, Westmorel, and George 2001). However, these disadvantages have been overcome recently with the commercially available kits of cell-repellent, U-bottomed and V-bottomed 96-well plates (CELLSTAR®, Greiner bio-one, UK) (Maritan, Lian and Mulligan, 2017).

Microwells fabrication on hydrophobic surfaces

Using hydrophobic materials which prevent cell attachment coupled with a fabrication technique to produce microwells allows control over shape, size and geometry of generated spheroids (Napolitano *et al.* 2007; L. Y. Wu, Di Carlo, and Lee 2008; Dean *et al.* 2007). The geometry of the fabricated surface guides the cell suspension to aggregate in the microwells, depending on gravity and hydrodynamic forces. The flexibility of shape, size and co-culture possibilities make this method of generating spheroids appealing. However, expertise in technology and specialised facilities are needed, which makes this method unattractive for small laboratories (**Figure 1.5** C).

Rotary bioreactors

Cells in suspension cultured in a standard bottle with a stirrer results in aggregates of cells resembling spheroids (Moscona, 1961; Schleich, 1967). This technique is simple, reproducible, and generates high numbers of spheroids (**Figure 1.5** D). Nonetheless, it exposes the cells to unnaturally high shear force, which affects cell physiology and function (Fang and Eglen 2017). Moreover, various shapes and sizes of spheroids are generated (Song *et al.* 2004). The National Aeronautics and Space Administration (NASA) have improved this method to a rotatory cell culture system with a unique gravity environment that eliminates most of the rotation shear force (Unsworth and Lelkes 1998; M. Ingram *et al.* 1997).

Spheroids from cell sheets

Cell culture surfaces coated with polymers that offer a weak cell attachment allow cells to attach and proliferate to confluency. When the force of cell-cell attachment reaches a certain threshold, a full dissociation of the monolayer from the surface occurs, creating a cell sheet (H.-F. Lu *et al.* 2003; Du *et al.* 2007; Tzanakakis, Hansen, and Hu 2001). Moreover, thermo-responsive polymers can be used to induce monolayer detachment upon change of culture temperature (**Figure 1.5** E). Upon further culture, for various times depending on cell type, this cell sheet shrinks,

condenses, and ends with spheroid formation (Ueno *et al.* 1992; Takezawa, Mori, and Yoshizato 1990; Takezawa *et al.* 1993). Compared to other methods of generating spheroids, this method is time consuming, labour intensive, and difficult to mass produce (Ueno *et al.* 1992; Takezawa *et al.* 1993).

Forced spheroid generation for cell types with weak cell-cell attachment

Cells with weak inter-cellular attachments need the use of physical forces to compel cells to aggregate. Examples of such physical forces include low-speed centrifugation (**Figure 1.5** F) (Akiyama *et al.* 2006), imposing magnetic fields (Ino, Ito, and Honda 2007), or standing traps of ultrasound waves (Jian Liu *et al.* 2007). However, the need for specialised equipment and difficulty of mass production hinders the use of this method.

1.2.4 3D culture as a tool to study the enthesis and its 3D culture requirements

3D culture is essential for enthesis research. Several studies have been performed on enthesial cells in 2D (Wang *et al.* 2007; Calejo *et al.* 2018). However, as discussed earlier in this chapter, 2D culture provides an unnatural environment in which the cells are evenly distributed with direct access to nutrients, oxygen, metabolites and signalling molecules. In contrast, cells in native tissues have different levels of exposure to these elements (Kinney *et al.* 2014) (**Figure 1.3** B and C, **Figure 1.4**). In 3D tissue cultures, the cells are formed in a multilayer structure, that is a step closer to representing the normal structure by forming a thick construct of tissue. Accordingly, 3D culture provides better cell-cell interaction, proliferation, function and a microenvironment that closely represents the microenvironment *in vivo* (Tibbitt and Anseth 2012). Furthermore, the enthesis has a gradient of four layers with different ECM composition and mechanical characteristics. Therefore, identification of critical mechanical properties of each layer is needed to set goals for scientists to achieve with 3D culture. Thus, a suitable scaffold-dependent or scaffold-less model is adopted for enthesis 3D culture. If a scaffold-dependent approach is targeted, then a mechanically relevant scaffold must be developed. This should be followed by a choice of biomaterial or a combination of biomaterials that can sustain these mechanical properties and provide biocompatibility.

Key points of this section:

- 3D culture better mimics the natural environment of cells in the tissue, which in turn results in better cellular communication, proliferation and function.

- Use of 3D culture techniques has good potential to be employed for enthesis engineering.
- Choosing the correct 3D culture methodology has to be carefully considered according to the study aim. Especially with the wide range of 3D culture options and techniques, there are no clear standards for choosing the best 3D culture.
- Hydrogel provides an excellent scaffold for cell encapsulation as it allows flexible manipulation of structure and easier manufacturing and handling.
- Significant resources and future development are directed toward spheroid culture

1.3 Co-culture methodology as a tool to study cellular interaction

Use of co-culture techniques have been documented in many fields of biomedical sciences, including mammalian cell studies, microbial studies and medical applications (Goers, Freemont, and Polizzi 2014). Uses of co-culture has included studying: cell-cell interactions (Bogdanowicz and Lu 2013; Wang *et al.* 2007), population control via toggle switches (Saeidi *et al.* 2011), tumour targeting (Hong, Song, and Shin 2013; Anderson *et al.* 2006) and delivery of therapeutic proteins (Bermúdez-Humarán *et al.* 2011). The main drive for such techniques is the limited representation of monocultures for normal cellular interaction in tissues where there are many cell types in the cell environment. Cellular phenotype is believed to be the result of the interaction of the genotype and culture environment of cells (Goers, Freemont, and Polizzi 2014). Therefore, various co-culture systems have been designed in the wider field of biomedical sciences and drug discovery in an attempt to study cell-cell interactions and advance biological studies into more realistic tissues, tumours or disease models (J. Bin Kim 2005; Alain and Querellou 2009; Harcombe 2010; Hesselman *et al.* 2012; Moraes *et al.* 2012; M.-H. Wu, Huang, and Lee 2010; Zengler *et al.* 2002; Beloqui *et al.* 2008) (**Figure 1.6**). Co-culture of spheroids in which two or more cell types are used to generate spheroids have been used in the literature to study cell-cell interaction (**Figure 1.6** Biii).

The effect of co-culture ranges from improved viability, protein secretions and ECM formation in pancreatic tissues (Shin *et al.* 2015; Wittig *et al.* 2013), to spheroid neovascularisation (Alajati *et al.* 2008; Walser *et al.* 2013; Road 2003; Beger *et al.* 1998). Therefore, the possibilities to explore the effects of co-culture on different cell type combinations are endless.

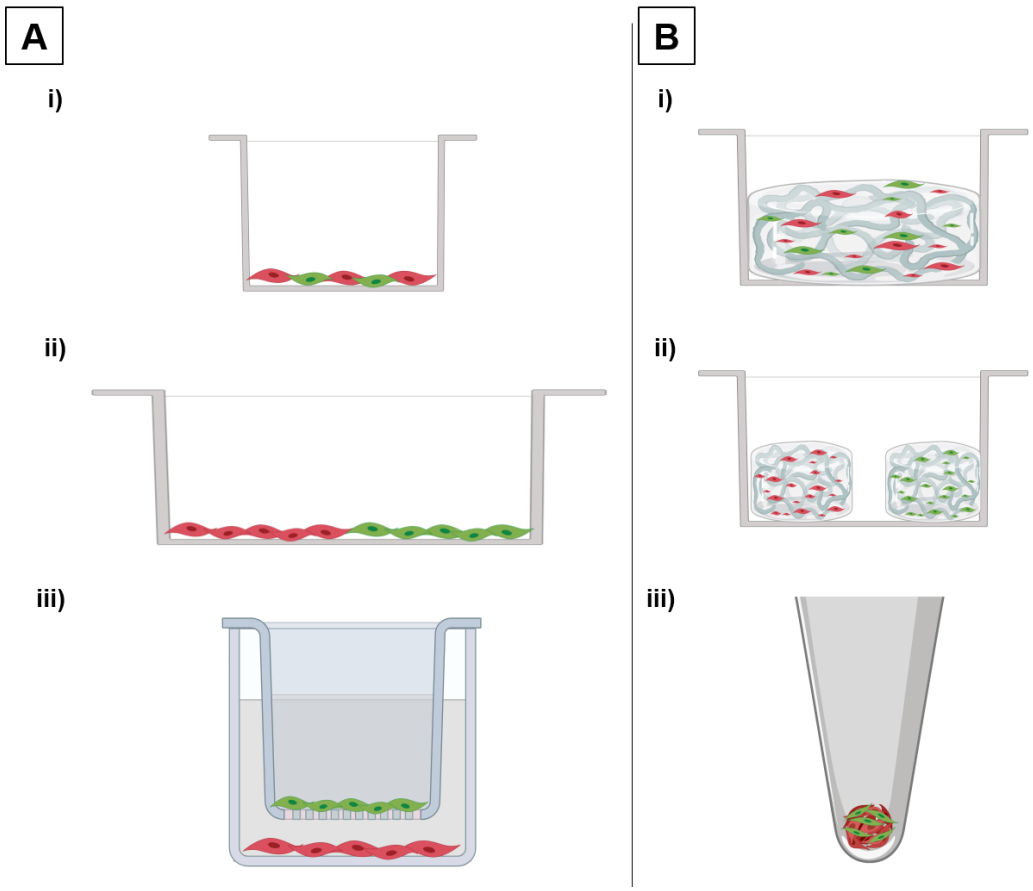

Figure 1.6: Examples of two distinct co-cultures of cell populations. *A) 2D, as a homogenised mixture of cells (i) (Calejo et al. 2018), cellular contact at one interface (ii) (Prasad Nayak et al. 2010; Wang et al. 2007), and paracrine effect through culturing two distinct cells in a common growth medium (iii) (Bacchus et al. 2012; Hatherell et al. 2011). B) 3D co-culture can be achieved in a homogenised mixture of hydrogel-encapsulated cells (i) (Albrecht et al. 2006), two separately cell-encapsulated hydrogels with common growth medium (ii) (S. K. Hamilton et al. 2013), and spheroid co-culture (iii) (Dilley and Morrison 2014).*

1.3.1 Variables affecting co-culture

Co-cultures are very complex techniques that can be affected by numerous variables. The variables are interconnected and dependent on each other; therefore, it is challenging to standardise all variables and test one variable only. However, for description purposes, the most significant variable will be discussed as follows:

1.3.1.1 Number of distinct populations

Although the term ‘co-culture’ suggests ‘two’ populations, more distinct populations can be added to co-cultures. However, most currently investigated co-cultures involve two populations. More than three distinct populations in a culture results in an unmanageable level of complexity, even if all other variables are standardised

(Zeidan, Radstrom, and van Niel 2010). Moreover, it is not always beneficial to have more than two distinct populations for co-culture, as Hatherell *et al.*, 2011 reported.

1.3.1.2 Degree of difference between the two distinct populations

Difference between populations can be as little as a fluorescent label for one population of the same cell type (Frimat *et al.* 2011; Albrecht *et al.* 2006) or as vast as culturing two different species (Goers, Freemont, and Polizzi 2014). The degree of difference between the two distinct populations depends on the aim of the experiment. Variable relationships between the two distinct populations add further depth to the complexity of the system. For example, the relationship between the two distinct populations cand be complementary, competitor, or prey and predator (Goers, Freemont, and Polizzi 2014).

An important application of co-culture is in research of tissue and artificial organ engineering. Co-culture between different tissues of the same species to study their cellular interaction and effect of co-culture is an integral part of regenerative medicine (C. P. Huang *et al.* 2009; Fukuda *et al.* 2006; Williams and Wick 2005; van der Wal *et al.* 1997; Yeh *et al.* 2011; S. C. Slater *et al.* 2011; Campbell *et al.* 2011).

1.3.1.3 Degree of contact between the two distinct populations

As different applications of co-culture require a specific degree of contact, the two distinct populations could be a homogenised mixture (Albrecht *et al.* 2006) (**Figure 1.7** A) or two separate cultures sharing the same growth media, as in transwells (Hatherell *et al.* 2011; Bacchus *et al.* 2012; Campbell *et al.* 2011) (**Figure 1.7** C), or the sharing of the same air to assess volatile material effect (Weber, Daoud-El Baba, and Fussenegger 2007) (**Figure 1.7** D). Choosing the correct method of cellular interaction between the two populations depends on the hypothesis and aim of the study. Additionally, an important aspect of cellular contact is defining the interaction as two-way or one-way, and designing the system accordingly. Controlling the population of each cell group in a co-culture needs optimisation, as different cell types have different proliferation rates. The starting cell number for culture can be optimised in ratios to prevent a cell type from completely overgrowing the other. For migration studies, the use of a separator or a simple gap between the two distinct populations can be used (Wang *et al.* 2007).

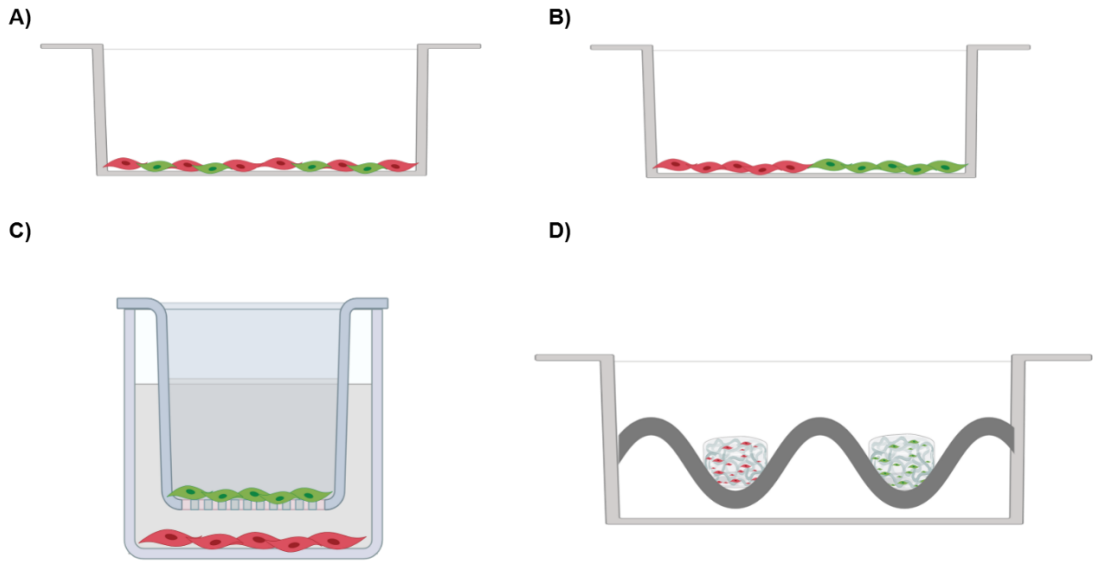

Figure 1.7: The degree of contact between two cell populations can help differentiate direct cell contact and paracrine effects in a co-culture. *A) A homogenised 2D co-culture (Calejo et al. 2018), B) a single interface cellular contact (Prasad Nayak et al. 2010; Wang et al. 2007), C) paracrine effect through separate cultures with common growth medium (Bacchus et al. 2012; Hatherell et al. 2011), and D) volatile gaseous exchange of separate cultures with their own growth medium but sharing the same gaseous environment (Albrecht et al. 2006).*

1.3.1.4 Scale of co-culture

Depending on the aim of the study, a co-culture could potentially be conducted at any volume. However, two opposing forces in the field of biotechnologies are pushing either to down-scale co-culture to allow high-throughput screening of different factors and optimisation steps, or to up-scale co-culture for industrial production yields (El-Ali, Sorger, and Jensen 2006).

Small-scale high-throughput are usually more cost-effective, with no need for specialisation in industrial-type production and equipment, which makes this scale suitable for laboratory exploration of an optimal culture environment. Most co-culture systems of this scale are in the range of one millilitre and can be used with standard laboratory culture consumables. Use of this scale has been reported with 96-well plates (Brenner, You, and Arnold 2009; Chuang, Rivoire, and Leibler 2010; Linden, Driessen, and McGuckin 2007), microdroplets on petri dishes (Byun *et al.* 2013) and microfluidic systems (Hesselman *et al.* 2012; Hong, Song, and Shin 2013; Frimat *et al.* 2011; C. P. Huang *et al.* 2009; Yeh *et al.* 2011; van der Meer *et al.* 2013; Balagadde *et al.* 2008; Chung *et al.* 2009; H. J. Kim *et al.* 2008). An ultimate down-scaling was reported by Frimat *et al.*, 2011 as they co-cultured single cells to investigate cell-on-cell effect.

In contrast, large-scale co-culture is needed for efficient production and supply. Litre-range co-cultures can be produced with bioreactors (Bacchus *et al.* 2012; Zeidan, Radstrom, and van Niel 2010; Gehin *et al.* 1996) or with hydrogel encapsulation (Albrecht *et al.* 2006). Disadvantages of large-scale co-culture include maintenance difficulty, asymmetric co-cultures and decreased viability (Shou, Ram, and Vilar 2007).

In general, there is a lack of sufficient detail about size of co-cultures, which restrains progress and manufacturing improvement. As the significance of co-culturing techniques increases, a general improvement and greater detail about co-culture specifications will arise (Goers, Freemont, and Polizzi 2014).

1.3.1.5 Time factor scale of co-culture

The length of time that two distinct cell populations are co-cultured so that they develop complex interactions is an important factor to consider (Jessup *et al.* 2004). The exposure of the two cell populations to one another could be performed for a short period of time, followed by separating and then studying the effect of that brief co-culture on the two populations. However, if a specific transformation path is required, then co-culture time can be extended (Balagadde *et al.* 2008).

1.3.2 Technology incorporation into co-culture models

Co-culture can be performed using several techniques, including: transwell plates (Miki *et al.* 2012; van der Wal *et al.* 1997; Hatherell *et al.* 2011), microfluidic platforms (El-Ali, Sorger, and Jensen 2006; Moraes *et al.* 2012; M.-H. Wu, Huang, and Lee 2010), hydrogels (Ahearne 2014; Sahoo *et al.* 2011), three-dimensional scaffolds (Campbell *et al.* 2011) or microarrays (Felton *et al.* 2012). There is a tendency towards developing techniques that are cost-effective and easily available (Javaherian, O'Donnell, and McGuigan 2011). One of the major challenges of developing a co-culture system is incorporating a suitable control model. The availability of systems including a separator that can be removed for the experiment and placed for the control, allows standardisation of all variables except the co-culture. A good standard for the ease of use is the simplicity of a transwell in making a co-culture. if the concept of transwell culture could be developed for more complex co-culturing models, including 3D cultures, then feasibility of co-culture use in 3D can increase. Moreover, models that support use of existing imaging and robotic equipment can improve applications of co-culture use.

1.3.3 Challenges in the co-culture field

There is an important compatibility issue for co-culture techniques since most of the analysis assays are designed for monoculture. As mentioned earlier, establishing a suitable control is a major issue in co-culture. Additionally, due to the presence of two cell populations in one environment, studying the effect of co-culture requires thorough individual characterisation of each cell population in the system. Upon completion of monoculture characterisation, co-culture experimentation can be conducted (Payne, Smith, and You 2012). A useful technique in studying the co-culture is to use fluorescently labelled cells for migration studies. On the other hand, measuring gene expression, protein synthesis, and other techniques requiring requiring use of a fully co-cultured sample, lack the ability to specify which cell type population was more affected (Wang *et al.* 2007).

1.3.4 Co-culture as a tool to study the enthesis and its 3D co-culture requirements

Due to the natural arrangement of the enthesis as a gradient of structural ECM and cell populations, co-culture is an essential tool to further examine the role of different cellular components and their effect on each other. A system with direct-contact 3D co-culture can improve understanding of cell-cell interaction within the enthesis and its role on enthesis development and function. Combining 3D culture methods and co-culture tools provides exciting opportunities to explore the enthesis in particular, and all tissue interfaces in general. Furthermore, a co-culture system that has a flexible method to adjust cellular contact to study effects of direct contact and paracrine effect (i.e. direct physical contact can be changed using common growth medium without physical contact) is required.

Key points of this section:

- Co-culture is essential for enthesis tissue engineering as the enthesis hosts populations of more than one cell type.
- Establishing different fluorescent labels for the two co-cultured cell populations is an important first step in monitoring migration effect.
- Studying the effect of co-culture requires an initial full characterisation of individual cell cultures.
- Co-culture requires careful consideration to assign suitable controls.

1.4 Current progress in enthesis tissue engineering research

The field of enthesis research is expanding and gaining more attention. The main objective is ultimately to find treatment options for enthesis injury that restore patients' quality of life for a considerable length of time. Several approaches to enthesis research started in many fields of science, including anatomy, biology, biochemistry, stem cell research, genetics, molecular biology and mechanical engineering. In all of these fields, enthesis related research has been established. The current focus is on two aspects of enthesis research: 1) understanding normal development, biomechanics, gene expression and signalling pathways of the enthesis, and 2) finding a suitable and implantable scaffold that restores enthesis function.

1.4.1 Understanding the normal structure of the enthesis and its development

Several studies aimed to explore normal development of the enthesis using different approaches. Rossetti *et al.* (2017) explored the use of micromechanical, structural, compositional and proteomic characterisation methods to identify microscopic mechanisms that give the enthesis its physiological function. They identified an area of ~500 µm depth at the junction of the calcaneal tendon of pigs and used this sample to perform mechanical testing fixed on a confocal fluorescent microscope (CFM) platform, documenting the changes to collagen fibrin structure when exposed to various uniaxial strain deformities. They also characterised a change in collagen fibres from thick type I collagen (105 ± 21 µm diameter), in the fibrous layer of the enthesis, to thinner (13 ± 4 µm diameter) and splaying type II collagen fibres, before inserting into the periosteum of the bone. Proteomics was also compared between mid-substance tendon and enthesis to identify key protein differences between them. They identified 22 enrichments of proteins in the enthesis tissue compared to the tendon, out of 433 proteins investigated. The same research group further identified the differences in a sequencing transcriptome study between tendon, enthesis and cartilage (Kuntz *et al.* 2018). The study detected a total of 34468 transcripts in tendon, cartilage and enthesis. They reported 13798 overlapping transcripts that were identified in all three tissues. Furthermore, they identified the number of specific transcripts for tendon, cartilage and enthesis, and reported them as 30, 61 and 1, respectively. Additionally, the jointly expressed transcripts between tendon/enthesis, tendon/cartilage and cartilage enthesis were reported as 69, 39 and 34, respectively. These studies have provided the field of enthesis tissue engineering with a standard of gene expression, proteomics and transcriptomics that can be used to assess true cell differentiation and gene expression in enthesis models and scaffolds.

1.4.2 Developing a suitable and implantable scaffold that restores enthesis function

New choices of biomaterials and manufacturing techniques have helped advance the research of scaffolds for enthesis reconstruction. Park *et al.* (2018) have described the printing of 3D biodegradable scaffolds that allow cell integration. The use of these scaffolds with mesenchymal stem cells (MSCs) showed a smooth bone to tendon transition, including a broad area of fibrocartilage formation compared to non-seeded 3D bioprinted scaffolds. These findings prove that cellular addition in scaffold design for enthesis repair better mimics the natural tissue. Another approach to produce an implantable scaffold is using decellularisation techniques to produce an implantable natural scaffold. The advantage of such techniques is the use of already made ECM that provides similar biochemical and mechanical properties to the implanted enthesis (Gilbert, Sellaro, and Badylak 2006; Badylak 2004). Xu *et al.* (2018) reported the development of a decellularisation protocol for a porcine enthesis, which used a complete structure containing tendon, enthesis and bone for better cell integration and retention of function. However, supply of such a scaffold has always been a limiting factor to its widespread use. Furthermore, the manufacture of an *in vitro* tissue engineered sinew model that can be formed using xenogenous fibroblasts and then decellularized, could be a potential replacement to such models (Lebled, Grover, and Paxton 2014).

1.4.3 Novel research and project aims

The overall aim of this thesis is to design, develop and assess the use of 3D co-culture systems to model cellular interaction in the enthesis. This was achieved by further study of three main aims:

1) Design and development of a 3D co-culture system that allows two distinct cell type populations to have a single interface. Establishing this model will allow study of the effect of co-culture on cells and ECM formation. Specific objectives to achieve this aim were to:
    a. Identify candidate materials and/or methodologies suitable for co-culture creation;
    b. Establish methods to distinguish between two distinct cell type populations using fluorescent labels;
    c. Investigate usability and reproducibility of the system to mimic an *invitro* 3D co-culture.

2) Use the hydrogel-based, scaffold-dependent 3D culture method developed in chapter 3 to assess candidate hydrogels for cellular biocompatibility and the effect of 3D co-culture on ECM formation. Specific objectives of this aim were to:
    a. Compare cell attachment, cell viability and cell density in cell-encapsulated agarose, gellan, fibrin and collagen hydrogels;
    b. Chose the most suitable hydrogel for use in the revised scaffold-dependent co-culture system;
    c. Assess ECM formation in cell-encapsulated bone-only, tendon-only, and bone-tendon co-culture in hydrogels;
    d. Assess the effect of bone and tendon cell-encapsulated hydrogel co-culture on ECM formation compared to bone-only and tendon-only cell-encapsulated hydrogel culture.
3) Assess the use of spheroid culture for the formation of bone and tendon spheroids that could be used for co-culture. Establishing this model will allow study of the effect of co-culture on cells and ECM formation. Specific objectives of this aim were to:
    a. Establish a standard method to produce tendon-only and bone-only spheroids;
    b. Produce co-cultures of minimum-contact (mini-coculture) and maximum-contact (max-coculture);
    c. Examine the difference in spheroid size over time of tendon-only, bone-only, mini-coculture and max-coculture spheroids to determine the time point of complete spheroid formation (smallest size) and growth thereafter;
    d. Correlate between size, cell density and ECM formation of spheroids to assess the effect of co-culture over time;
    e. Investigate the effect of different degrees of contact in co-culture (i.e. mini-coculture vs max-coculture) on gene expression.

Chapter 2. General Materials and Methods

2.1 General cell culture related materials and methods

Cell culture work was performed in a sterile environment. A laminar flow hood was used to conduct cell work. All materials were sterilised by autoclaving or 70% alcohol spray before being placed inside the hood.

2.1.1 Autoclaving

Phosphate buffered saline, distilled water, glassware and instruments were autoclaved at 115^{o}C for 30 minutes (Astell Scientific, UK). Other materials sterilised by autoclaving will be stated in their relevant chapter's specific materials and methods.

2.1.2 Phosphate buffered saline solution

Phosphate buffer saline (PBS) tablets were used to make 0.01 M phosphate buffered saline solution, 0.0027 M potassium chloride and 0.137 M sodium chloride (Sigma, UK). The tablets were dissolved in a ratio of one tablet/200 ml distilled water.

2.1.3 Cell sources

Ethical approval was not needed to conduct experiments with animal cells. Genetic modification for primary cell lines did not require ethical approval (all cells used in this thesis are primary cell lines). Accordingly, all cell culture work was performed in accordance with the UK Animals (Scientific Procedures) Act 1986.

Chick tendon fibroblasts with or without green fluorescent protein label (CTF/CTF-GFP):

Embryonic chick tendon fibroblasts (CTF) and CTF with incorporated green fluorescent protein (CTF-GFP) were isolated from the metatarsal tendons of dissected chick embryo hind limbs. The chick embryos were of age 13.5 days at the time of culling as, after 14 days of age, chick embryos sacrifice had to be performed by licenced laboratory and individual. Dissected tendons were placed in 5 % antibiotic/antimycotic (ABAM, HyClone, GE Healthcare Life Sciences) PBS solution. After three washes with sterile PBS in the laminar flow hood, the cells were isolated from tendon by a collagen digestion method. The tendons were digested by submersion in 0.1% collagenase type II DMEM and incubated for 1.5 hours at 37^{o}C, 5% CO_2. The cells were isolated from the solution by using a 100 µm cell strainer (BD Falcon, USA). Cells were moved to a T-175 cm^2 flask and incubated at 37^{o}C, 5% CO_2 (Paxton *et al*. 2012) and cultured according to the general culturing procedure.

Mouse osteoblasts (MC3T3):

This cell line has been established from mouse calvaria and was acquired from the European Collection of Authenticated Cell Cultures (ECACC, UK). Cells are osteogenic precursor cells that can differentiate into osteoblasts and osteocytes. They were thawed on receiving and cultured in standard cell culture media as described in **section 2.1.4** and incubated at 37ºC, 5% CO_2.

Dog primary tendon fibroblasts (DPF):

DPFs were isolated from the calcaneal tendons of dogs, obtained from the veterinary school at The University of Edinburgh. Dissected tendons were stored in 5 % ABAM in PBS solution. After three washes with sterile PBS in the laminar flow hood, the cells were isolated from tendon by a collagen digestion method. The tendons were digested by submersion in 0.1% collagenase type II DMEM and incubated overnight at 37ºC, 5% CO_2. The cells were isolated from the solution by using a 100 µm cell strainer (BD Falcon, USA). Cells were moved to a T-175 cm^2 flask and incubated at 37ºC, 5% CO_2 and cultured according to the general culturing procedure.

Rat tendon fibroblasts (RTF):

Adult rats were dissected to harvest calcaneal tendons. The dissection was conducted on a bench top in the laboratory. The lower halves of the rats were collected from the animal house immediately after animal culling. The lower half was rinsed generously with 70% alcohol. Autoclaved forceps and scissors were used in addition to sterile, disposable scalpels. First, skinning was performed to expose the area of the calcaneal tendon, with great caution not to touch the tissues with non-sterile equipment. The muscles and fat around the calcaneal tendon were dissected carefully; then the calcaneal tendon was excised from its calcaneal attachment while holding the tendon with forceps. The muscle tissues attached to the tendon were carefully dissected, and the tendon was excised. The excised tendons were stored and submerged in 5% ABAM PBS solution until ready to extract the cells. To isolate the cells, tendons were cut by a scalpel into small pieces measuring approximately 3x3 mm and then digested in Dulbecco's modified eagle's medium (DMEM) with 0.1% collagenase type II for 18 hours. The solution was shaken vigorously after digestion to help disintegration of tendons. Isolation of cells was facilitated by a 100 µm cell strainer, and the final solution was moved to a T-175 cm^2 flask cultured in standard growth media (described in **section 2.1.4**) at 37ºC, 5% CO_2.

Differentiated rat osteoblasts (dROb):

A rat osteoblastic cell line (ROb) was acquired (CELL applications, Inc., USA). The cells were cultured according to provider protocols. Differentiation was achieved by culturing the cells at full confluency for 14 days, which resulted in the cells changing their morphology from large, spindle-shaped cells to small, rounded cells (dRObs).

2.1.4 Cell culture

Cells were cultured in T-75 cm^2 flasks and passaged to T-175 cm^2 when 80% confluency was reached. The media used for general cell culture was Dulbecco's modified eagle's medium (DMEM; Sigma, UK) supplemented with 10% fetal bovine serum (Labtech, UK), 2.4% L-glutamine (Life Technologies, UK), 2.5% 4-(hydroxyethyl)-1-piperazineethanesulfonic acid (HEPES) buffer (Life Technologies, UK), and 1% penicillin/streptomycin (Life Technologies, UK). Supplemented DMEM (sDMEM) was the standard growth media, and all cells were incubated at 37^{o}C, 5% CO_2 for the duration of the experiments. All experiments were conducted under a laminar flow class 2 safety cabinet, after sterilisation of all work-related surfaces and equipment with Distel solution (1 part Distel, 9 parts autoclaved water), 1% Vircon, and 70% ethanol solution.

2.1.5 Cell dissociation from flasks

Anchorage-dependent cells were washed with pre-warmed PBS once before treatment with TrypLE Express (Catalogue number: 12604, Giboco, UK). To detach the cells from plastic surfaces of flasks and culture-wells, appropriate amounts of TrypLE were added according to manufacturer recommendations. After 3-5 minutes, the cells detached from the flask and were resuspended in sDMEM.

2.1.6 Cell counting

A haemocytometer counting chamber (Cat number AC1000, Hawksley, UK) was loaded with a cell suspension solution. Five large squares (corner squares and centre square) were counted on the haemocytometer (**Figure 2.1**). The average of the five counts was then calculated and multiplied by 10,000, which resulted in the number of cells/1 ml. The result was multiplied by the cell suspension solution volume to obtain the total cell number.

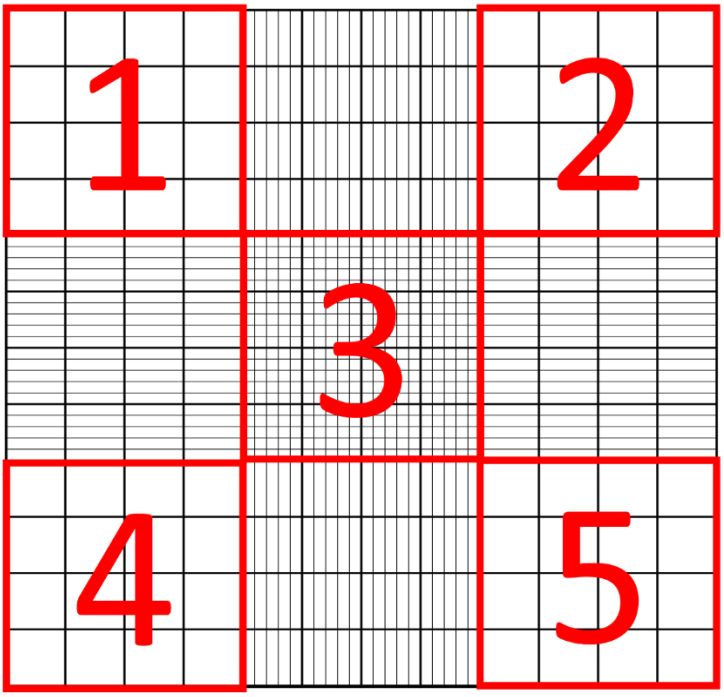

Figure 2.1: Large squares at the corners and the centre of the haemocytometer were calculated

2.1.7 Cell storage

All cell types were cultured in T-175 cm^2 flasks with the aim of cryopreservation storage. The cells were dissociated from the flask surface by TrypLE while cells were in the exponential stage of growth (70-80% confluent). After counting the cells, the solution was centrifuged for 3 minutes at 1000 rpm, and the pellet of cells was resuspended at a concentration of 1 million cells/ml using a pre-chilled freezing medium at 4-8^{o}C. The freezing medium was prepared as 10% dimethyl sulfoxide (DMSO, Sigma, UK) DMEM. One ml cryopreservation vials (Cryo-S, Greiner bio-one, UK) were used to store 1 ml of the cell solution. The vials were placed in a “Mr Frosty” freezing container (catalogue number 5100-0001, ThermoFisher Scientific, UK) and stored in a - 80^{o}C freezer overnight. The vials were moved to liquid nitrogen storage (-196^{o}C) the following day.

2.1.8 Cell thawing

To use a vial of cells after storage in liquid nitrogen, the cells were thawed quickly in a water bath at 37^{o}C for 1 minute. The 1 ml cell solution in the vial was then transferred to a 50 ml centrifuge tube that contained 9 ml of sDMEM. The solution was shaken to homogenise content before centrifuging for 3 minutes at 1000 rpm. The supernatant was discarded, and 15 ml of sDMEM were used to disrupt the cell pellet and form a

homogenous cell suspension. The fresh cell suspension was transferred to a T-75 cm^2 flask and cultured at 5% CO_2 and 37^oC in an incubator.

2.2 Co-culture system

General materials and methods of the co-culture system are described in this section. Technique-specific materials and methods are described in their relevant chapters. There were two methodologies used for the co-culture system: 1) scaffold-dependent, 2) scaffold-less systems. In this section, a description of the materials followed by the methods used to create each co-culture system is provided.

2.2.1.1 Scaffold-dependent co-culture system

The original co-culture system design was developed and reported by previous work in the laboratory (Bellamy. D. 2015). The design was a simple mould-based system. PDMS (polydimethylsiloxane) Sylgard 184 silicone (Dow Corning, Midland, MI, USA) was prepared according to the manufacturer's instructions and poured into 6-well plates (Greiner bio-one, UK). Immediately after pouring the Sylgard, 3D printed blocks in shapes of the desired mould for the co-culture were placed in the silicone (**Figure 2.2** A, College of Art, University of Edinburgh, UK). The plates containing the Sylgard were kept at room temperature for seven days to allow the Sylgard to polymerise. After seven days, the 3D printed blocks were then removed, creating a hollow mould to be used for co-culture (**Figure 2.2** B). To sterilise the system, the plates containing the moulds and the 3D printed blocks were soaked in 70% alcohol for 30 minutes and left to dry in a laminar flow hood for one hour.

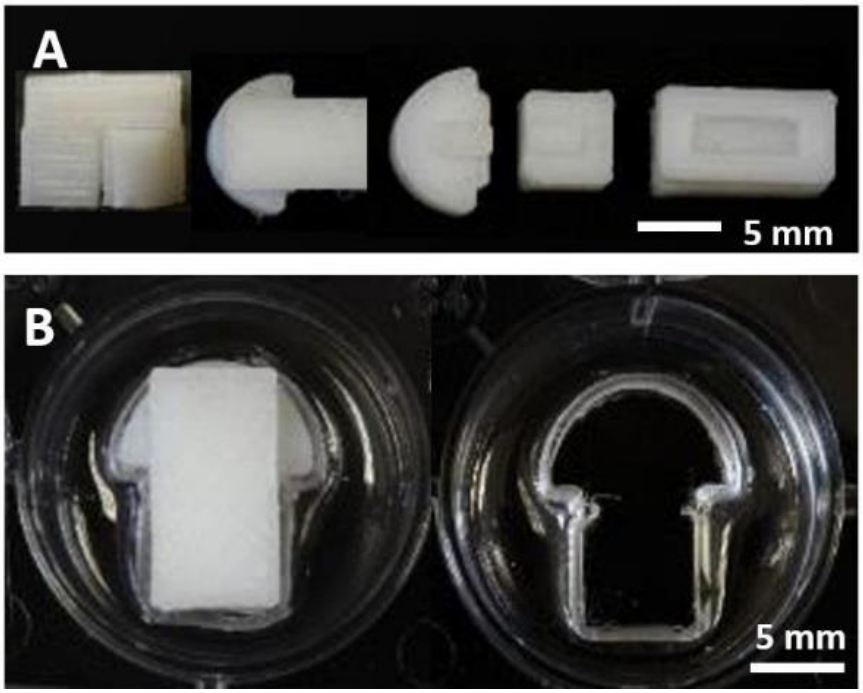

Figure 2.2: A) 3D printed block designs. B) Using Sylgard silicone to make a hollow template in a 12-well plate by using 3D printed blocks.

This methodology was revised in the improved co-culture system by creating half-well plugs. These half-well plugs were made by pouring Kemsil silicone (Kemdent, UK), prepared according to the manufacturer's instructions, into 24-well plate wells (Greiner Bio-one, UK). The Kemsil silicone polymerises in 10 minutes, creating a well-plug (**Figure 2.3** A). The well-plugs were collected from wells and cut in half (**Figure 2.3** B) by using a number 23 scalpel (Swann-Morton, UK). The half-well plugs were sterilised by submerging in 70% alcohol for 30 minutes. Before use for tissue culture, the half-well plugs were kept in a laminar flow hood for 30 minutes to dry.

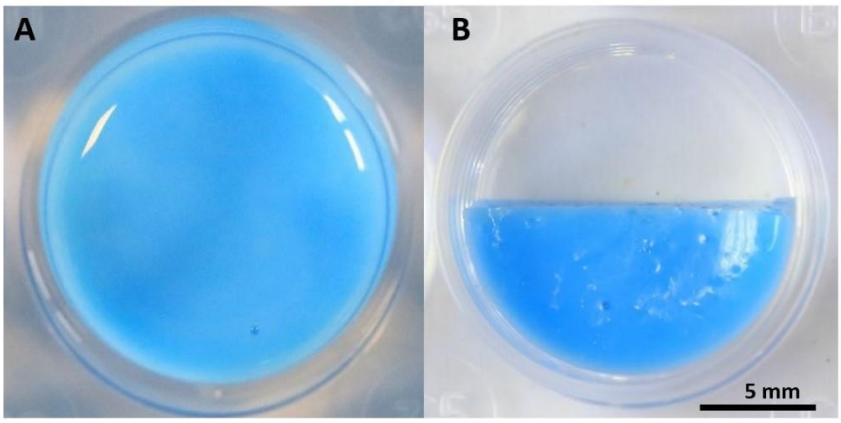

Figure 2.3: A) Kemsil silicone well-plug made in a 24-well plate. *B) A half-well plug created by cutting the well-plug into two halves.*

2.2.1.2 Scaffold-less co-culture system

Spheroids of cells were made by culturing the cells in U-bottomed, cell repellent, 96-well plates (CELLSTAR®, Greiner bio-one, UK). The anchorage-dependent nature of the cells forced them to attach to other cells, creating a spheroid of cells.

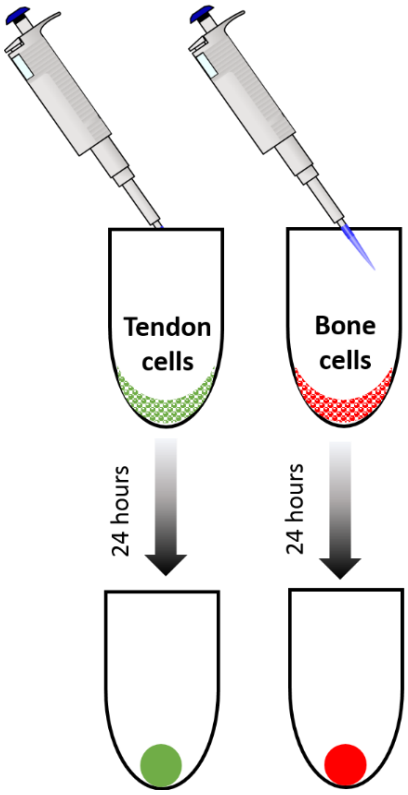

Figure 2.4: Formation of scaffold-less 3D culture spheroids in 24 hours.

2.2.2 Hydrogels

Hydrogels were used as scaffolds for cell encapsulation to create a 3D culture. The materials and methods required to make each hydrogel are described below:

2.2.2.1 Agarose

Agarose hydrogels were prepared by mixing 1 g of UltraPure™ low melting point (LMP) agarose powder (16520050, Invitrogen, UK) with 99 ml of distilled water and raising the temperature gradually until the powder fully dissolved to a final concentration of 1% agarose solution. The agarose was sterilised by autoclaving. The cell solution was mixed with agarose at no more than 40^{o}C inside a laminar flow hood in a 1:1 ratio, resulting in 0.5% agarose hydrogel with suspended cells. The 0.5% cell-suspended agarose was freshly prepared for each experiment and cultured at 37^{o}C, 5% CO_2 for the duration of each experiment.

2.2.2.2 Gellan

Gellan powder was hydrated by mixing with deionised water at 70-80^{o}C. After complete hydration of the powder, the gellan hydrogel was immediately autoclaved. When the autoclave cycle finished, the gellan hydrogel was transferred to a laminar flow hood to be mixed with cells in a 1:1 ratio at a temperature no higher than 40^{o}C.

2.2.2.3 Fibrin

Preparation of fibrin hydrogel required the use of fibrinogen and thrombin. Other supplements, used to prevent protein digestion, were aminohexanoic acid and aprotinin. A thrombin mix was prepared by adding 97.1% cell suspension in sDMEM, 2.4% thrombin, 0.2% aprotinin and 0.2% aminohexanoic acid. To make fibrin hydrogel, a solution of one part fibrinogen and five parts thrombin mix was made. The construct was then incubated for one hour to allow the hydrogel to polymerise. The volume of fibrin hydrogel is specified in the methodology section of the relevant chapter.

2.2.2.3.1 Thrombin

Thrombin (200 U/ml) was prepared by dissolving a vial of 1000U thrombin powder (Calbiochem, UK) in 5 ml of 0.1% Bovine serum albumin (BSA, Sigma, UK) in Ham's F-12K (Kaighn's) Medium (F12K, Catalogue number 21127022, ThermoFisher scientific, UK). The thrombin solution was transferred to Bijou tubes and frozen at -20^{o}C. To use the prepared thrombin, the Bijou tube of thrombin was removed from the freezer and defrosted at room temperature.

2.2.2.3.2 Fibrinogen

To prepare 20 mg/ml (2%) of fibrinogen solution, 1 g of fibrinogen powder (F8630, Sigma, UK) was dissolved in 50 ml of F12K. The fibrin solution was kept in a 37^{o}C water bath and gently shaken every 30 minutes for a minimum of 4 hours to ensure complete dissolution of fibrinogen powder. Sterilisation of fibrinogen solution was achieved by vacuum filtration using 0.22 µm filters (Corning, UK). The sterile fibrinogen was stored in 15 ml tubes (Greiner bio-one, UK) and kept in a -20^{o}C freezer. When fibrinogen was needed, the 15 ml tubes were removed from the freezer and defrosted at room temperature. The fibrinogen powder used for all experiments in this thesis was sourced from the same batch.

2.2.2.3.3 Aminohexanoic acid

Powder form of 6-aminohexanoic acid (VWR, UK) was weighed to obtain 0.292 g and dissolved in 10 ml of sterile PBS, producing a ratio of 1:34.2 aminohexanoic acid (g) to water (ml). The solution was sterile filtered through a 0.2 µm syringe filter. The working solution was stored in the fridge to be used when needed.

2.2.2.3.4 Aprotinin

Preparing aprotinin required dissolving 10 mg of aprotinin (Roche, UK) in 1 ml of sterile PBS to obtain a 1:100 ratio. The aprotinin solution was sterile filtered after dilution. The solution was then stored as 100 µl aliquots in autoclaved 1.5 ml reaction tubes (Greiner bio-one, UK) in a -20^{o}C freezer. When needed, the solution was defrosted at room temperature.

2.2.2.4 Collagen

Collagen required pH correction for use as a 3D scaffold for tissue engineering. Mixing nine parts of collagen hydrogel (pH 2) with one part 0.2 sodium phosphate (pH 11.2) resulted in an optimum collagen hydrogel for 3D cell encapsulation (pH 7), which had a final concentration of 6 mg/ml pepsin soluble collagen, as supplied and described by the manufacturer (CB-008, Collagen solutions, UK). Supplemented DMEM was used to dilute collagen to a final concentration of 3 mg/ml. Collagen required a temperature of 2-10^{o}C for storage and during cell encapsulation. Polymerising collagen hydrogel was achieved by incubation at 37^{o}C, 5% CO_2. Collagen used for all experiments in this thesis was sourced from the same batch.

2.2.3 Cell labelling

Labelling different cells with specific fluorescent proteins enabled visualisation and tracking of distinct cell types in a co-culture, essential for the progress of this study. Using fluorescent labels to identify live and dead cells to study viability was also important. In the following sections, a description is given of the materials and methods of each cell labelling technique.

2.2.3.1 Transfection

Transfection was used to incorporate a fluorescent label into different cell types. The process of transfection ran through three stages: establishing kill curves for different cell types, addition (transfection) of desired proteins, and selecting competent cells. Details of each stage are stated below.

2.2.3.1.1 Kill curve for different cell types

Kill curves of G418 antibiotic (AB) treatment to different cell types were established. Cells were seeded in a 24-well plate in a 0.1 x 10^6 density and incubated overnight before experimenting. Five concentrations of AB in S-DMEM were investigated: 0.1, 0.25, 0.5, 1 and 2 mg/ml. Daily photographs were taken of all cells in different concentrations and visual assessment was used to determine viability. Viability was compared to live cells in negative control wells.

2.2.3.1.2 Transfection

Several transfection protocols were investigated for both Liopofectamine® 2000 (11668030, Life Technologies, UK) and Lipofectamine® 3000 transfection reagents (L3000-001, Life Technologies, UK). Both original manufacturer protocols were used to incorporate an empty plasmid vector with a red fluorescent protein (RFP) (mCh-alpha-tubulin was a gift from Gia Voeltz, Addgene plasmid # 49149; RRID: Addgene_49149). Moreover, optimisation of the protocol was performed to improve results. Contact time between cells and transfection reagent was optimised to 4 hours instead of 24 hours in Lipofectamine® 2000, and the same variable was also optimised in Lipofectamine® 3000 from 48 hours to 4 hours. Decreasing the reagent-cell contact time aimed to improve cell viability.

2.2.3.1.3 Selection with AB

The results of the kill curve stage were used to add an optimised AB concentration to the culture media of different cell types. The cells were cultured as standard, and the optimised media was changed every other day. Fluorescent microscope pictures

combined with bright field pictures of the same field were compared to differentiate between transfected and non-transfected cells. Addition of optimised media was performed either after 24 or 72 hours to further optimise the protocols.

2.2.3.2 Cell tracker

Red cell tracker was used to label MC3T3 and dROb cells (C34552, CellTracker™ Red CMTPX, Life Technologies, UK) and green cell tracker (C7025, CellTracker™ Red CMTPX, Life Technologies, UK) was used to label RTF cells. Preparation of cell tracker working solution was performed according to the manufacturer's protocol to a final concentration of 15 µM. Briefly, 50 µg of cell tracker powder was dissolved in 7.3 µl of DMSO to make a 10 mM cell tracker dye solution. This was followed by diluting the solution to a standard working concentration of 15 µM of cell tracker dye.

2.2.3.3 Calcein/Propidium iodide solution

The dye solution was freshly prepared in a dark environment for each experimental time-point. The required amount of dye solution was prepared with DMEM growth media supplemented with 0.7% of 50 µg/ml Calcein AM (C34852, Invitrogen Molecular Probes®, UK), staining live cells green, and 2% of 1mg/ml Propidium Iodide (PI) (P4170 ,Sigma, UK) staining dead cells red. Non-fluorescent Calcein AM substrate was taken up by live cells and hydrolysed into fluorescent calcein. In contrast, PI bound to DNA proteins for fluorescence, which could be achieved only in dead cells due to the defects in cell and nuclei membrane integrity.

2.2.3.4 Hoechst 33342

Hoechst 33342 stain (R37165, Invitrogen Molecular Probes®, UK) was used to stain the nuclei of live cells. The stain was cell permeable, which allowed it to bind to the cell DNA and emit fluorescence when excited at 360 nm. Emission was detected at 460 nm using a confocal microscope.

2.3 Imaging modalities

2.3.1 Light microscopy

A Leica light microscope was used to monitor cell cultures and to image samples (Leica DMi1, UK). The microscope was used at a magnification of 5x, 10x and 20x for monitoring the health of cell cultures and for detection of possible infection. Methods of relevant experiments are described in detail in their chapters.

2.3.2 Fluorescent microscopy

Assessing fluorescent 2D cultures was performed using a Leica fluorescent microscope (Leica DMi8, UK) with 10x and 20x atmospheric lenses. Samples were imaged to observe fluorescent tag bleaching for cell tracker and successful transfection assessment. The detector gain and laser intensity were fixed during these experiments to ensure that the bleaching effect was assessed. Images obtained were processed using ImageJ (National Institute of Health, USA) and Imaris software (Bitplane, Oxford Instruments, UK).

2.3.3 Confocal fluorescent microscopy (CFM)

Data sets of confocal images were obtained from an inverted confocal laser scanning microscope system (Nikon A1R, Nikon, UK). The system allowed for live imaging of unopened culture plates so sterility could be maintained. The atmospheric lenses used were 4x and 10x, according to experimental needs. Laser intensity and detector gain were adjusted according to experimental need, considering labelling quality, number of cells, photobleaching, depth of images and background noise. Data sets obtained were analysed by NIS Elements (Nikon, UK), imageJ (National Institute of Health, USA) and Imaris software (Bitplane, Oxford Instruments, UK).

2.4 Statistical analysis

As the aim of experiments was to establish a reliable and reproducible method, the cells used in experiments were acquired from a single animal source. Therefore, the results in this thesis were aimed to verify the stability of the system and not to generalise the results to the animal population. Therefore, sample data is presented as ‘Nn’, where ‘N’ indicates the number of independent experiments started from cell thawing after liquid nitrogen storage (and not from a different animal) while ‘n’ indicates the number of technical replicates per experiment. An exclusion to this rule is implemented for the cell attachment experiment in section (4.4.1.1) in which the “nn” number indicates all the total number of technical replicates for all experimental repeats. This is adopted because independent experiments had different numbers of technical replicates.

Excel software was used with all quantitative data to calculate averages and determine standard curves (Excel 2016, Microsoft office, USA). Statistical tests were performed using GraphPad Prism (Version 8.1.1, GraphPad Software Incorporation, USA), and specific tests are indicated in relevant chapters’ methods. The analysis included unpaired two-tailed *t*-tests, one-way analysis of variance (ANOVA), two-way

ANOVA and a mixed effect model. The use of each test is indicated in the figure legend of each graph, including the use of Tukey's post-test multiple comparison test.

Unless otherwise stated, all data was tested for normal distribution using the Shapiro-Wilk test. In figures where GraphPad Prism software was used to conduct statistical analysis, asterisks denote significance levels as follows: * $p < 0.05$, ** $p < 0.01$, *** $p < 0.001$, and **** $p < 0.0001$; p values not reaching the level of significance are indicated (ns). Error bars where statistical analysis has been conducted always represent the standard deviation. No standard error of means was presented or calculated.

Chapter 3. Designing a 3D tissue interface model: creating a reproducible methodology for establishing 3D co-culture systems

3.1 Introduction

Improving treatment methods for enthesis injuries is limited by the current knowledge gap in enthesis development and healing processes. Understanding the developmental process of the enthesis will help in determining factors to consider when researching therapeutic options or engineering an enthesis *in vitro*. Indeed, understanding healing processes occurring at the enthesis after injury and their limitations will help determine better intervention time points and methods. Nonetheless as entheses are affected by repeated daily life activity and the stress exerted on them, they wildly differ from one person to another in terms of size and composition (Apostolakos *et al.*, 2014). Therefore, creating a model system to engineer a standardised artificial enthesis would help investigate cellular interaction, observe tissue development and identify specific therapeutic targets or interventions.

An *in vitro* interface model between two of the main cell types present at the enthesis has been engineered previously by Wang et al. (2006). This interface model was designed to culture osteoblasts and fibroblasts in direct contact. Then, GAGs, alkaline phosphatase (ALP), and chondrogenic gene markers such as cartilage oligomeric matrix protein (COMP) and type II collagen were investigated as indicators of chondrogenic transformation resulting from bone and tendon cell co-culture. This study showed that direct contact between osteoblasts and fibroblasts caused an up-regulation of the chondrogenic markers COMP, aggrecan and type II collagen in the cells of the interface region, compared to the cells in the pure osteoblast or fibroblast regions. However, this study was performed in a 2D setting, which does not represent the natural physiological environment of cells in tissues. It is now well recognised that 2D cell cultures do not represent the natural cellular environment or structure (Edmondson *et al.*, 2014) and therefore it is not ideal to assume that cell response and behaviour in 2D culture is a valid imitation of native tissue (Brendon M Baker and Chen, 2012). Accordingly, 3-dimensional (3D) tissue culture methods are a promising alternative to re-evaluate direct contact between osteoblasts and tendon fibroblasts.

3.2 Chapter aim and objectives

To design and develop a 3D co-culture system that allows two distinct cell type populations to have a single interface. Establishing this model will allow study of the effect of co-culture on cells and ECM formation.

Specific objectives for this chapter are to

1. Identify candidate materials and/or methodologies suitable for co-culture creation;
2. Establish methods to distinguish between two distinct cell type populations using fluorescent labels;
3. Investigate the usability and reproducibility of the system to mimic an *invitro* 3D co-culture.

3.3 Materials and Methods

3.3.1 Establishing fluorescently labelled cells

Visualisation of different cell populations was important to determine a successful co-culture. Therefore, two labelling techniques to introduce different fluorescent proteins into different cell populations were attempted.

3.3.1.1 Assessment of permanent cell labelling (transfection)

An attempt to transfect MC3T3 cells was performed as described in **section 2.2.3.1** (N=2 independent experiments, n=3 technical repeats). As a positive control, CTF and DPF cells were examined at the same time. 60k samples of each cell type were seeded in a tissue culture 24-well plate in addition to transfection reagent-free wells, vector-free wells and cells-only negative control wells. Two transfection kits (Lipofectamine™ 2000 and Lipofectamine™ 3000, Thermofisher, UK) were optimised and used to transfect an empty vector with RFP fluorescent label (as described in **section 2.2.3.1**). Fluorescence of transfected cells was assessed by imaging cells using a Nikon fluorescent microscope (DMi8, Leica, UK) with a low power objective lens (x5 dry) and an RHOD filter cube (excitation at 517-563nm and emission detection at 590nm).

3.3.1.2 Temporary cell labelling usability (Cell tracker)

A temporary fluorescent label was assessed for use to distinguish between cells. Cell tracker (CellTracker™ Red CMTPX, Life Technologies, UK) was used to label cells with a temporary red fluorescent label (N=3 independent experiments, n=3 technical repeats). The fluorescent label freely passes through the cell membrane and the chloromethyl group in the dye reacts with thiol groups, utilising a glutathione S-transferase–mediated reaction. In most cells, glutathione levels are high, and glutathione transferase is ubiquitous. The reaction product was retained in the cells and passed down to the daughter cell. The CellTracker™ Red product in the cells has a peak excitation value at 577nm, and peak emission was detected at 602nm. The

duration of use before fluorescence faded was evaluated for different concentrations of CellTracker™ Red labelled MC3T3 cells.

3.3.1.2.1 CellTracker use in 2D culture

MC3T3 cells were cultured in three groups of T-25 cm^2 flasks (Greiner Bio-one). Each group of flasks had a concentration of either 5 µM, 10 µM or 15 µM of CellTracker™ Red to be investigated. Subsequently, a fluorescent microscope (DMi8, Leica, UK), fitted with a RHOD filter cube (excitation at 517-563nm and emission at 590nm), was used to take pictures of the three groups of flasks at days 0, 2, 5 and 8. To stabilise different variables while using the fluorescent microscope, emission parameter settings were standardised, i.e., laser intensity, detector gain and pinhole size.

3.3.1.2.2 CellTracker use in 3D culture

The optimum concentration of cell tracker used in 2D was assessed with 3D MC3T3 cell-encapsulated hydrogels to evaluate exposure to CFM lasers for a longer period. Bleaching effect was investigated in 3D by exposing the same area of interest in the full thickness of MC3T3 cell-encapsulated hydrogel, labelled with CellTracker™ red, for CFM lasers to acquire datasets of images over days 0, 2, 5 and 8. Then the final image at day 8 was compared to an image of a day 8 sample which was not exposed to the CFM laser.

3.3.2 Designing a co-culture system

3.3.2.1 Vertical scaffold-dependent co-culture system

This experiment aimed to create a single interface between two stacked hydrogel layers. This was attempted by using agarose, gellan, fibrin and collagen hydrogels in flat-bottomed, cell repellent 96-well plates (Greiner bio-one, UK). The gross assessment was performed using red and green food colours with agarose and gellan hydrogels to help visualise the formation of the single interface, as illustrated in **Figure 3.1**. Alternatively, for fibrin hydrogel, pink and clear coloured hydrogels were produced by using either DMEM (producing a pink hydrogel) or 1X PBS (producing a clear hydrogel) in the thrombin mix (as described in **section 2.2.2.3**), as the use of food colours interfered with the natural formation of the fibrin hydrogel. Similarly, collagen hydrogel was coloured yellow or clear by using either DMEM (producing a yellow hydrogel in response to the low pH of DMEM containing phenol red) or 1X PBS (producing a white hydrogel), when diluting the 6 mg/mL to 3 mg/mL collagen (as described in **section 2.2.2.4**).

3.3.2.1.1 Cell-free vertical interface assessment

For each hydrogel, 80 µl of two differently coloured layers were stacked in a single well (**Figure 3.1)**. A side-view image was taken for each of the stacked layers of hydrogels by a digital single lens reflex camera (Canon D6 DSLR, Canon, Japan) equipped with a 100 mm macro lens (Canon EF 100mm f2.8 USM Macro Lens, Canon, Japan).

3.3.2.1.2 Cell-encapsulated vertical interface assessment

Microscopic evaluation of the formed interface was performed. CTF cells were encapsulated in a hydrogel and 80 µl was cast at the bottom of the well (**Figure 3.1** A). Following setting of the hydrogel, 80 µl of hydrogel encapsulated with MC3T3 cells was cast on top (**Figure 3.1** B). After the hydrogel had set, sDMEM was added to each well and the construct was assessed by CFM immediately after formation. Datasets of images were analysed and processed using Imaris software (Bitplane, Oxford Instruments, UK).

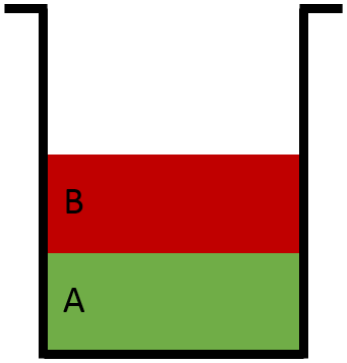

Figure 3.1: Vertical co-culture system. A) First layer of stacked hydrogel. B) Second layer of stacked hydrogel.

3.3.2.2 Horizontal scaffold-dependent co-culture system

A horizontal co-culture system was required to overcome the disadvantages of the vertical co-culture system (discussed in section 3.4.2.2). Accordingly, two horizontal scaffold-dependent co-culture systems were designed and developed.

3.3.2.2.1 Original scaffold-dependent co-culture system

This original system has been designed and developed by previous work in the laboratory (Bellamy. D. 2015). The materials of the original scaffold-dependent co-culture system have been described in **section 2.2.1.1**. Using a 3D printed block to seal one side of a well, 300 µl of cell-encapsulated hydrogel (at a cell concentration of 50K/100 µl hydrogel solution) was cast in the empty half of the system (**Figure 3.2**

B). When the hydrogel set, the 3D printed block was removed (**Figure 3.2** C), and another 300 µl of cell-encapsulated hydrogel was cast in the empty side of the well (**Figure 3.2** D). This created a single 3D interface between the two cell-encapsulated hydrogels. The shape of the mould was used to grossly identify which cell type was in which side of the system, i.e., the square side contained tendon cells and the half-circle contained bone cells. CFM was used to examine the formation of a single 3D interface between the two cell-encapsulated hydrogels using a low power objective lens (x10 dry, excitation lasers: 488 nm and 561 nm). The cells used were CTF-GFP and MC3T3. The MC3T3 cells were temporarily labelled with cell tracker red as described in **section 2.2.3.2**. The datasets acquired from CFM were processed using ImageJ software (Schindelin *et al.*, 2012) to make a z-axis projection single image.

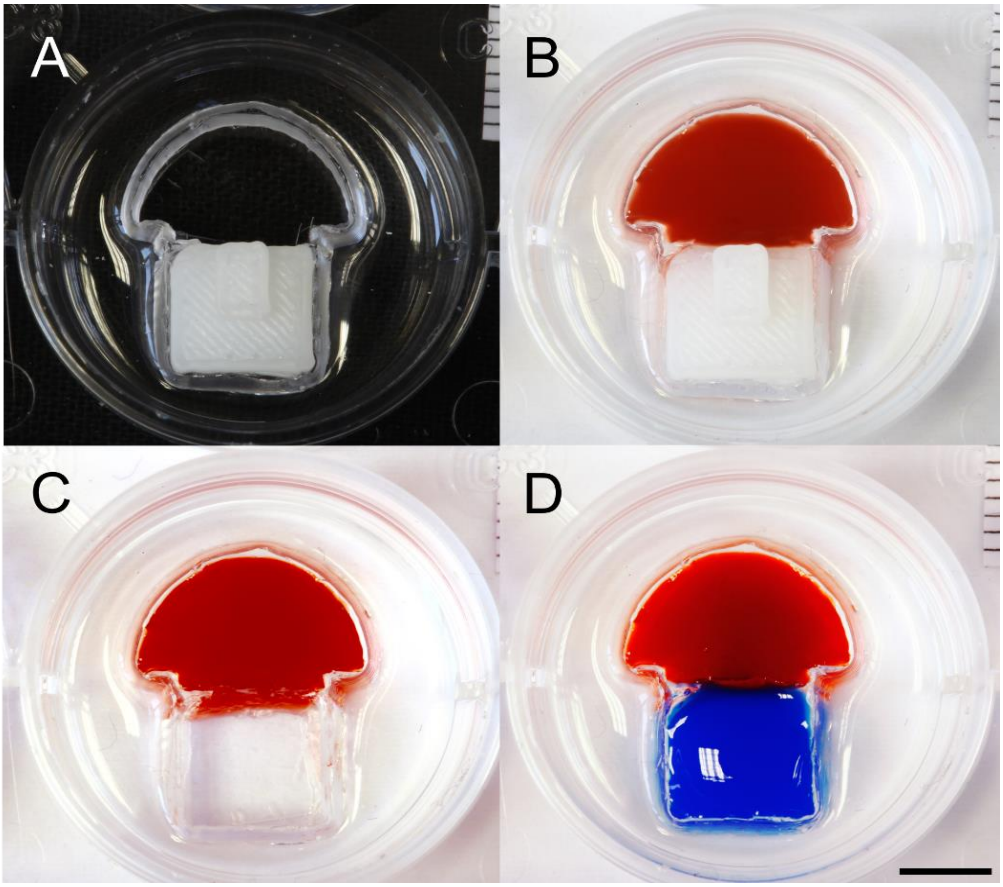

Figure 3.2: Original protocol for scaffold-dependent co-culture system. *A) A 3D block was inserted in the hollow mould to block one side. B) A cell-encapsulated hydrogel was cast in the exposed side of the system. C) After the hydrogel set, the 3D block was removed, exposing the other side of the system. D) The other cell type was encapsulated in the hydrogel and cast in the empty space. Pseudo red and blue colours were used with agarose gel for demonstration purposes. (Scale bar = 5 mm)*

3.3.2.2.2 Revised scaffold-dependent co-culture system

The original scaffold-dependent co-culture system had several disadvantages that limited its use. Leakage around and below the 3D printed block caused cell-encapsulated hydrogel to leak to the other side of the system. Moreover, time, cost and difficulty in inserting/removing the 3D printed blocks were other factors that encouraged revision of the original scaffold-dependent system. This was improved by creating half-well plugs, as described in **section 2.2.1.1**. The concept of the revised system was the same as the original system, in allowing creation of a single 3D interface between the two cell-encapsulated hydrogels. By using the materials described in **section 2.2.1.1**, half-well plugs were created. These half-well plugs were used to seal half a well of a non-tissue culture treated 24-well plate (Greiner bio-one, UK) (**3.3** A). Cell-encapsulated hydrogels were cast as described in **section 3.3.2** and shown in (**Figure 3.2**). The interface between the cell-encapsulated hydrogels was imaged at the same location for all samples on days 0, 1, 2 and 4. Five samples of agarose, gellan, fibrin and collagen were investigated in this experiment. This experimental method was repeated using non-tissue culture treated 24-well plates.

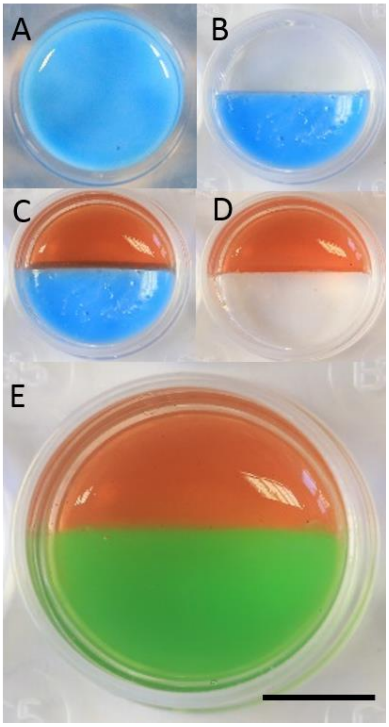

Figure 3.3: Improved scaffold-dependent co-culture system protocol. *A) A half-well plug was inserted into the well. B) A cell-encapsulated hydrogel was poured into the exposed side of the system. C) After the hydrogel had set, the 3D block was removed, exposing the other side of the system. D) The other cell type was encapsulated in the hydrogel and poured into the empty space. Pseudo red and green colours were used with agarose gel for demonstration purposes only. (Scale bar = 5 mm)*

3.3.2.3 Scaffold-less co-culture system

Spheroid 3D culture is a popular methodology in the fields of drug discovery, cancer research and tissue engineering. This technique was used as an alternative methodology to achieve a 3D co-culture of two distinct populations.

3.3.2.3.1 Spheroid formation and co-culture

CTF-GFP (tendon cells) and MC3T3 (bone cells) labelled with temporary cell tracker, as described in **section 2.2.3.2,** were used in this experiment. The aim was to observe the formation of bone and tendon spheroids, as described in **section 2.2.1.2,** and monitor the interface of their co-culture. Four groups of spheroids were made: tendon-only, bone-only, minimum-contact co-culture (mini-coculture) and maximum-contact co-culture (max-coculture). To make bone and tendon spheroids, 50 K of each cell type were seeded in a U-bottomed, cell-repellent 96-well plate (**Figure 3.4**) (Greiner bio-one, UK). To make a mini-coculture spheroid, one tendon and one bone spheroid was placed in the same well after formation (**Figure 3.4**). To make a max-coculture spheroid, 100 K of a homogenised cell suspension of equal numbers of tendon and bone cells mixed together was seeded in a U-bottomed, cell-repellent 96-well plate (**Figure 3.4**) (Greiner bio-one, UK). CFM was used to image all groups of spheroids at day 1, 2, 4 and 6. Datasets were processed using ImageJ (Schindelin *et al.*, 2012) to observe the spheroid formation and assess the co-localisation of cell types in the co-culture.

3.3.2.3.2 Spheroid cross-sectional area (CSA) assessment for spheroid size and co-culture effect

Four groups were compared: single tendon spheroids, single bone spheroids, mini-cocultures and max-cocultures. A light microscope (Leica DMi1, UK) with an objective lens of 10x magnification was used to take images of all groups at days 1, 3, 5, 7 and 10 (independent experiments N=5, technical repeats n=4), followed by cross-sectional surface measurement using ImageJ software (Schindelin *et al.*, 2012). Averages of the cross-sectional area were calculated using Excel software (Excel 2016, Microsoft office, USA). Mixed effect model statistical analysis was performed, followed by Tukey's honest significance test for multiple comparisons, using GraphPad Prism (version 8.1.1 for Windows, GraphPad Software, California, USA).

3.3.3 Confocal fluorescent microscopy (CFM)

Datasets of CFM images were obtained from an inverted confocal laser scanning microscope system (Nikon A1R, Nikon, UK). The system allowed for live imaging with

culture plates unopened to maintain sterility. The atmospheric lenses used were 4x or 10x according to experimental needs. Laser intensity and detector gain were adjusted according to experimental needs, considering fluorescent labelling quality, number of cells, photobleaching, depth of images and background noise. Data sets obtained were analysed by NIS Elements (Nikon, UK), ImageJ (National Institute of Health, USA) and Imaris software (Bitplane, Oxford Instruments, UK). ImageJ software was used to perform a z-axis projection of fluorescence, producing a single figure that represented the collective of all the detected fluorescence in a dataset of images. Imaris software was used to reconstruct CFM datasets into 3D digital models and inspect the samples' side-plane views.

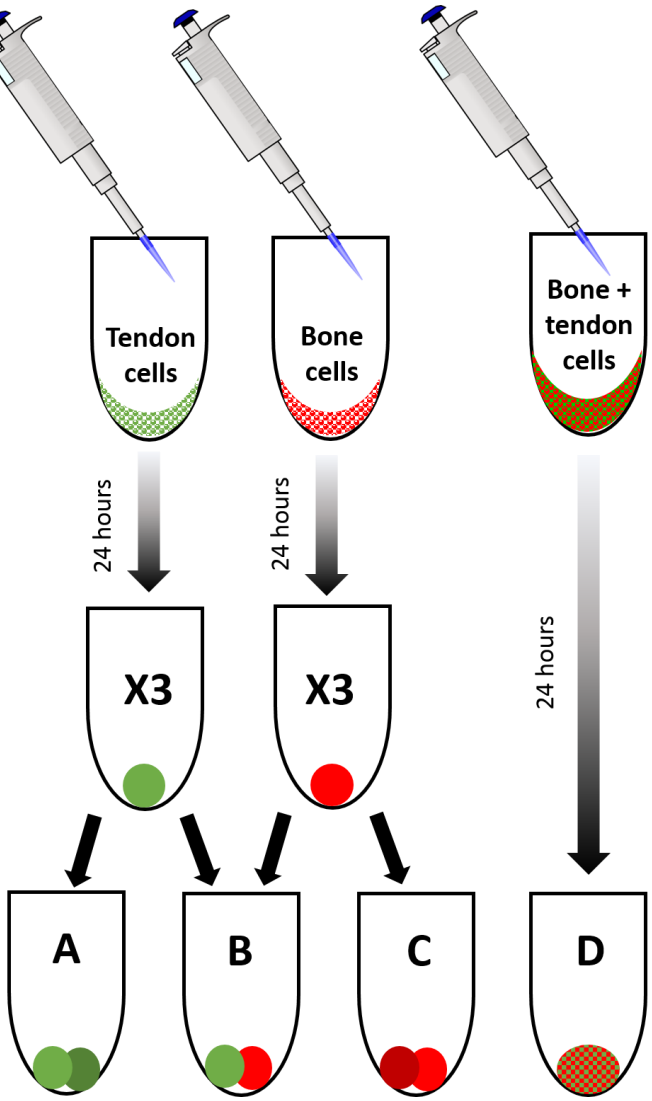

Figure 3.4: Scaffold-less co-culture system protocol. *Cells of bone and tendon were seeded separately on cell-repellent, U-bottomed 96-well plates. After one day of culture, A) two tendon-only, B) mini-coculture, C) two bone-only, and D) max-coculture spheroid groups were produced.*

3.4 Results

3.4.1 Cells Fluorescent labelling of cells

Visualisation of different cell populations was important to determine a successful co-culture. Therefore, two labelling techniques to introduce different fluorescent proteins into different cell populations was attempted: permanent and temporary labels.

3.4.1.1 Permanent fluorescent cell labelling (transfection) assessment

A permanent fluorescent label in the cells would facilitate long term observation of the co-culture system, including studies to assess cell proliferation and migration. Transfection of MC3T3 cells with an RFP was attempted using six protocols, including the manufacturer protocol for Lipofectamine® 2000 and 3000 transfection kits. Fluorescence from MC3T3 cells was not detected in any of the six transfection protocols after 1 week of culture (**Figure 3.5**). Compared to the positive control group, fluorescence was detected in CTF cells using the Lipofectamine® 2000 optimised by adding selecting AB after 24 hours, and the Lipofectamine® 3000 optimised by adding the selecting AB after 72 hours of culture (**Figure 3.6** B), indicating a successful transfection of CTF cells. Moreover, transfection of the RFP fluorescent label in DPF cells was successful when performed using Lipofectamine® 2000 optimised by adding selecting AB after 24 hours and 72 hours, Lipofectamine® 3000 original protocol, and Lipofectamine® 3000 optimised by adding selecting AB after 72 hours of culture (**Figure 3.7** B, C, D and F).

In contrast, the failure to detect fluorescence from MC3T3 cells indicated an unsuccessful transfection. Despite repeating the experiment two times with 6 different protocols, MC3T3 cells were not successfully transfected, while CTF and DPF cells were. This indicated that MC3T3s were not compatible with Lipofectamine® 2000 and 3000 transfection kits and couldn't be used to introduce RFP. The advantage of a permanent fluorescent cell label is for long term labelling. However, this experiment aimed to label the cells with an RFP to aid visualisation of the cells in the co-culture and assess the formation of a single 3D interface immediately after culture. Therefore, a permanent fluorescent label is not necessary if labelling could be achieved temporarily. Consequently, a temporary fluorescent labelling protocol was then investigated.

3.4.1.2 Temporary fluorescent cell labelling assessment

As a permanent fluorescent cell label was not successfully achieved, an alternative method needed to be established. Therefore, a temporary fluorescent label produced by CellTracker™ red was investigated and optimised for use with MC3T3 cells. Fluorescence was detected from MC3T3 cells in all concentrations of cell tracker (**Figure 3.8**). However, the duration of fluorescence was variable between different cell tracker concentrations (**Figure 3.8**).

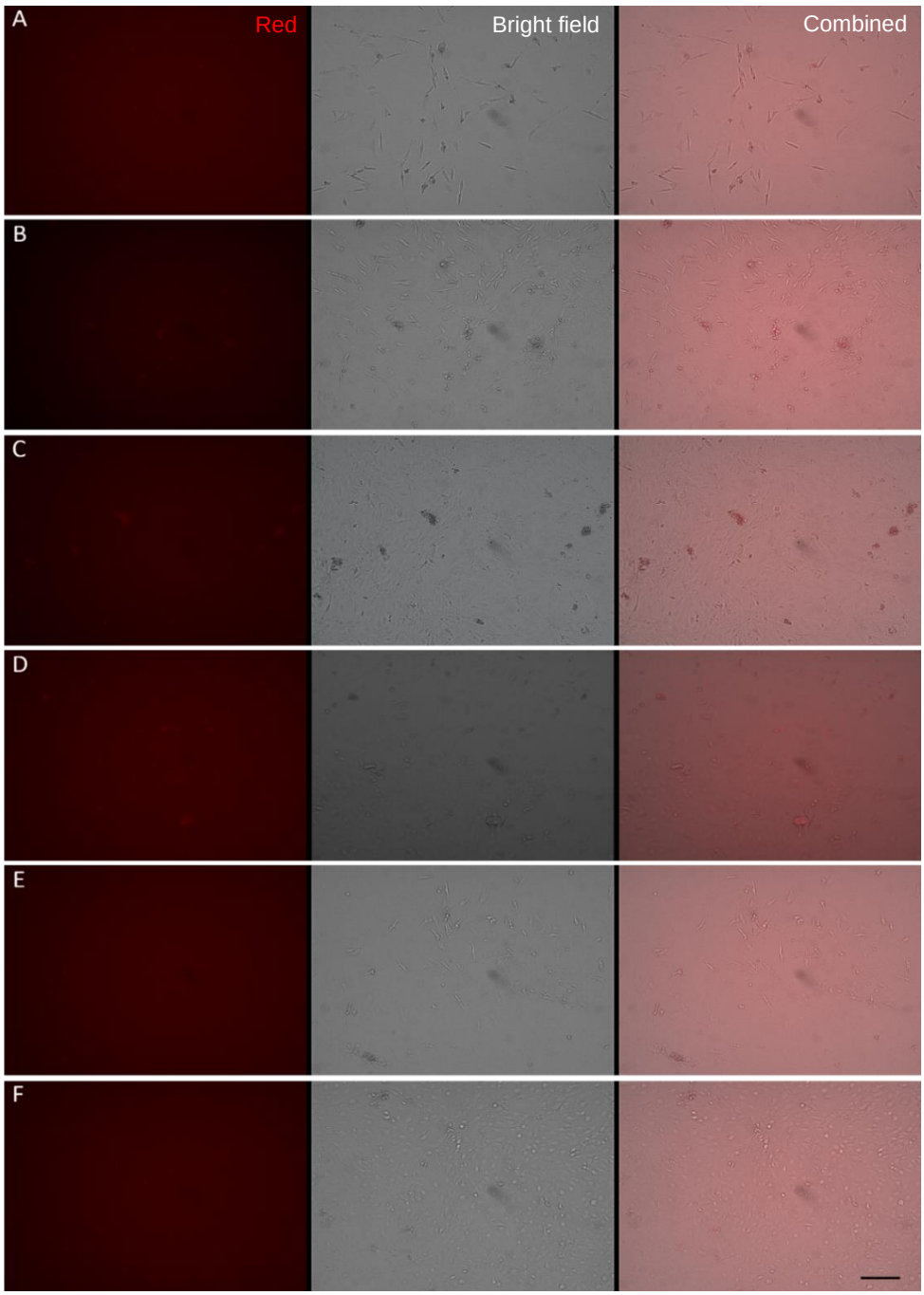

Figure 3.5: Transfection of MC3T3 cells was attempted using six transfection protocols. *A) Manufacturer protocol for Lipofectamine® 2000 transfection kit. B) An optimised Lipofectamine® 2000 protocol by adding selecting AB after 24 hours of transfection. C) Selecting AB was added 72 hours after transfection of cells with Lipofectamine® 2000. D) Manufacturer protocol for Lipofectamine® 3000 transfection kit. E) An optimised Lipofectamine® 3000 protocol by adding selecting AB after 24 hours of transfection. F) Selecting AB was added 72 hours after transfection of cells with Lipofectamine® 3000. All these protocols were used to transfect MC3T3 cells with an empty vector containing RFP label. An efficient transfection was not achieved in any protocol. Images were taken using the red channel, bright field, and the combined view of FM. Representative images were chosen from a library of images acquired during the experiment. (Scale bar = 200 µm)*

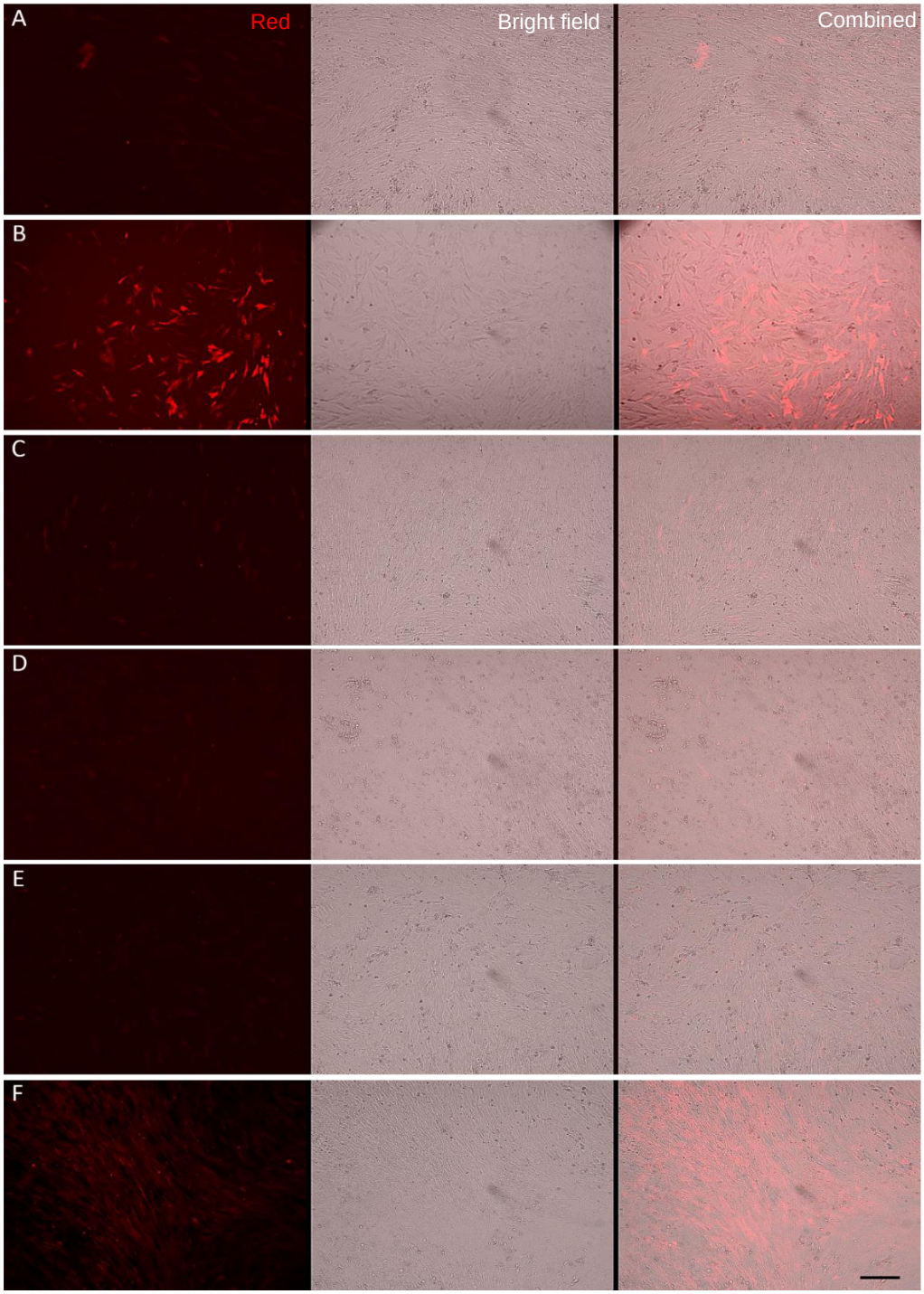

Figure 3.6: CTF cells were used as a positive control for transfection protocols. *A) Manufacturer protocol for Lipofectamine® 2000 transfection kit. B) An optimised Lipofectamine® 2000 protocol by adding selecting AB after 24 hours of transfection. C) Selecting AB was added 72 hours after transfection of cells with Lipofectamine® 2000. D) Manufacturer protocol for Lipofectamine® 3000 transfection kit. E) An optimised Lipofectamine® 3000 protocol by adding selecting AB after 24 hours of transfection. F) Selecting AB was added 72 hours after transfection of cells with Lipofectamine® 3000. All these protocols were used to transfect CTF cells with an empty vector containing RFP label. An efficient transfection was achieved using protocols B and F. Images were taken using the red channel, bright field, and the combined view of FM. Representative images were chosen from a library of images acquired during the experiment. (Scale bar = 200 µm)*

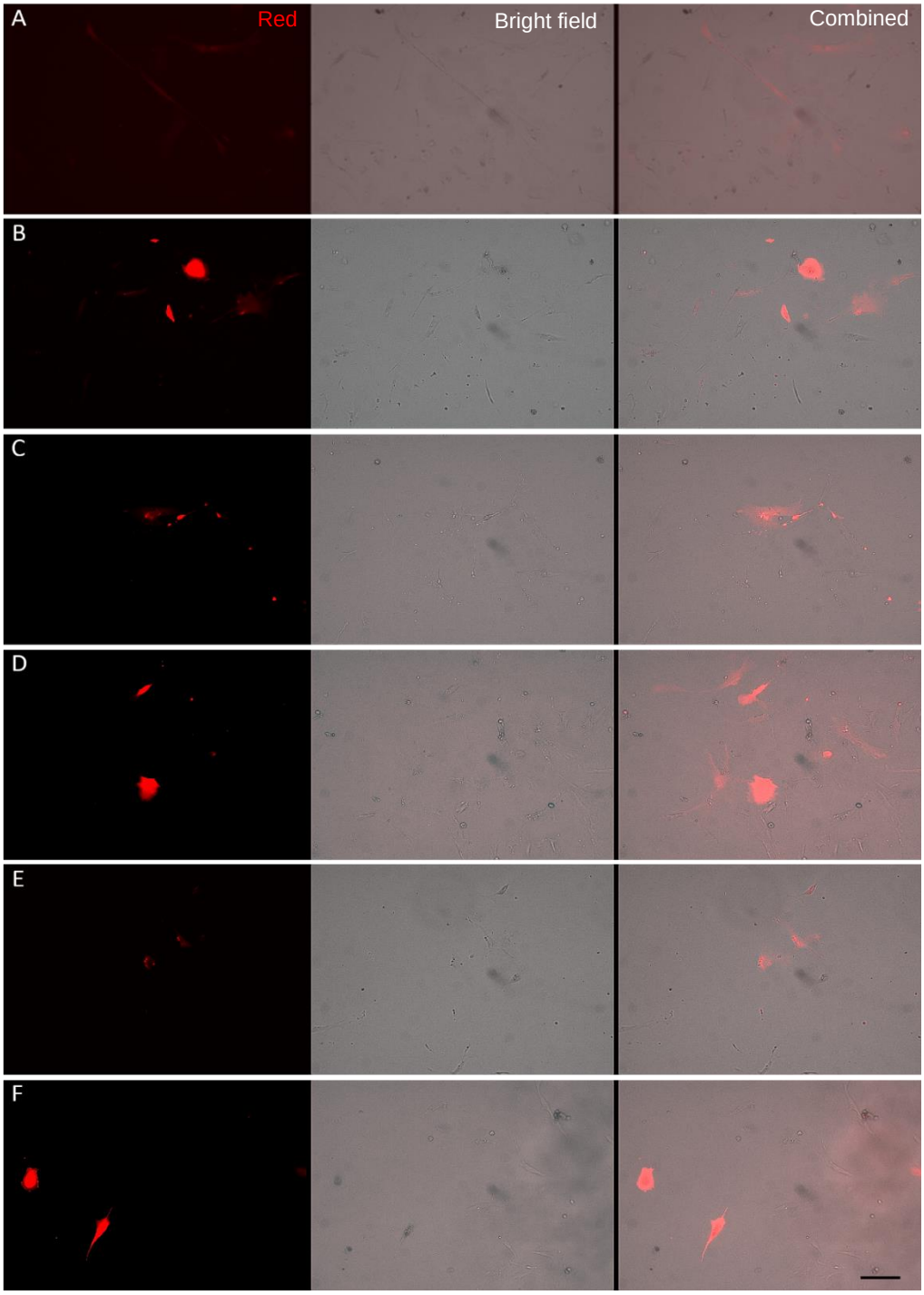

Figure 3.7: DPF cells were used as a positive control for transfection protocols. *A) Manufacturer protocol for Lipofectamine® 2000 transfection kit. B) An optimised Lipofectamine® 2000 protocol by adding selecting AB after 24 hours of transfection. C) Selecting AB was added 72 hours after transfection of cells with Lipofectamine® 2000. D) Manufacturer protocol for Lipofectamine® 3000 transfection kit. E) An optimised Lipofectamine® 3000 protocol by adding selecting AB after 24 hours of transfection. F) Selecting AB was added 72 hours after transfection of cells with Lipofectamine® 3000. All these protocols were used to transfect DPF cells with an empty vector containing RFP label. An efficient transfection was achieved using protocols B, C, D and F. Images were taken using the red channel, bright field, and the combined view of FM. Representative images were chosen from a library of images acquired during the experiment. (Scale bar = 200 µm)*

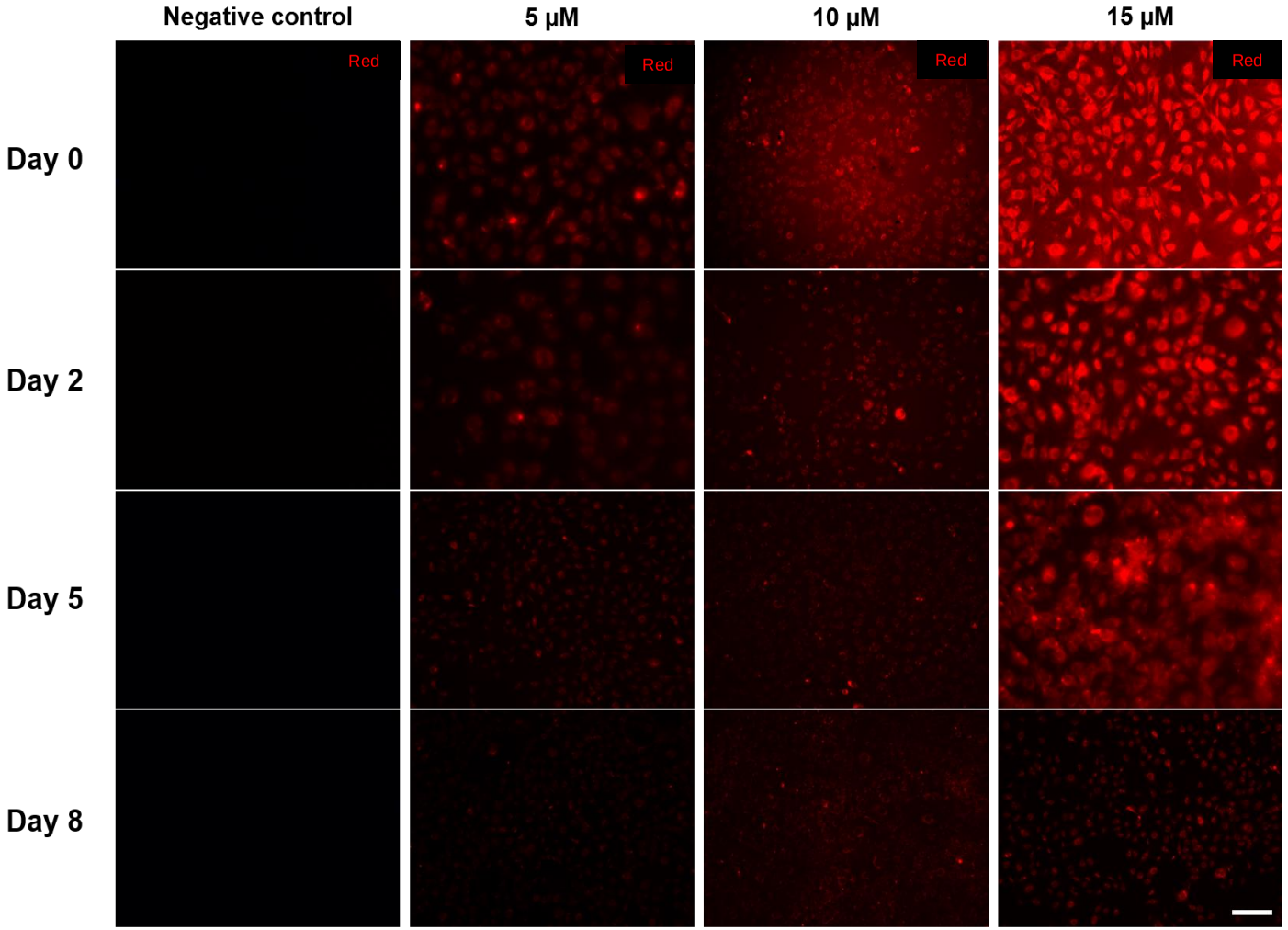

Figure 3.8: Fluorescent microscope images of the red channel showing decreased signal detection of cell tracker used to label MC3T3 cells cultured in T-25 cm² flasks over time. *The cells were treated with different concentrations of red cell tracker to assess duration of usability for the label. Images were taken using the red channel of CFM. Representative images were chosen from a library of images acquired during the experiment. (Scale bar = 200 µm)*

The general observation was that the higher the concentration of cell tracker, the longer the MC3T3 cells exhibited fluorescence (**Figure 3.8**). The time limit for fluorescence in MC3T3 cells was set to 5 days after labelling the cells with 15 µM of cell tracker. The temporary fluorescent cell labelling protocol provided the required fluorescent label to visualise and identify different MC3T3 cells in a 2D culture. However, MC3T3 cells were intended to be used in a cell-encapsulated hydrogel. Additionally, CFM had to be used to visualise the MC3T3 cell-encapsulated hydrogel, which required more laser power to excite the CellTracker™ red, which could result in bleaching of fluorescent proteins. Therefore, a comparison between a sample that has been imaged with CFM over 4 time points (days 0, 2, 5 and 8) was compared to a sample that was imaged at a single time point (day 8). This showed that CellTracker™ red fluorescent proteins were hard to visualise at day 8 (**Figure 3.9** D and **3.10** A) compared to the non-bleached sample at day 8 (**Figure 3.10** B). Accordingly, CellTracker™ red was used as a fluorescent label for MC3T3 cells to investigate the formation of a single 3D interface in the following sections. Nevertheless, the use of cell tracker as a cell marker was limited to 5 days.

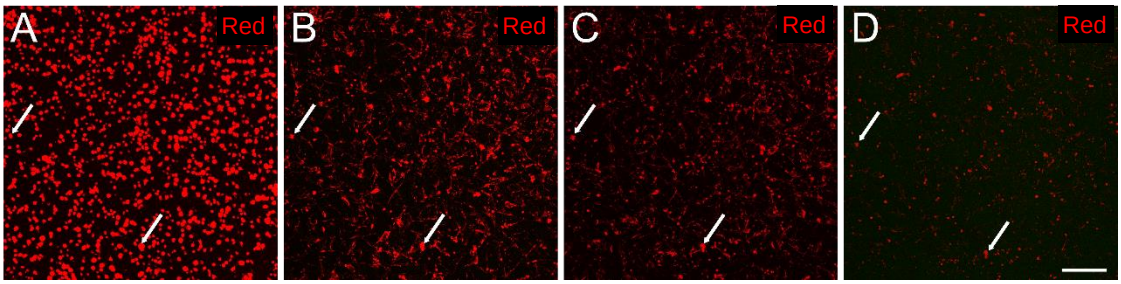

Figure 3.9: MC3T3 cells encapsulated in fibrin hydrogel and labelled with CellTracker red. A, B, C and D are days 0, 2, 5 and 8, respectively (N=3, n=3)*. Images were taken using the red channel of CFM. The imaging was performed at the same area of interest to monitor bleaching of the fluorescent label. Arrows point to landmarks of the same area of interest. Representative images were chosen from a library of images acquired during the experiment. (Scale bar = 200 µm)*

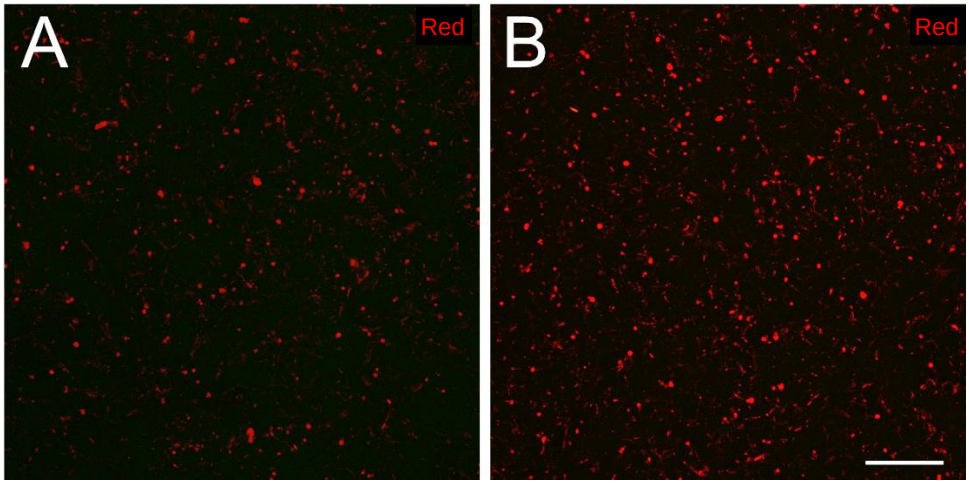

Figure 3.10: Comparison between A) Bleached CellTracker red fluorescent label of MC3T3 cells at day 8, and B) Unbleached sample of fluorescently labelled MC3T3 with CellTracker red. *The comparison showed a notable bleaching effect caused by five exposures to the CFM laser (N=3, n=3). Images were taken using the red channel of CFM. Representative images were chosen from a library of images acquired during the experiment. (Scale bar = 200 µm)*

3.4.2 Vertical interface of cell-encapsulated 3D co-culture system

The simplest method of acquiring a co-culture using hydrogel was to layer two cell encapsulated hydrogels in a well. The feasibility of this method was assessed by gross examination and CFM visualisation.

3.4.2.1 Gross assessment of interface formation

The use of agarose, gellan, fibrin and collagen hydrogels to create a vertical interface was evaluated. The hydrogels were vertically stacked in two layers to create an interface (**Figure 3.11**). However, it was not clear if the interface was formed because of the lack of contrast between the two layers of hydrogels. As a proof of concept, two layers of agarose and gellan hydrogels were coloured red and green to assess the formation of the interface grossly. An interface was successfully observed between the differently coloured agarose and gellan hydrogels **(Figure 3.12** A and B). Similarly, two layers of fibrin and collagen hydrogels were differentiated with pink and clear layers (**Figure 3.12** C and D). This was because the colours used for staining agarose and gellan interfered with the setting process of fibrin and collagen. Hence, formation of a successful interface was grossly observed using fibrin and collagen hydrogels (**Figure 3.12** C and D). Notably, surface tension between the well wall and the liquid form of the different hydrogels before setting caused the interface shape to be concave instead of flat.

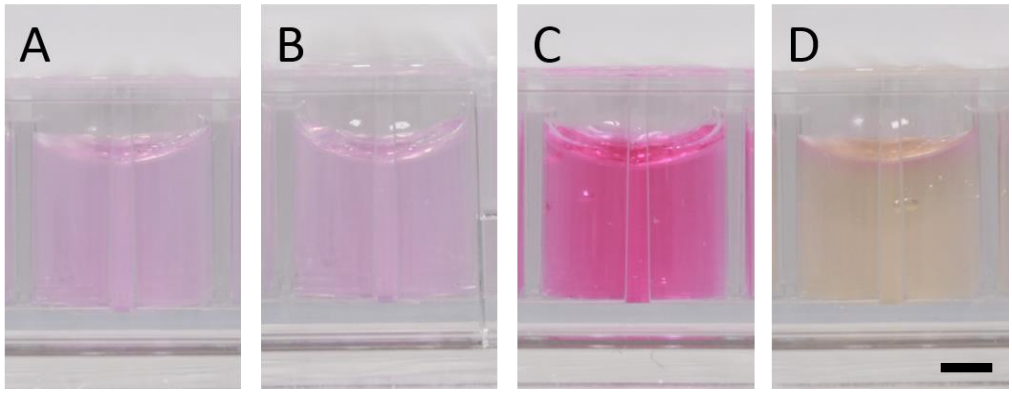

Figure 3.11: Side-view of CTF and MC3T3 cell-encapsulated and stacked layers of A) agarose, B) gellan, C) fibrin, and D) collagen hydrogels. *The interface was not visible due to the lack of colour contrast between the two stacked layers of hydrogels. (Scale bar = 2 mm)*

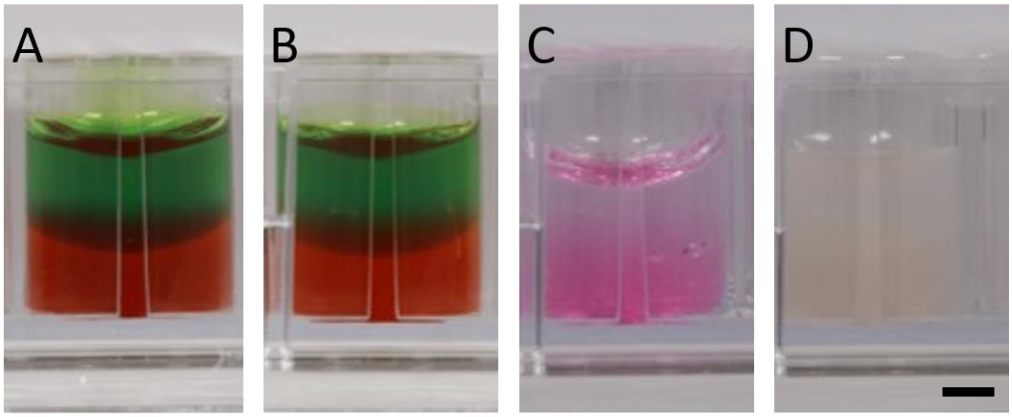

Figure 3.12: Side-view of coloured and stacked layers of A) agarose, B) gellan, C) fibrin, and D) collagen hydrogels*. Gross observation of interface formation when two layers of hydrogel were stacked. Notably, surface tension between the well wall and the liquid form of the hydrogel before setting caused the interface shape to be concave instead of flat. (Scale bar = 2 mm)*

3.4.2.2 CFM assessment of single interface formation and co-culture structure integrity

The interface formed between two stacked layers of distinct cell-encapsulated populations in agarose, gellan, fibrin and collagen hydrogels was assessed (**Figure 3.13**). A single interface was observed between CTF-GFP and MC3T3 cells when encapsulated in agarose and gellan (**Figure 3.13** A and B). However, when the CTF-GFP and MC3T3 cells were encapsulated in fibrin and collagen hydrogels, the interface formed extended between the wall of the well and the bottom layer of the hydrogel, due to a leak from the top layer of the cell-encapsulated hydrogel (**Figure 3.13** C and D).

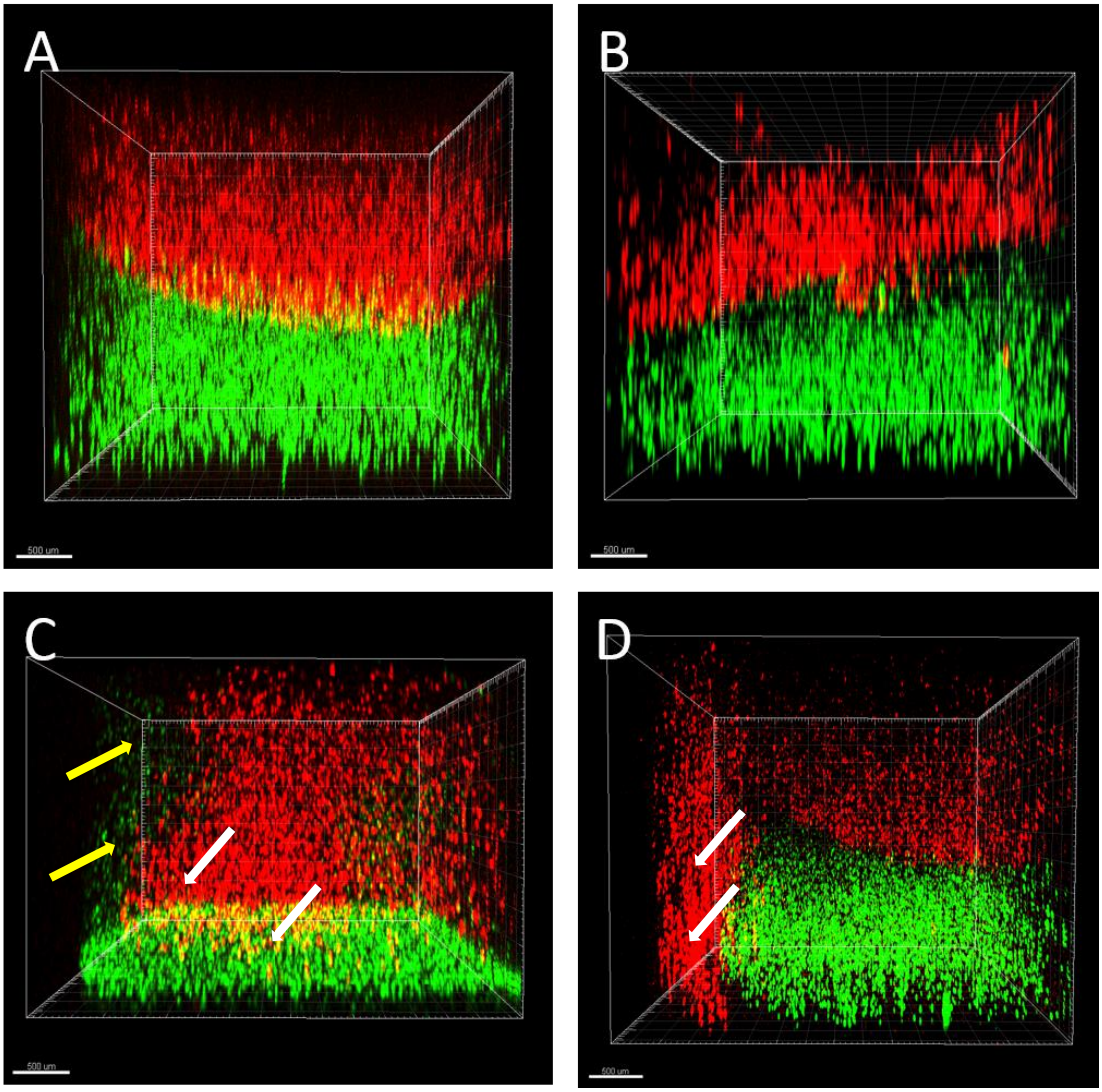

Figure 3.13: 3D digital models rendered from CFM datasets were used to observe the formed vertical interface between MC3T3 (red) and CTF (green) cells (N=3, n=3). *Agarose, gellan, fibrin and collagen hydrogels were used to encapsulate MC3T3 and CTF cells in A, B, C and D, respectively. Surface tension affected the shape of hydrogels. More importantly, fibrin and collagen hydrogels showed signs of leakage as MC3T3 (red) cells were observed occupying parts of the bottom half of the vertical co-culture system (white arrows). Furthermore, tendon cells were displaced from bottom layer to top layer (yellow arrows). Representative images were chosen from a library of images acquired during the experiment. (Scale bar = 500 µm)*

Notably, the interface formed between the two stacked layers of hydrogels was observed as concave and not a flat interface (**Figure 3.13** A and D). This was the result of the surface tension between the wall of the well and the liquid hydrogel before it set. This was observed in all hydrogel types. Additionally, fibrin and collagen hydrogels showed leakage from the top layer of the stacked hydrogel between the wall of the well and the bottom layer of the hydrogel. This increased the interface surface area considerably for fibrin and collagen hydrogels, making them

incomparable to agarose and gellan. Another consideration was the exposure to nutrients and media. As the cells encapsulated in the top layer of the stacked hydrogel had direct access to media and nutrients, the cells encapsulated in the bottom layer were reliant on media and nutrient diffusion through the top layer to the bottom layer. Therefore, a horizontal interface of 3D co-culture system was attempted.

3.4.3 Horizontal interface of 3D cell-encapsulated co-culture system

3.4.3.1 Original scaffold-dependent co-culture system

Bone and tendon cells were labelled with red and green fluorescent labels, respectively. They were then cultured in the original co-culture system (**figure 3.1**). After one day of culture, the area that connects the two cell-encapsulated hydrogels was imaged using CFM to confirm that the two cell-encapsulated hydrogels had an interface between them. The separation indicated that an artificial interface had been established between the two cell-encapsulated hydrogels. An artificial interface in agarose, gellan, fibrin and collagen hydrogels was created (**Figure 3.14** A, B, C and D, respectively). Importantly, a noticeable difference in cell morphology was observed in cells cultured in different hydrogels. Cells encapsulated in gellan and agarose exhibited a spherical morphology (**Figure 3.14** A and B). In contrast, when encapsulated in fibrin and collagen, CTF cells showed elongated morphology and MC3T3 cells showed a polygonal structure (**Figure 3.14** C and D).

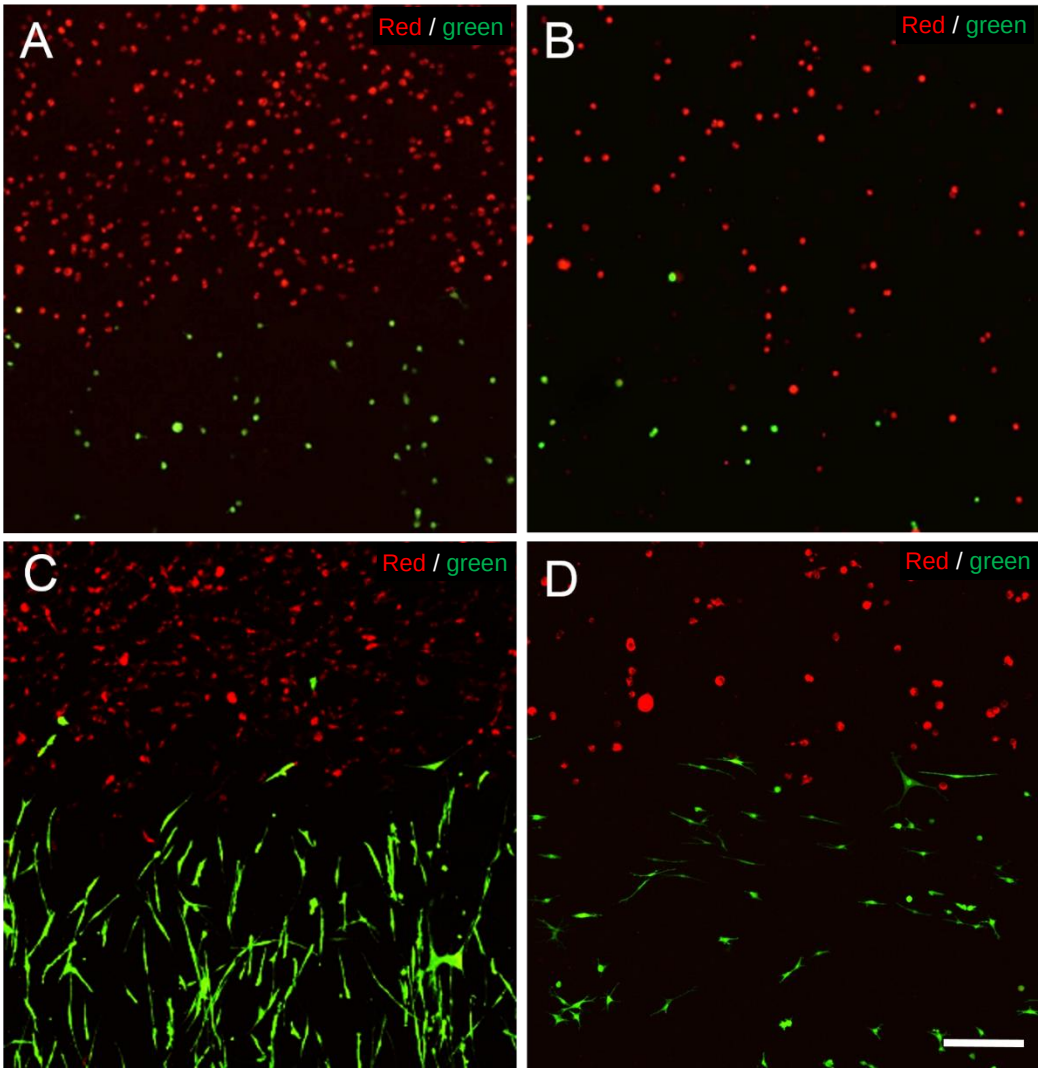

Figure 3.14: CFM dataset, processed using ImageJ to stack a Z-axis projection of the total signal in the dataset. *Green-labelled cells were CTFs, whereas red-labelled cells were MC3T3s that were encapsulated in A) agarose, B) gellan, C) fibrin, and D) collagen hydrogels. The CTF and MC3T3 cells occupied opposite sides of the field and are in direct physical contact. Images were taken using combined red and green channels of CFM. Representative images were chosen from a library of images acquired during the experiment. (Scale bar = 200 µm)*

3.4.3.2 Revised scaffold-dependent co-culture system

The original scaffold-dependent co-culture system had several advantages and limitations. The most important limitation was the leakage around the 3D printed block when the first cell-encapsulated hydrogel was cast in the co-culture system (**Figure 3.2**). A revision of the scaffold-dependent co-culture system was conducted using a different material to achieve the same result of co-culturing two cell-encapsulated hydrogels in the system. As a result, a revised co-culture system was developed that was achieved by creating half-well plugs of Kemsil silicone that can be used to block one side of a 24-well plate.

3.4.3.2.1 Gross assessment of co-culture formation

The suitability of the revised system for creating a single horizontal interface by encapsulating CTF and MC3T3 cells in agarose, gellan, fibrin and collagen hydrogels (**Figure 3.15**) was evaluated. However, to grossly assess the formed interface, the hydrogels needed to be coloured. Two volumes of agarose were separately coloured red and green, and they were then used in the system as described in **section 3.3.2.2.2**. A single horizontal interface was observed between them (**Figure 3.16** A). Similarly, the gellan hydrogel was assessed, and a horizontal interface was observed (**Figure 3.16** B).

In contrast, fibrin and collagen hydrogels were coloured pink and clear and an interface was observed between these two differently coloured hydrogels (**Figure 3.16** C and D). An improved seal, preventing leakage of solution, was observed in the revised scaffold-dependent co-culture system compared to the original scaffold-dependent co-culture system. Moreover, preparation before the experiment was reduced from one week in the original design to 2 hours in the improved design. Furthermore, the improved design could be scaled more easily compared to the 3D-printer-dependent original design. A comparison of advantages and limitations for the original and revised scaffold-dependent co-culture systems are listed in (**Table 3.1**).

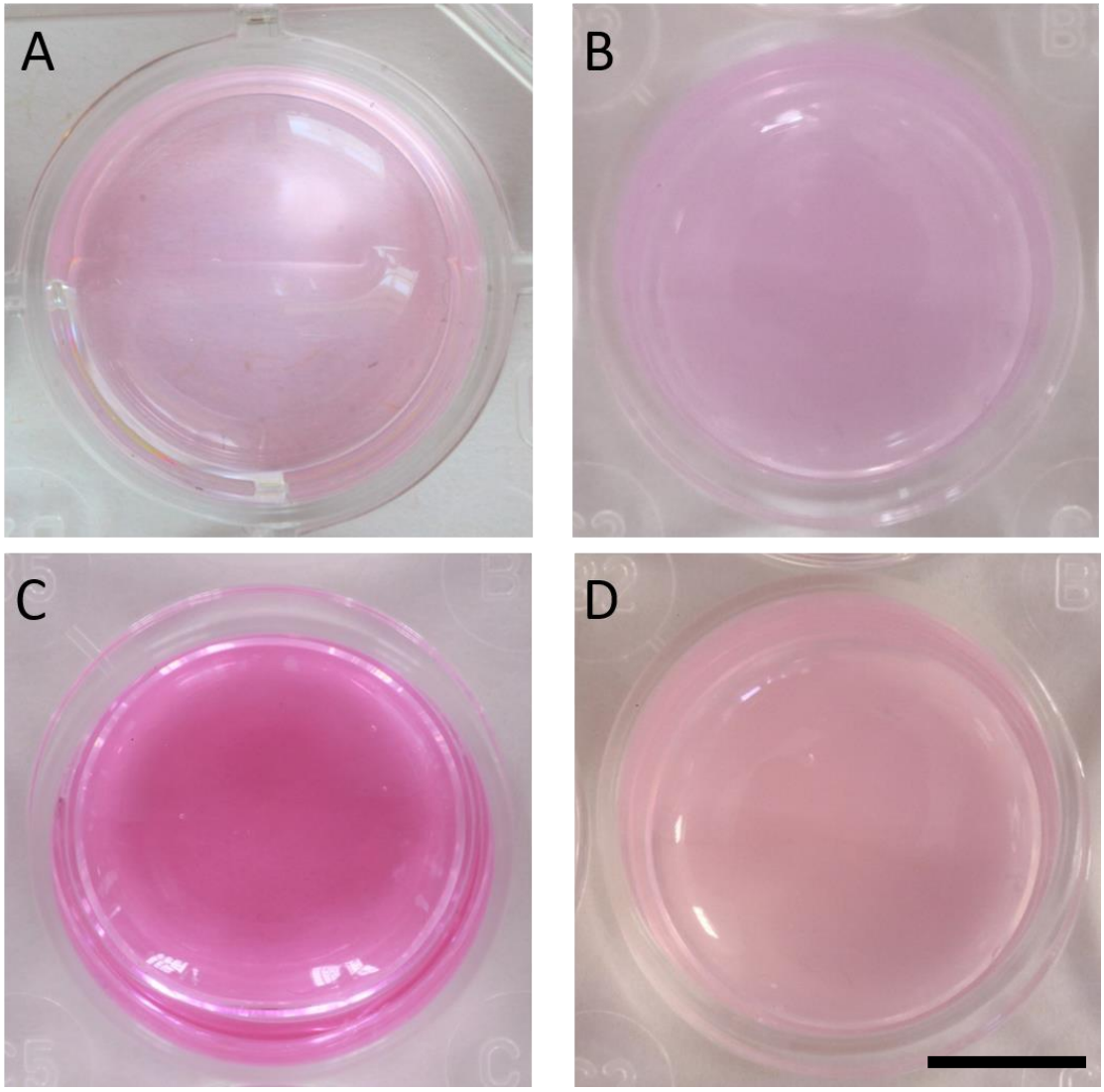

Figure 3.15: Gross appearance of the horizontal co-culture system cell-encapsulated hydrogels*. MC3T3 and CTF cells were encapsulated in A) agarose, B) gellan, C) fibrin and D) collagen hydrogels. (Scale bar = 5 mm)*

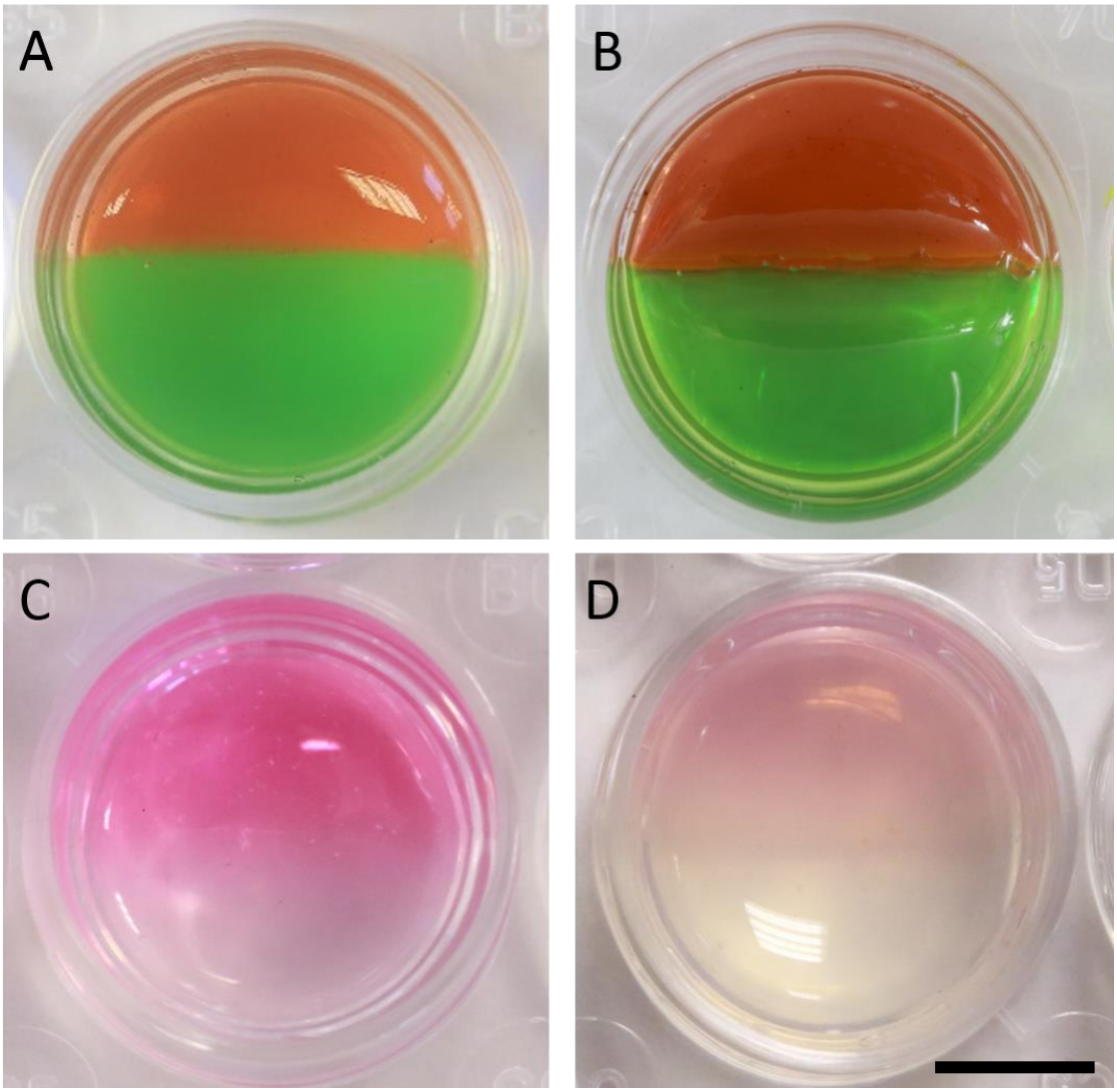

Figure 3.16: Gross assessment of the interface formed by using the horizontal co-culture system. *A) Agarose and B) gellan hydrogels were coloured with red and green food colours, whereas C) fibrin and D) collagen hydrogels were coloured with DMEM (pink) and PBS (clear). (Scale bar = 5 mm)*

Table 3.1: Comparing the original co-culture system design to the revised co-culture system*. Advantages and limitations of each method are listed for relevant specifications.*

Specifications	**Observations**	
Type of culture	**Original co-culture system**	**Revised co-culture system**
Ease of use	Labour intensive preparation and use of the system for co-culture	Easier system preparation and use
Cost	Expensive materials such as Sylgard silicone (£ 200/kg) and 3D printing of blocks	Cheap materials, only Kemsil silicone needed (£ 29.22/kg)
Sterilisation	Both 3D printed blocks and plates needed sterilisation with 70% alcohol; more risk of infection	Only the half-well plugs needed sterilisation with 70% alcohol; less risk of infection
Water seal	Poor sealing caused cell-encapsulated hydrogel to leak into the other side of the system	Better sealing achieved
Cell type identification	Easy, depending on the different sides' shape	Required careful documentation and/or systematic setup
Scalability	Expensive, and required cooperation with the art school	Could be done easily in the lab

3.4.3.2.2 CFM assessment of single interface formation between two distinct cell-encapsulated hydrogel co-cultures

An experiment was conducted to test the formation of a 3D single interface between encapsulated hydrogels with different cell types. The observation was conducted for 3 days to further monitor the behaviour of different cells in the cell-encapsulated hydrogels at the 3D single interface region. In agarose, a 3D single interface formed between CTF and MC3T3 cell-encapsulated hydrogels (**Figure 3.17** A). Cell

morphology in agarose remained spherical throughout the duration of the experiment, without showing any sign of cell attachment to agarose nor cell proliferation (**Figure 3.17** A). In gellan, the 3D single interface was successfully established (**Figure 3.17** B). Like agarose, cells encapsulated in gellan did not show signs of attachment to the hydrogel throughout the experiment. (**Figure 3.17** B). CTF cells qualitatively showed an increase in cell crowdedness over time when encapsulated in fibrin and collagen hydrogels, indicating the suitability of these hydrogels for cell proliferation (**Figure 3.17** C and D). These results suggested a preference to use the fibrin and collagen hydrogels for further experimentation to determine their usability as scaffolds for a tissue interface model.

The scaffold-dependent co-culture system required the cell-encapsulated hydrogel to have a firm consistency to hold its form when the half-well plug was removed from the system (**3.3** C and D). This was a crucial step in forming a perpendicular 3D single interface between the two cell-encapsulated hydrogels. If the stiffness of the cell-encapsulated hydrogel was not appropriate to the system, a random oblique interface formed. To assess structural integrity, the hydrogels' interface side-profile plane was investigated to determine the interface angle. Agarose, gellan and fibrin produced an acceptably semi-perpendicular 3D interface (**Figure 3.18** A, B and C). However, collagen co-culture demonstrated an oblique interface that could not be reproduced consistently and was not suitable for accurate imaging using CFM (**Figure 3.18** D). The CFM required a perpendicular projection of lasers on samples to investigate the interface formed between the two cell-encapsulated hydrogels. Consequently, imaging of an oblique interface could show false results of mixed cells at the interface. Due to this limitation, collagen was excluded from further investigations using the scaffold-dependent co-culture system.
Another important consideration was that the plates used were tissue-culture treated plates, i.e. they promote cell attachment and proliferation on the plastic surface of the well It was therefore not clear whether the cell crowding of CTF and MC3T3 cells were inside the fibrin hydrogel or on the plastic surface of the well. Consequently, non-tissue culture treated plates were used to repeat the same experiment as before with the tissue-culture treated plates (**Figure 3.19**). The cell-encapsulated agarose hydrogel showed the same spherical morphology of both CTF and MC3T3 cells, but the number of fluorescently detected cells decreased as the experiment progressed, suggesting either bleaching of fluorescent proteins or decrease in cell number (**Figure**

3.19 A). A similar result was also observed in cells encapsulated in gellan (**Figure 3.19** B).

Conversely, cells encapsulated in fibrin showed a qualitative increase in cell crowdedness that can be attributed to the proliferation of cells, which is the same result observed in the previous experiment using the tissue-culture treated 24-well plates. However, examining the z-axis projection of fluorescent proteins in the CTF and MC3T3 cells showed a similar appearance and no clear evidence of whether cell growth was inside the encapsulated hydrogel or on the plastic surface of the well plate (**Figure 3.20**). Therefore, to prove cell crowding happened in the cell-encapsulated hydrogel rather than on the plastic surface, a side plane view of the interface was examined in the samples produced using the tissue-culture treated plates, compared to samples produced using the non-tissue-culture treated plates (**Figure 3.21**). This experiment showed that the location of the CTF and MC3T3 cells encapsulated in the fibrin hydrogel were mostly present on the plastic surface by day 4 of the experiment, despite their presence in the hydrogel during day 0 and 1 of the experiment with the tissue-culture treated plates (**Figure 3.21** A). On the other hand, when using the non-tissue culture treated plates, CTF and MC3T3 cells maintained their presence in the hydrogel throughout the experiment with heavier crowding in the lower half of the encapsulated hydrogel. This could have been due to the effect of gravity (**Figure 3.21** B). Nonetheless, the cells maintained their presence in the encapsulated hydrogel, and the crowding observed could be attributed to proliferation inside the encapsulated hydrogel, and not on the plastic surface of the well plate. Consequently, non-tissue culture treated 24-well plates were used for all future investigations of the effect of co-culture on different cell types' viability, extracellular matrix formation and content (see **chapter 4**).

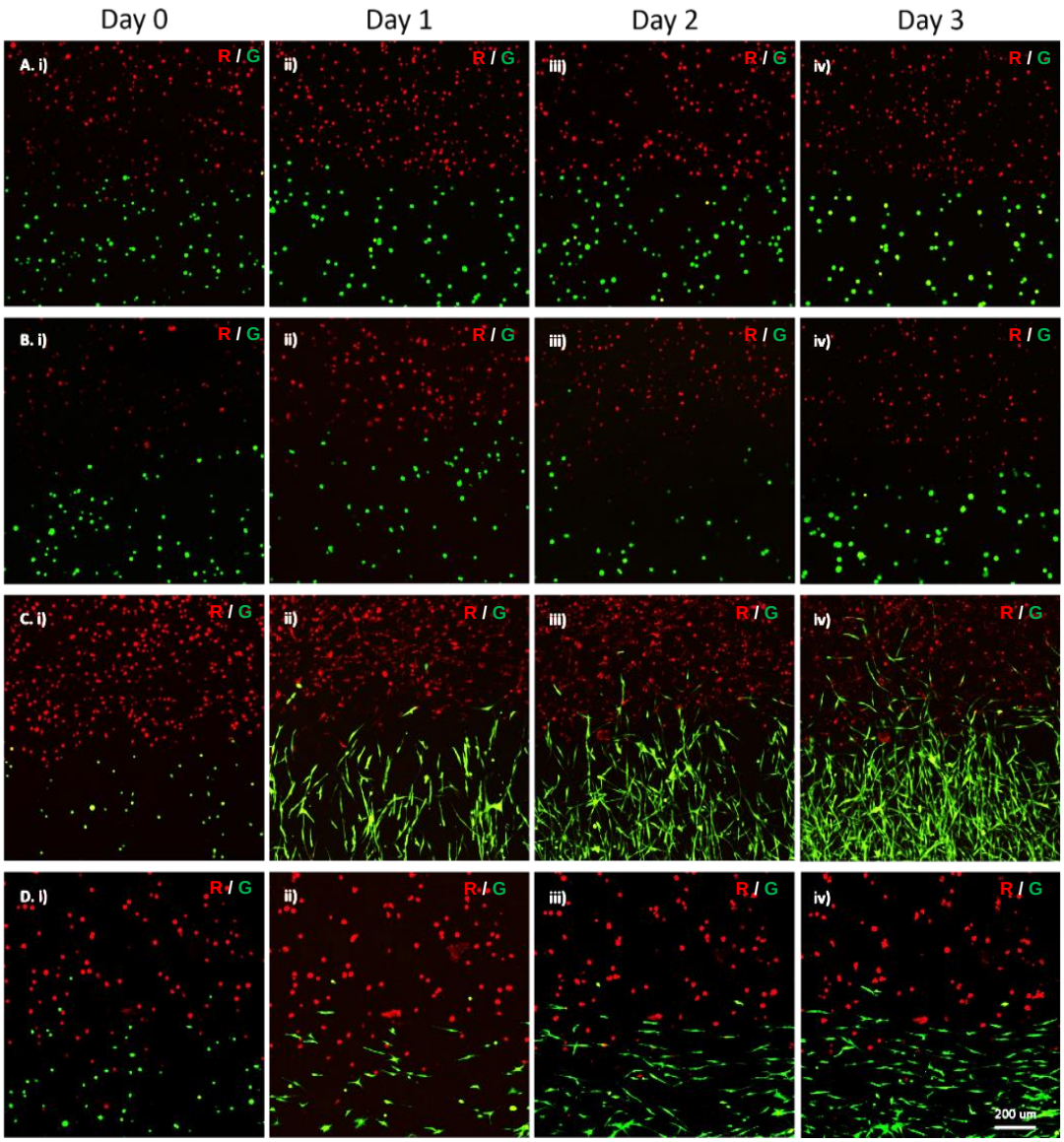

Figure 3.17: Short-term observation experiment to assess cell morphology in different hydrogels using CFM (N=3, n=4). *A noticeable difference in cell morphology could be observed when comparing cells in A) agarose and B) gellan to cells in C) fibrin and D) collagen. In A) and B) the cells exhibited a spherical morphology. Whereas in C) and D), the cells exhibited morphological changes relevant to their cell type. It was notable that CTF cells encapsulated in fibrin (C. iv) showed migratory action by invading the MC3T3 side of the co-culture after three days. In this experiment, tissue-culture treated 24-well plates were used. Images were taken using combined red (R) and green (G) channels of CFM. Representative images were chosen from a library of images acquired during the experiment. (Scale bar = 200 µm)*

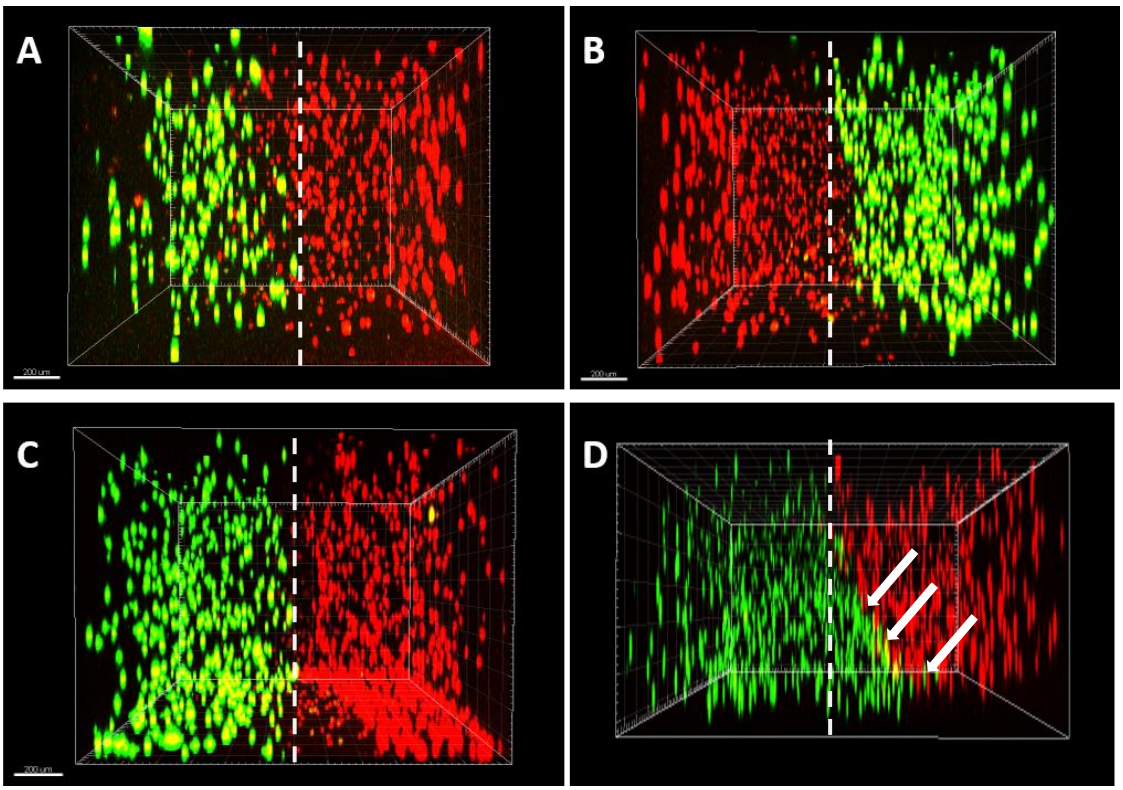

Figure 3.18: 3D digital models of the interface rendered from the CFM datasets were used to assess the interface plane by examining the side profile of the model. *Agarose, gellan and fibrin showed an acceptably perpendicular interface, whereas collagen showed an angled interface (white arrows). Representative images were chosen from a library of images acquired during the experiment (N=3, n=4). (Scale bar = 200 µm)*

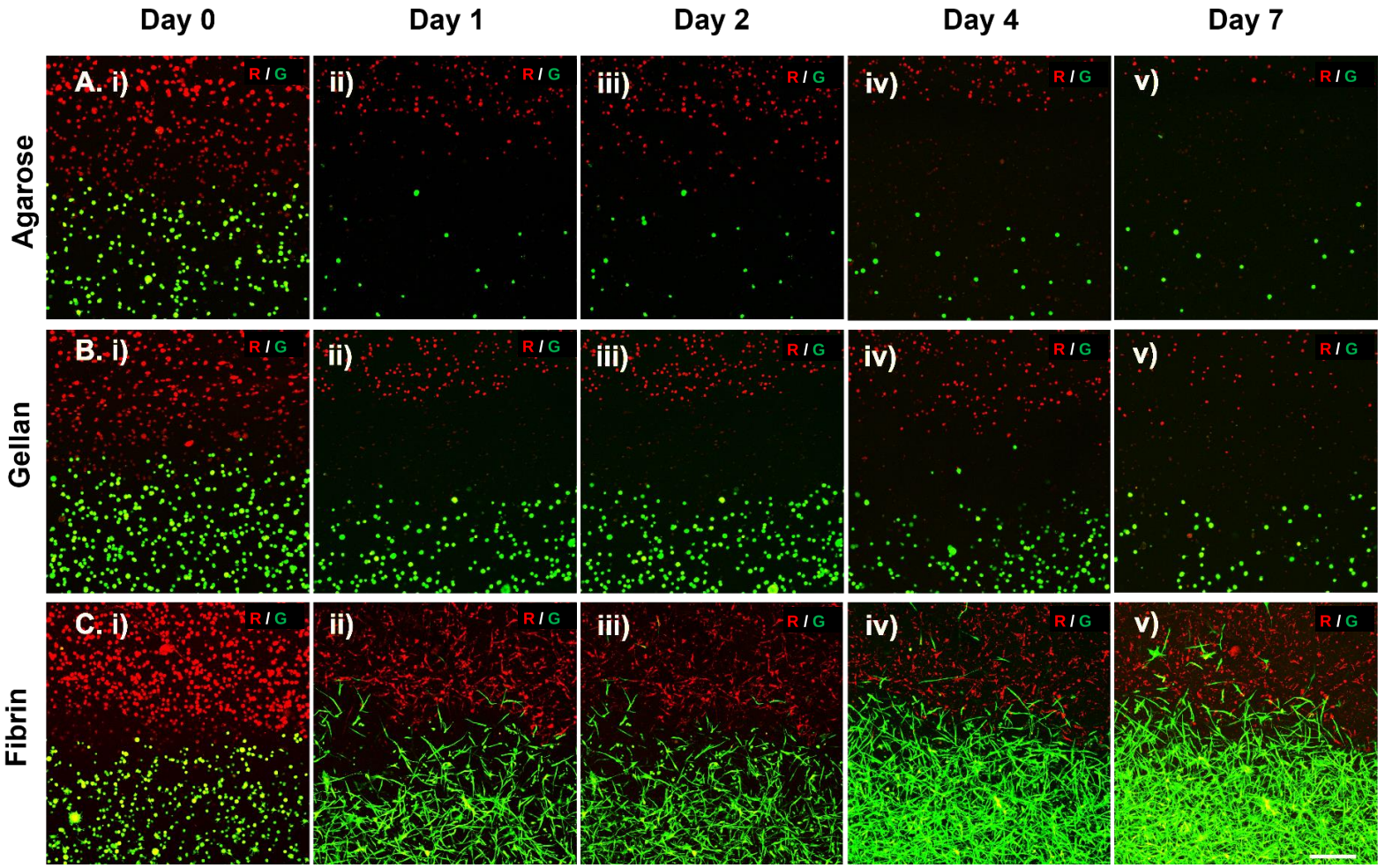

Figure 3.19: Short-term observation experiment repetition in non-tissue culture treated plates. *The same results were observed in terms of cell crowdedness and migratory action in fibrin. Representative images were chosen from a library of images acquired during the experiment (N=3, n=4). Images were taken using combined red (R) and green (G) channels of CFM. (Scale bar = 200 µm)*

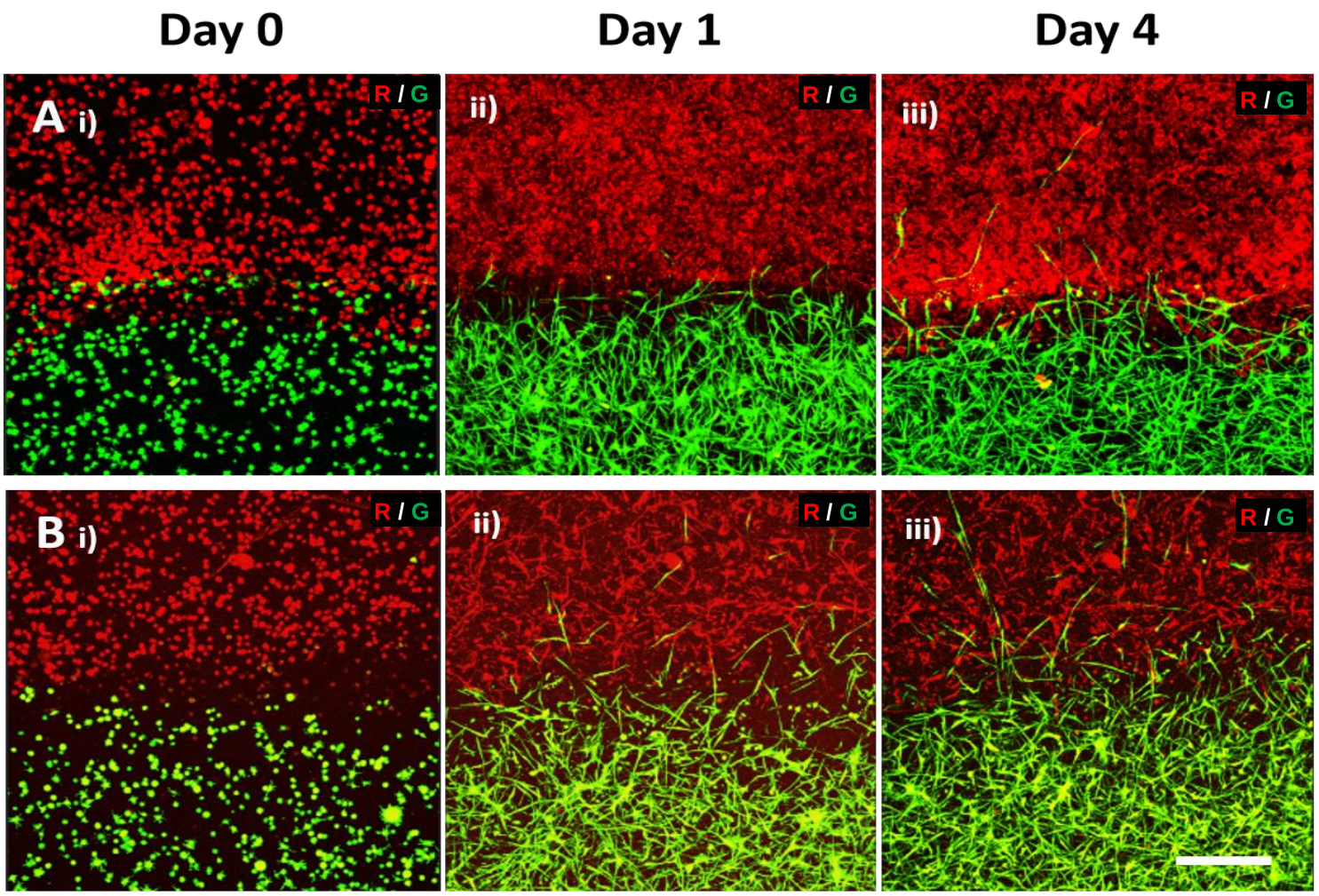

Figure 3.20: The interface between two cell-encapsulated hydrogels was compared between A) tissue-culture treated 24-well plates and B) non-tissue-culture treated 24-well plates. *The interface formed using the two plate types appears similar using the z-axis projection view. Images were taken using combined red (R) and green (G) channels of CFM. (Scale bar = 200 µm)*

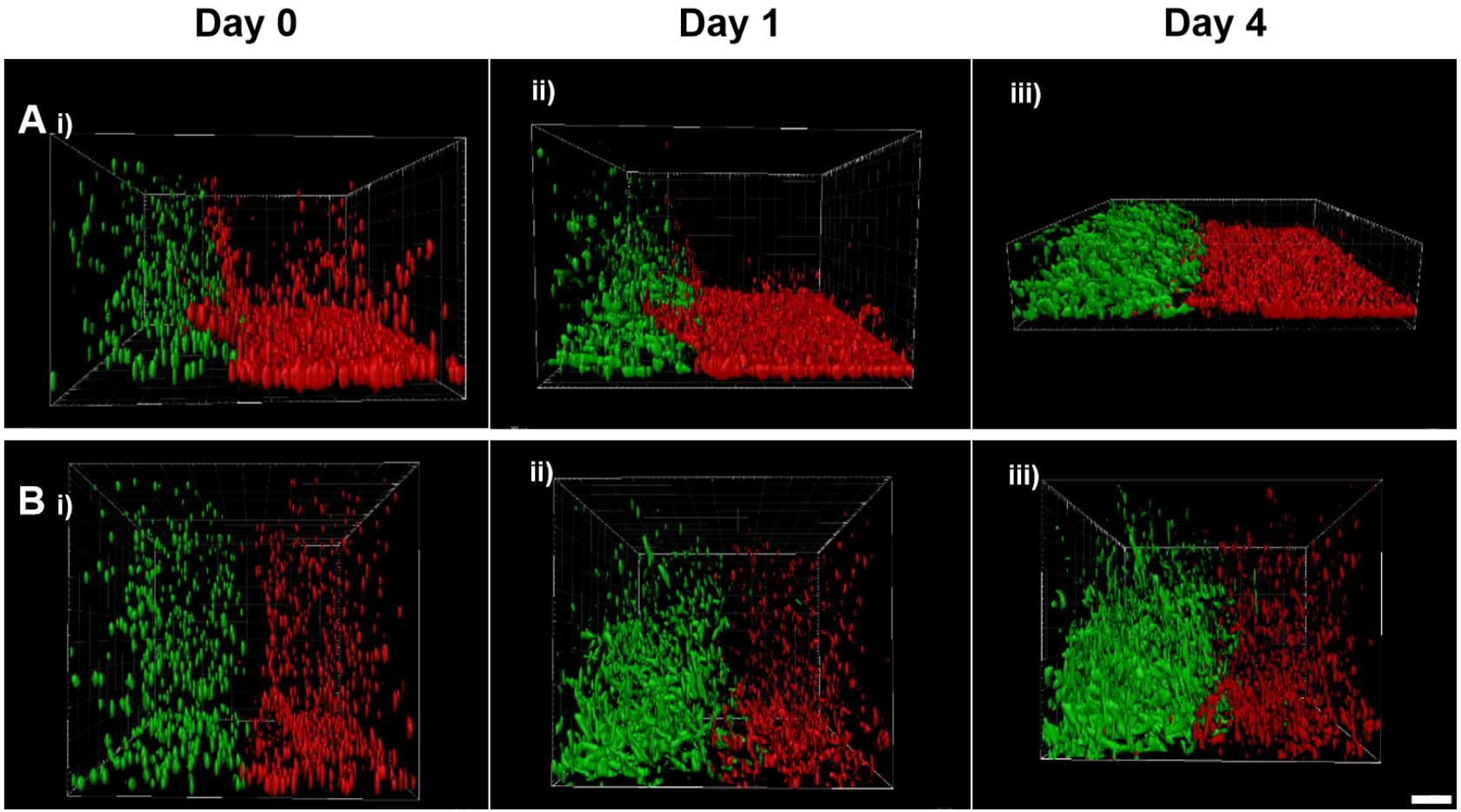

Figure 3.21: Comparison of side-plane projection view of the interface between two cell-encapsulated fibrin hydrogels. *A) Interface made using tissue-culture treated 24-well plates, showing presence of cells inside the fibrin hydrogel at day 0 followed by detection of cells at the plastic surface of the 24-well plate at day 4. This suggested that the cell crowding observed was due to proliferation on the plastic surface. B) Interface made using non-tissue-treated 24-well plates, showing presence of CTF and MC3T3 cells inside the fibrin hydrogel throughout the experiment with an increase in cell crowding (Scale bar = 200 µm)*

3.4.4 Scaffold-less 3D co-culture system

Scaffolds presented challenges during trials in retrieving cells from the scaffold-dependent co-culture system. Retrieving cells from the scaffolds was essential to quantify proliferation (**sections 4.4.1.4.2** and **4.4.3**). Moreover, the scaffold-dependent co-culture system allowed only a small percentage of tendon and bone cells to have physical contact with the other cell population. Therefore, a system that provided more cell-cell contact was pursued. The scaffold-less 3D co-culture system was achieved by producing tendon and bone spheroids (**Figure 3.22** A and B) after one day of culture in a U-bottomed, cell-repellent 96-well plate (Greiner bio-one, UK).

After the formation of tendon and bone spheroids, they were transferred to a single well for a minimum cell-cell contact co-culture (**Figure 3.22** C). For maximum cell-cell contact, a homogenised mixture of tendon and bone cells was used to produce a single spheroid of co-cultured bone and tendon cells (**Figure 3.22** D). This system allowed for faster investigations and minimised the number of cells needed for each experiment, compared to the scaffold-dependent 3D co-culture. A proof-of-concept study to assess the use of spheroid culture for interface formation between tendon and bone cells was performed. The study involved co-localisation of tendon and bone cells within a co-culture and measurement of the CSA of different groups of spheroids in order to assess the effect of co-culture.

3.4.4.1 Co-localisation of cells in mono- and co-culture of spheroids

Intra-spheroid cell organisation of CTF-GFP and MC3T3 cells in monoculture, mini-coculture and max-coculture was observed after 1, 2, 4 and 6 days of culture. The aim of this experiment was to observe cell migration and self-organisation in a co-culture compared to monoculture.

3.4.4.1.1 Tendon-only spheroid co-localisation

Two tendon-only spheroids and two bone-only spheroids were also monitored as a reference for the interaction of the same type of cells. Two tendon-only spheroids were placed together after one day of culture of spheroid formation (**Figure 3.23**). The two spheroids merged into an oval-shaped spheroid at day 2 (**Figure 3.23**). At day 4, the two spheroids had merged completely and formed a single spheroid, which was a relatively similar size to a tendon spheroid at day 1 (**Figure 3.23**). Despite the two spheroids being cultured for 4 days, there was no evidence of an increase in spheroid size. Finally, at day 6, there was no significant change in the spheroid size, indicating

either contraction of cells in the spheroid, decreased cell density or decreased ECM formation (**Figure 3.23**).

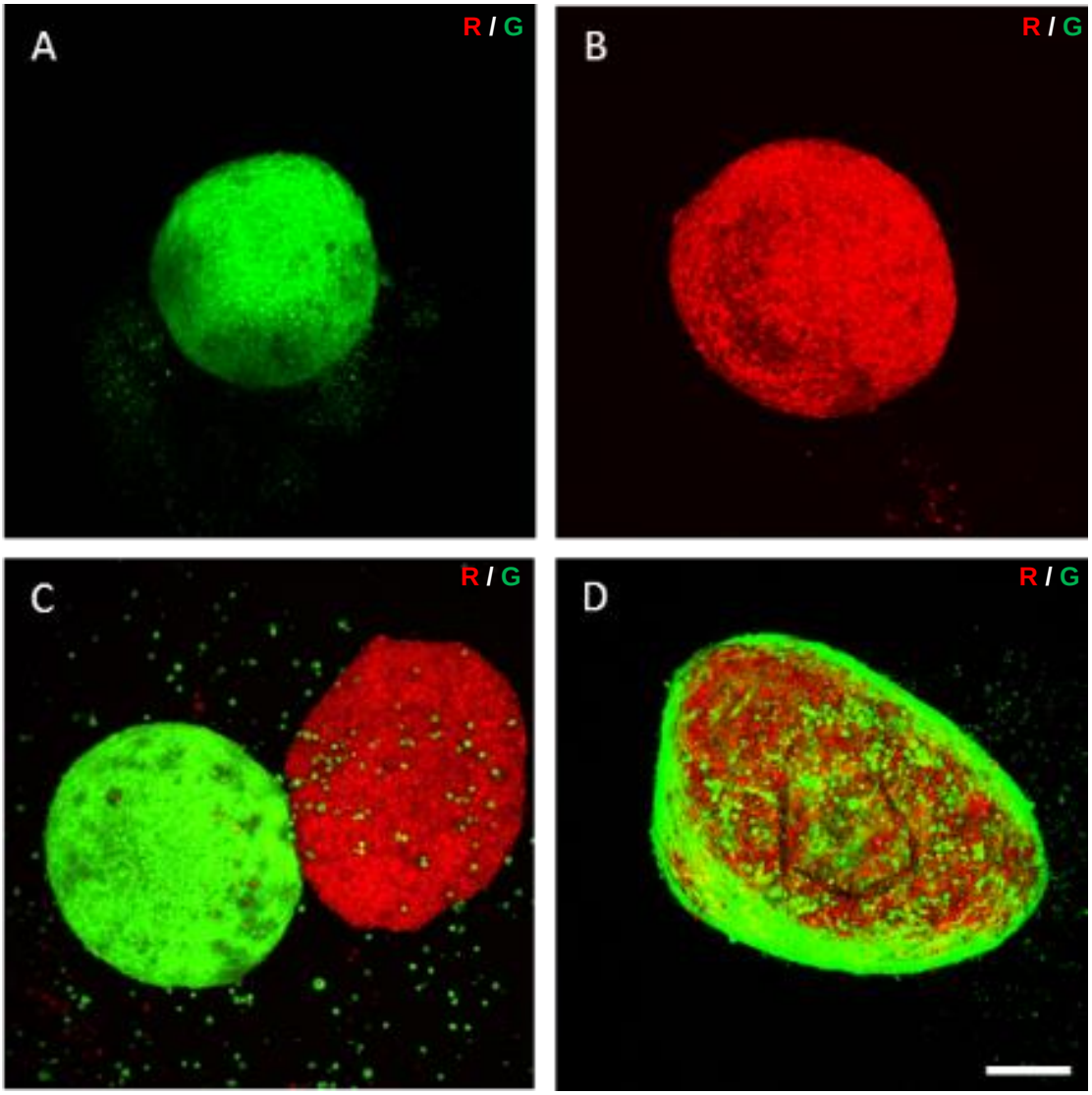

Figure 3.22: Groups of spheroids were produced using U-bottomed, cell repellent 96-well plates. *A) Tendon cell spheroid after one day of culture. B) Bone cell spheroid after one day of culture. C) Tendon and bone spheroids together at day 1 after being cultured separately for one day, for minimum contact 3D co-culture. D) A homogenised mixture of tendon and bone cells cultured together for one day, for maximum contact 3D co-culture. Images were taken using combined red (R) and green (G) channels of CFM. Representative images were chosen from a library of images acquired during the experiment (N=3, n=4). (Scale bar = 200 µm)*

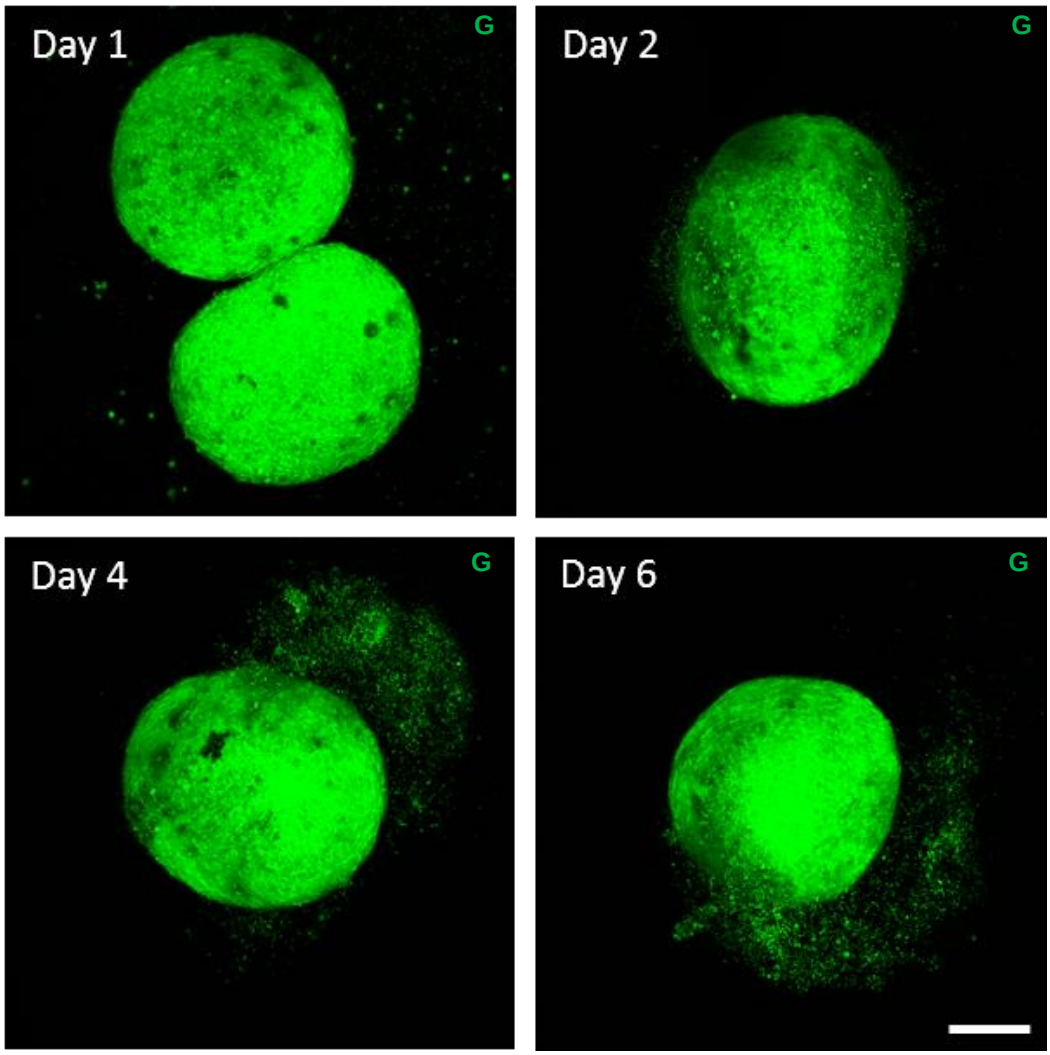

Figure 3.23: Scaffold-less system product imaged using the CFM. *Two CTF cell (green) spheroids were co-cultured in a single well. At day 1, the two tendon cell spheroids were placed in a single well of a cell-repellent and U-bottomed 96-well plate. At day 2, the two spheroids merged into a single spheroid. Day 4 showed a smaller spheroid, indicating cell contraction. Day 6 showed a more compact spheroid that was comparable in size to day 1 spheroids. Images were taken using the green (G) channel of CFM. Representative images were chosen from a library of images acquired during the experiment (N=3, n=4). (Scale bar = 200 µm)*

3.4.4.1.2 Bone-only spheroid co-localisation

Two bone-only spheroids were placed together after spheroid formation at day 1 (**Figure 3.24**). The two spheroids remained separate, with space visible between them when observed at day 2 and 4 (**Figure 3.24**). However, at day 6, bone spheroids were not visible as the CellTracker™ red usability had reached its limit (**Figure 3.24**). This contrasting observation between culturing two tendon spheroids and two bone spheroids indicated that tendon cells have weaker cell-cell attachments compared to bone cells. The bone cells' stronger cell-cell attachment did not allow the cells of the two spheroids to merge and attach to each other.

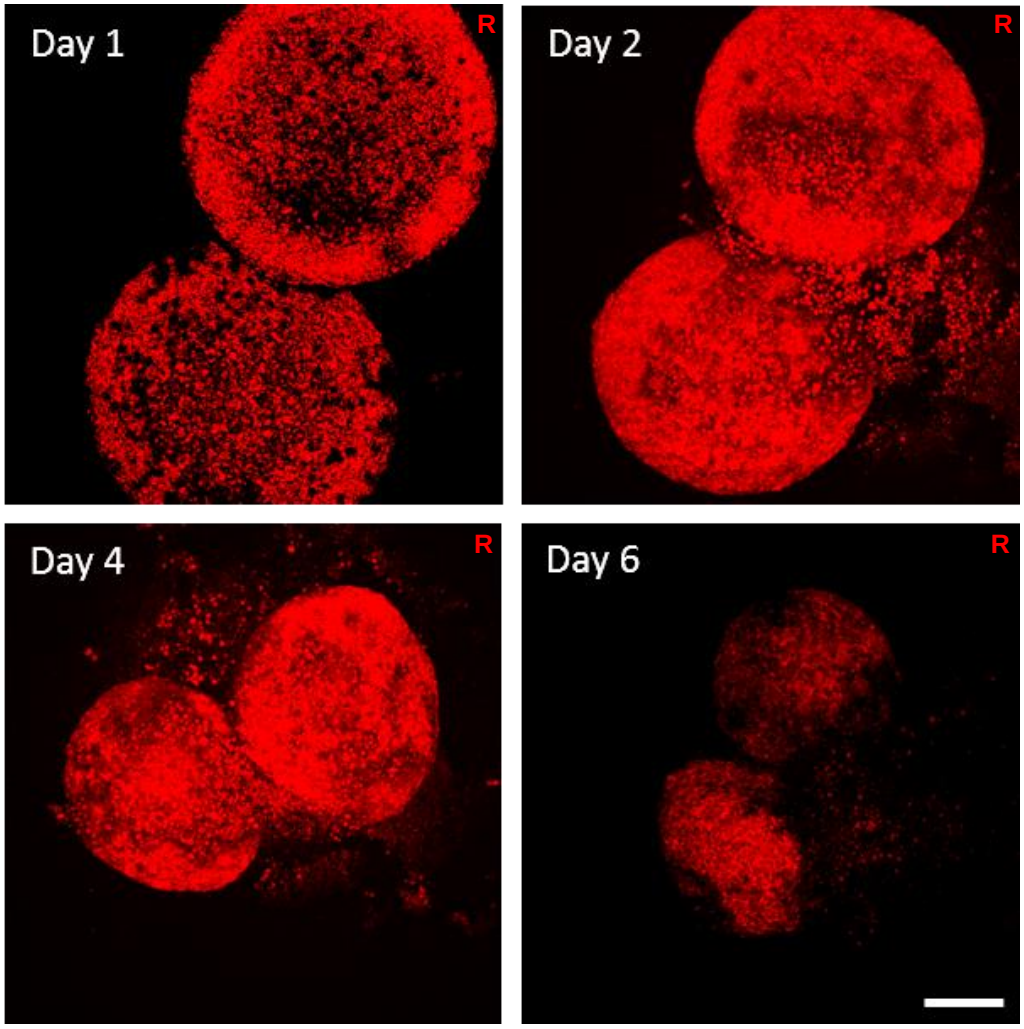

Figure 3.24: Scaffold-less system product imaged using the CFM. *Two MC3T3 cell (red) spheroids were co-cultured in a single well. At day 1, the two bone cell spheroids were placed in a single well of a cell-repellent and U-bottomed 96-well plate. At day 2, the two spheroids retained their shape and did not show signs of merging. At day 4, smaller spheroids indicating cell contraction without merging of the spheroids. At Day 6, the two spheroids appeared to be separate, but contraction could not be assessed due to the loss of the fluorescent label. Images were taken using the red (R) channel of CFM. Representative images were chosen from a library of images acquired during the experiment (N=3, n=4). (Scale bar = 200 µm)*

3.4.4.1.3 Mini-coculture spheroid localisation

Mini-coculture of CTF-GFP and MC3T3 cells was achieved by transferring a formed single tendon and single bone spheroid to one well at day 1 (**Figure 3.25**). The two spheroids had not merged at day 2, but the size of each spheroid was relatively smaller, indicating contraction of cells (**Figure 3.25**). Observation of the mini-coculture at day 4 showed that the tendon spheroid had started to merge with the bone spheroid, as the tendon spheroid boundary was disrupted and had started surrounding the bone spheroid (**Figure 3.25**). Finally, at day 6, the size of both spheroids had decreased, with the tendon spheroid cells almost surrounding the bone cells (**Figure 3.25**). Accordingly, when a bone spheroid and tendon spheroid were cultured in one well for 6 days, they merged (**Figure 3.25**). This merging was perhaps driven by the weak cell-cell attachment of the CTF-GFP cells, which allowed them to surround the strongly attached MC3T3 cells. In contrast, when two bone spheroids were cultured in one well, they did not merge (**Figure 3.24**).

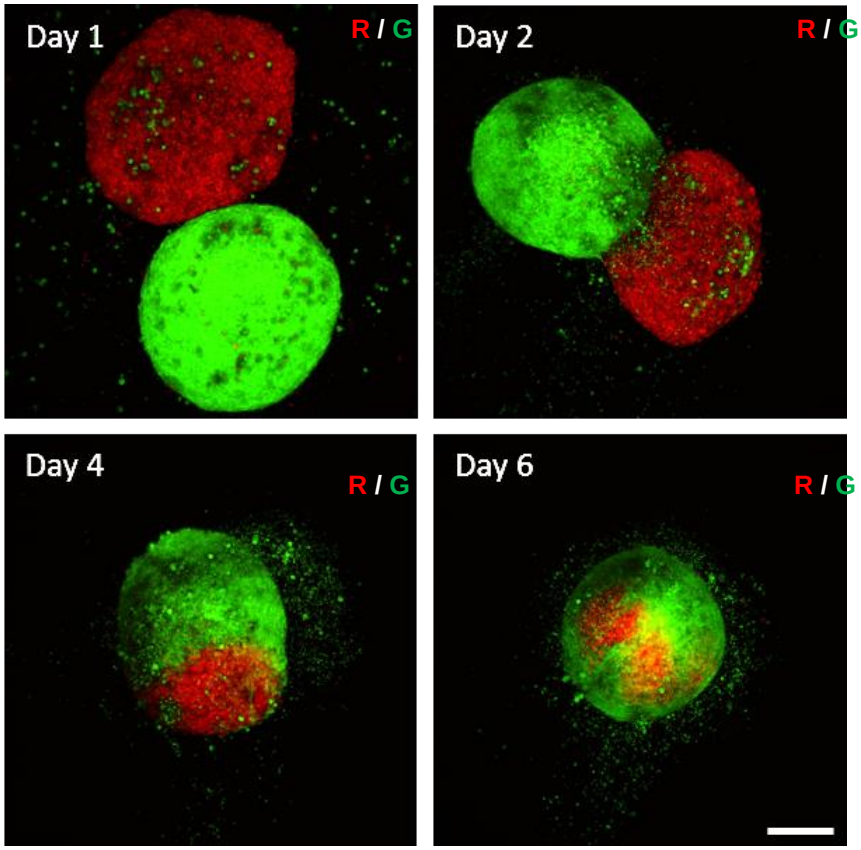

Figure 3.25: Scaffold-less co-culture system of mini-coculture imaged using CFM. A spheroid of *CTF cells (green) and MC3T3 cells (red) was co-cultured in a single well. At day 1, the bone and tendon spheroids were placed together in a single well of a cell-repellent and U-bottomed 96-well plate. At day 2, an interface had formed between the two spheroids. Day 4 showed the CTF spheroid starting to surround the MC3T3 spheroid. Day 6 showed the MC3T3 spheroid completely surrounded by the CTF spheroid. Images were taken using combined red (R) and green (G) channels of CFM. Representative images were chosen from a library of images acquired during the experiment (N=3, n=4). (Scale bar = 200 µm)*

The max-coculture of CTF-GFP and MC3T3 cells was achieved by using similar cell numbers of the two cell types to create a homogenised solution for spheroid generation. After one day of culture, the homogenised mixture was maintained with a thin rim of CTF cells surrounding the spheroid (**Figure 3.26**). At day 2, the CTF-GFP cells were visible at the periphery of the spheroid, while MC3T3 cells were at the core of the spheroid (**Figure 3.26**). Finally, at days 4 and 6, the MC3T3 cells remained at the core of the spheroid while the CTF-GFP cells were at the periphery (**Figure 3.26**). This result was similar to what was observed in the mini-coculture experiment, indicating that CTF-GFP cells had weaker cell-cell attachment, allowing them to surround the strongly attached MC3T3 cells (N=3, n=4).

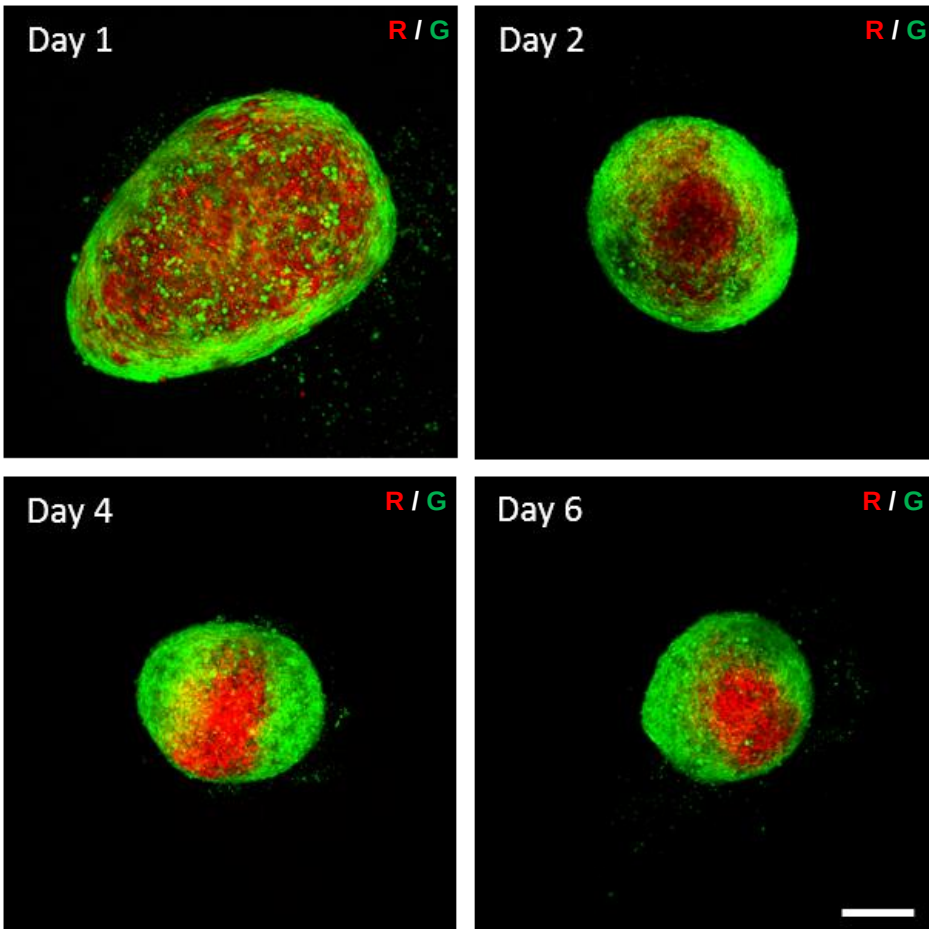

Figure 3.26: Scaffold-less co-culture system of max-coculture imaged using the CFM. *CTF cells (green) and MC3T3 cells (red) were mixed and cultured at day 0 in a single well of a cell-repellent and U-bottomed 96-well plate. At day 1, CTF cells concentrated around the peripheries of the mixed spheroid while many CTF cells were still visible at the centre. At day 2, most of CTF cells were around the periphery of the spheroid while the centre of the spheroid was occupied by MC3T3 cells. The spheroid also appeared to be smaller than its original size from day 1. At days 4 and 6, the mixed spheroid appeared smaller, with CTF cells surrounding MC3T3 cells. Images were taken using combined red (R) and green (G) channels of CFM. Representative images were chosen from a library of images acquired during the experiment (N=3, n=4). (Scale bar = 200 µm)*

3.4.4.2 Cross-sectional surface area (CSA) of spheroid types

The CSA measurements of different spheroid groups showed a decreasing pattern over time (**Figure 3.28**). Tendon spheroids had an average of 23.34 µm² ± 3.16 at day 1, which marginally decreased at day 3 to 19.54 µm² ± 1.73 ($p= 0.0321$). There was no significant difference between CSA measurements at days 3, 5 (17.70 µm² ± 1.68), 7 (17.67 µm² ± 0.91) and 10 (16.79 µm² ± 0.96), which indicated stabilisation of spheroid formation (**Figure 3.27** A). It was expected that cell proliferation in the spheroid would cause an increase in CSA measurement. Bone spheroids showed an evident decrease in CSA measurement over time from 61.79 µm² ± 2.73 at day 1 to 17.97 µm² ± 1.05 at day 20 (**Figure 3.27** B). The decrease in CSA measurements appeared to decelerate at days 7 (18.84 µm² ± 1.70) and 10 (17.97 µm² ± 1.05) as there was no significant change in CSA ($p= 0.9779$). CSA measurements of mini-coculture and max co- coculture spheroids showed a similar decreasing pattern of CSA measurements (**Figure 3.27** C and D). CSA measurements of mini-coculture at day 1 were 66.74 µm² ± 3.58, which decreased to 19.09 µm² ± 2.05 by day 10 (**Figure 3.27** C). Likewise, CSA measurements of max-coculture spheroids were 70.34 µm² ± 1.64 at day 1, which decreased to 19.34 µm² ± 2.20 at day 10 (**Figure 3.27** D). Both mini-coculture and max-coculture CSA measurements showed a deceleration of the decrease in CSA measurements at days 7 and 10, when their SCA measurements were not significantly different (day 7 vs day 10: mini-coculture $p= 0.9030$, max-coculture $p= 0.3745$) (**Figure 3.27** C and D). All measurements of different spheroid groups at all time points are also listed in **Table 3.2**.

.

Table 3.2: CSA measurements of tendon-only, bone-only, mini-coculture and max-coculture at days 1, 3, 5, 7 and 10.

Spheroid type	day of culture	Mean CSA	Standard Deviation	Number of samples
Tendon	Day 1	61.79	2.7319	5
	Day 3	41.40	3.9152	5
	Day 5	23.34	1.6963	5
	Day 7	18.84	1.6973	5
	Day 10	17.97	1.0526	5
Bone	Day 1	23.34	3.1611	5
	Day 3	19.54	1.7318	5
	Day 5	17.70	1.6800	5
	Day 7	17.67	0.9102	5
	Day 10	16.79	0.9576	5
Mini-coculture	Day 1	66.74	3.5968	5
	Day 3	44.48	2.2797	5
	Day 5	26.68	2.5147	5
	Day 7	21.10	2.4340	5
	Day 10	19.65	2.0573	5
Max-coculture	Day 1	70.34	1.6369	5
	Day 3	49.77	2.1856	5
	Day 5	28.88	3.2239	5
	Day 7	22.13	2.4103	5
	Day 10	19.34	2.1935	5

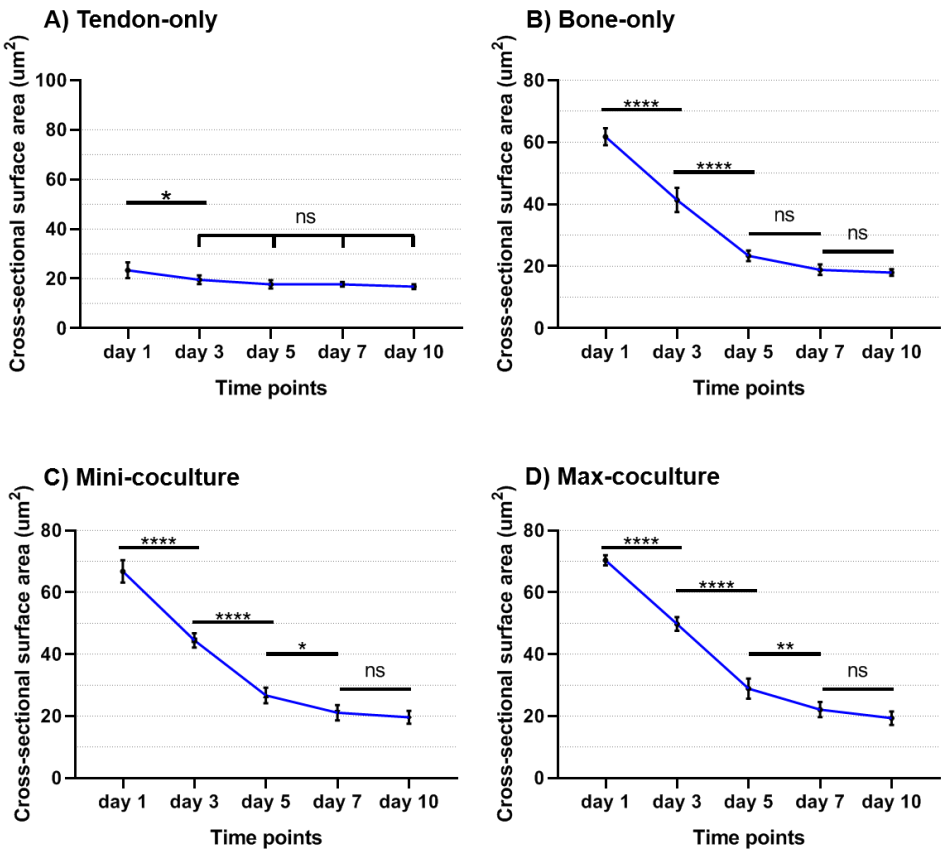

Figure 3.27: Data from Table 3.2 plotted on a graph to show the effect over 10 days of culture on CSA of A) tendon, B) bone, C) mini-coculture, D) max-coculture*. One-way ANOVA with Tukey's multiple comparisons post-test was conducted for each group with error bars showing the standard deviation (N=5, n=4).*

In addition to studying the effect of time on the CSA of each spheroid group, the difference between spheroid groups at each time point was compared by replotting the data from **Figure 3.27** in **Figure 3.28** and **Table 3.3**. At day 1, tendon-only spheroid CSA measurements were significantly less than all other groups (all p values = <0.0001). Bone-only spheroid CSA measurements at day 1 (61.79 µm² ± 2.73) was significantly different from max-coculture (70.34 µm² ± 1.64, p= 0.0029), while not significantly different to mini-coculture (66.74 µm² ± 3.58, p=0.1493). Interestingly, despite these differences at day 1 between all spheroid groups, CSA measurements at day 10 were not statistically different between all groups (**Table 3.3**)

Table 3.3: Tukey's multiple comparisons of CSA measurements of spheroids groups at different time points.

Day	Comparison	Significant?	P value
Day 1	Bone vs. Tendon	Yes	<0.0001
	Bone vs. Mini-coculture	No	0.1493
	Bone vs. max-coculture	Yes	0.0029
	Tendon vs. Mini-coculture	Yes	<0.0001
	Tendon vs. max-coculture	Yes	<0.0001
	Mini-coculture vs. max-coculture	No	0.278
Day 3	Bone vs. Tendon	Yes	0.0002
	Bone vs. Mini-coculture	No	0.4787
	Bone vs. max-coculture	Yes	0.0209
	Tendon vs. Mini-coculture	Yes	<0.0001
	Tendon vs. max-coculture	Yes	<0.0001
	Mini-coculture vs. max-coculture	Yes	0.0236
Day 5	Bone vs. Tendon	Yes	0.0033
	Bone vs. Mini-coculture	No	0.1501
	Bone vs. max-coculture	No	0.0529
	Tendon vs. Mini-coculture	Yes	0.0013
	Tendon vs. max-coculture	Yes	0.0019
	Mini-coculture vs. max-coculture	No	0.644
Day 7	Bone vs. Tendon	No	0.564
	Bone vs. Mini-coculture	No	0.3887
	Bone vs. max-coculture	No	0.1435
	Tendon vs. Mini-coculture	No	0.1056
	Tendon vs. max-coculture	Yes	0.0405
	Mini-coculture vs. max-coculture	No	0.9046

Table 3.3: continued

Day 10	Bone vs. Tendon	No	0.3199
	Bone vs. Mini-coculture	No	0.4325
	Bone vs. max-coculture	No	0.6161
	Tendon vs. Mini-coculture	No	0.1123
	Tendon vs. max-coculture	No	0.1893
	Mini-coculture vs. max-coculture	No	0.9955

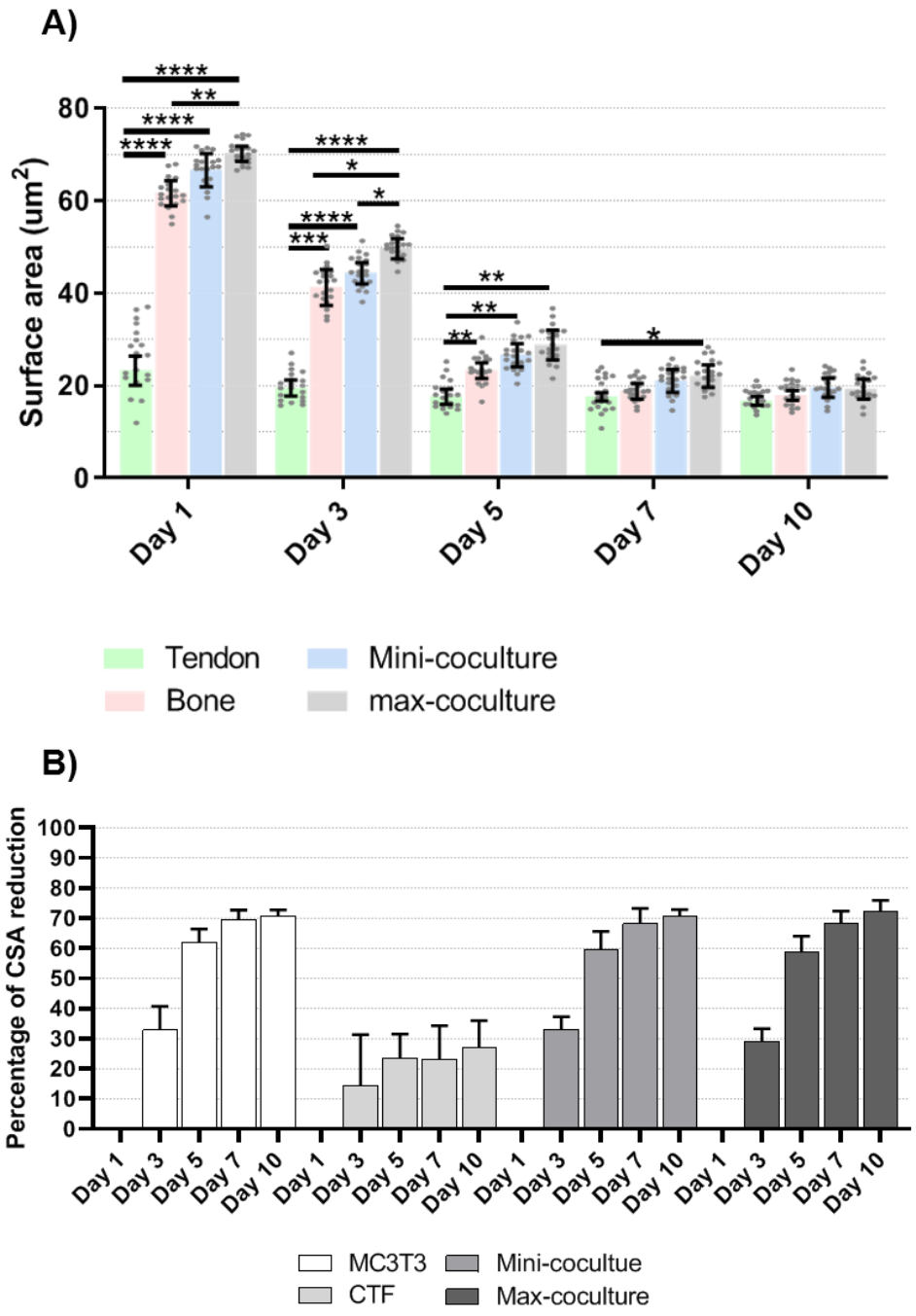

Figure 3.28: Data from Table 3.3 was plotted on a graph to show A) CSA measurements for tendon-only, bone-only, mini-coculture and max-coculture spheroids, re-plotted to show the comparison between groups at each time point. B) The percentage of CSA reduction in spheroids is shown. *Mixed effect model analysis with Tukey's multiple comparison post-test was performed with error bars showing the standard deviation (N=5, n=4).*

Finally, the effect of co-culture was assessed by comparing the combined CSA measurement of mono-culture tendon-only and bone-only spheroids, with mini-coculture

and max-coculture measurements (**Figure 3.29**). Accordingly, the co-culture of tendon and bone cells using spheroids resulted in the decrease of CSA measurements in the mini-coculture (19.65 µm² ± 2.06, p= <0.0001) and max-coculture (19.34 µm² ± 2.19, p= <0.0001) compared to the summation of mono-cultures of tendon and bone spheroids (34.75 µm² ± 1.07).

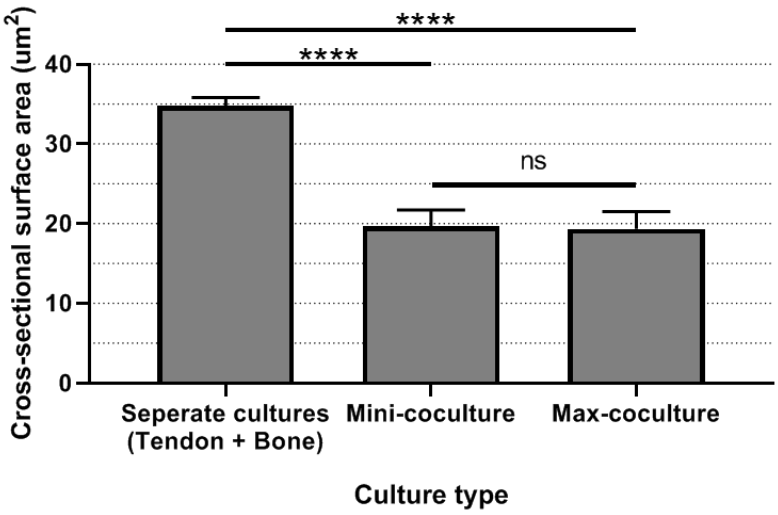

Figure 3.29: The summation of CSA of separate tendon and bone spheroid mono-culture at day 10 was significantly more than mini-coculture and max-coculture. *This result showed an inhibitory effect of co-culture, resulting in smaller sized spheroids. One-way ANOVA with Tukey's multiple comparisons post-test was conducted with error bars showing the standard deviation (N=5, n=4).*

3.5 Discussion

To study the development and healing mechanisms of tissue interfaces, an enthesis *invitro* model must be developed. Accordingly, Wang et al. (2007) and Calejo *et al.* (2018) described the development of a 2D interface model of bone and tendon cells. They reported a chondrogenic transformation of the co-cultured cells caused by the interaction between bone and tendon cells. However, both studies were conducted in a 2D environment. Cell communication and function were found to be significantly different between 2D and 3D tissue cultures, with the latter showing better cell-cell interaction, proliferation, function and a microenvironment that closely represented *in vivo* (Kim, 2005; Tredan *et al.*, 2007; Tibbitt and Anseth, 2009; Gurski *et al.*, 2010; Szot *et al.*, 2011; B. M. Baker and Chen, 2012; Xu *et al.*, 2012; Yip and Cho, 2013; Hongisto *et al.*, 2013; Huang *et al.*, 2013; Edmondson *et al.*, 2014). Therefore, a 3D co-culture model of a tissue interface is needed.

3.5.1 Introducing fluorescent cell labels

An essential criterion for the co-culture system is to allow visualisation of different cell populations using live imaging. Live imaging is superior to standard immunohistochemistry studies which require an end-point sample usage. Thus, the movement of cells in the same sample cannot be monitored over several time points. Therefore, the use of live fluorescent imaging to distinctively visualise tendon and bone cells was essential for this study. This was achieved for CTF cells by harvesting tendon fibroblast cells from chicks that have been genetically modified to express GFP in all their cells. However, MC3T3 cells were purchased as a primary cell line that does not have a fluorescent label. Consequently, the introduction of a permanent fluorescent label was attempted. Two transfection agents were tested and optimised as described by the manufacturer to induce a fluorescent label, but both failed to transfect the MC3T3 cell type and (**Figure 3.7**). However, both transfection agents were used successfully to transfect two control cell types: CTF and DPF cells (**Figures 3.5** and **3.6**). Therefore, it was concluded that MC3T3 were challenging to transfect and specialised expertise, further time and more funding was required for successful transfection, which was not available.

Instead, a temporary cell tracker was used and optimised to visualise MC3T3 cells (**Figure 3.8**). The disadvantages of cell tracker use were the need to label the cells for each experiment, bleaching of the fluorescent label, dilution of the label as cells proliferated and the total cost of labelling the cells for each experiment. However, for the scope of this study, it was decided that using cell tracker achieved the desired outcome, which was to introduce a fluorescent label to the MC3T3 cells for distinctive visualisation against the CTF-GFP cells when observing the interface using CFM (**Figure 3.14**).

Other possible methods of introducing a fluorescent label include the use of nuclear (DNA) fluorescent labels (Martin, Leonhardt and Cardoso, 2005), such as Hoechst 33258 (Durand and Olive, 1982) and DRAQ5 (Leonhardt *et al.*, 2000). However, these nuclear labels do not show cell morphology as they are confined to the nucleus of the cells (i.e. they do not also stain the cytoplasm). Another option to distinctively label tendon and bone cells is the use of fluorescent magnetic nanoparticle transfection (Tseng, Di Carlo and Judy, 2009). Nonetheless, these nanoparticles are in the range of 50-100 nm in diameter, and the fluorescent label is applied to one side of these particles, which might decrease the efficiency of fluorescent detection depending on the orientation of the nanoparticle in the cells. Moreover, these nanoparticles are of a physically solid form

which will block the excitation optical source from reaching deeper areas of a 3D construct. It is this solid physical form that will also increase individual cell weight and could further influence the observed cell migration to the bottom of the 3D hydrogel (**Figure 3.21**). Luminescent semiconducting nanocrystals (Bruchez *et al.*, 1998; Wu *et al.*, 2003) are also another possible alternative to distinctively label tendon and bone cells. However, these crystals contain toxic cadmium, which was found to be leaching out and affecting cell viability under specific biological conditions (Leonhardt *et al.*, 2000).

3.5.2 Designing a 3D co-culture system with an interface

The original 3D co-culture system was designed and used to produce a single interface in a co-culture (**Figure 3.14**). Four hydrogels were used as scaffolds to examine the system. The system resulted in the formation of an interface in all four hydrogels (**Figure 3.14**). However, a striking difference in cell morphology was observed (**Figure 3.14**). The cells cultured in fibrin exhibited unique morphology relevant to their cell types. CTF cells showed an elongated cell structure, while MC3T3 cells were polygonal in shape (**Figure 3.14** C). These cell morphologies observed in the fibrin hydrogel culture were distinctly different from the spherical shapes of both CTF and MC3T3 cells observed in agarose and gellan cultures (**Figure 3.14** A and B). CTF and MC3T3 cells were anchorage-dependent cells, i.e. they needed surface attachment to exhibit normal cell function and behaviour. These different cell morphology responses were recorded after one day of cell culture in each hydrogel. To investigate if this response was culture-time dependent, further investigations of the effect of longer culture time on cell morphology response were conducted (**Figure 3.17**).

The original scaffold-dependent system had several limitations. The most important was poor water sealing, which allowed liquid hydrogel to leak to the other side of the system. Moreover, materials used to make the system were expensive and preparation was time-consuming. Other limitations and disadvantages were listed in **Table 3.1**. Therefore, an improved design of the scaffold-dependent co-culture system was made (**3.3**). This design had better water sealing and was cheaper and easier to implement. Advantages and limitations of the improved co-culture system were listed in **Table 3.1**.

Using the improved co-culture system for longer observational studies of cell morphology and migration was investigated (**Figures 3.17** and **3.19**). The cells were cultured in agarose, gellan, fibrin and collagen. The interface was imaged at the same interface area of the cell-encapsulated hydrogel at day 0, 1, 2 and 3. The cell morphology in agarose

and gellan was spherical (**Figure 3.17** A and B), which is not the morphology observed in 2D or in native tissue histology. Some studies in the literature describe the modification of hydrogels that do not usually support cell attachment into cell-attachment supporting hydrogels. Gellan was shown in this thesis to not support cell attachment; other studies in the literature have demonstrated similar findings, such as the work of Ferris *et al.,* (2013). Other studies have described methods to modify gellan hydrogel to support cell attachment, as reported by da Silva *et al.* (2018) and Ferris *et al.* (2013).

On the other hand, CTF cells exhibited a bi-polar, elongated, spindle-like morphology in fibrin and collagen hydrogels, whereas MC3T3 cells showed polygonal morphology (**Figure 3.17** C and D). These findings suggested that the cells were able to anchor to the naturally present anchorage proteins expressed in fibrin and collagen (Doyl *et al.* 2016). The cells used in this study were anchorage-dependent cell types. This means that attachment of the cells was vital for their viability and function (Merten *et al.* 2015). Furthermore, cell crowding increased in fibrin culture compared to agarose and gellan cultures (**Figure 3.17**). This suggested that the cells proliferated in fibrin.

Nevertheless, because the well-plates used were of the tissue-culture treated type, cell proliferation on the well plastic surface could not be excluded. Therefore, non-tissue culture treated plates were used to repeat the experiment. The non-tissue culture treated plates do not provide a suitable attachment surface for the cells to anchor, which limits cell proliferation in the hydrogel. As a result, the cell proliferation observed in (**Figure 3.19**) can be attributed to the 3D co-culture system and not to the plastic surface, according to evidence of intra-hydrogel attachment and growth presented in (**Figure 3.21**). CTF cells in these experiments showed migratory action as they invaded the side containing the MC3T3 cells (**Figure 3.19** C).

To use this developed system to study the effect of co-culturing tendon and bone cells, it is vital to assess the suitability and usability of candidate hydrogels. Assessment can include studies of cell attachment, cell viability, cell proliferation and hydrogel structure integrity. This is a crucial step before using this hydrogel-based co-culture system to study the effect of co-culture. Moreover, studying the effect of co-culture is challenging. One of the challenges is in selecting a proper investigation which would be able to depict the effect of co-culture distinctively. Suggested factors include assessing the co-culture effect on cell density, ECM formation and gene expression. Another critical challenge is choosing a suitable control that could be compared to the co-culture. As the two

distinctive cell types are cultured together, they can be distinguished by their fluorescent label when using CFM. However, in end-point analysis studies which involve digestion of the sample, it is not possible to separate, for example, proteins produced by tendon cells from proteins produced by bone cells. This includes RNA extraction, protein synthesis assays and enzymatic digestion assays. Accordingly, if there is an effect of co-culture, it cannot be attributed to tendon or bone cells even with the use of monoculture controls of tendon and bone cells.

Another candidate system for co-culture in the literature uses brushite cement to produce a bone-like scaffold. These brushite cement anchors are moulded as a small anchorage structure that can create a ligament-like construct when tendon fibroblasts are seeded on fibrin hydrogel in a 35mm petri dish, as described in Paxton *et al.* (2010). However, this system was a monoculture of fibroblasts only, therefore, populating these cement anchors with osteoblasts could make a potentially promising co-culture system.

3.5.3 Scaffold-less co-culture system

As 3D culture and tissue engineering offer many possible methodologies to culture cells in 3D, there is no single method that can be considered the best option. Therefore, another different approach to making a co-culture system was developed. 3D culture of spheroids is a method that has been first described in the literature by Moscona and Moscona (1952). Several techniques for spheroid generation have been described, including hanging-drop, rotary bioreactors, ultra-low cell attachment surfaces and microfabricated hydrophobic surfaces (Lin and Chang, 2008). In this study, the ultra-low cell attachment surface method was used to produce tendon and bone spheroids (**Figure 3.22** A and B). The generated bone and tendon spheroids were cultured together in one well after formation to create a 3D co-culture, which was labelled as mini-coculture (**Figure 3.22** A). Moreover, a homogenised cell suspension containing tendon and bone cells was used to create max-coculture spheroids using the same technique (**Figure 3.22** D). This was another novel method to study a 3D co-culture model of bone and tendon cells.

As a proof of concept, CSA of tendon-only, bone-only, mini-coculture and max-coculture spheroids was measured to firstly characterise the size of each spheroid group over time, and secondly to assess the effect of co-culture on CSA. The effect of co-culture was examined by comparing the summation of the CSA of tendon-only and bone-only monocultures to the CSA of the co-culture. A secondary aim was to evaluate if different levels of CTF/MC3T3 cell-cell contact (i.e. mini-coculture and max-coculture) affected

CSA. Accordingly, the CSA of all spheroid groups showed a decreasing pattern from day 1 to day 10 (**Figure 3.27**). A notable finding was that, despite all groups having a significantly different spheroid size (CSA) on day 1, the CSA at day 10 was not significantly different between the groups (**Figure 3.28**). Moreover, the co-culture of tendon and bone cells in spheroids resulted in a decrease in the size of the co-culture (**Figure 3.29**). This decreasing change in CSA measurements could be hypothesised as the result of either reduction in cell density, ECM formation, or as a natural cell contraction. Therefore, further studies based on these findings would be to assess cell density, ECM formation and CSA for a longer period of time.

In conclusion, the field of enthesis research is in need of a 3D enthesis model. In this chapter, two co-culture methodologies have been explored and assessed. These systems could be used to investigate various interfaces between different cell types. Examples of these interfaces include bone-tendon, bone-ligament, bone-cartilage, muscle-tendon and muscle-nerve interfaces. The main interest of this study was to develop 3D bone-tendon interface models. This was achieved by two methodologies, scaffold-dependent co-culture and scaffold-less co-culture. The formation of an interface between the two populations of cells was confirmed by labelling them with identifying fluorescent labels and imaging them by CFM. The two developed models were used to study the effect of co-culture on bone and tendon cells in 3D. The scaffold-dependent 3D co-culture model is discussed in **chapter 4**.

A proof of concept study showed that spheroid 3D co-culture of bone and tendon cells produced a decrease in spheroid size caused by co-culture. This has raised important questions about the cause of this decrease, which will be addressed further in **chapter 5**. On the other hand, as described in the next chapter, hydrogel-based co-culture required further testing and evaluation of different hydrogel materials to choose the most suitable candidate hydrogel. Assessment included cell attachment, cell viability, cell density and hydrogel structure integrity. Based on these investigations, a candidate hydrogel was used for further evaluation of the effect of co-culturing bone and tendon cells in a cell-encapsulated hydrogel co-culture system.

Chapter 4. 3D co-culture of tendon and bone scaffolds: hydrogel evaluation and assessment of co-culture effect

4.1 Introduction

4.1.1 Enthesis tissue engineering

The focus of this study was to evaluate the potential of using 3D tissue engineering methodologies to create a tissue interface model between tendon and bone tissues. Tissue engineering a 3D model can be performed by two general approaches, scaffold-dependent or scaffold-less (see **chapter 1**, **section 1.2.2**). In this chapter, the focus will be on the scaffold-dependent method that includes the use of 3D scaffolds to culture cells in a 3D environment.

As discussed in **section 1.2.2.2**, scaffolds are the mainstay of any 3D scaffold-dependent tissue-engineered product. A scaffold in 3D tissue engineering acts as an artificial extracellular matrix (ECM) to mimic the biological and mechanical properties of normal tissue (B. Kim, Baez, and Atala 2000). The natural ECM provides the tissue with structural integrity and mechanical properties like stretching, resistance and weight bearing. It is also the ECM that stores different growth factors and potentiates their action (Chan and Leong 2008). Therefore, developing tissue-specific scaffolds that can function as an artificial ECM of that tissue is of great importance to 3D tissue engineering.

For this study, the intended use of scaffolds was to allow the formation of a co-culture between two distinct cell type populations in 3D. Therefore, a system was designed to host two cell-encapsulated hydrogels in a co-culture. Hydrogels were considered suitable candidates due to their superior moulding flexibility and allowing of a homogenous cell distribution encapsulated within. As the scaffold needed for cell-encapsulated co-culture experiments was intended to replace the ECM formed by the cells, natural biodegradable hydrogels were assessed for suitability. The candidate hydrogel to be used for cell-encapsulation co-culture and ECM assessment had to meet specific criteria. These criteria included the hydrogel being of proper solid form to allow side by side co-culture, allowing cells to attach, supporting cell growth by showing an increase in cell density, not causing significant cell death during the preparation and cell encapsulation process, and showing consistent results.

Assessment of scaffold usability depends on the intended use. Possible assessments include toxicity assays, proliferation assays, migration studies, mechanical studies and protein synthesis assays. For this chapter, evaluation of scaffold usability included three components: hydrogel suitability, cell density and ECM formation. For hydrogel suitability, cell attachment, percentage of live cells and cell proliferation were assessed.

Whereas for ECM formation, collagen and glycosaminoglycans (GAGs) content were quantified. ECM of tendons, ligaments, cartilages, bones and enthesis all consist mainly of collagen (Benjamin *et al.* 2006; Eriksson, Kindblom, and Wredmark 2000; Screen *et al.* 2015; Wilson *et al.* 2010; Young 2003). Proteoglycans are core proteins which have abundant GAGs proteins attached. They provide hydration and swelling pressure to tissues, giving them compressive force resistance. Therefore, cartilages have high proteoglycans content (Couchman and Pataki 2012). In contrast, tendons, ligaments and bones have lower proteoglycans presence. Notably, enthesis has a cartilaginous component, which in turn has a higher proteoglycans content. Therefore, GAGs assessment was used as a marker for ECM formation and co-culture effect on tendon and bone cell-encapsulation co-culture.

4.2 Chapter aims and objectives

The two main aims of this chapter were to 1) assess hydrogel suitability for cell encapsulation, and 2) study the effect of cell-encapsulated hydrogel 3D co-culture.

The specific objectives were to:

1. Compare cell attachment, cell viability and cell density in cell-encapsulated agarose, gellan, fibrin and collagen hydrogels;
2. Choose the most suitable hydrogel for use in the revised scaffold-dependent co-culture system to study 3D co-culture effect;
3. Assess the ECM formation in cell-encapsulated bone-only, tendon-only, and bone-tendon co-culture in hydrogels;
4. Assess the effect of bone and tendon cell-encapsulated hydrogel co-culture on ECM formation and cell number, compared to bone-only and tendon-only cell-encapsulated hydrogel monocultures;
5. Evaluate the difference in ECM formation between standard 2D culture and cell-encapsulated 3D culture.

4.3 Materials and methods

4.3.1 Assessment of cell anchorage and attachment to hydrogels

Assessing cell anchorage to hydrogels was performed to determine hydrogel suitability for use in the developed system. Cell anchorage and attachment is vital for anchorage-dependent cells' function and viability (Ahmad Khalili and Ahmad 2015; Merten 2015; Ruoslahti and Reed 1994). Agarose, gellan, fibrin and collagen hydrogels were

encapsulated with 50 K/100 µl cells. Two cell types were used separately to assess their attachment: CTF-GFP and MC3T3. After cell encapsulation in the assessed hydrogels, the encapsulated hydrogels were cultured for 24 hours at 37°C and 5% CO_2. The CTF-GFP cells were genetically encoded with GFP. However, the MC3T3 cells were labelled with RFP as a red cell tracker (CellTracker™ Red CMTPX, Life Technologies, UK). After 24 hours of incubation, the cells were visualised using CFM. Cell attachment to hydrogels was assessed visually by using an attachment criterion. Criteria of attachment included 1) loss of refractile appearance of the cell membrane, 2) presence of cell extensions and cell processes, and 3) visible and distinguishable nucleus (Ahmad Khalili and Ahmad 2015; Engler *et al.* 2009). The cells were examined against these criteria to determine their attachment to hydrogels and categorised as either attached or non-attached cells. Experimental samples were compared to examples of attached and non-attached cells (**Figure 4.1**)

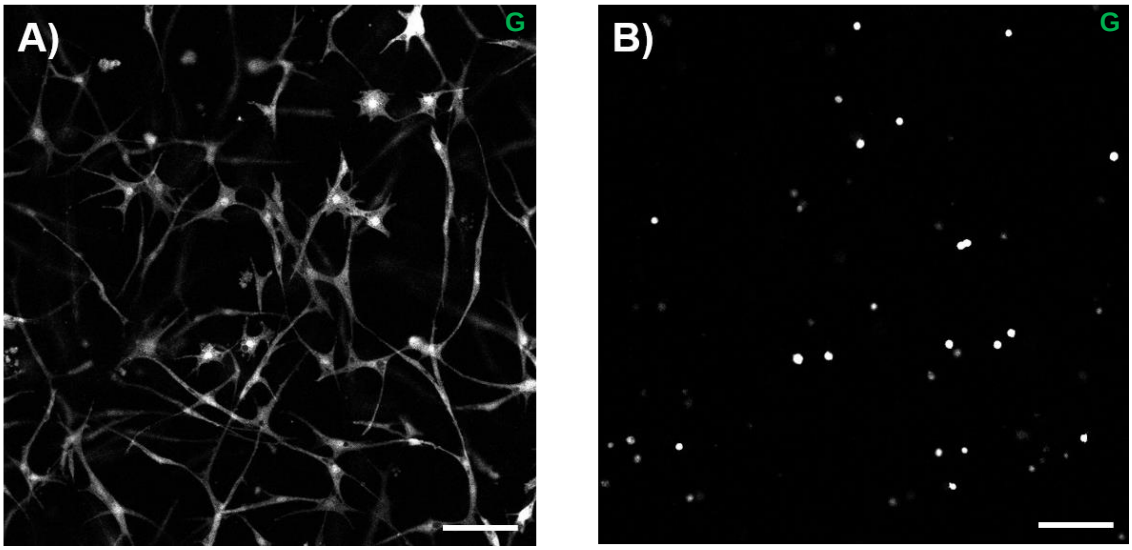

Figure 4.1: Examples of attached cells in fibrin (A) and non-attached cells in agarose (B). *Cell attachment assessment was performed for cells in agarose, gellan, fibrin and collagen. Images were taken using the green (G) channel of CFM. (Scale bar = 200 µm)*

4.3.2 Live/dead assay using calcien/PI staining

Cell viability was assessed using calcein AM and propidium iodide to evaluate dead cells. The dye solution was freshly prepared for each time point in a dark environment. The dye solution was prepared as described in (**2.2.3.3**). 100 µl of dye solution was added to each well, then each cell/hydrogel combination was incubated for an hour in 37°C, 5% CO_2. The dye solution was then removed, and fresh sDMEM was added before visualisation.

4.3.2.1 CTF and MC3T3 cell viability

The cell-encapsulated agarose, gellan, fibrin and collagen hydrogels were prepared as described in **section 2.2.2** in a ratio of 500K cells to 1 ml of hydrogel, then 100 µl of the solution was cast in eight wells of flat-bottomed, cell repellent 96-well plates (Greiner bio-one, UK). Live/dead staining was performed on days 0, 2 and 4 at each time point (N=3, n=3). Fluorescent images were taken at 4X magnification throughout the depth of each construct. These images were then saved as a dataset and processed to produce a single image of fluorescent z-axis projection using Fiji (Fiji, Schindelin *et al.* 2012).

4.3.2.2 RTF and dROb cell viability

The cell-encapsulated fibrin hydrogels were prepared as described in **section 2.2.2** in a ratio of 500K cells to 1 ml of hydrogel, then 100 µl of the solution was cast in eight wells of flat-bottomed, cell repellent 96-well plates (Greiner bio-one, UK). Live/dead staining was performed on days 0, 4, 7 and 10 at each time point (N=3, n=4). Fluorescent images were taken at 4X magnification throughout the depth of each construct. These images were then saved as a dataset and processed to produce a single image of fluorescent z-axis projection using Fiji (Fiji, Schindelin *et al.* 2012).

4.3.3 Percentage of live cells in hydrogels

The percentage of live cells encapsulated in hydrogels was investigated. The aim of the experiment was to compare cell viability when encapsulated in agarose, gellan, fibrin and collagen hydrogels. CTF and MC3T3 cell viability, when encapsulated in these hydrogels, was assessed at day 0 and day 7 (N=4, n=4). The cell-encapsulated hydrogels were prepared as described in **section 2.2.2** in a ratio of 500K cells to 1 ml of hydrogel. 100 µl of the solution was cast in eight wells of flat-bottomed, cell repellent 96-well plates (Greiner bio-one, UK) in a single-blinded sampling procedure for each cell/hydrogel type combination and a list of all wells with cell/hydrogel occupant combination documented (**Figure 4.2**). Living cells were labelled with calcein AM while dead cells were labelled with PI, using a calcein/propidium iodide solution as described in **section 2.2.3.3**. The cell-encapsulated agarose and fibrin hydrogels were incubated in calcein/PI solution for an hour, the solution was removed, then the cell-encapsulated hydrogels were washed once with 1x PBS. CFM was used to image the cell-encapsulated hydrogels at day 0 and day 7; the examiner was blinded to which combination of cell/hydrogel was being examined (**Figure 4.2**). The datasets of images obtained from the CFM were analysed using Imaris software (Bitplan, Oxford Instruments, UK) to calculate live and dead cells.

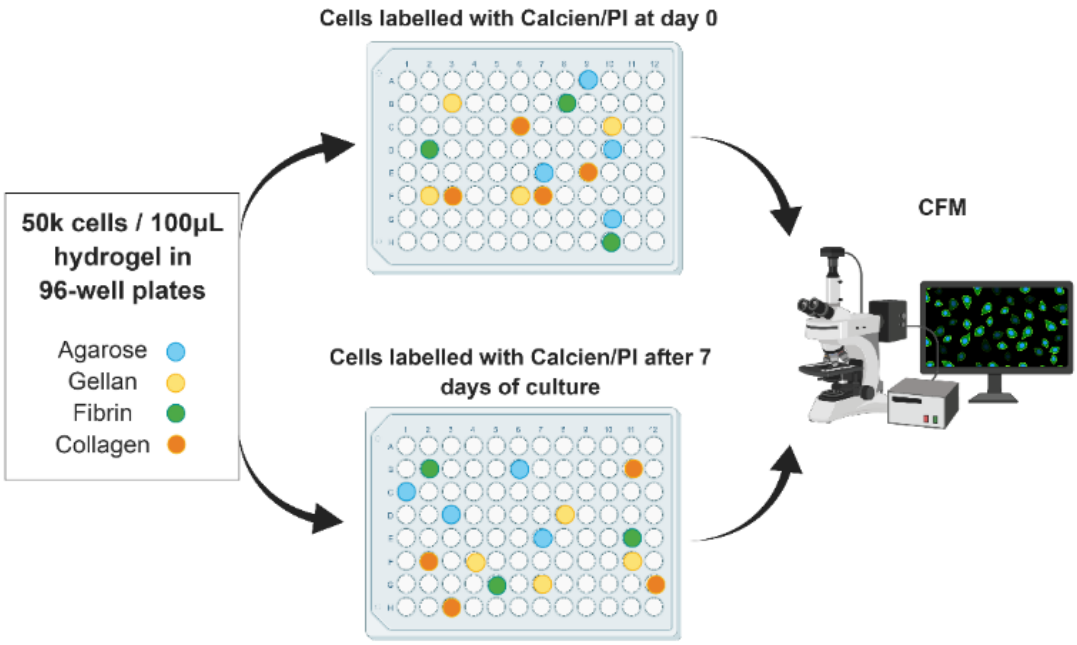

Figure 4.2: A diagram of cell viability percentage experiment single blinded sampling methodology to collect datasets of live and dead cells using CFM. *Cells were encapsulated in hydrogels at day 0 in two groups; one was immediately labelled with calcein/PI and imaged, the other was cultured for 7 days then labelled with calcein/PI and imaged by CFM (N=4, n=4).*

4.3.4 Dead cells' nuclei clearing by FBS enzymes.

Cell culture media used for cell-encapsulated hydrogel maintenance contained FBS, which contained various enzymes, including DNases. Therefore, to rule out false counting of dead cells in the previous experiment (**section 4.3.2**), the effect of FBS enzymes on the dead cells' nuclei count was investigated. Calcein/PI solution was prepared and used as described in **section 2.2.3.3** to label live and dead CTF and MC3T3 cells. 10K, 20K, 40K, 60K and 100K dilutions of live and dead cell groups were transferred to 1.5mL reaction tubes (Greiner bio-one, UK) and centrifuged at 1000 rpm for 3 minutes (Micro Centaur, MSE, UK). Cells in the dead groups were killed by resuspending the cells in 1 ml of 70% alcohol in each reaction tube and incubating for 5 minutes before centrifugation at 1000 rpm for 3 minutes to decant the 70% alcohol. The separate live and dead cells' dilution pellets were resuspended using the calcein/PI solution and cultured at 37°C, 5% CO^2 for one hour. This was followed by centrifugation at 1000 rpm for 3 minutes, then the calcein/PI solution was decanted. The dilutions were washed with 1 ml of 1xPBS and then resuspended in 500 µl of 1xPBS. 200 µl of the final solutions were transferred to regular 96-well plates (Greiner bio-one, UK) for

fluorescence detection using a microplate reader (GloMax® Explorer, Promega, UK). The results were used to create standard curves of live and dead CTF and MC3T3 cells.

To examine the effect of FBS enzymes on nuclear material digestion, 40K of live CTF and MC3T3 cells were seeded separately in tissue culture treated 6-well plates (Greiner Bio-one, UK) (N=3, n=3). At the same time, similar cell numbers were killed as described earlier and seeded in tissue-culture treated 6-well plates (Greiner bio-one, UK). These live and dead CTF and MC3T3 cells were cultured for 5 days. The live cells and one group of dead cells were cultured in sDMEM, while another group of dead cells was cultured in FBS-free sDMEM. A negative control of sDMEM with no cells was also used. No media changes were made to avoid loss of dead cells. After 5 days of culture, all cell groups were collected and assayed using calcein/PI solution (**Figure 4.3**) as described earlier.

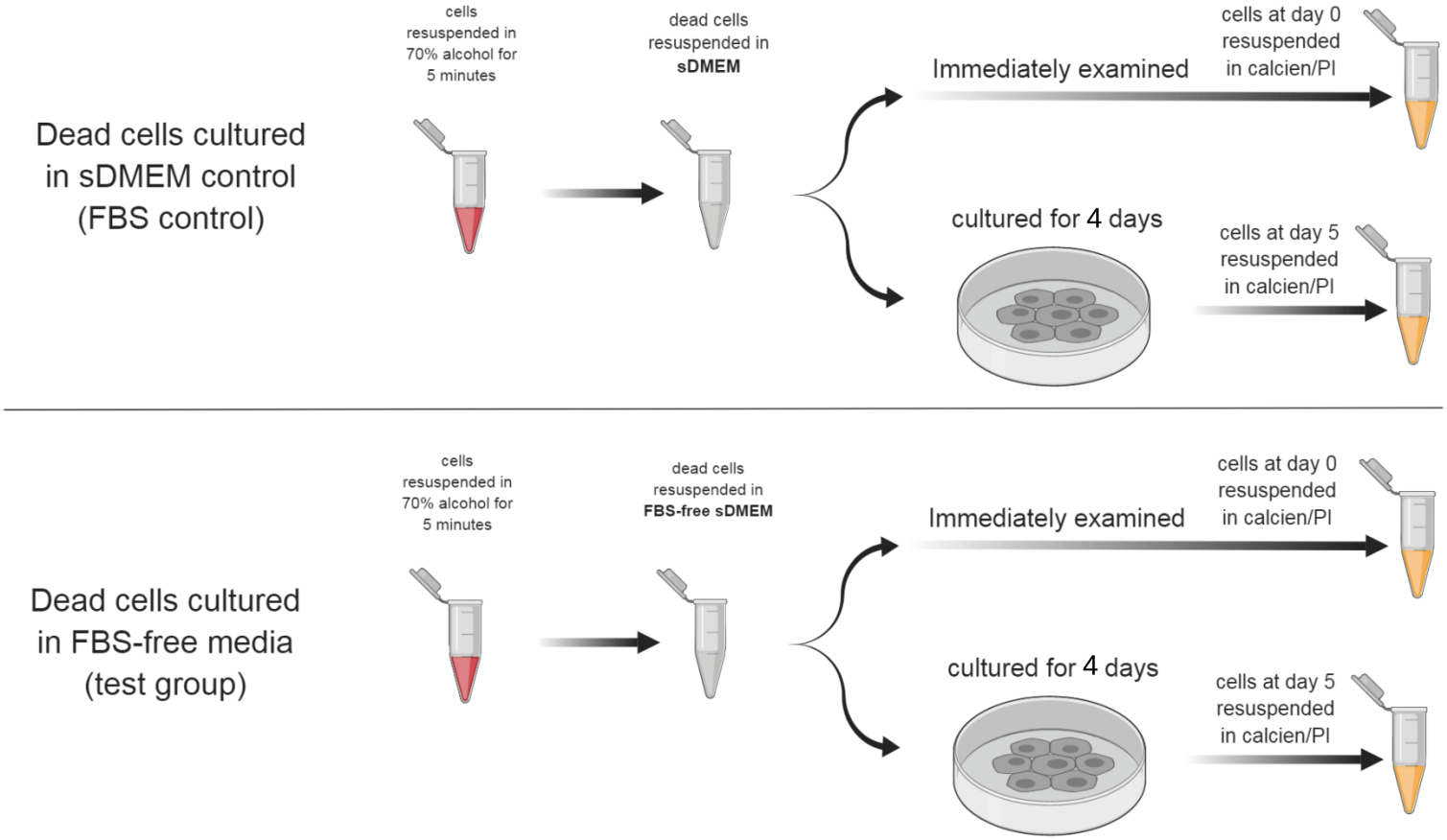

Figure 4.3: Work-flow diagram of FBS enzyme effects on disappearance of dead cells' nuclear materials when labelled with PI. Groups for experiment included negative control of sDMEM without cells, positive control of live cells, dead cells cultured with sDMEM, dead cells cultured with FBS-free sDMEM.

4.3.5 Cell proliferation in hydrogels

The DNA content of the CTF and MC3T3 cells in the cell-encapsulated agarose and fibrin hydrogels was assessed (CyQuant™ cell proliferation assay, Invitrogen, UK). CTF/MC3T3 cell-encapsulated agarose and fibrin hydrogels were prepared as described in **section 2.2.2** in a ratio of 500 K cells to 1 ml of hydrogel. On the day of cell-encapsulation, four samples of each cell/hydrogel combination were stored in a -80°C freezer as day 0 samples (N=3, n=4). The other four samples were cultured for 7 days then washed with 1x PBS and stored at -80°C (N=3, n=4). The CyQuant™ cell proliferation assay was not designed to assess DNA content of cells encapsulated in hydrogels. Therefore, hydrogel-specific cell-isolation protocols were used before starting the CyQuant™ assay. On the day of assay, all samples were thawed, and hydrogel-specific preparation was performed for the test as described below:

4.3.5.1 Agarose hydrogel

The cells encapsulated in agarose were retrieved by incubating collagen at 75°C for 30 minutes and centrifuging the cells for 5 minutes at 2000 rpm (1-13 microfuge, Sigma, UK). The agarose was discarded, and the pellet of cells was used for the CyQuant™ assay, as described by the manufacturer, to quantify DNA content.

4.3.5.2 Fibrin hydrogel

Cell retrieval from fibrin hydrogel to quantify DNA (cell density) was attempted using two methodologies. A physical and a chemical homogenisation method were trialled.

4.3.5.2.1 Homogenisation of fibrin hydrogel method for DNA measurements

Retrieval of DNA from CTF and MC3T3 cells encapsulated in fibrin hydrogel was attempted. The cell-encapsulated fibrin hydrogel was minced with a disposable sterile scalpel blade number 10a (Swann-Morton, UK). The minced cell-encapsulated hydrogel was sonically disrupted to form a homogenised solution (SSE-1 Digital Sonifier, Branson, UK). The homogenised solution was used for the CyQuant™ assay, as described by the manufacturer, to quantify DNA content.

4.3.5.2.2 Use of Nattokinase for fibrin hydrogel digestion and cell retrieval

As described in Carrion *et al.* (2014), the use of Nattokinase fibrinolytic enzyme activity to retrieve cells encapsulated in fibrin hydrogel was performed, with a small modification to digestion time. Nattokinase powder (NSK-SD; Japan Bio Science Laboratory Co. Ltd, USA) was dissolved in PBS containing 1 mM EDTA (Sigma, UK) to a final concentration of 50 FU/ml. Samples in 1.5 ml microtubes were washed with 1x PBS, then 1 ml of

Nattokinase solution was added to samples and cultured at 37°C, 5% CO_2 overnight (in the Carrion *et al.* study, the digestion period with Nattokinase was from 30-90 minutes using fibrin hydrogels of lower concentrations). After incubation, samples were centrifuged at 1000 rpm for 3 minutes then used for the CyQuant™ assay.

4.3.6 ECM formation and content evaluation

The collagen and GAGs content of ECM, formed within cell-encapsulated fibrin hydrogels culture, were assessed (Sircol™ and Blyscan™, Biocolor, UK). Separate RTF and dROb cell-encapsulated fibrin hydrogels were prepared as described in **section 2.2.2.3** in a ratio of 500K cells to 1 ml of hydrogel. The cell-encapsulated fibrin hydrogel solutions were then used in the revised scaffold-dependent co-culture system, described in **section 3.3.4,** to produce three groups of cell-encapsulated fibrin hydrogel: 300 µl RTF-only, 300 µl dROb-only, and 300 µl from each to form the RTF/dROb cell-encapsulated co-culture. The revised scaffold-dependent co-culture system was used with the half-well plug blocking half the system in the RTF-only and dROb-only groups (**Figure 4.4**), whereas the co-culture of RTF and dROb cell-encapsulated hydrogels were used as described in **section 3.3.4**. Twelve samples were collected at days 5, 10, 15 and 20 from each group and six were used for collagen content assessment using Sircol™ soluble and insoluble collagen assays, as described in the manufacturer protocol (N=1, n=6). Another six samples at each time point were used to assess GAGs using Blyscan™ GAGs assay (Blyscan™, Biocolor, UK) (N=1, n=6). Optimisation was performed by repeating the experiment with different time points. Optimised time points were day 0 and day 20 (N=3, n=4). The optimisation was necessary to subtract the collagen and GAGs formed during 2D cell growth and expansion, before cell-encapsulation in fibrin hydrogel culture (**Figure 4.5**).

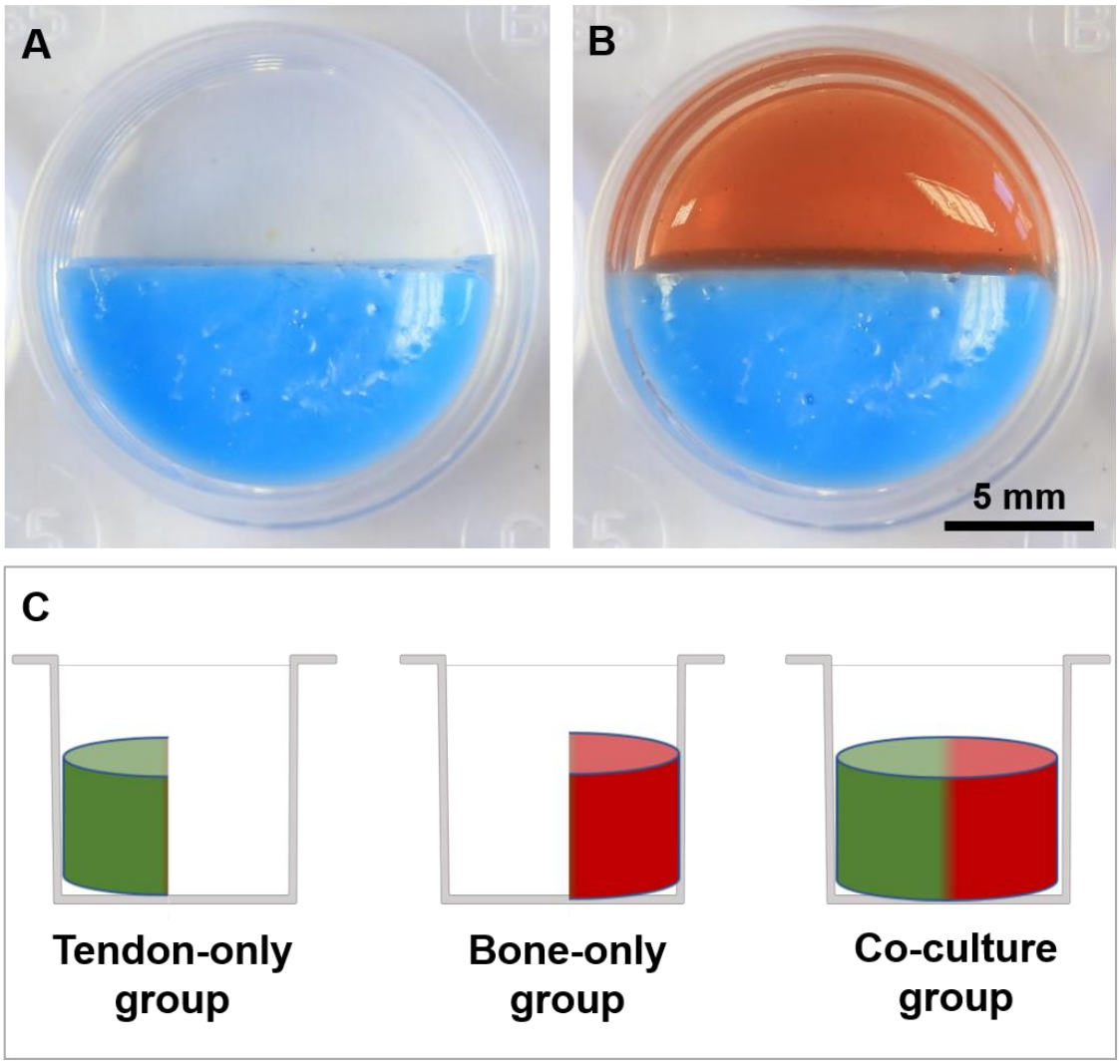

Figure 4.4: A) A half-well plug was used to block half of the well. *B) The RTF-only and dROb-only hydrogels were cultured separately without removing the half-well plug (red pseudocolor was used for illustration purposes), whereas the RTF and dROb co-culture was performed using the full system as described in* ***section (3.3.4).*** *C) Groups of samples used to assess the effect of co-culture.*

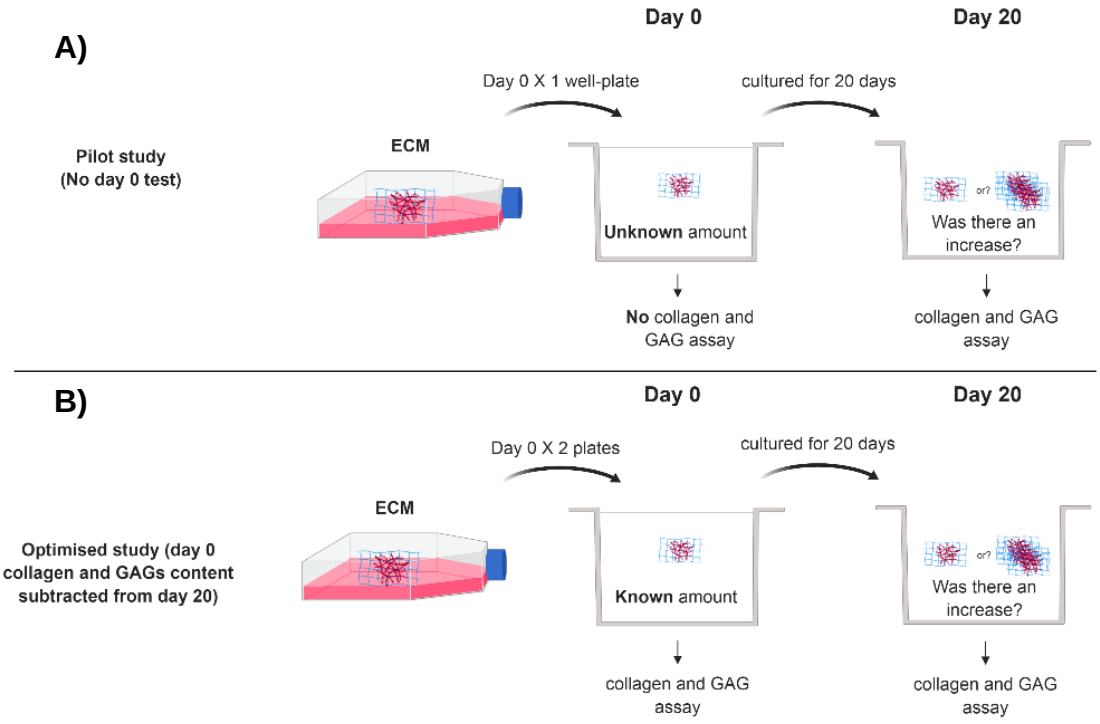

Figure 4.5: A) The pilot study compared to B) optimised experiment of ECM formation, collagen and GAGs content*. Collagen and GAGs content were not assessed at day 0 in the pilot study, which was performed in the optimised experiment. The collagen and GAGs results of day 0 were subtracted from the collagen and GAGs results after 20 days of culture to show the collagen and GAGs formation due to 3D cell-encapsulated fibrin hydrogel culture.*

4.3.7 Cell density experiment

Cell density in cell-encapsulated fibrin hydrogels was assessed (CyQuant™ cell proliferation assay, Invitrogen, UK). Separate RTF and dROb cell-encapsulated fibrin hydrogels were prepared as described in **section 2.2.2.3** in a ratio of 500K cells to 1 ml of hydrogel. The cell-encapsulated fibrin hydrogel solutions were then used in the revised scaffold-dependent co-culture system described in **section 3.3.4** to produce three groups of cell-encapsulated fibrin hydrogel: 300 µl RTF-only, 300 µl dROb-only, and 300 µl from each to form the RTF/dROb cell-encapsulated co-culture. The revised scaffold-dependent co-culture system was used with the half-well plug blocking half of the system in the RTF-only and dROb-only groups (**Figure 4.4** A), whereas the co-culture of RTF and dROb cell-encapsulated hydrogels were used as described in **section 3.3.4**. Four samples were collected at days 5, 10, 15 and 20 from each group and used for the CyQuant™ assays as described in the manufacturer's protocol (N=1, n=4). Optimisation

for the experiment was performed by repeating the experiment at different time points. Optimised time points were day 0 (N=3, n=4) and day 20 (N=3, n=4).

4.3.8 2D vs 3D experiments

Culture of RTF and dROb cells was compared between standard 2D culture and 3D cell-encapsulation in fibrin hydrogel after 20 days of culture. Both types of cultures were conducted in 24-well plates. However, 2D cell culture was conducted in cell-culture-treated 24-well plates, whereas 3D cell culture was conducted in a non-cell-culture-treated 24-well plate to prevent cells migrating from hydrogel encapsulation and attaching to the 2D plastic surface of the well plate. Three experiments were conducted: cell number determination, collagen, and GAGs content measurements. Cell number was determined using the CyQuant™ assay. This was an essential step to compare cell number after 20 days of either 2D or 3D culture.

Moreover, the cell numbers were used to calculate how much collagen and GAGs were produced per cell. This provided comparable results of collagen and GAGs in 2D vs 3D culture. Collagen and GAGs measurements were performed as described in **section** 4.3.6.

4.4 Results

The investigations pursued were either to compare the suitability of hydrogels for cell-encapsulation or to assess ECM formation. Investigations of hydrogel suitability included the study of their support of cell attachment, cell viability and cell proliferation. Suitability of different hydrogels was determined based on these studies combined with results presented in **section 3.4.1**, and a hydrogel was then selected for cell-encapsulation and ECM formation assessment accordingly. ECM formation investigations were designed to assess the ECM content resulting from bone-only, tendon-only, and co-culture in cell-encapsulated hydrogels.

4.4.1 Hydrogel suitability for cell encapsulation

To study the effect of co-culture on cell density and ECM formation, a suitable hydrogel for the co-culture system required selection. This selection was based on the following experiments conducted on agarose, gellan, fibrin and collagen hydrogels.

4.4.1.1 Cell attachment

Agarose, gellan, fibrin and collagen hydrogels' support for cell anchorage and attachment was assessed. The assessment was based on visual confirmation of cell attachment criteria. The criteria described in Ahmad Khalili and Ahmad 2015; Engler *et al.* 2009 and stated in **section**

3.4.1 were used to differentiate between attached and non-attached cells. The assessment was to answer one question:

Did the cells attach?	No ✗	Yes ✓

CTF and MC3T3 cells did not show any signs of attachment to agarose or gellan hydrogels when encapsulated within. In contrast, they fulfilled the attachment criteria when encapsulated in fibrin and collagen hydrogels (**Table 4.1**). This was a result for consideration in the process of selecting the most suitable hydrogel for ECM production evaluation, as cell attachment was essential for cell function and viability (Ahmad Khalili and Ahmad 2015; Merten 2015; Ruoslahti and Reed 1994).

Table 4.1: Cell attachment observations of encapsulated CTF and MC3T3 cells in agarose, gellan, fibrin and collagen hydrogels. (nn represents technical replicas of all independent experiments)

	Agarose	Gellan	Fibrin	Collagen
CTF	✗ N=9 (nn=47)	✗ N=8 (nn=42)	✓ N=12 (nn=56)	✓ N=15 (nn=88)
MC3t3	✗ N=12 (nn=58)	✗ N=8 (nn=44)	✓ N=7 (nn=39)	✓ N=11 (nn=59)

4.4.1.2 Live/dead assay of CTF and MC3T3 cells when encapsulated in different hydrogels

Qualitative assessment of viability was performed using calcein/PI staining, as described in **section 2.2.3.3**. Agarose, gellan, fibrin and collagen hydrogels were imaged using CFM across the z-axis, and a projection along the z-axis was produced as a single image at days 0, 2 and 4 of cell-encapsulated 3D culture. CTF cells qualitatively showed good viability when encapsulated in gellan and fibrin across time (**Figure 4.6** B and C). CTF cells encapsulated in collagen hydrogel showed moderate cell death at day 2 (**Figure 4.6** D), and at day 4 when encapsulated in agarose hydrogel (**Figure 4.6** A). Furthermore, it was visually evident that MC3T3 cells were viable across all time points when encapsulated in fibrin hydrogel (**Figure 4.7** C). In contrast, MC3T3 cells did not show good viability in agarose, gellan or collagen gels, as more red (dead) cells were detected (**Figure 4.7** A, B, and D).

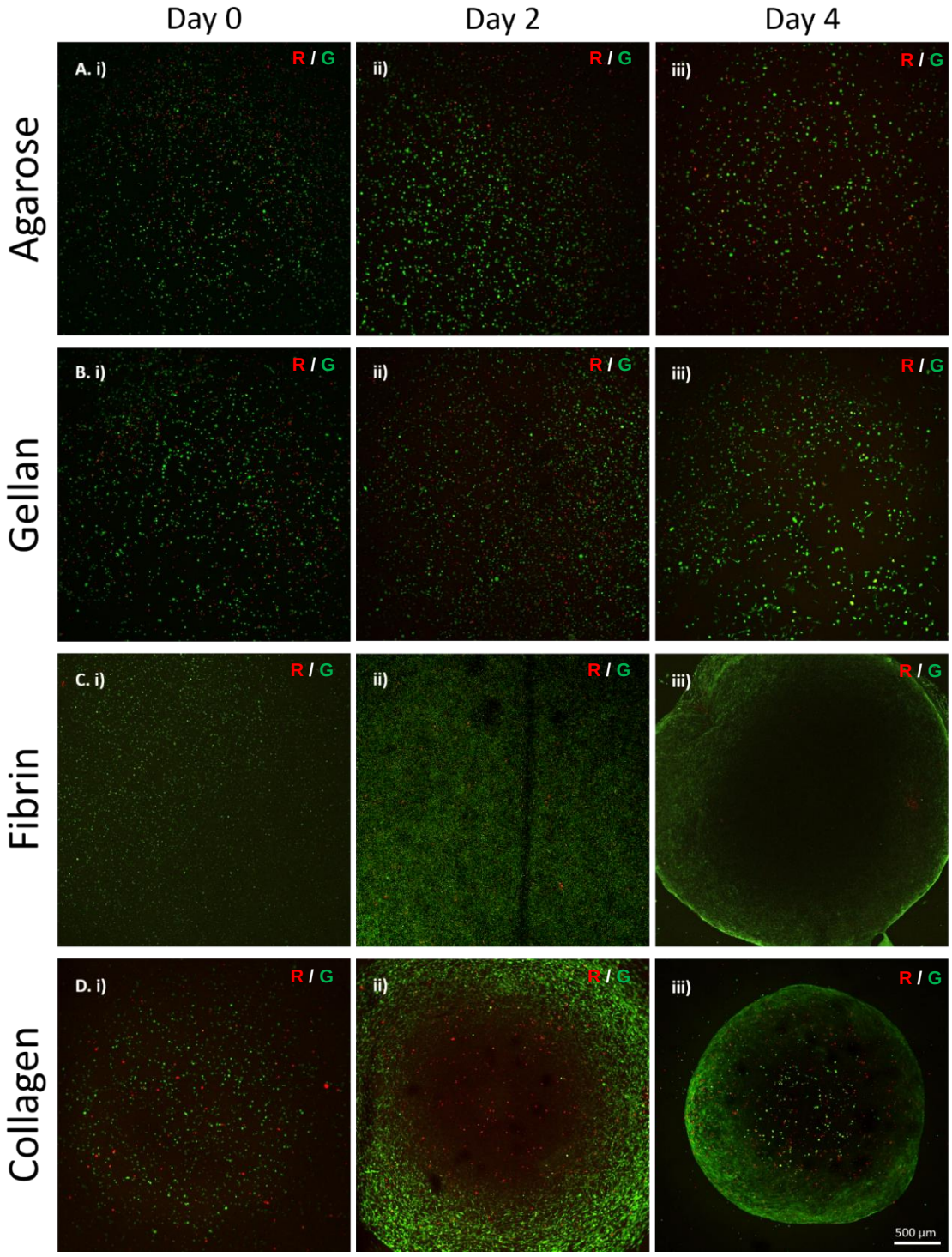

Figure 4.6: CTF cells encapsulated in A) agarose, B) gellan, C) fibrin, and D) collagen, stained with calcien (stains live cells green) and PI (stains dead cells red). *Agarose, gellan and fibrin qualitatively showed good viability of cells as the presence of dead cells was not significant. However, the collagen hydrogel showed a dead core of cells at day 2. Images were taken using combined red (R) and green (G) channels of CFM. Representative images were chosen from a library of images acquired during the experiment. (N=3, n=4)*

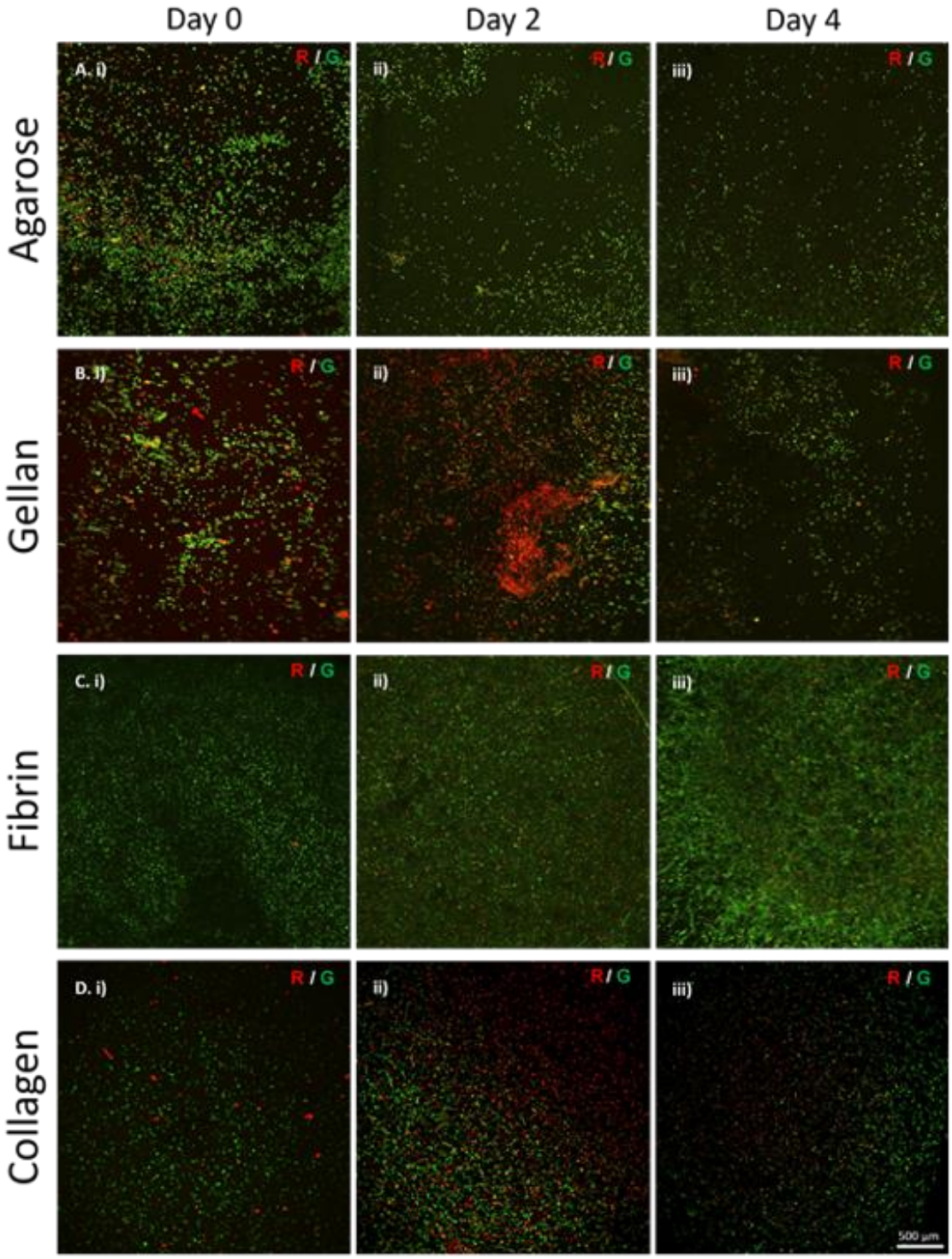

Figure 4.7: MC3T3 cells encapsulated in A) agarose, B) gellan, C) fibrin and D) collagen, stained with calcien (stains live cells green) and PI (stains dead cells red). *Fibrin qualitatively showed good viability of cells as the presence of dead cells was not significant. However, agarose at day 1, and gellan and collagen at day 2, showed a significant presence of dead cells at day 2. Images were taken using combined red (R) and green (G) channels of CFM. Representative images were chosen from a library of images acquired during the experiment. (N=3, n=4)*

4.4.1.3 Percentage of live cells in hydrogels

Viability of cells encapsulated in a hydrogel was an important factor for deciding a suitable hydrogel, which would then be used for experiments on ECM formation and content in cell-encapsulated hydrogels. The live and dead cells in cell-encapsulated agarose, gellan, fibrin and collagen hydrogels were counted at day 0 and at day 7. The percentage of live CTF cells was quantified and presented in **Figure 4.8**. The percentage of live CTF cells in agarose was 53.94% at day 0 and 81.16% at day 7. It was 58.97% at day 0 and 49.71% at day 7 when CTF cells were cultured in gellan. CTF cells in fibrin hydrogel had a 94.81% viability at day 0 and 77.78% at day 7. When CTF cells were cultured in collagen, 89.45% were live at day 0 and 38.41% at day 7. These viability percentages were taken from 5 technical repeats of one experiment as a pilot study. A more rigorous assessment was performed for agarose and fibrin hydrogels and was statistically analysed (N=4, n=5) (**Figure 4.9**). The percentage of live CTF cells in agarose was significantly increased after 7 days of culture, at 61% ± 2.50 on day 0, compared to day 7 (88.20% ± 4.82, p = < 0001). On the other hand, the percentage of live cells was not significantly different between day 0 (94.90% ± 00.81) and day 7 (87.45% ± 06.31), when cells were cultured in fibrin hydrogel.

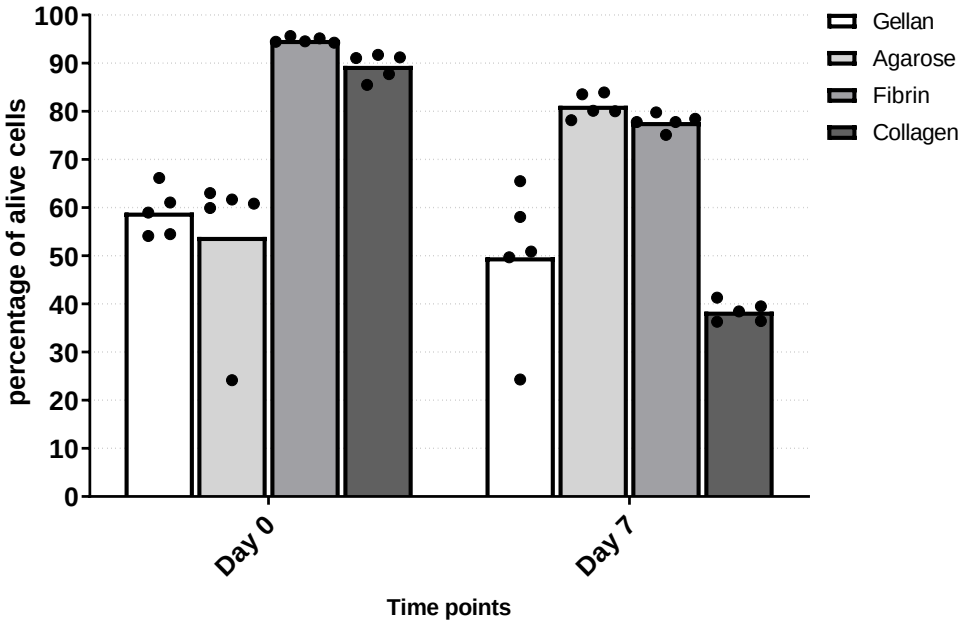

Figure 4.8: Pilot study of the percentage viability of CTF cells when encapsulated in gellan, agarose, fibrin and collagen hydrogels at days 0 and 7. *(N=1, n=5), scattered points were technical repeats of one experiment.*

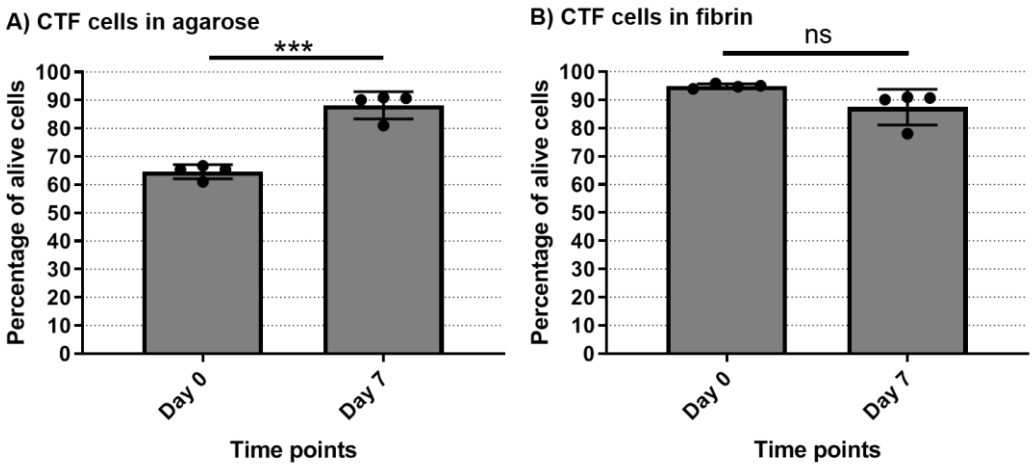

Figure 4.9: Percentage of live CTF cells when encapsulated in A) agarose and B) fibrin hydrogels*. Unpaired, two-tailed t-test was conducted with error bars showing the standard deviation (N=4, n=4).*

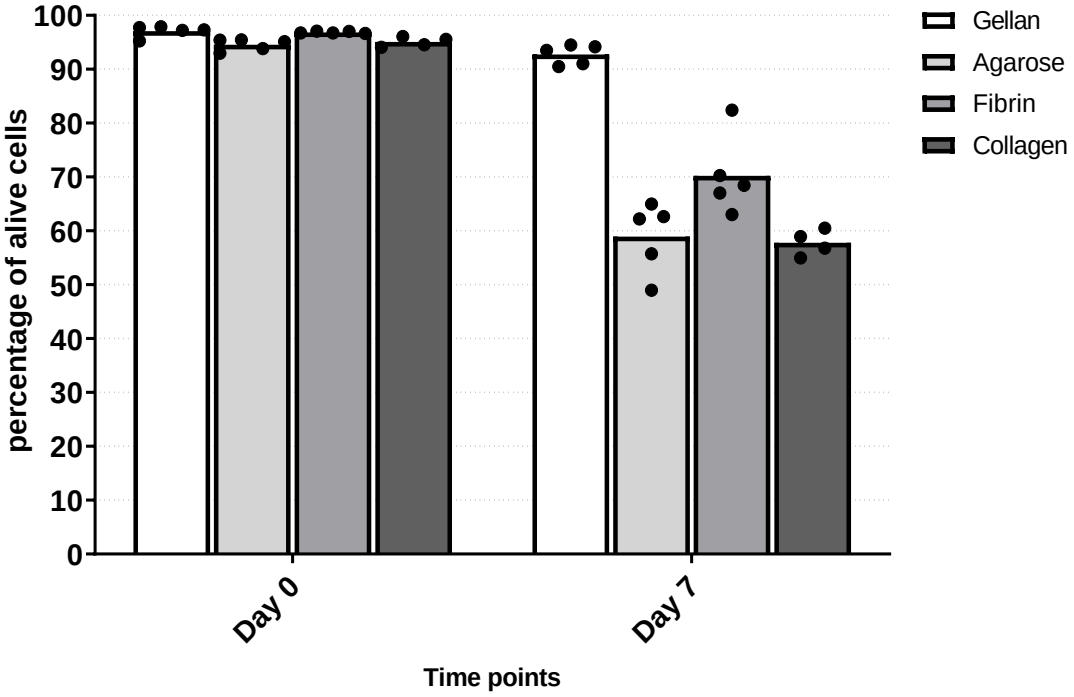

Figure 4.10: Pilot study of the percentage of viability of MC3T3 cells when encapsulated in gellan, agarose, fibrin and collagen hydrogels at days 0 and 7. *(N=1, n=5), scattered points were technical repeats of one experiment.*

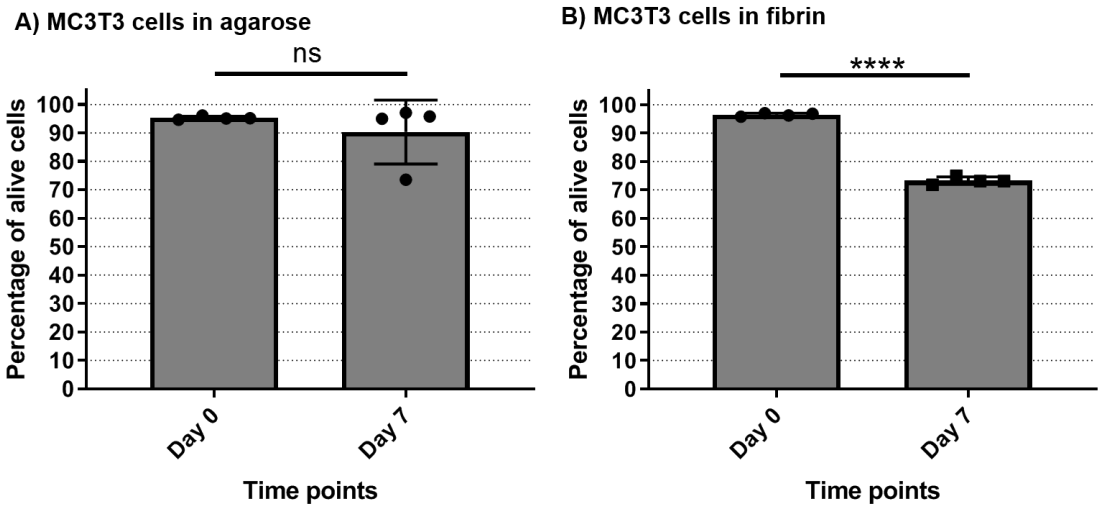

Figure 4.11: Percentage of live MC3T3 cells when encapsulated in A) agarose and B) fibrin hydrogels. *Unpaired, two-tailed t-tests were conducted with error bars showing the standard deviation (N=4 n=4).*

Gellan and collagen hydrogels were not assessed beyond the pilot study as they were eliminated as candidates for a cell-encapsulated hydrogel, as discussed in **section 3.4.4**. The qualitative results of live cell percentages encapsulated in agarose, gellan and fibrin hydrogels (**chapter 3**, **Figure 3.11**) showed an increase in CTF cells crowding when encapsulated in fibrin hydrogel and a decrease of CTF and MC3T3 crowding when encapsulated in agarose and gellan over time. Surprisingly, contradicting results were observed when CTF and MC3T3 cells were counted manually depending on their fluorescent labels in **Figures 4.8, 4.9, 4.10** and **4.11**. It was hypothesised that the presence of nucleases in FBS used for cell culture might have influenced disintegration of the dead cells' nuclei. This, in turn, could have influenced the count of dead cells, as it depended on the PI label binding to dead nuclei to generate fluorescence, ultimately resulting in lower dead cell count and a false higher percentage of live cells. Therefore, an experiment to test the effect of FBS enzymes on dead cells' nuclei was designed and performed. This experiment showed no significant difference in the number of dead CTF cells detected when they were cultured for 4 days with sDMEM (53.26K ± 2.61) compared to FBS-free sDMEM (45.81K ± 6.87, p = 00.15, **Figure 4.12**). Same findings were also observed after evaluating MC3T3 cells (number of cells after 4 days of culture in sDMEM = 40.75K ± 12, FBS-free sDMEM = 38.71 ± 10.90, p = 0.76, **Figure 4.13**).

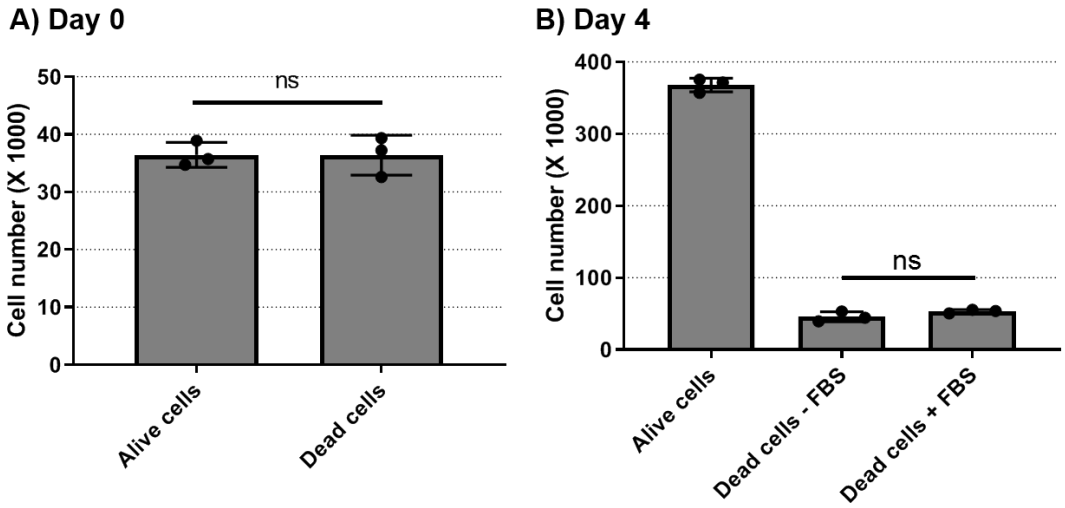

Figure 4.12: Assessment of the effect of FBS enzymes supplemented in culture media on nuclear material clearance at day 0 and day 4. *A) Number of live control CTF cells and dead cells at day 0. B) Insignificant difference between dead CTF cells cultured with FBS enzymes compared to dead CTF cells without FBS enzymes after 4 days of culture. Unpaired, two-tailed t-tests were conducted with error bars showing the standard deviation (in B, only dead cells without FBS and with FBS were included in the t-test) (N=3, n=4).*

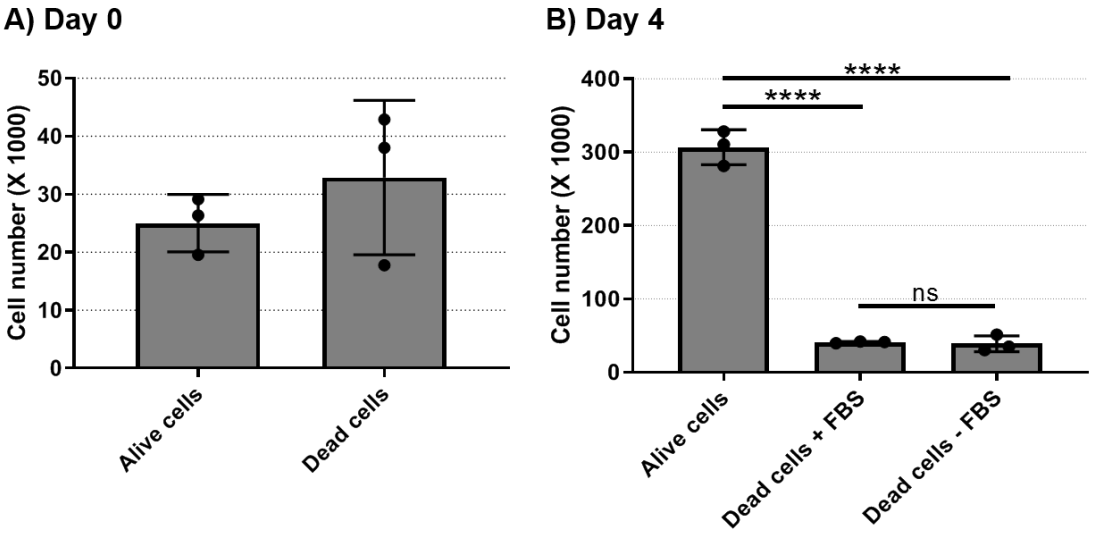

Figure 4.13: The effect of FBS enzymes supplemented in culture media on nuclear material clearance at day 0 and day 4. *A) Number of live and dead MC3T3 cells control at day 0. B) Insignificant difference between dead MC3T3 cells cultured with FBS enzymes compared to dead MC3T3 cells without FBS enzymes. Unpaired, two-tailed t-tests were conducted with error bars showing the standard deviation (in B, only dead cells without FBS and with FBS were included in the t-test) (N=3, n=4).*

4.4.1.4 Cell density by DNA quantification

Cell proliferation was an important indicator of hydrogel suitability for testing ECM formation and content. Hydrogels were expected to allow encapsulated cells to proliferate and form their ECM. However, if the hydrogel did not support cell proliferation, the encapsulated cells cannot produce ECM in abundance to replace the biodegradable scaffold. Therefore, agarose and fibrin hydrogels' support of cell proliferation was assessed by quantifying the DNA content of CTF and MC3T3 cells in the encapsulated hydrogels at day 0 and day 7.

4.4.1.4.1 Quantifying DNA of cells encapsulated in agarose hydrogel

DNA content of CTF cells encapsulated in agarose had increased significantly from day 0 (64.62 ng/ml ± 1.46) to day 7 (94.71 ng/ml ± 16.63) ($p = 0.03$, **Figure 4.14** A). Similarly, MC3T3 cells' DNA content was quantified when encapsulated in agarose hydrogel, which showed a significant decrease from 50 ng/ml ± 88 at day 0 to 28.33 ng/ml ± 0.75 at day 7 ($p = 0.01$, **Figure 4.15** A). DNA content of cells encapsulated in agarose showed a decrease and an increase in results, showing that both an increase and a decrease were possible, which gave confidence that the cell retrieval protocol used to isolate the cells from agarose was successful.

4.4.1.4.2 Quantifying DNA of cells encapsulated in fibrin hydrogel

Cell lysis buffer and homogenisation by sonication method

DNA content of CTF cells fell sharply from day 0 (34.62 ng/ml ± 9.52) to day 7 (8.10 ng/ml ± 3.54) when encapsulated in fibrin hydrogel ($p = 0.01$, **Figure 4.14** B). Also, the DNA content of MC3T3 cells when encapsulated in fibrin significantly decreased from 20 ng/ml ± 4.90 at day 0 to 10.71 ng/ml ± 1.27 at day 7 ($p = 0.03$, **Figure 4.15** B).

The decrease of DNA content over time when cells were encapsulated in fibrin hydrogel was unexpected as qualitative data had shown an increase in crowding of CTF cells over time (**Figures 4.6, 3.17,** and **3.19**). This could have been because of an unsuccessful cell retrieval method for fibrin hydrogel. Therefore, another methodology to retrieve cells from fibrin hydrogel was adopted from Carrion *et al.* (2014).

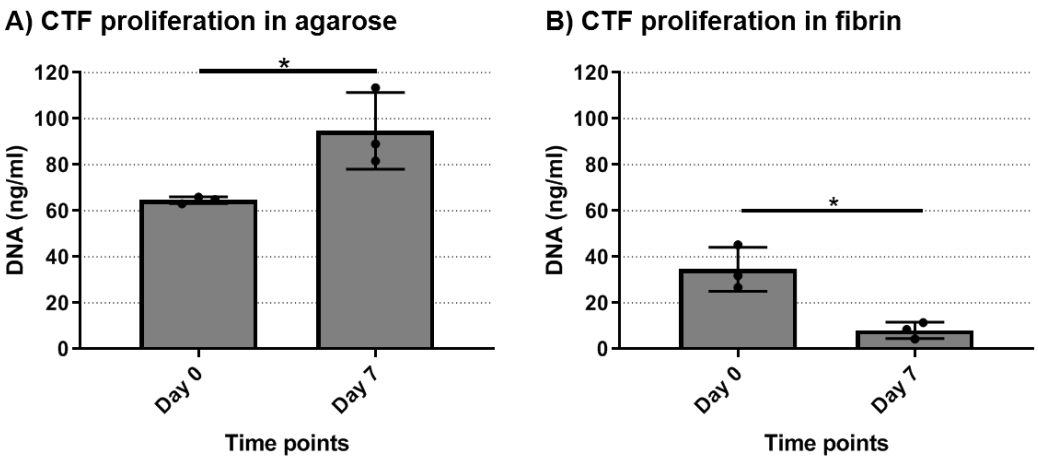

Figure 4.14: Proliferation of CTF cells when encapsulated in A) agarose, compared to B) fibrin*. The assessment was performed at days 0 and 7. Unpaired, two-tailed t-tests were conducted with error bars showing the standard deviation (N=3, n=4).*

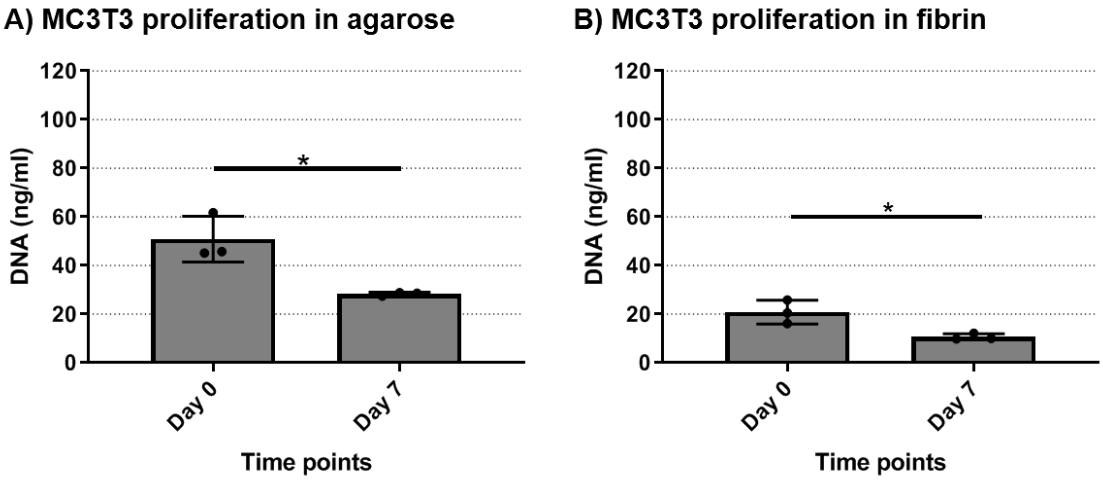

Figure 4.15: Proliferation of MC3T3 cells when encapsulated in A) agarose, compared to B) fibrin. *The assessment was performed at days 0 and 7. Unpaired, two-tailed t-tests were conducted with error bars showing the standard deviation (N=3, n=4).*

Nattokinase use to digest fibrin hydrogel method for cell retrieval

Fibrin hydrogel digestion was performed using nattokinase, as described in **section** 4.3.5.2.2. DNA quantification of CTF cells encapsulated in fibrin hydrogel and retrieved by the nattokinase method showed an increase from 79.39 ng/ml ± 41.51 at day 0 to 1680.00 ng/ml ± 95.85 at day 7 (p = <0.0001, **Figure 4.16** A). Similarly, MC3T3 cells' DNA quantification showed an increase from 128.00 ng/ml ± 32.30 at day 0 to 591.70 ng/ml ± 127.00 at day 7 (p = 0.0004, **Figure 4.16** B). These results showed that cells encapsulated in hydrogel increased their cell density over time. This came in support of the qualitative data presented in **section 3.4.3.2.2**.

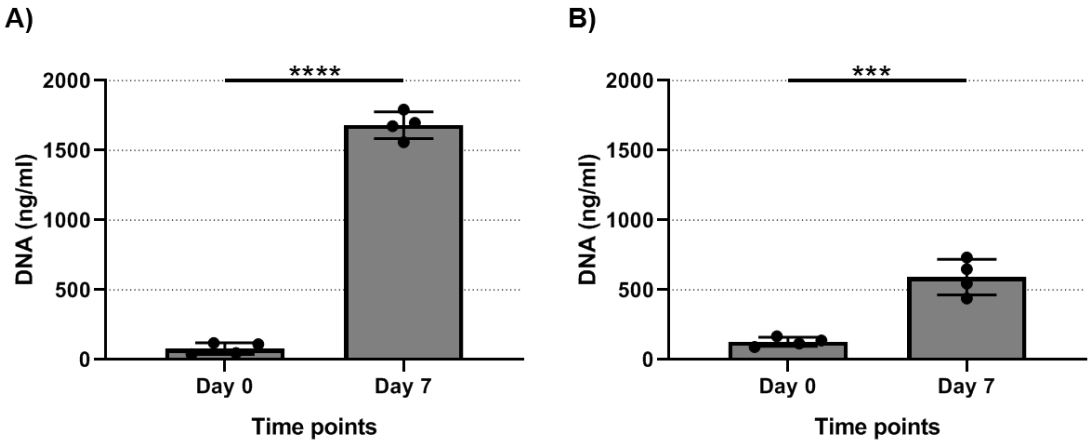

Figure 4.16: Cell numbers determined after quantification of DNA. *A significant increase in cell density can be observed after 7 days of culture in A) CTF and B) MC3T3 cells. Unpaired, two-tailed t-tests were conducted with error bars showing the standard deviation (N=4, n=3).*

Table 4.2: Summary characteristics of agarose, gellan, fibrin and collagen hydrogels for cells encapsulation.

	Repeatability *	Interface plane	Cell attachment	DNA quantification	Suitability for assays **	Ease of use
Agarose	✓	✓	×	✓	✓	✓
Gellan	×	✓	×	n/a	×	×
Fibrin	✓	✓	✓	✓	✓	✓
Collagen	×	×	✓	n/a	×	✓

* Repeatability refers to the ability to produce identical cell-encapsulated hydrogels.

** Suitability of hydrogel for various assays. Some assays require cell retrieval from the hydrogel. This couldn't be achieved easily in some of the hydrogels.

4.4.2 ECM formation

Bone and tendon cells used for previous experiments were sourced from different species (chick tendon fibroblasts and mouse osteoblasts), which was acceptable for system evaluation and hydrogel assessment. However, for a functional assessment of the co-culture effect on cellular communication, tendon and bone cells from the same species were needed.

To change to a single source of tendon and bone cells, rat tendon fibroblasts and osteoblasts were acquired as described in **sections 2.1.3.3 and 2.1.3.4**. The suitability of these cells for fibrin hydrogel encapsulation was tested by encapsulating the cells in fibrin and assessing their viability by qualitative calcein/PI cell viability staining as described in **section 4.3.2**.

Both RTF (rat tendon fibroblasts) and dROb (differentiated rat osteoblasts) showed good viability when observed at days 0, 4, 7 and 10 (**Figures 4.17** and **4.18**). These results showed that fibrin hydrogel was suitable for RTF and dROb cell encapsulation and was an appropriate option for further experimentation.

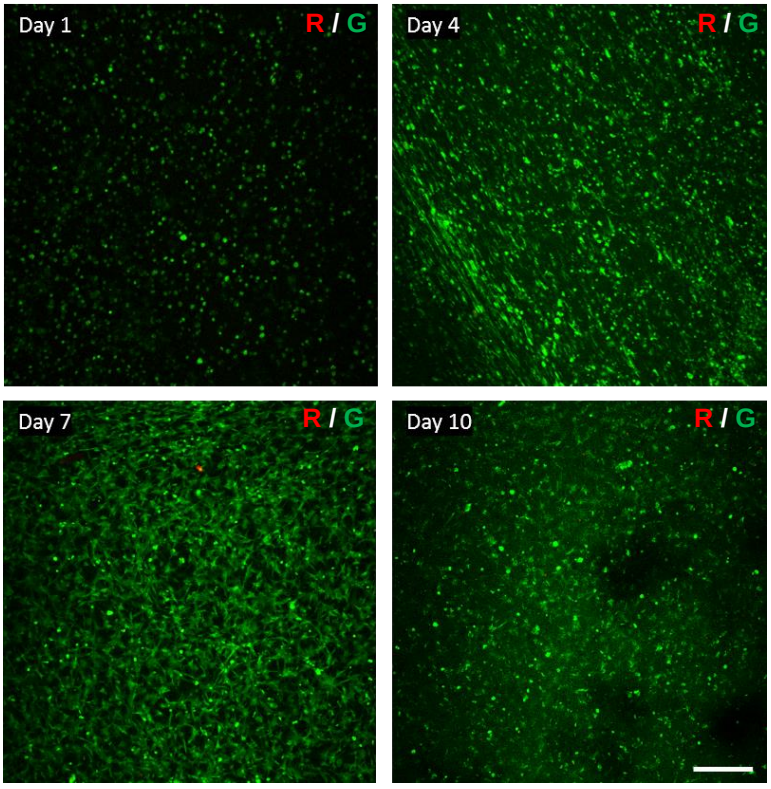

Figure 4.17: RTF cells maintained their viability when encapsulated in fibrin hydrogel over time. Calcein stained live cells green and PI stained dead cells red (N=3, n=3, representative images were chosen from a library of images acquired during the experiment). *Images were taken using combined red (R) and green (G) channels of CFM. Representative images were chosen from a library of images acquired during the experiment (N=3, n=4). (Scale bar = 500 µm)*

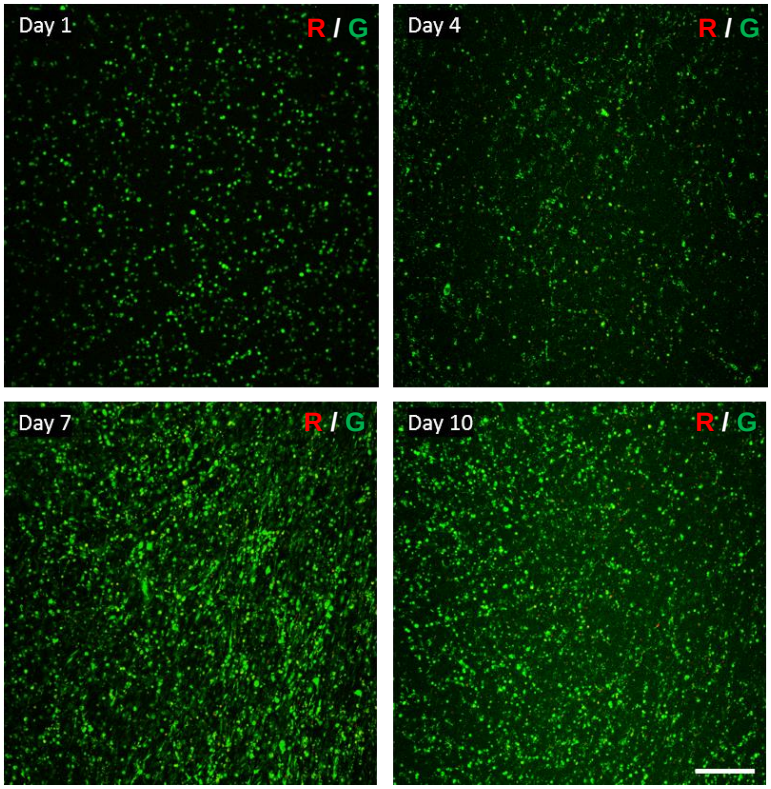

Figure 4.18: dROb cells maintained their viability when encapsulated in fibrin hydrogel over time. Calcien stained live cells green, and PI stained dead cells red (N=3, n=3, representative images were chosen from a library of images acquired during the experiment). *Images were taken using combined red (R) and green (G) channels of CFM. Representative images were chosen from a library of images acquired during the experiment (N=3, n=4). (Scale bar = 500 µm)*

4.4.2.1 Collagen content measurements in cell-encapsulated fibrin hydrogel

4.4.2.1.1 Pilot study

ECM collagen content in cell-encapsulated fibrin hydrogels was assessed to determine the effect of co-culture on the ECM formation of RTF and dROb cell-encapsulated hydrogels. Collagen content of cultured RTF-only cell-encapsulated fibrin hydrogels was measured at days 5 (51.01 µg/sample), 10 (64.51 µg/sample), 15 (61.80 µg/sample) and 20 (78.80 µg/sample) (**Figure 4.19** A). The time-point averages of collagen content were made from 6 repeats of RTF-only cell-encapsulated hydrogels for each time-point, which showed a notable difference between day 5 and day 20 (**Figure 4.19** A). Similarly, collagen content of dROb-only cell-encapsulated hydrogel was measured at days 5 (101.70 µg/sample), 10 (104.10 µg/sample), 15 (114.70 µg/sample) and 20 (135.50 µg/sample) (**Figure 4.19** B). For co-culture of RTF and dROb cell-encapsulated hydrogels, collagen measurements at days 5, 10, 15 and 20 were 125.40, 130.10, 131.70 and 166.80 µg/sample, respectively (**Figure 4.19** C). To compare the effect of co-culture

on ECM collagen content, the summation of RTF-only and dROb-only cell-encapsulated hydrogels' collagen content was compared to the RTF and dROb cell-encapsulated co-culture. Collagen content after the summation of separate RTF-only and dROb-only cell-encapsulated hydrogels at days 5, 10, 15 and 20 was 152.67, 168.65, 176.47 and 214.28 µg/sample, respectively (**Figure 4.19** D).

However, this experiment lacked experimental repeats and a day 0 measurement. The collagen content of cells that had been produced in the flasks during 2D cell culture and expansion before transferring them to their cell-encapsulated hydrogel might have had an influence on these results (**Figure 4.5**). Therefore, a day 0 collagen content measurement was needed to subtract the collagen content that had been transferred from cell expansion and 2D culture.

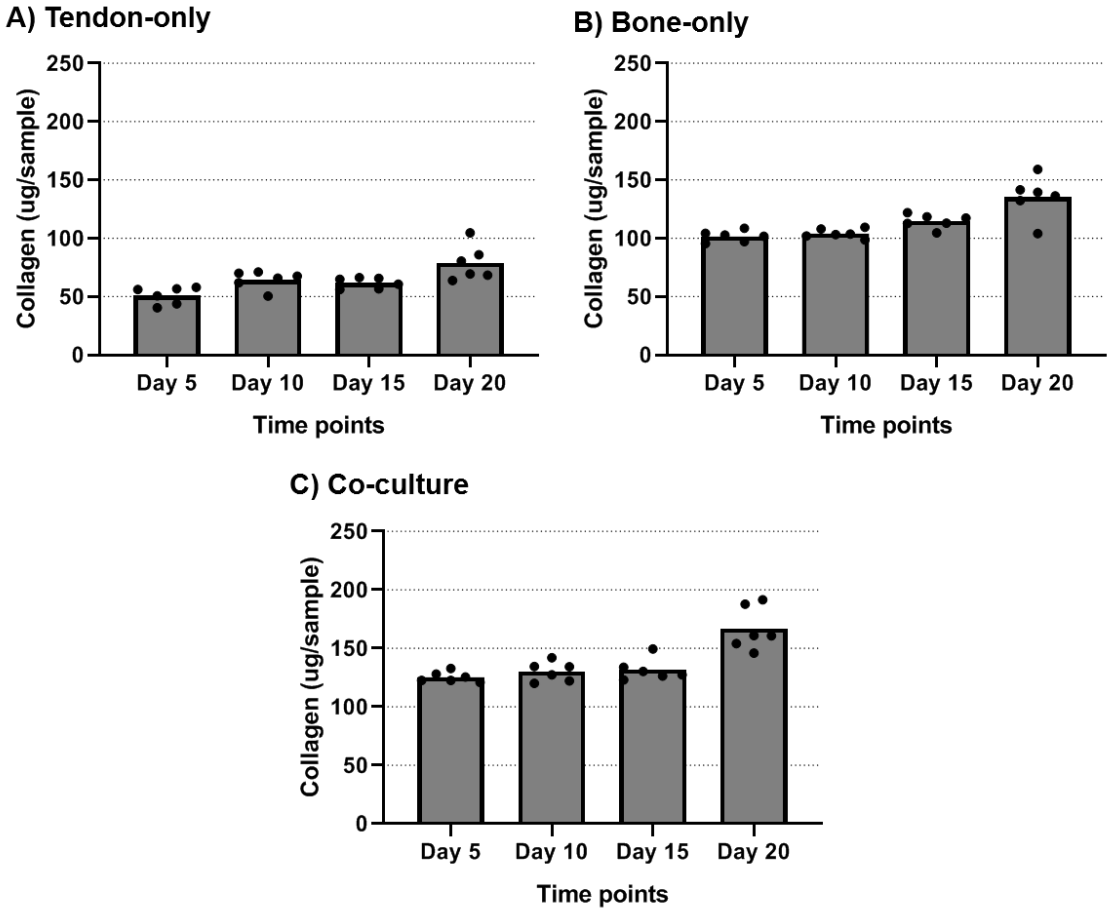

Figure 4.19: Pilot study for ECM collagen content. *ECM collagen content of A) RTF-only cell-encapsulated hydrogels, B) dROb -only cell-encapsulated fibrin hydrogels, and C) RTF and dROb cell-encapsulated co-culture. (N=1, n=6), scatter plot of technical repeats.*

4.4.2.1.2 Collagen measurements of cell-encapsulated fibrin hydrogel

As described previously, day 0 collagen content measurements are needed to quantify collagen produced during 3D cell-encapsulation culture. Additionally, the increasing trend of collagen measurements was visibly greater at day 20 compared to days 5, 10 and 15. Therefore, this experiment was designed to assess collagen measurements at day 0 and day 20.

Accordingly, collagen measurements of tendon-only cell-encapsulated hydrogels increased significantly from 14.34 µg/sample ± 2.18 at day 0 to 22.87 µg/sample ± 0.98 at day 20 (p = 0.0035, **Figure 4.20** A). Similarly, bone-only cell-encapsulated hydrogel collagen content increased significantly from 5.04 µg/sample ± 0.80 at day 0 to 214.50 µg/sample ± 26.12 at day 20 (p = 0.0002, **Figure 4.20** B). The co-culture of tendon and bone cells in cell-encapsulated hydrogels also resulted in a significant increase of collagen measurements from day 0 (34.13 µg/sample ± 7.69) to day 20 (231.80 µg/sample ± 17.28) (p = <0.0001, **Figure 4.20** C).

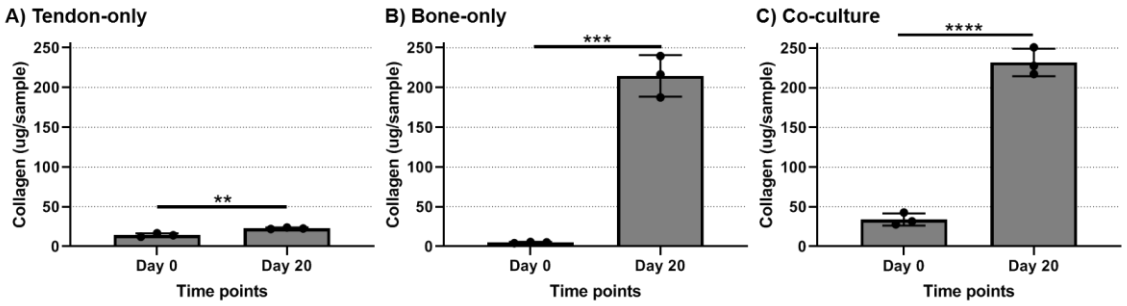

Figure 4.20: ECM collagen content measurements at day 0 and day 20 in A) tendon-only, B) bone-only, C) their co-culture encapsulated in fibrin hydrogel. *Unpaired, two-tailed t-tests were conducted with error bars showing the standard deviation (N=3, n=4).*

4.4.2.2 GAGs content measurements in cell-encapsulated fibrin hydrogel

4.4.2.2.1 A pilot study of GAGs measurements

ECM GAGs content in cell-encapsulated fibrin hydrogels was assessed to determine the effect of co-culture on the ECM formation of RTF and dROb cell-encapsulated hydrogels. GAGs content of cultured RTF-only cell-encapsulated fibrin hydrogels was measured at days 5 (2.87 µg/sample), 10 (1.92 µg/sample), 15 (2.71 µg/sample), and 20 (23.85 µg/sample) (**Figure 4.20** A). Similarly, GAGs content of dROb-only cell-encapsulated hydrogels was measured at days 5 (7.26 µg/sample), 10 (5.79 µg/sample), 15 (6.36 µg/sample) and 20 (15.09 µg/sample) (**Figure 4.20** B). The co-culture of RTF and dROb

cell-encapsulated hydrogels' collagen measurements at days 5, 10, 15,and 20 were 125.40, 130.10, 131.70 and 166.80 µg/sample, respectively (**Figure 4.20** C). To compare the effect of co-culture on ECM collagen content, the summation of RTF-only and dROb-only cell-encapsulated hydrogels' collagen content was compared to the RTF and dROb cell-encapsulated co-culture. Collagen content after the summation of separate RTF-only and dROb-only cell-encapsulated hydrogels at days 5, 10, 15 and 20 were 21.04, 24.28, 22.90 and 23.01 µg/sample, respectively (**Figure 4.20** D).

However, as the GAGs content of cell-encapsulated fibrin hydrogels was not assessed at day 0, it was not clear if the GAGs content was produced during 2D cell growth and expansion in the flasks or due to the 3D cell-encapsulated hydrogel culture (**Figure 4.5**). Therefore, the experiment was not repeated and re-designed to include day 0 as a reference to subtract GAGs content produced before cell-encapsulation in the fibrin hydrogel.

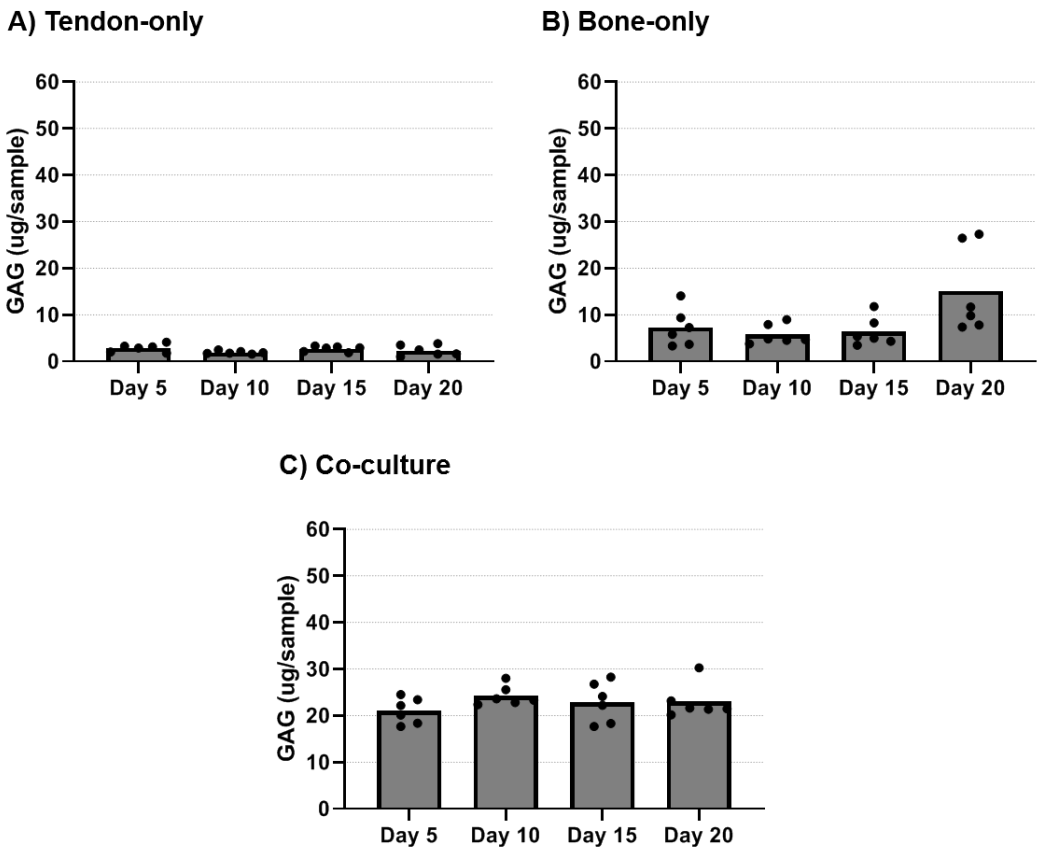

Figure 4.21: Pilot study for ECM GAGs content*. ECM GAGs content of A) RTF-only cell-encapsulated hydrogels, B) dROb-only cell-encapsulated fibrin hydrogels, and C) RTF and dROb cell-encapsulated co-culture. (N=1, n=6), scatter plot of technical repeats.*

4.4.2.2.2 GAGs measurements of cell-encapsulated fibrin hydrogel

As described previously, day 0 GAGs content measurements were needed to quantify the GAGs produced during 3D cell-encapsulation culture. Therefore, this experiment was designed to assess GAGs measurements at day 0 and day 20.

GAGs measurements of tendon-only cell-encapsulated hydrogels increased significantly from 3.64 µg/sample ± 0.92 at day 0 to 11.97 µg/sample ± 1.29 at day 20 (p = 0.0008, **Figure 4.22** A). Similarly, bone-only cell-encapsulated hydrogel collagen content increased significantly from 0.05 µg/sample ± 0.03 at day 0 to 16.88 µg/sample ± 3.27 at day 20 (p = 0.0009, **Figure 4.22** B). The co-culture of tendon and bone cells in cell-encapsulated hydrogels also resulted in a significant increase in collagen from day 0 (34.13 µg/sample ± 7.69) to day 20 (231.80 µg/sample ± 17.28) (p = <0.0001, **Figure 4.22** C).

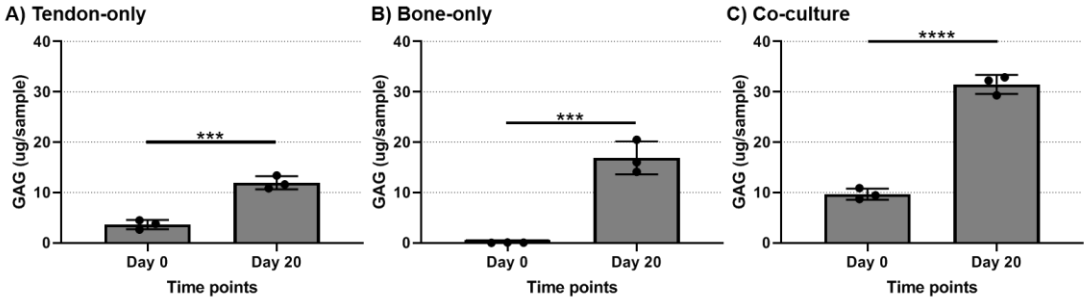

Figure 4.22: ECM GAGs content measurements at day 0 and day 20 in A) tendon-only, B) bone-only, and C) their co-culture encapsulated in fibrin hydrogel. *Unpaired, two-tailed t-tests were conducted with error bars showing the standard deviation (N=3, n=4).*

4.4.2.3 Studying the effect of 3D co-culture on ECM

Assessment of the cellular interaction effect in a 3D co-culture on ECM formation and cell density was performed. ECM collagen and GAGs content in cell-encapsulated scaffolds were assessed to determine the effect of co-culture on the ECM formation in tendon and bone cell-encapsulated hydrogels. Whereas, cell density was assessed by quantifying DNA content in cell-encapsulated hydrogels. The collagen, GAGs and cell density of the summation of tendon-only and bone-only encapsulated fibrin hydrogels were compared to a co-culture of tendon and bone encapsulated fibrin hydrogels. The assumption of the experiment was that the summation of RTF-only and dROb-only encapsulated fibrin hydrogels' collagen, GAGs and DNA content should equal the cell-encapsulated co-cultured fibrin hydrogel if cellular interaction in 3D co-culture did not affect ECM formation and cell density. However, if the co-culture

of RTF and dROb cell-encapsulated fibrin hydrogels was different than the summation of their monocultures, then co-culturing influenced ECM formation and DNA content (**Figure 4.23**). This experiment aimed to assess: 1) the effect of cellular interaction in the developed 3D co-culture, and 2) chondrogenic transformation caused by cellular interaction via measurement of GAGs content. This was hypothesised as chondrocytes produce significantly more GAGs than osteoblasts and tenocytes.

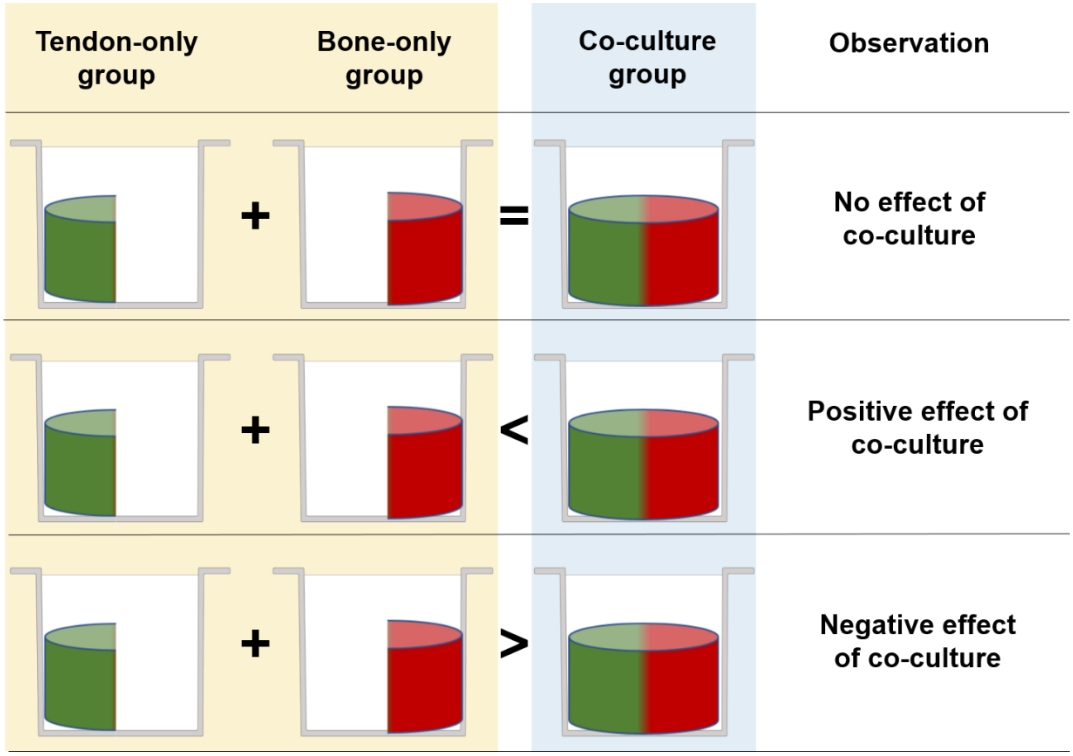

Figure 4.23: Assumptions of the effect of cellular interaction in a 3D co-culture on ECM formation and DNA content

4.4.2.3.1 Effect of co-culture on ECM collagen content

The ECM collagen of the summation of tendon-only and bone-only cell-encapsulated hydrogel monocultures was compared to their co-culture after 20 days of culture (**Figure 4.23**). This showed no significant difference between the summation of monocultures' collagen content and the co-culture collagen content ($p = 0.38$, **Figure 4.24**). The separate monocultures' summation of collagen content was 197.70 µg/sample ± 22.37 compared to 217.00 µg/sample ± 25.42 in the co-culture after 20 days. This observation meant that co-culturing bone and tendon cells using the developed 3D scaffold-dependent co-culture system did not influence ECM collagen content.

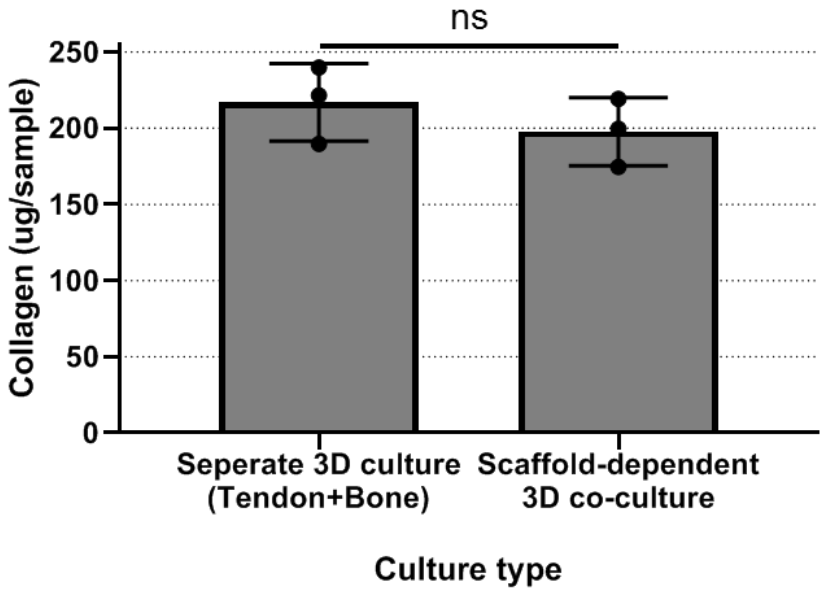

Figure 4.24: ECM collagen content after 20 days of culture with day 0 collagen content subtracted. *The summation of RTF-only and dROb-only compared to the co-culture of RTF and dROb cell-encapsulated hydrogels. Unpaired, two-tailed t-tests were conducted with error bars showing the standard deviation (N=3, n=4).*

4.4.2.3.2 Effect of co-culture on ECM GAGs content

Similarly, the ECM GAGs of the summation of tendon-only and bone-only cell-encapsulated hydrogel monocultures was compared to their co-culture after 20 days (**Figure 4.23**), and no significant difference found ($p = 0.38$, **Figure 4.25**). The GAGs content of summated separate monocultures was 25.15 µg/sample ± 5.48 compared to 21.81 µg/sample ± 2.99 in their co-culture after 20 days. This observation meant that co-culturing bone and tendon cells using the developed 3D scaffold-dependent co-culture system did not influence ECM GAGs content.

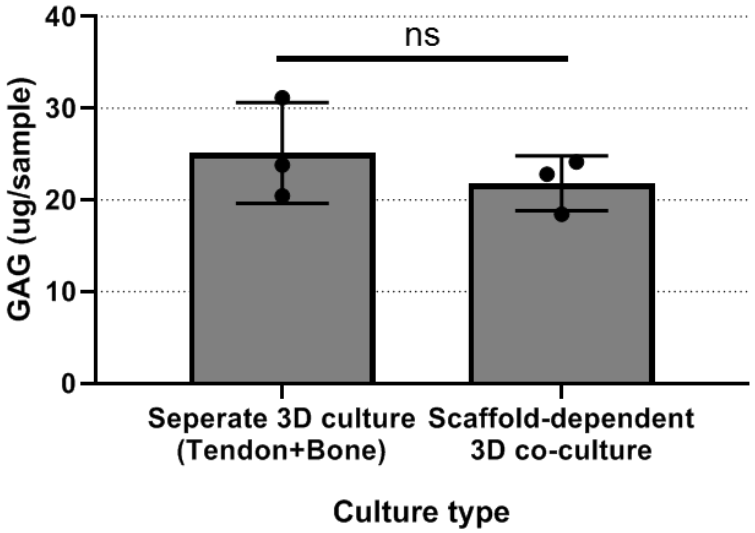

Figure 4.25: ECM GAGs content after 20 days of culture with day 0 GAGs content subtracted. *The summation of RTF-only and dROb-only compared to the co-culture of RTF and dROb cell-encapsulated hydrogels. Unpaired, two-tailed t-tests were conducted with error bars showing the standard deviation (N=3, n=4)*

4.4.3 Cell density measurements in cell-encapsulated fibrin hydrogel

Similar to ECM formation studies, cell density characterisation in 3D culture was performed. Also, the effect of co-culture of cell-encapsulated fibrin hydrogels with tendon and bone cells on cell density was assessed in the following sections.

4.4.3.1 A pilot study of cell density measurements

Examining cell density over time was performed to evaluate the proliferation of cells when encapsulated in fibrin hydrogel. An increase in cell number can increase ECM formation capacity. Therefore, DNA quantification was performed on tendon-only, bone-only, and their co-culture while encapsulated in fibrin hydrogel. In the pilot study, tendon-only cell-encapsulated fibrin hydrogels did not show an increase in cell density when measured at days 5 (11.91 ng/ml), 10 (15.15 ng/ml) and 15 (8.56 ng/ml). However, at day 20, cell density appeared to have increased to 65.33 ng/ml (**Figure 4.26** A). Bone-only cell-encapsulated fibrin hydrogel showed moderately more cell density than tendon cells at day 5 (93.85 ng/ml), 10 (319.10 ng/ml) and 15 (236.40 ng/ml). Similar to tendon-only cell density at day 20, the cell density of bone-only fibrin hydrogel showed an increase at day 20 (759.10 ng/ml) (**Figure 4.26** B). Furthermore, the co-culture of bone and tendon cell-encapsulated hydrogels showed a sharp increase in cell density between days 5 (43.78 ng/ml) and 10 (1306.24 ng/ml), then again between days 15 (1290.45 ng/ml) and 20 (2240.18 ng/ml) (**Figure 4.26** C). Nevertheless, this was a pilot study that was performed only once with 4 technical

repeats. Accordingly, no statistical analysis was performed on this data. Another study was performed that included testing cell density at days 0 and 20 (**Figure 4.27**).

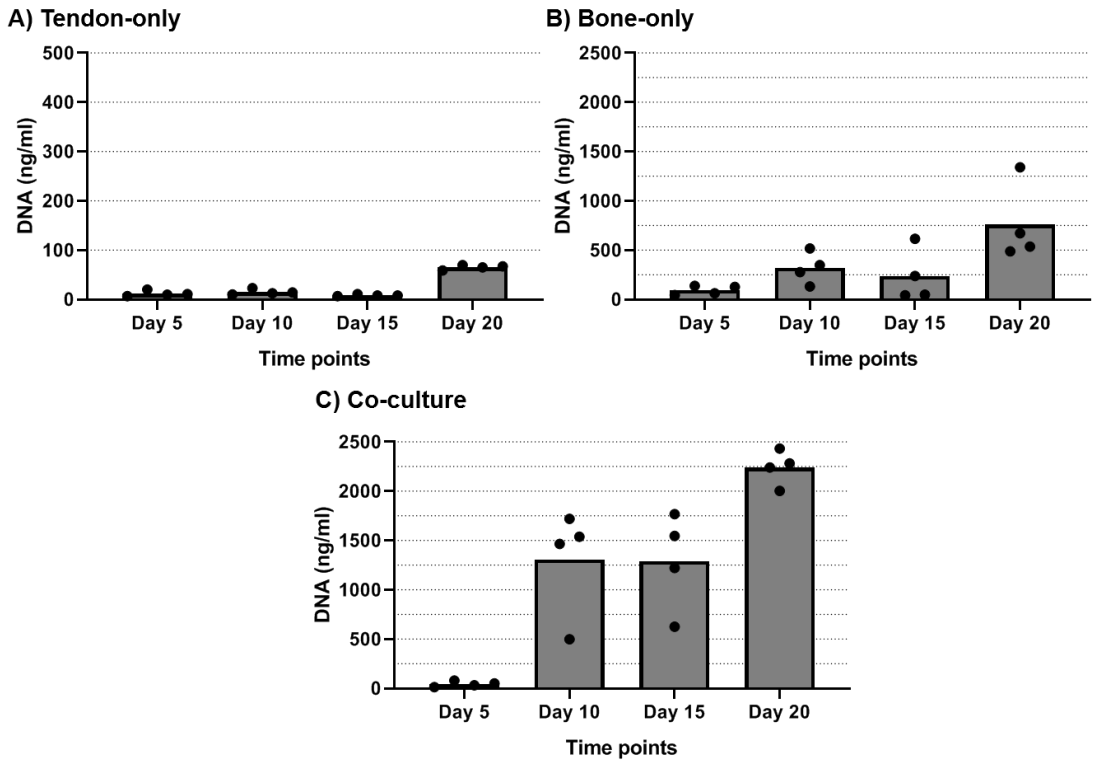

Figure 4.26: Pilot study for cell density content. *Cell density of A) RTF-only cell-encapsulated hydrogels, B) dROb-only cell-encapsulated fibrin hydrogels, and C) RTF and dROb cell-encapsulated co-culture. (N=1, n=4), scattered plot represents technical repeats of cell density measurements.*

4.4.3.2 Cell density measurements of cell-encapsulated fibrin hydrogel

Three independent experiments were performed to test cell density in cell-encapsulated fibrin hydrogels. All groups of samples from tendon-only, bone-only, and their co-culture in cell-encapsulated fibrin hydrogels showed a significant increase in cell density over time (**Figure 4.27**). Tendon-only cell-encapsulated fibrin hydrogels showed an increase from 121.40 ng/ml ± 38.31 at day 0 to 517.40 ng/ml ± 131.10 at day 20 ($p = 0.0074$ **Figure 4.27** A). Similarly, bone-only cell-encapsulated hydrogels' cell density increased significantly from 192.80 ng/ml ± 25.89 at day 0 to 1563.12 ng/ml ± 341.40 at day 20 ($p = 0.0023$, **Figure 4.27** B). Furthermore, the co-culture of tendon and bone cell-encapsulated fibrin hydrogel exhibited a significant increase over time from day 0 (284.00 ng/ml ± 2464) to day 20 (1876.67 ng/ml ± 307.030) ($p = 0.0009$, **Figure 4.27** C).

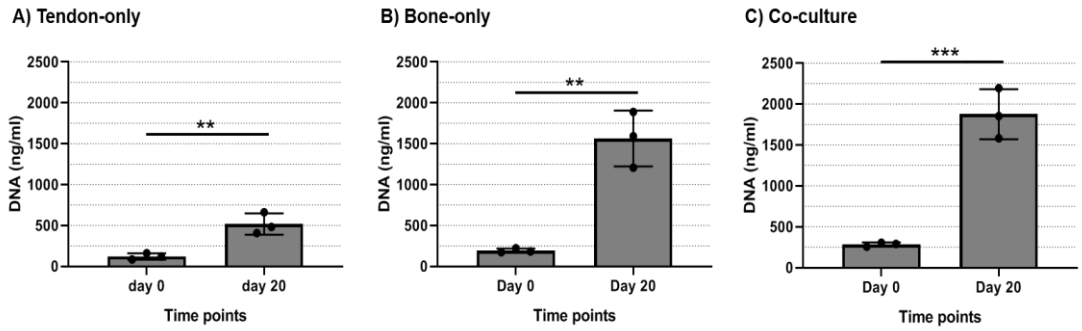

Figure 4.27: Cell density measurements at day 0 and day 20 in A) tendon-only, B) bone-only, and C) their co-culture encapsulated in fibrin hydrogel. *Unpaired, two-tailed t-tests were conducted (N=3, n=4).*

4.4.3.3 Effect of co-culture on cell density

Again, the cell density of the summation of tendon-only and bone-only cell-encapsulated hydrogel monocultures was compared to their co-culture after 20 days of culture (**Figure 4.23**), showing no significant difference (p = 0.58, **Figure 4.28**). The separate monocultures' summation of cell density was 2047.16 ng/ml ± 382.30 compared to 1876.45 ng/ml ± 307.30 in the co-culture after 20 days. This observation meant that co-culturing bone and tendon cells using the developed 3D scaffold-dependent co-culture system did not influence cell density.

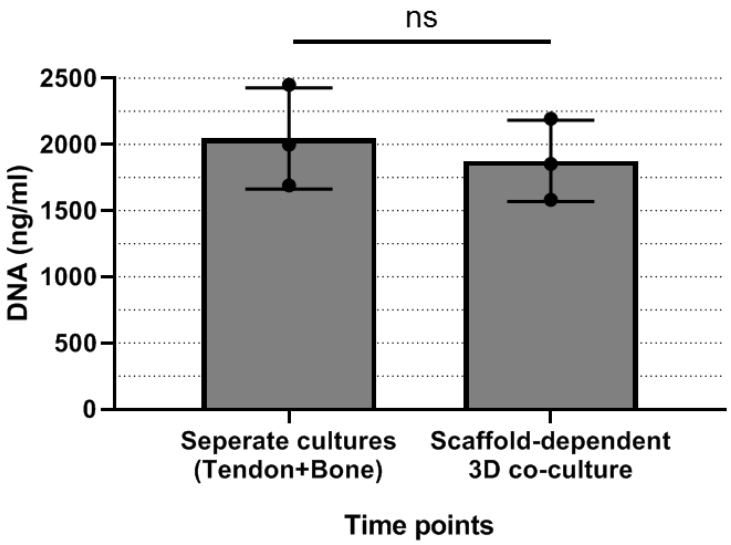

Figure 4.28: No significant effect of bone and tendon cell-encapsulated hydrogels 3D co-culture on cell density. *An unpaired, two-tailed t-test was conducted with error bars showing the standard deviation (N=3, n=4).*

4.4.4 Comparing 2D culture to the developed 3D scaffold-dependent culture

The use of 3D culture has been reported to result in an increase in cell proliferation, ECM formation and cell-cell communications (Tibbitt and Anseth 2012). Accordingly,

studies to investigate the difference between 2D and 3D culture in cell density and ECM formation (i.e. collagen and GAGs) after 20 days of culture was conducted using RTF and dROb cells. For a fair comparison between 2D and 3D, collagen and GAGs measurements were normalised to cell number (i.e. collagen and GAGs content per cell in each sample was presented instead of content per sample).

The number of cells in a single well of a 24-well plate was compared to their numbers when cultured in the scaffold-dependent 3D culture method, also performed in a 24-well. The number of tendon cells after 20 days of culture in 2D was 218.20K cells ± 42.85, which was significantly less than 111.00K cells ± 29.01 when cultured in cell-encapsulated fibrin hydrogel 3D culture ($p = 0.0230$, **Figure 4.29** A). On the other hand, the number of bone cells in 2D (330.47K cells ± 20.36) culture was significantly less than their numbers in 3D (1484.21K cells ±.326.30) ($p = 0.0036$, **Figure 4.29** B).

ECM collagen content in 2D culture of tendon cells (0.026 ng/cell ± 0.005) was significantly higher than cell-encapsulated 3D culture in fibrin hydrogel (0.015 ng/cell ± 0.005) ($p = 0.04$, **Figure 4.30** A). Likewise, ECM collagen content in 2D culture of bone cells (0.495 ng/cell ± 0.070) was significantly higher than cell-encapsulated 3D culture in fibrin hydrogel (0.140 ng/cell ± 0.047) ($p = 0.0019$, **Figure 4.30** B).

Moreover, the ECM GAGs content of 2D culture of tendon cells at day 20 was 0.222 ng/cell ± 0.024, which was significantly higher than 3D cell-encapsulated culture in fibrin hydrogel (0.016 ng/cell ± 0.003) ($p = 0.0001$, **Figure 4.31** A). Also, GAGs content in 2D culture of bone cells (0.171 ng/cell ± 0.011) was significantly higher than 3D cell-encapsulated culture in fibrin hydrogel (0.011 ng/cell ± 0.001) ($p = 0.0001$, **Figure 4.31** B).

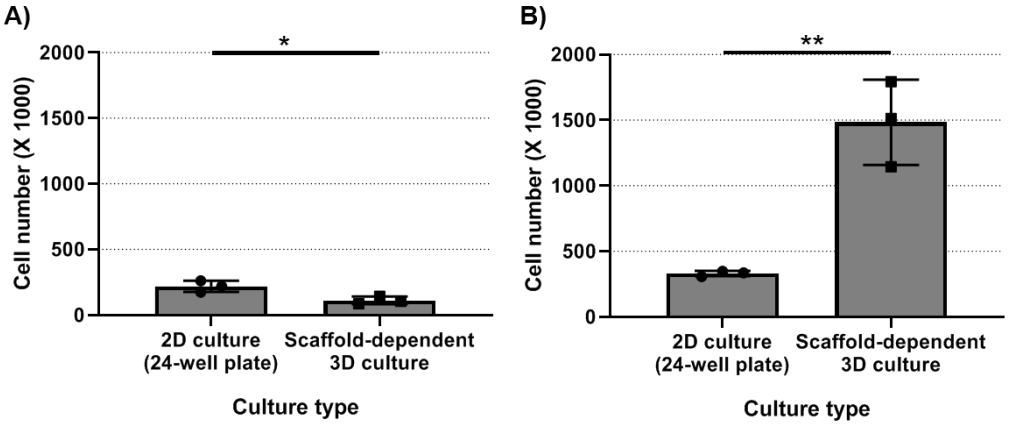

Figure 4.29: Cell numbers compared between 2D (24-well plate) and 3D scaffold-dependent cultures of A) tendon cells and B) bone cells. *Unpaired, two-tailed t-tests were conducted with error bars showing the standard deviation (N=3, n=4).*

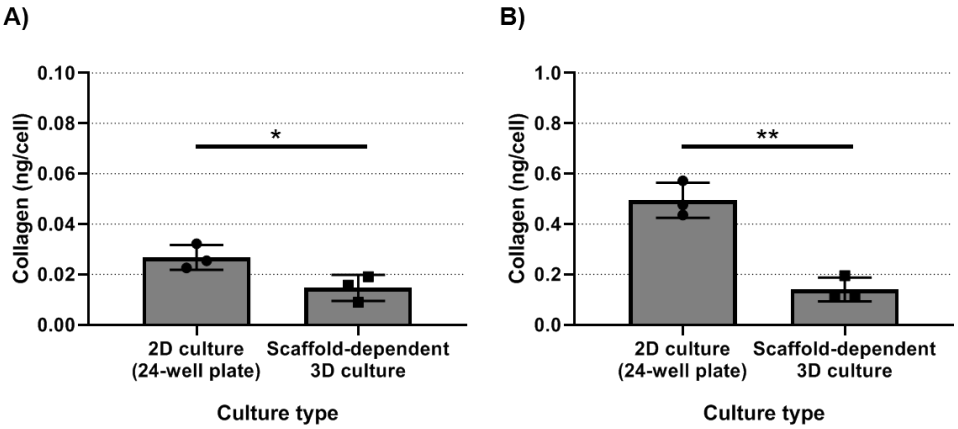

Figure 4.30: Collagen content of ECM after normalisation to cell number compared between 2D (24-well plate) and 3D scaffold-dependent cultures of A) tendon cells and B) bone cells. *Unpaired, two-tailed t-tests were conducted with error bars showing the standard deviation (N=3, n=4).*

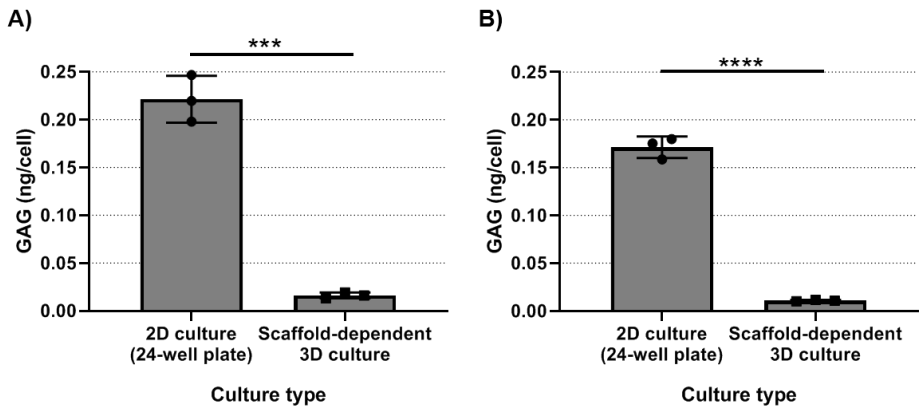

Figure 4.31: GAGs content of ECM after normalisation to cell number compared between 2D (24-well plate) and 3D scaffold-dependent cultures of A) tendon cells and B) bone cells. *Unpaired, two-tailed t-tests were conducted with error bars showing the standard deviation (N=3, n=4).*

In summary, the suitability of agarose, gellan, fibrin and collagen hydrogels for cell-encapsulation was assessed. Collagen and fibrin hydrogels were suitable for cell attachment for both CTF and MC3T3 cells. Whereas, CTF cells' viability was best in fibrin and improved over time in agarose, compared to gellan and collagen. On the other hand, MC3T3s showed better viability in gellan and fibrin. Additionally, the DNA content of CTF cells showed an increase when cultured in fibrin. This was supported by the qualitative evidence of increased cell crowding, presented in **section 3.4.1**.

Moreover, these results were correlated with the interface-plane results of **section 3.3.4**. These results showed that collagen hydrogel was not suitable for side-by-side co-culture, which lost its form and resulted in a tilted interface-plane. This could cause false-positive migration results when assessed by the perpendicular projection of CFM. Therefore, fibrin hydrogel was chosen as the most suitable hydrogel for cell-encapsulated scaffold-dependent 3D co-culture. A results summary of hydrogel support for cell culture is presented in **Table 4.2**.

Characterisation of ECM collagen and GAGs content in cell-encapsulated fibrin hydrogel with tendon and bone cell monocultures and their co-culture after 20 days was performed. It was shown that collagen and GAGs content increased over time (**Figures 4.20** and **4.22**). These results were used to study the effect of co-culture on ECM content of collagen and GAGs in the following section. Moreover, 3D co-culture of tendon and bone cells in the scaffold-dependent system did not affect collagen and GAGs content of the ECM significantly (**Figures 4.24** and **4.25**).

Also, in the cell density results section, cell density was characterised in cell-encapsulated fibrin hydrogel with tendon and bone cell monocultures, and their co-culture over 20 days. It has been shown that ECM collagen and GAGs content increase over time (**Figure 4.27**). These results were used to study the effect of co-culture on cell density and showed no significant difference between the summation of tendon and bone monocultures and their co-culture (**Figure 4.28**).

Finally, the number of tendon cells in 2D was higher than their numbers in the 3D cell-encapsulated fibrin hydrogel (**Figure 4.29** A). In contrast, the number of bone cells in 2D was significantly less than their numbers in 3D cell-encapsulated fibrin hydrogel (**Figure 4.29** B). Moreover, 2D culture was compared to 3D cell-encapsulated hydrogel culture of bone and tendon cells, showing less ECM collagen and GAGs content when compared to 2D culture after 20 days (**Figures 4.30** and **4.31**).

4.5 Discussion

The two main aims of this chapter were to assess hydrogel suitability for cell encapsulation and to determine the effect of bone and tendon cell-encapsulated hydrogel co-culture on ECM formation and cell density. This was achieved by using the 3D cell-encapsulated hydrogel co-culture system designed and developed in chapter 3. However, the 3D cell-encapsulated hydrogel co-culture needed to support cell attachment, viability, proliferation and ECM formation. These were important aspects of creating a successful tissue interface model. Therefore, agarose, gellan, fibrin and collagen hydrogels were investigated to choose a suitable hydrogel for use in the 3D cell-encapsulated hydrogel co-culture system. This was followed by the investigation of ECM formation by quantifying collagen and GAGs content of the chosen hydrogel cell-encapsulated co-culture, in addition to cell density, over 20 days of culture. This was followed by studying the effect of 3D co-culture on cell density, and ECM collagen and GAGs content after 20 days of culture. Moreover, a comparison between standard 2D cell culture and 3D cell-encapsulated hydrogel was performed to assess the advantage of 3D culture over 2D culture.

Hydrogel choices for 3D cell culture were numerous (**Table 1.1**). However, a selection of four hydrogels was performed based on successful 3D culture and widespread use (Aufderheide and Athanasiou 2005a; Bayrak and Yilgor Huri 2018; Dean *et al.* 2007; Ferris *et al.* 2013; Font Tellado, Balmayor, and Van Griensven 2015; Silva-Correia, Oliveira, and Reis 2016; Stevens *et al.* 2016). These hydrogels were agarose, gellan, fibrin and collagen. Subsequently, the most suitable hydrogel of these choices would be used for ECM investigations. Therefore, these hydrogels were studied regarding their support for cell attachment, viability and proliferation. As fibrin and collagen are normal cellular hosts in animals, they present attachment proteins that facilitate cell attachment (Pierschbacher and Ruoslahti 1984; Ratner and Bryant 2004; Ruoslahti, Hayman, and Pierschbacher 1985). Whereas, agarose and gellan were not expected to support cell attachment as they were not a normal host for cells; however, they are widely used in the 3D culture field as delivery vehicles for drugs, non-anchorage dependent cell culture, or for 3D culture of anchorage-dependent cells after chemical hydrogel modification (Aufderheide and Athanasiou 2005; Batorsky *et al.* 2005; Cascone *et al.* 2001; Ferris *et al.* 2013). This was confirmed by the results of the cell attachment experiment (**Table 4.1**).

Further studies performed to choose a suitable hydrogel included determination of live cell percentage in cell-encapsulated agarose, gellan, fibrin and collagen hydrogels. The expectation at day 0 was that most of the cells would be alive. However, an interesting finding showed low viability for CTF cells at day 0 when encapsulated in agarose and gellan, compared to fibrin and collagen (**Figure 4.8**). Notably, the percentage of live MC3T3 cells at day 0 was high in all hydrogels (**Figure 4.10**). This observation meant that CTF cells were vulnerable to the cell-encapsulation process in agarose and gellan. This process involved using the hydrogels at 40°C to re-suspend a pellet of cells. It was hypothesised that their viability might have been affected by either the high temperature or viscosity of the cell-encapsulated hydrogels causing increased pressure on the CTF cells.

In contrast, fibrin and collagen were used at room temperature. Moreover, the viscosity of fibrin and collagen was much thinner during the process of cell-encapsulation. Surprisingly, on day 7, CTF-encapsulated agarose hydrogels showed an increase in the percentage of living cells (**Figure 4.9**). This surprising observation was seen in four separate independent experimental repeats (**Figure 4.9**). CTF-encapsulated gellan hydrogels showed no improvement in the percentage of living CTF cells from day 0; therefore, no further testing was performed. Another surprising finding was the percentage of live CTF and MC3T3 cells in collagen hydrogel. Interestingly, despite displaying a high percentage of live cells on day 0, the percentage fell considerably at day 7 (**Figures 4.8** and **4.10**). The fact that the percentage of live cells was high at day 0 eliminates methodological and preparation effect on cell viability, i.e., encapsulating the cells at 4°C during collagen hydrogel preparation did not have an effect on cells' viability. This finding raised serious concerns about the use of collagen for further investigation. Moreover, for ECM evaluation, a collagen quantification method was used which cannot be used if the cell were encapsulated in collagen hydrogel. However, cells encapsulated in fibrin hydrogel showed attachment signs, better cell viability, higher cell density and reliable structural integrity (**Table 4.2, Figures 4.9, 4.11, 4.14,** and **4.15**). Accordingly, fibrin hydrogel was chosen for ECM formation and cell density studies.

The aim of the live/dead assay experiment was to assess the viability of CTF and MC3T3 cells when encapsulated in hydrogels to choose a suitable candidate. However, the results were misleading as percentages of live cells did not reflect cell numbers. Accordingly, percentage of viability could be high even if the cells did not

proliferate. Therefore, manual counting of cells was attempted. Despite the total number of cells in each sample being known at day 0, and using the same methodology of acquiring datasets from CFM images, the total number of cells in each sample was non-comparable for several reasons. Firstly, the size of cell-encapsulated agarose, gellan, collagen and fibrin hydrogels changed over time. This change was hydrogel-type mediated. For example, fibrin and collagen cell-encapsulated hydrogel shrunk to 40% of their original size, compared to agarose and gellan hydrogels which retained almost the same size when CTF cells were encapsulated in them (**Figure 4.6** C and D). This shrinkage meant that under the same CFM settings, fibrin and collagen cell-encapsulated hydrogels pseudo-manifested more cells. Secondly, each hydrogel type showed various degrees of opacity over time. This interfered with CFM laser penetration levels for detecting fluorescence from cells. Therefore, more cells could have been detected in a clearer cell-encapsulated hydrogel type compared to a more opaque type. Accordingly, the number of cells in this study were not reliable, and another method to quantify cell density was required.

There are no reliable cell proliferation methods dedicated for use in 3D culture. The field of 3D cell culture is faced with difficulties to establish reliable and reproducible cell proliferation assays compared to the extensively researched 2D cell culture. This is because of the widely varied materials and techniques of 3D cell culture. Most of the current solutions for this are modifications of 2D cell culture and proliferation assays (**Table 4.3**). Those solutions are mostly case-specific to the condition of a specific 3D cell culture technique. For example, CellTiter-Glow 3D cell proliferation assay by Promega is designed to assess proliferation in 3D culture of spheroids, as per the manufacturer's description (Promega, UK). 2D cell culture proliferation assays are performed depending on quantification of either DNA presence, proliferation protein, cellular metabolism or live/dead cell visualisation and manual counting. A key obstacle to quantifying DNA from 3D cell culture was the difficulty of retrieving cells' DNA from the sample, as the cells were trapped and attached to the scaffold. This was particularly evident in cell-encapsulated hydrogel 3D cell culture. Similarly, retrieving cellular metabolites to assess cell proliferation was equally challenging as the penetration rates of different agents differ according to the scaffold used. Consequently, a trial for live/dead cell labelling and manual counting was attempted. The experiment of percentage of live cells was originally designed to show cell proliferation. The numbers of live and dead cells were intended to be used as a proliferation indicator over time. However, as mentioned earlier, due to the use of

multiple hydrogels and the distinct characteristics of these hydrogels, an accurate calculation of cell number was not possible.

Hydrogel characteristics like shrinkage over time affected the dimensions of the area of interest. Moreover, different inter-hydrogel transparency affected the fluorescence detection sensitivity with CFM in addition to intra-hydrogel transparency change over time. These were the two major reasons that the percentage of live cells did not reflect cellular proliferation, but rather a live cells percentage. This percentage could be useful as information about the status of the cells in terms of viability but cannot be used as an indicator of cell proliferation. Hence, another method needed to be adopted to measure cell density in the cell-encapsulated hydrogels over time.

Another attempt to quantify cells' DNA in cell-encapsulated hydrogels was through the optimisation of the 2D based CyQuant™ DNA quantification assay. CTF cells encapsulated in agarose and fibrin hydrogels were retrieved and assayed (**Figure 4.14**). The results showed an increase in DNA content of CTF cells in agarose after 7 days of culture (**Figure 4.14** A). However, surprisingly lower DNA of CTF cells was quantified at day 7 when CTF cells were encapsulated in fibrin hydrogel (**Figure 4.14** B). This was unexpected for two reasons. Firstly, CTF cells encapsulation in fibrin hydrogel showed an increase in cell crowding over time (**section 3.4.4**). Secondly, it had been proven that dead cells' DNA content did not disintegrate over culture time (**Figure 4.12**), which meant that the DNA content at day 0 should remain and be picked up at day 7. However, this was not the case, as the DNA content of CTF cells was significantly lower, which meant that the CTF cells encapsulated in fibrin hydrogel could not be retrieved from fibrin hydrogel after 7 days by the method described in **section 4.3.4.2** (**Figures 4.14** B and **4.15** B). Therefore, an alternative cell retrieval method was adapted.

Hydrogel-specific breakdown enzymes are available for some hydrogels, such as collagenase for collagen and nattokinase for fibrin (Caliari and Burdick 2016; Carrion *et al.* 2014). The use of these enzymes was expected to breakdown the cell-encapsulated hydrogel and release the cells. The cells theoretically could be collected after the hydrogel broke down, and cells' DNA could be quantified. As collagen hydrogel use for cell encapsulation was discarded earlier in the study, no further DNA assessment was conducted. The use of nattokinase enzyme to retrieve CTF and MC3T3 cells encapsulated in fibrin hydrogel was performed, followed by DNA quantification using CyQuant™ DNA quantification assay. This experiment showed a

significant increase in DNA presence after 7 days of culture in CTF and MC3T3 cells encapsulated in fibrin hydrogel (**Figure 4.16**).

Depending on earlier experiments, fibrin hydrogel was found to be the most appropriate hydrogel for cell-encapsulated co-culture studies to evaluate ECM formation and content (**Table 4.2**). Surprisingly, collagen hydrogel showed unfavourable conditions for cell culture in 3D. The solidifying conditions for collagen required the mixture of cells and collagen to be incubated for one hour (compared to the 5 minutes required for fibrin, agarose and gellan). This long waiting time caused the encapsulated cells to precipitate at the bottom of the culture well. Moreover, the side profile experiments in chapter 3 (**Figure 3.18**) showed an angled interface, which was not favourable for the system as it changes the interface contact surface area between the two cell populations and produces false positive results of cell migration when examined using CFM. Furthermore, encapsulated cells' viability in collagen was low compared to other hydrogels (**Figure 4.8** and **4.10**), which was also a surprising result as collagen has been used regularly in 3D cell culture. This could be the result of decreased supply of gases and nutrients to the cells due to impaired diffusion through the collagen hydrogel. For these reasons, collagen hydrogel was excluded from further examination.

A decision needed to be made about the cell types used in the experiments. The CTF and MC3T3 cells were from two different species, whereas most co-culture studies in the field have been performed in same species (Lu *et al.* 2010; Markham, Simpson, and Baker 2015; Takahashi *et al.* 2007; Yip and Cho 2013; Young 2003). For this reason, a single species of tendon and bone cells was required. Human tendon and bone cells were considered to replace CTF and MC3T3 cells. Nonetheless, due to technical and cost issues, such as the slow growth of the cells and the high cost of culture maintenance, alternative options were pursued. Rat cells were nominated as cells were easily accessible and could be adopted to the system without further optimisation. RTF cells were isolated from adult rat calcaneal tendon (RTF) while rat osteoblasts (dROb) were purchased (see cell sources **section 2.1.3**).

An experiment was conducted to confirm RTF and dROb cells' suitability for fibrin hydrogel encapsulation, showing qualitatively that viability of both cells was excellent at days 0, 4, 7 and 10. Moreover, it qualitatively showed an increase in cell crowding over time. This indicated proliferation of the encapsulated cells in the fibrin hydrogel (**Figures 4.17** and **4.18**).

Table 4.3: Examples of currently used techniques to assay cell proliferation in 3D cultures

Assay name	Detection method	Target	Type of assay	Cell extraction /digestion	Ease of use	reference
Cell counting Kit-8 (CCK-8)	Colorimetric	Metabolic	Continuous	Not required	Simple	(Liu et al. 2017)
Alamar Blue assay	Colorimetric	Metabolic	Continuous	Not required	Simple	(Li et al. 2016)
MTS assay	Colorimetric	Metabolic	Endpoint	Not required	Simple	(Radhakrishnan et al. 2018)
Manual DNA quantification	Spectrophotometer	Physical DNA	Endpoint	Required	Difficult	(Rajabi et al. 2018)
Quant-iT PicoGreen dsDNA reagent and kit	Fluorometric	Fluorescent probe	Endpoint	Required	Simple	(Chun et al. 2015; L. Wu, Lin, and Qin 2015)
CyQUANT Cell Proliferation Assay Kit	Fluorometric	Fluorescent probe	Endpoint	Required	Simple	(Nagai et al. 2012)
ATPlite 1Step 3D	Luminometric	Metabolic	Continuous	Required	Simple	New
CellTiter-Glo® 3D Cell Viability Assay	Luminometric	Metabolic	Endpoint	Required	Simple	(Edmondson, Adcock, and Yang 2016)

The RTF and dROb cells were used for ECM formation and content studies. The cells were acquired from a single animal source, as the experiments conducted were aimed to verify the reliability and reproducibility of the 3D co-culture system. Accordingly, the results can be used to prove the stability of the system but cannot be generalised over the rat population.

ECM of bone, tendon and enthesis is mainly composed of collagen (Adamczyk *et al.* 2008). Hence, it was important to monitor collagen formation and deposition in the ECM and the effect of co-culture on the collagen content of RTF and dROb cell-encapsulated hydrogel co-culture. On the other hand, GAGs are moderately present in bones and tendons and abundantly present in cartilages (Couchman and Pataki 2012). Accordingly, higher GAGs levels were expected if fibrocartilaginous tissue transformation occurred after co-culture of RTFs and dRObs in cell-encapsulated fibrin hydrogel when compared to RTF-only and dROb-only cell encapsulated monocultures as described, previously reported by Calejo *et al.* (2018) and Wang *et al.* (2007). However, these two studies were performed in 2D standard culture, which has already been established to not be an ideal culture to mimic natural tissues (see **section 1.2.2.1**). Consequently, quantitative collagen and GAGs assays were used to study the effect of 3D co-culture on ECM formation and content.

Sircol™ soluble and insoluble collagen assays were used to quantify collagen content in cell-encapsulated fibrin hydrogels. Soluble collagen assay detects newly formed collagen that is pepsin soluble. Whereas, insoluble collagen is used to identify mature collagen that is pepsin insoluble. The result of these two assays were summed together as total collagen and used to compare the total collagen production by co-culture of RTF and dROb cell-encapsulated hydrogel to the summation of total collagen detected in RTF-only and dROb-only cell-encapsulated hydrogels (**Figure 4.19**). Although a pilot study showed a decrease in collagen content due to co-culture, this was not a statistically significant difference when the experiment was repeated (N=3) (**Figure 4.24**).

GAGs in cell-encapsulated fibrin hydrogels were quantified using Blyscan™ GAGs assay. The results of this essay from RTF and dROb cell-encapsulated co-cultures was compared to the summation of RTF-only and dROb-only GAGs assay results. The pilot study of this experiment showed an increase in GAGs resulting from the RTF and dROb cell-encapsulated hydrogel co-culture (**Figure 4.21**). However, upon repeating the experiment, there was no statistically significant difference in GAGs content between co-cultured RTF and dROb cell-encapsulated hydrogels compared to the summation of RTF-only and dROb-only cell-encapsulated monocultures (**Figure 4.25**). A discrepancy in expectations of total ECM collagen and GAGs content was observed during the pilot studies for both assays (**Figures 4.19** and **4.21**). This was attributed to the fact that day 0 levels of collagen and GAGs were not subtracted

from the results. This was because of the collagen and GAGs that were formed during 2D cell growth and expansion in flasks before the cells were used for 3D cell-encapsulation in fibrin hydrogels (**Figure 4.5** A). Therefore, in the repetition of these pilot studies, day 0 collagen and GAGs content was calculated and subtracted from day 20 collagen and GAGs results (**Figures 4.5** B, **4.20**, and **4.22**). These experiments showed that there was no effect of 3D co-culture on collagen or GAGs content of the ECM (**Figures 4.24** and **4.25**).

Moreover, the cell density of cell-encapsulated hydrogels was assessed for tendon and bone cell monocultures and their co-cultures (**Figure** 4.26). It was evident that cells proliferated in the cell-encapsulated hydrogel, and their DNA quantification increased over time (**Figure 4.27**). The studying of the effect of co-culture on cell density did not include deletion of day 0 DNA quantification values, as known and similar starting cell numbers were used for both tendon and bone cells. Similar to collagen and GAGs assays, the cell density experiment did not reveal an effect of 3D co-culture on the tendon and bone cell-encapsulated fibrin hydrogel (**Figure 4.28**).

As a final investigation in this chapter, a comparison between 2D and 3D culture was conducted. The aim was to evaluate the performance of tendon (RTF) and bone (dROb) cells in the developed 3D cell-encapsulated culture. This showed that bone cells proliferated significantly more in the cell-encapsulated hydrogel in a 24-well plate compared to a standard 2D 24-well plate (**Figure 4.29** B). However, collagen and GAGs content of these bone cell-encapsulated hydrogels was significantly less compared to 2D culture when total values were divided by cell number (**Figures 4.30** B and **4.31** B). On the other hand, tendon cells showed significantly less cell numbers, collagen and GAGs content when encapsulated in fibrin hydrogel compared to their standard 2D culture (**Figures 4.30** A and **4.31** A). There are mixed reports in the literature about the effect of 3D culture on cell proliferation. Many studies have reported a decrease in cell proliferation (Chitcholtan, Sykes, and Evans 2012; Fallica *et al.* 2012; Luca *et al.* 2013; Maria *et al.* 2011; Yang and Marek-Sadowska 2018). Interestingly, one study had reported an increase in cell proliferation in 3D culture when cells were encapsulated in Matrigel (Hongisto *et al.* 2013). However, in the same study, the same cell type that showed an increase in proliferation in Matrigel displayed a significant decrease in proliferation when cultured on the synthetic poly(2-hydroxyethyl methacrylate).

In conclusion, a methodical approach to selecting a suitable hydrogel for cell encapsulation has been researched for use in a 3D co-culture study. A comparison between agarose, gellan, fibrin and collagen hydrogel was conducted, which resulted in selecting fibrin hydrogel as the most suitable hydrogel for cell encapsulation and usage in the revised 3D scaffold-dependent co-culture system. Fibrin hydrogel was used to assess ECM formation for bone-only and tendon-only cell-encapsulated hydrogels. Furthermore, these results were compared to a 3D scaffold-dependent cell encapsulated co-culture of tendon and bone cells. This showed no evidence of co-culture effect on ECM formation and content as collagen and GAGs in the ECM were assessed and compared. A number of limitations were encountered throughout the study. These included the low sample size, limited number of hydrogels, inability to normalise collagen and GAGs results to cell number, long experimental time limiting the number of repeats, and the expensive cost of CFM and Sircol™ and Blyscan™ assays.

Nonetheless, the system has provided a successful methodology to co-culture cell-encapsulated hydrogels with a single interface between two distinct cell populations. The effect of cell-encapsulated 3D co-culture in hydrogel could be further researched to explore possible immunohistochemical or gene expression changes. Moreover, the use of biochemical and physical stimuli is of interest to monitor the difference between a static bone and tendon cell-encapsulated fibrin hydrogel 3D co-culture compared to a biochemically and/or physically stimulated sample. Accordingly, the most important results from this chapter are 1) describing a methodology to create a successful 3D co-culture between two distinct populations of cells, 2) providing 3D-optimised cell/hydrogel suitability assessment techniques, and 3) showing how the system can be used to study the effect of 3D co-culture.

Chapter 5. Investigating the use of bone and tendon spheroids to create a 3D co-culture *in vitro*

5.1 Introduction

Cell-cell and cell-ECM interaction are crucial for most cells in the body to form a functional 3D tissue. Due to the disadvantages of 2D culture (discussed previously in **section 1.2.1**), attempts to culture cells in 3D have been made to bridge the gap between 2D monolayer cell culture and *in vivo* animal studies, in the hope of decreasing the ambiguity of 2D monolayer cell-based studies, saving time, animal resources and research funds. Various models of 3D culture have been documented in the literature in the past three decades. One of the earliest models for 3D culture that closely resembles native tissues was organotypic tissue explants. These models have been extensively used in most biomedical research fields. Nevertheless, this model has its challenges, such as difficulty in obtaining specimens and ethical approval. Moreover, typical explants depend on diffusion of nutrients from media to support tissue viability, which is difficult to achieve in the core of the tissue efficiently due to the size of explants (Lin and Chang, 2008).

Accordingly, a smaller sized 3D culture on the scale of 100-500 µm would create a feasible alternative to tissue explants. The first demonstration of such small scale 3D culture was reported by Holtfreter (Holtfreter, 1943) and Moscona (Moscona and Moscona, 1952), in which they reported the use of cell aggregates as a 3D culture forming a spheroid. This spheroid culture presented a greater similarity to native tissue over monolayer 2D culture (Lin and Chang, 2008). Subsequently, spheroid culture gained increasing interest in many fields of biomedical research, such as tissue engineering, cell biology, cancer research and drug discovery and development.

Spheroid culture use for enthesis research

When tendon cells and bone cells come into contact during foetal life, the formation of the enthesis is triggered (Lu and Thomopoulos, 2013). Moreover, an *in vitro* interface model between two of the main cell types present at the enthesis has been engineered previously by Wang and colleagues (Wang *et al.*, 2007). This interface model was designed to culture bone and tendon cells in direct contact. Then, chondrogenic transformation markers were investigated in the resulting interface region between the two cell regions. The study showed that direct contact between bone and tendon cells caused an up-regulation of chondrogenic markers in the cells of the interface region compared to the cells in the pure osteoblast or fibroblast regions. However, this study was performed in a 2-dimensional (2D) setting, which

does not represent the natural physiological environment of cells in tissues. It is now well recognised that 2D cell cultures do not represent the natural cellular environment or structure (Edmondson *et al.*, 2014) and accordingly, it is not ideal to assume that cell response and behaviour in 2D culture is a valid imitation of native tissue (Baker and Chen, 2012). To overcome this, spheroid culture can be used to re-evaluate the effect of direct contact between bone and tendon cells in 3D.

5.1.1 Chapter aim and objectives

The main aim of this chapter was to assess the use of spheroid culture for the formation of bone and tendon spheroids that could be used for co-culture. Establishing this model will allow study of the effect of co-culture on cells and ECM formation.

Specific objectives for this chapter were to

1. Establish a standard method to produce tendon-only and bone-only spheroids;
2. Produce co-cultures of minimum-contact (mini-coculture) and maximum-contact (max-coculture);
3. Examine the difference in spheroid size over time of tendon-only, bone-only, mini-coculture and max-coculture spheroids to determine the time point of complete spheroid formation (smallest size) and growth thereafter;
4. Correlate between size, cell density and ECM formation of spheroids to assess the effect of co-culture over time;
5. Investigate the effect of different degrees of contact in co-culture (i.e. mini-coculture vs max-coculture) on gene expression.

5.2 Methods

5.2.1 Spheroid generation and co-culture

RTF and dROb cells were used to make tendon and bone spheroids, respectively. The method of generating spheroids depended on culturing the cells on a cell-repellent surface in the form of U-bottom 96-well plates (CELLSTAR®, Greiner bio-one, UK) as described in **section 3.3.2.2**. To generate a single spheroid for one cell type, 50K cells were cultured in a well of a cell-repellent, U-bottom 96-well plate for 24 hours (**Figure 5.1**).

There were two co-culture variants used, a mini-coculture and a max-coculture. The mini-coculture was produced by generating a spheroid for tendon and bone cells

separately. Then single bone and tendon spheroids were moved together into an empty well, producing two spheroids, one tendon and one bone, in a single well. For max-coculture, 50K of RTF cells were mixed with 50K of dROb cells in a homogenised solution to make a single spheroid.

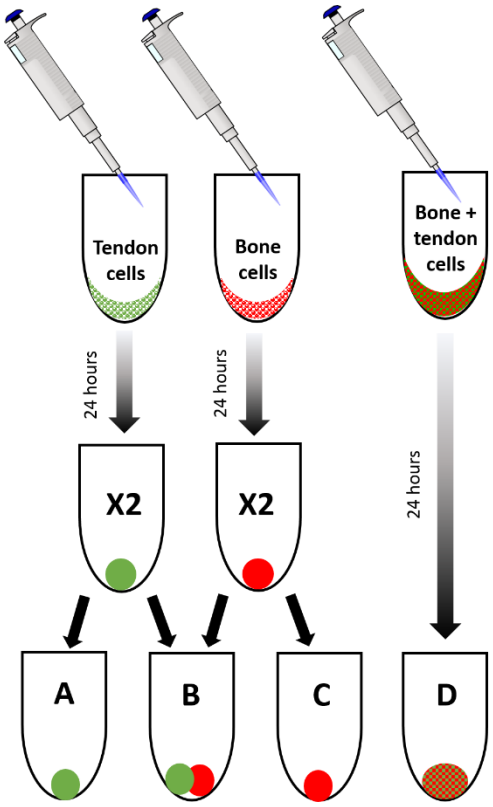

Figure 5.1: Protocol for generating spheroids of different groups for all experiments in this chapter <u>except</u> the co-localisation experiment. *After one day of culture, A) tendon-only, B), mini-coculture, C) bone-only, and D) max-coculture spheroid groups were produced.*

5.2.2 Co-localisation of cell types in spheroids

RTF cells were labelled with GFP using a green cell tracker (CellTracker™ green CMFDA, Life Technologies, UK), while dRObs were labelled with an RFP using a red cell tracker (CellTracker™ Red CMTPX, Life Technologies, UK). CFM was used to image 4 groups: two-tendon spheroids, two-bone spheroids, mini-coculture, and max-coculture (**Figure 5.2**). Imaging was conducted on days 1, 2, 4 and 6 (N=3, n=3). The datasets acquired from CFM were processed using ImageJ software (Schindelin *et al.*, 2012) to produce a single image of z-axis projection. Laser intensity and detector gain were adjusted according to experimental need, considering fluorescent labelling quality, number of cells, photobleaching, depth of images and background noise, with a 4x atmospheric lens. Data sets obtained were analysed by NIS Elements (Nikon,

UK), ImageJ (National Institute of Health, USA), and Imaris software (Bitplane, Oxford Instruments, UK). ImageJ software was used to create a z-axis projection of fluorescence acquired from datasets to produce a single figure that represented the collective of all fluorescence detected in a dataset of images.

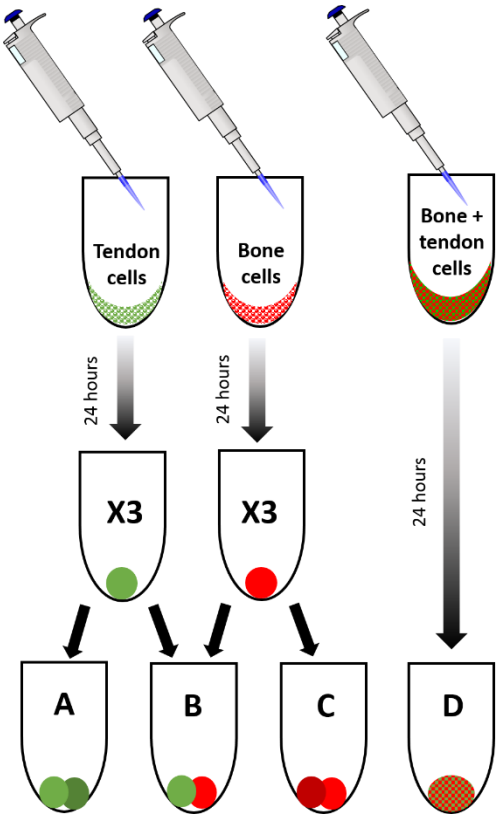

Figure 5.2: Protocol for generating spheroids of different groups for the co-localisation experiment*. After one day of culture, A) two tendon-only, B) mini-coculture, C) two bone-only, and D) max-coculture spheroid groups were produced.*

5.2.3 Spheroid cross-sectional surface area (CSA) comparison

Four groups were compared: single tendon spheroid, single bone spheroid, mini-coculture, and max-coculture. A light microscope (Leica DMi1, UK) with an objective lens of 10x magnification was used to take images of all groups at days 1, 3, 5, 7, 10, 15 and 20 (N=8, n=3). Cross-sectional surface was measured using an automated process that was recorded as a macro for Fiji software (Fiji is just imageJ, Schindelin *et al.*, 2012). The process of generating data and its analysis steps is depicted in **Figure 5.3**.

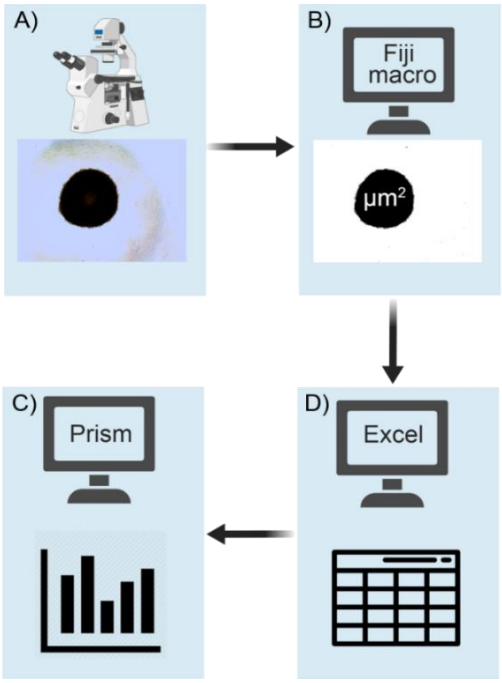

Figure 5.3: Process for obtaining CSA of spheroids. *A) Brightfield views of spheroids were imaged using an inverted microscope with an objective lens of 10x magnification. B) Images were analysed by Fiji software to calculate surface area. C) Means were calculated using Excel software. Finally, D) results were statistically analysed using Prism software.*

5.2.4 Cell density in spheroids

DNA content of spheroids was measured at different time points to determine cell density (CyQUANT™ Cell Proliferation Assay Kit, Molecular Probes, Invitrogen, UK). The DNA content of the four groups described in (**5.2.3**) was compared to determine the effect of different degrees of co-culture on cell density (N=3, n=4).

5.2.5 ECM evaluation

The collagen and GAGs content of ECM formed after spheroid formation was assessed (Sircol™ and Blyscan™, Biocolor, UK). Four groups of spheroids were measured: tendon-only, bone-only, mini-coculture, and max-coculture spheroid groups, which were prepared as described in **section 5.2.1**. Twelve samples were collected at days 5, 10, 15, and 20 from each group and 6 of them were used for collagen content assessment using Sircol™ soluble and insoluble collagen assays as described in the manufacturer's protocol (N=1, n=6). The other six samples of each time point were used to assess GAGs using Blyscan™ GAGs assay (Blyscan™, Biocolor, UK) (independent experiment N=1, technical repeats n=6). For one sample in the collagen and GAGs assays, 10 spheroids were used. This was due to the limitation of collagen and GAGs' range of sensitivity detected by the assays.

Optimisation was performed by repeating the experiment at different time points. Optimised time points were day 0 and day 20 (N=3, n=4). The optimisation was necessary in order to subtract the collagen and GAGs formed during 2D cell growth and expansion before spheroid formation.

5.3 Results

5.3.1 Spheroid formation

Qualitative proof of tendon-only, bone-only, mini-coculture, and max-coculture spheroids formation was obtained after 1 day of culture (**Figure 5.4**) (N=3, n=2). 50K RTF and dROb cells were cultured separately in U-bottomed, cell-repellent 96-well plates for 24 hours, which resulted in the formation of tendon and bone spheroids (**Figure 5.4** A and B). For mini-coculture, a single bone and tendon spheroid was transferred to one well after 24 hours of separate culture (**Figure 5.4** C). For max-coculture, a homogenised mixture of bone and tendon cells (50K each) was cultured for 24 hours, resulting in the formation of a single spheroid (**Figure 5.4** D). These results confirmed the formation of a bone-only, tendon-only, mini-coculture, and max-coculture spheroids, which could be used to study RTF and dROb cells' co-localisation, density, ECM formation and gene expression in different levels of contact in 3D co-culture.

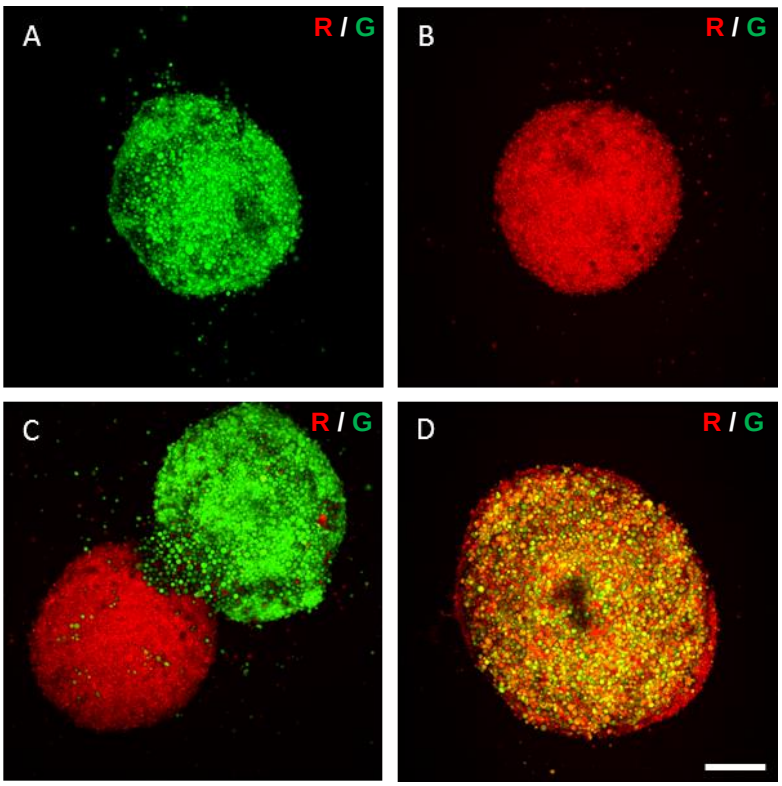

Figure 5.4: Z-axis projection of CFM datasets of A) tendon, B) bone, C) mini-coculture, and D) max-coculture spheroids after 1 day of culture. *Images were taken using combined red (R) and green (G) channels of CFM. Representative images were chosen from a library of images acquired during the experiment (N=3, n=4). (Scale bar = 500 µm)*

5.3.2 Co-localisation of RTF and dROb cells in spheroid co-culture

Intra-spheroid cell organisation of RTF and dROb cells in mini-coculture and max-coculture was observed after 1, 2, 4 and 6 days of culture. Moreover, two tendon-only spheroids and two bone-only spheroids were monitored as a reference for the interaction of the same type of cells.

Two tendon-only spheroids were placed together after one day of culture for spheroid formation (**Figure 5.5**). The two spheroids remained separate, with space visible between them when observed at day 2 (**Figure 5.5**). At day 4, the two spheroids showed signs of merging, as the space between them was lost, and the spheroid boundaries were lost between them (**Figure 5.5**). Finally, at day 6, the two spheroids formed one oval shaped spheroid marking their complete merger (**Figure 5.5**).

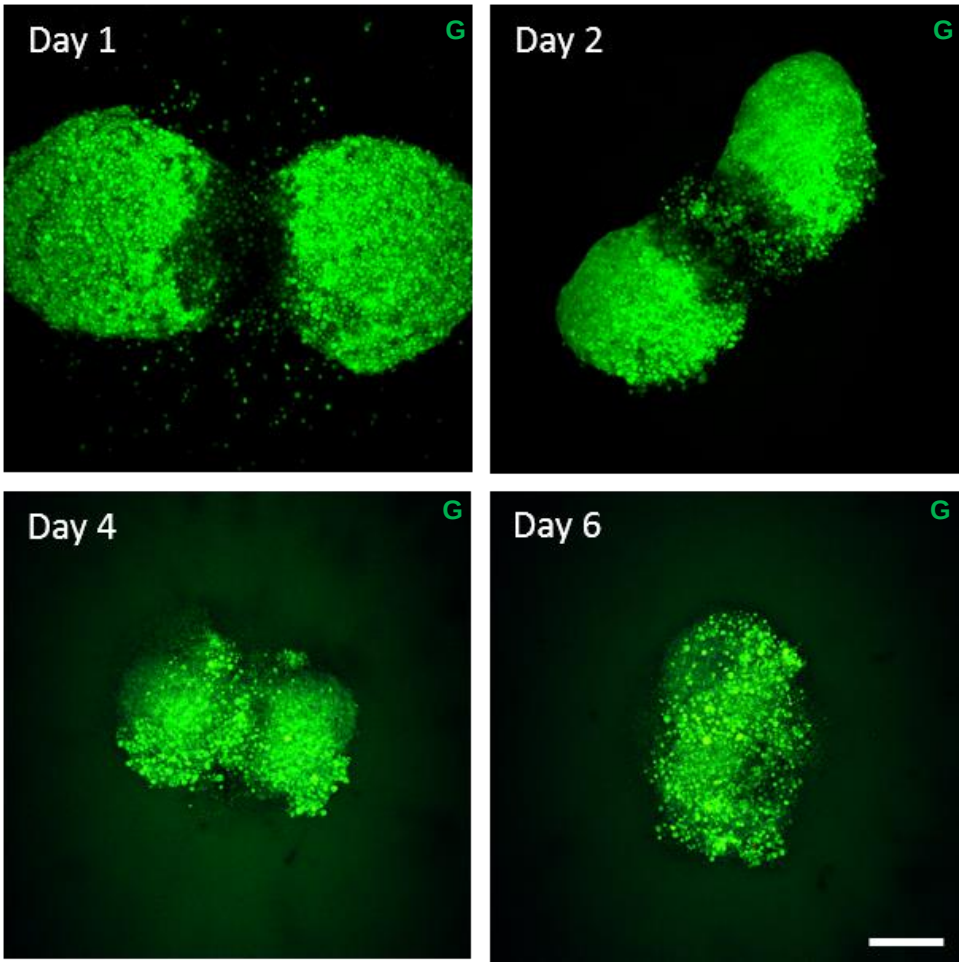

Figure 5.5: Z-axis projection of CFM datasets of two tendon spheroids*. The two spheroids started merging by day 4, finally fusing completely by day 6. Images were taken using the green (G) channel of CFM. Representative images were chosen from a library of images acquired during the experiment (N=3, n=4). (Scale bar = 500 µm)*

Two bone-only spheroids were also moved together after spheroid formation at day 1 (**Figure 5.6**). The two spheroids started merging, as the space between them was lost, and the opposing two spheroid boundaries started to blur at day 2 (**Figure 5.6**). The merging was still not complete at day 4 as the two spheroids were still distinguishable (**Figure 5.6**). However, at day 6, the two spheroids were completely indistinguishable, creating a single spheroid, which did not have clear boundaries probably because of cell proliferation at different rates on different sides of the spheroids (**Figure 5.6**). This experiment showed that if two spheroids of the same cell type (RTF or dROb) are cultured together, they merge completely by day 6 of culture (N=3, n=4).

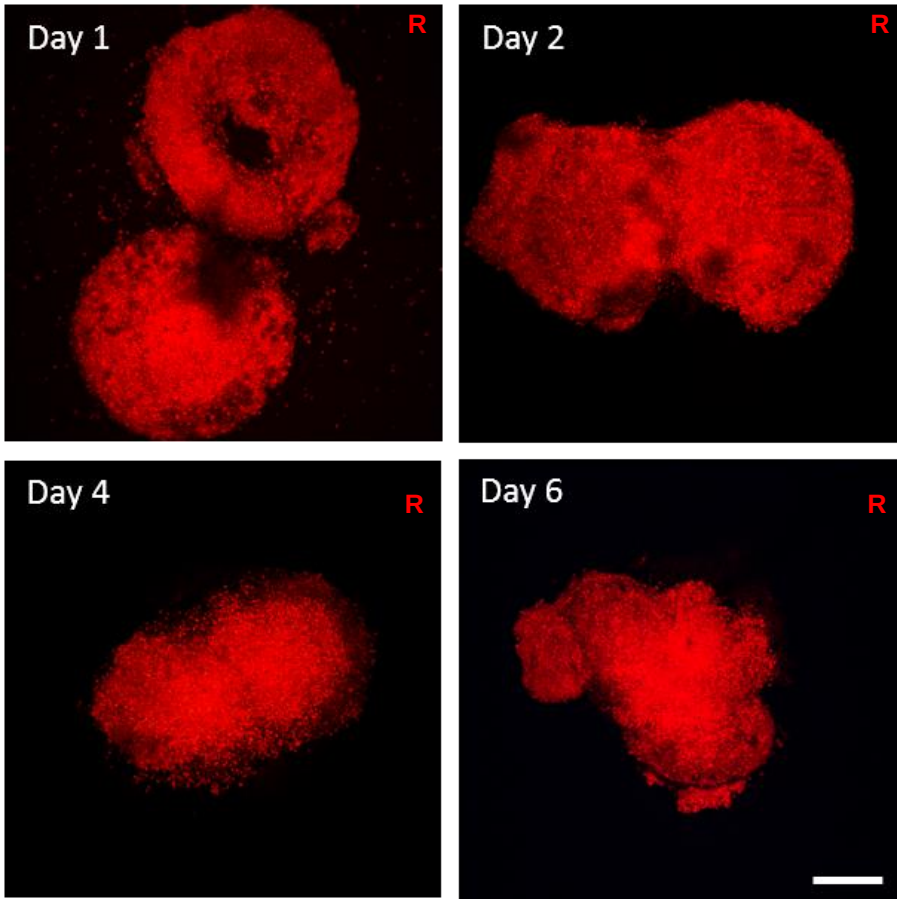

Figure 5.6: Z-axis projection of CFM datasets of two bone spheroids. *The two spheroids started merging by day 2, finally fusing completely by day 6. Images were taken using the red (R) channel of CFM. Representative images were chosen from a library of images acquired during the experiment (N=3, n=4). (Scale bar = 500 µm)*

Mini-coculture of RTF and dROb cells was achieved by transferring an already formed single tendon and single bone spheroid into one well at day 1 (**Figure 5.7**). The two spheroids did not merge at day 2, but the size of each spheroid had decreased (**Figure 5.7**). Monitoring at day 4 showed that the tendon spheroid further decreased in size and maintained its boundary, but the bone spheroid boundary showed disruption and growth towards the tendon spheroid (**Figure 5.7**). Finally, at day 6, the size of both spheroids decreased, with both spheroids maintaining their boundaries (**Figure 5.7**). Accordingly, when a bone spheroid and tendon spheroid were cultured in one well for 6 days, they did not merge (**Figure 5.7**). On the other hand, when two spheroids of the same cell type were cultured in one well, they did merge (**Figures 5.5** and **5.6**). This indicated that spheroids of RTFs and dRObs adhered only to their same cell type spheroid. Nonetheless, this attachment and merging observation was lost when a spheroid was introduced to another spheroid of a different cell type (**Figure 5.7**) (N=3, n=4).

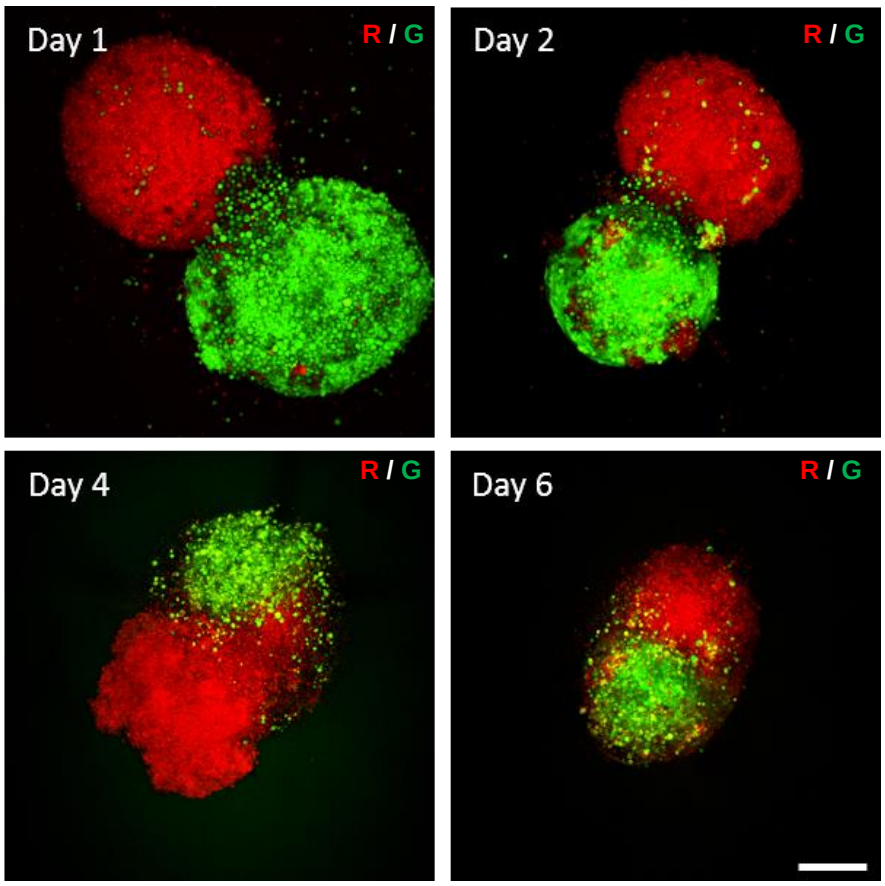

Figure 5.7: Z-axis projection of CFM datasets of mini-coculture. *The two spheroids retained their boundaries and did not completely merge at days 2, 4 and 6. The mini-coculture size appeared to be influenced more by the tendon spheroid as it decreased in size, mimicking what was seen when two tendon spheroids were cultured together and in contrast to when two bone spheroids were cultured together. Images were taken using combined red (R) and green (G) channels of CFM. Representative images were chosen from a library of images acquired during the experiment (N=3, n=4). (Scale bar = 500 µm)*

The max-coculture of RTF and dROb cells was achieved by using similar cell numbers of the two cell types to create a homogenised solution that was used for spheroid generation. After one day of culture, the homogenised mixture was maintained with a thin rim of dROb cells surrounding the spheroid (**Figure 5.8**). At day 2, the RTF cells concentrated at the centre of the spheroid while the previous rim of dROb cells disseminated through the spheroid and the size of the spheroid decreased (**Figure 5.8**). Finally, at day 6, dROb cells reorganised at the core of the spheroid while the RTF cells were on the periphery of the spheroid (**Figure 5.8**). This result supported the previous observation that cells of the same type adhere and attach with no evidence of inter-cellular attachment (N=3, n=4).

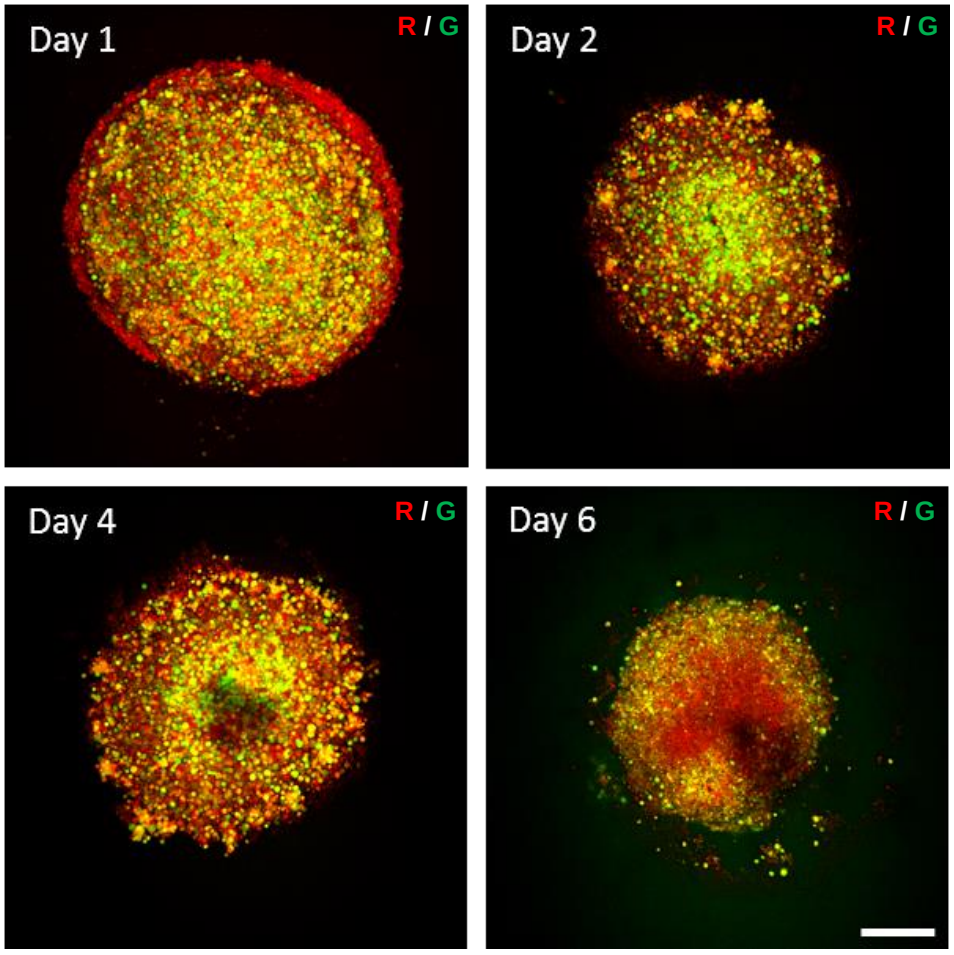

***Figure 5.**8**: Z-axis projection of CFM datasets of max-coculture.** The spheroid retained its homogenised heterogenous cell type at day 2, with more tendon cells at the centre. However, by day 6, most of the core of the spheroid appeared to be composed of bone cells, with tendon cells pushed to the periphery. The max-coculture size appeared to be influenced more by the tendon cells as it decreased in size, mimicking what was seen when two tendon spheroids were cultured together and in contrast to when two bone spheroids were cultured together. Images were taken using combined red (R) and green (G) channels of CFM. Representative images were chosen from a library of images acquired during the experiment (N=3, n=4). (Scale bar = 500 µm)*

5.3.3 Cross-sectional surface area of spheroid types

Tendon spheroids' cross-sectional surface area (CSA) exhibited a decline over time. The CSA at day 1 was at its largest (82.16 µm² ± 24.85, N=8, n=4) and reached its smallest at day 20 (10.09 µm² ± 0.66, N=8, n=4), representing one-eighth of the original size at day 1 (**Figure 5.9** A). In contrast, bone spheroids demonstrated a parabolic pattern in which they started to decline from day 1 (48.36 µm² ± 2.19, N=8, n=4) until day 7 (40.19 µm² ± 3.17, N=8, n=4), when their CSA started growing to regain their day 1 CSA at day 10 (54.11 µm² ± 2.16, N=8, n=4) (**Figure 5.9** B). Interestingly, CSA of bone spheroids doubled in size by day 20 (106.00 µm² ± 7.56, N=8, n=4) compared to its original size at day 1 (48.36 µm² ± 2.19) (**Figure 5.9** B).

Mini-coculture of RTF and dROb cells' CSA was at its largest at day 1 (99.90 µm² ± 15.66, N=8, n=4) (**Figure 5.9** C). It showed a similar parabolic pattern, with CSA declining to its lowest at day 5 (52.75 µm² ± 2.50, N=8, n=4), starting to increase at day 10 (62.00 µm² ± 2.67, N=8, n=4) (**Figure 5.9** C). The CSA of mini-coculture regained its day 1 original size (99.90 µm² ± 15.66, N=8, n=4) at day 20 of culture (106.30 µm² ± 6.07, N=8, n=4) (**Figure 5.9** C). On the other hand, the CSA of max-coculture did not regain its original day 1 size (114.20 µm² ± 4.03, N=8, n=4) by day 20 of culture (104.40 µm² ± 5.37, N=8, n=4) (**Figure 5.9** D). Although, it showed a similar parabolic pattern of decreasing CSA to its lowest at day 5 (52.55 µm² ± 5.50, N=8, n=4), then starting to regain size by day 7 (55.21 µm² ± 3.99, N=8, n=4) (**Figure 5.9**).

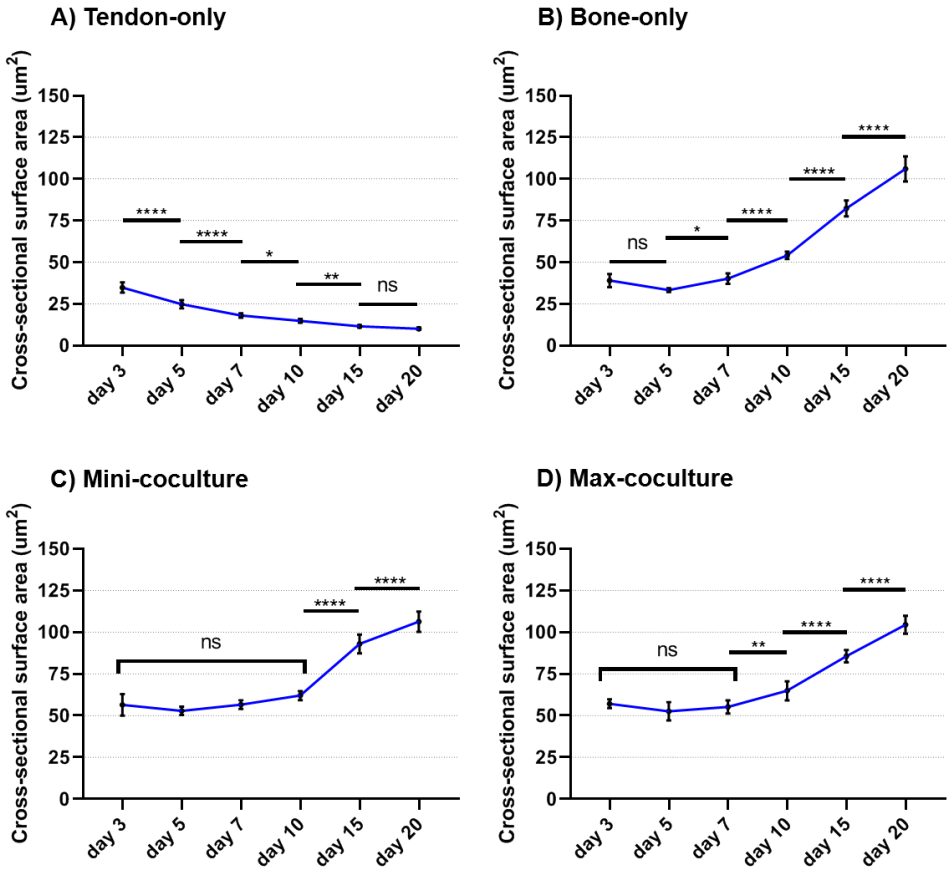

Figure 5.9: CSA measurements of spheroids as an indication of spheroid size*. A) tendon-only spheroids exhibited a decreasing pattern in size, reaching one-eighth of its original size. B) Bone-only spheroids demonstrated an initial decrease in CSA until day 5, followed by an increase to double its original size. C) Both mini-coculture and D) max-coculture spheroids displayed a steep decline in CSA pattern, followed by an increase starting at day 10 to finally reach their starting CSA size by day 20. One-way ANOVA with Tukey's multiple comparison post-test was conducted for each group with error bars showing the standard deviation (N=8, n=3).*

CSA of the mini-coculture and the max-coculture were not significantly different throughout the experiment, except for day 15 when the mini-coculture had a faster increase in size compared to the max-coculture (p values for days: 1 = 0.19, 3 = 0.97, 5 = 0.99, 7 = 0.85, 10 = 0.58, 15 = 0.41, 20 = 0.92) (**Figure 5.10**). Interstingly, bone spheroid CSA increased over time to be not significantly different from max-coculture CSA at day 15 (average of CSA for: bone = 82.30 μm^2 ± 4.72, and max-coculture = 85.61 μm^2 ± 3.69, p value = 0.43, N = 8, n = 4) (**Figure 5.10**). Furthermore, at day 20, bone spheroid CSA was similar to mini-coculture and max-coculture as there was no statistically significant difference between the three groups (average of CSA for: bone = 106.02 μm^2 ± 7.56, mini-cocultue = 106.26 μm^2 ± 60.7, and max-coculture = 104.42 μm^2 5.37) (**Figure 5.10**). This indicated that bone cells (i.e. dRObs) were the major contributors to the mini-coculture and max-coculture CSA size.

The results of CSA for the tendon spheroids raised questions about possible reasons for the decrease in CSA pattern observed (**Figure 5.9** A). Moreover, it was essential to understand what influenced the increase of CSA in bone-only, mini-coculture and max-coculture spheroids (**Figure 5.9** B, C, and D). Possible reasons for CSA increase could be due to an increase in cell density and/or ECM formation. Therefore, studies to quantify DNA in spheroids and ECM content were performed next.

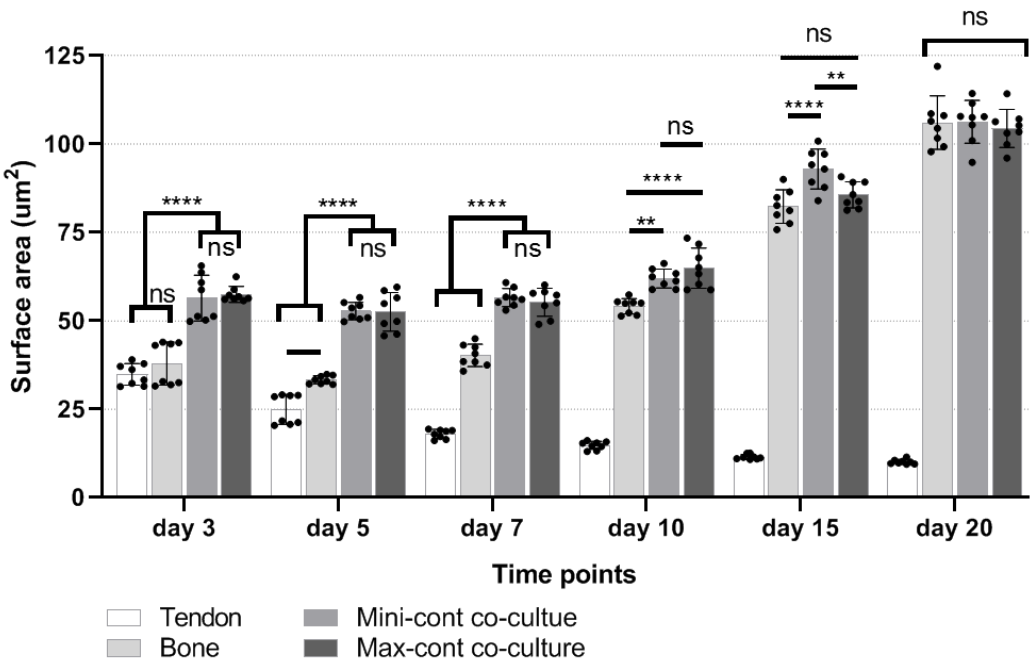

Figure 5.10: CSA measurements of spheroids as an indication of spheroids size*. Mixed effects model with Tukey's multiple comparison post-test was conducted with error bars showing the standard deviation (N=8, n=3). This result showed that CSA was not different by day 20 between bone-only, mini-coculture and max-coculture, indicating that bone cells were contributing to most of mini-coculture and max-coculture CSA by day 20. Notably, mini-coculture and max-coculture were not different throughout the experiment, suggesting no difference in the effect of varying co-culture RTF/dROb cell-cell contact levels.*

5.3.4 Cell density in spheroids

DNA measurement of tendon spheroids showed a decreasing trend similar to what was observed for CSA (**Figure 5.11**), which was at its highest at day 0 (161.24 ng/ml, N=1, n=6) and at its lowest at day 20 (31.08 ng/ml, N=1, n=6). On the other hand, bone spheroids' DNA content showed an increasing pattern starting at day 0 (123.93 ng/ml, N=1, n=6), with its highest measurement at day 20 (347.41 ng/ml, N=1, n=6) (**Figure 5.11**). The DNA measurement of mini- and max-cocultures (287.19 ng/ml and 284.44 ng/ml, respectively) (**Figure 5.11**) at day 0 were near to the summation of tendon and bone spheroids' DNA measurements at day 0 (summation = 289.68 ng/ml). These measurements were taken from one independent experiment; therefore, no statistical analysis was performed.

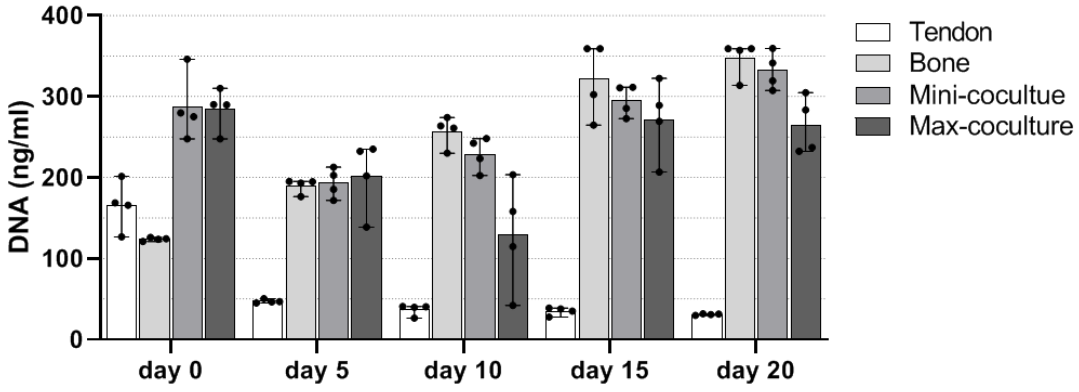

Figure 5.11: DNA quantification as an indicator of cell density for spheroid culture. *DNA content of tendon spheroids showed a decreasing pattern, indicating cell loss, while bone spheroids showed an increasing pattern, indicating cell proliferation. On the other hand, mini-coculture and max-coculture showed an initial decrease, corresponding with tendon cells' loss observed in tendon spheroids, followed by an increase, matching bone cells behaviour in bone spheroids. No statistical tests were used as only one independent experiment was performed, with error bars showing the range of data (N=1, n=4).*

Further measurements were performed to confirm findings, including day 0 and day 20. Tendon spheroids' DNA measurements had decreased significantly from day 0 (165.80 ng/ml ± 37.49, N=3, n=4) to day 20 (43.67 ng/ml ± 2.48, N=3, n=4) (**Figure 5.12** A), whereas bone spheroids' DNA measurements increased over time from 123.9 ng/ml ± 2.68 at day 0 to 335.80 ng/ml ± 4.09 at day 20 (N=3, n=4, **Figure 5.12** B). DNA measurements for mini-coculture spheroids were not significantly different between day 0 (289.70 ng/ml ± 39.40, N=3, n=4) and day 20 (308.80 ng/ml ± 42.43, N=3, n=4) (**Figure 5.12** C). Similarly, max-coculture did not have a significantly different DNA content between day 0 (289.70 ng/ml ± 39.40, N=3, n=4) and day 20 (340.00 ng/ml ± 38.54, N=3, n=4) (**Figure 5.12** D). Moreover, at day 0, tendon and bone spheroids' DNA measurements were not significantly different (day 0 tendon vs bone p value = 0.31) (**Figure 5.13**). The same observation was true for mini-coculture and max-coculture at day 0 (day 0 mini-coculture vs max-coculture p value = 0.98) (**Figure 5.13**). Notably, DNA measurement of bone, mini-coculture and max co-culture were not significantly different at day 20 (day 20 p value of: bone vs mini-coculture = 0.66, bone vs max-coculture = 0.99, and mini-coculture vs max-coculture = 0.56) (**Figure 5.13**). These results clearly showed that bone spheroid cells (i.e. dROb) were the major contributor for the DNA content and CSA size of mini-coculture and max-coculture spheroids.

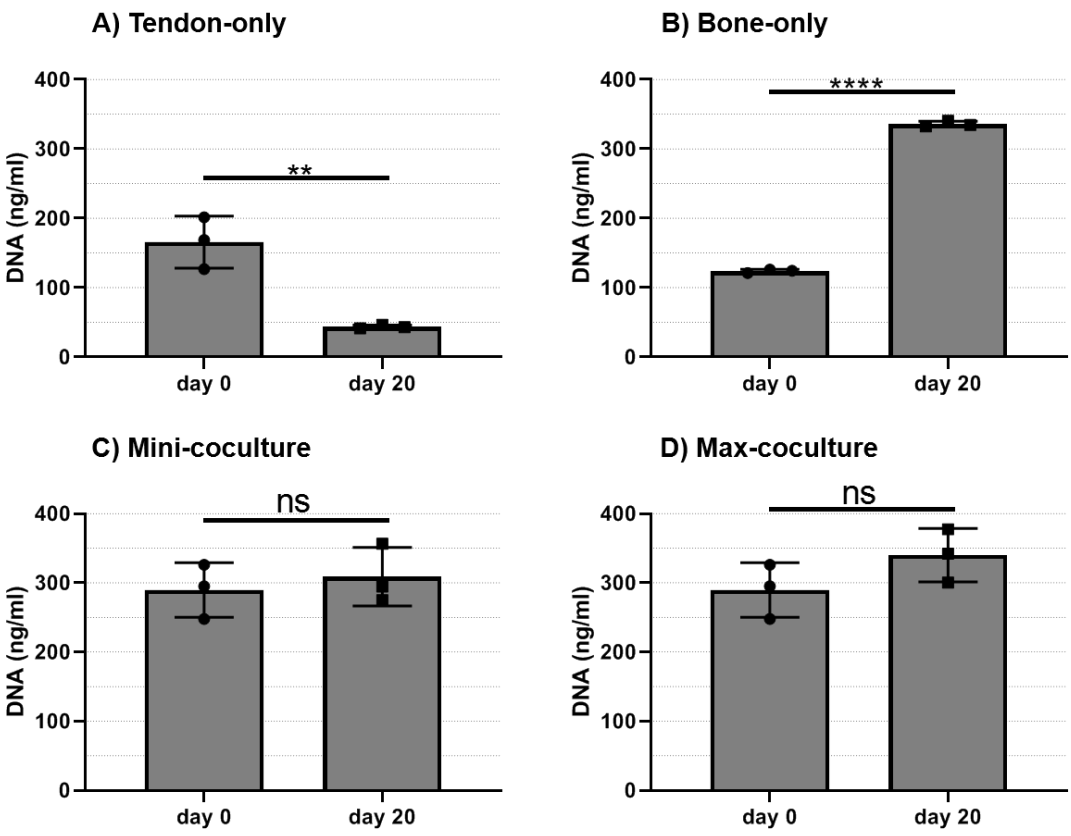

Figure 5.12: DNA quantification as an indicator of cell density for spheroid culture. *DNA content of tendon spheroids (A) showed a statistically significant decrease from day 0 to day 20, indicating cell loss, while bone spheroids (B) showed a significant increase, indicating cell proliferation. On the other hand, mini-coculture (C) and max-coculture (B) presented no difference in cell density when day 0 DNA content was compared to day 20. Unpaired, two-tailed t-tests were performed on each group with error bars showing the standard deviation (N=3, n=4).*

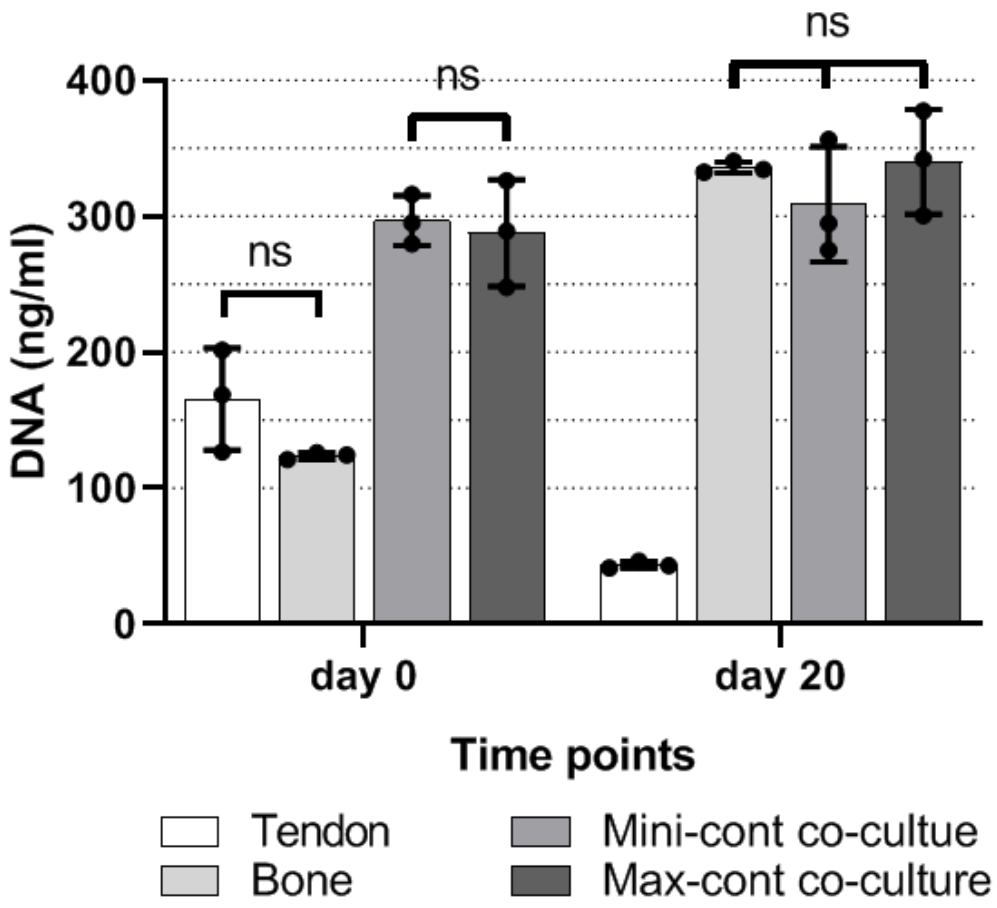

Figure 5.13: Data from Figure 5.13 was replotted to show DNA quantification compared between spheroid groups at day 0 and day 20*. At day 0, 50 k of RTFs and 50 k of dRObs, used to make tendon and bone spheroids respectively, did not have a statistically significant difference in DNA content. Moreover, using 50 k of RTFs and 50 k of dRObs for mini-coculture and max-coculture at day 0 resulted in a non-significantly different DNA content between them. By day 20, DNA content of tendon cells was statistically different from all other groups, while the other groups were not statistically different from one another. Two-way ANOVA with Tukey's multiple comparison post-test was conducted with error bars showing the standard deviation (N=3, n=4). Only non-significant results are labelled.*

5.3.5 ECM formation

As use of the Sircol™ collagen assay kit was limited by the range of collagen detection, aims of this experiment were to: 1) determine suitable starting cell number of RTF and dROb cells for spheroid formation and collagen content detection after culturing different starting cell numbers of RTF and dROb cells for 20 days, and 2) observe ECM content of collagen and GAGs in mini-coculture and max-coculture after 20 days.

5.3.5.1 Collagen in the ECM

A suitable starting cell number for spheroid formation and collagen detection was assessed for both tendon and bone spheroids (**Figures 5.14** and **5.15**). The total collagen at day 0 that was transferred over from the 2D cell expansion and growth before starting the spheroid formation process was measured and subtracted from day 20 collagen results. Tendon spheroids' collagen measurements at day 0 for 25K (4.56 µg/sample ± 2.24), 50K (7.01 ug/sample ± 0.68), and 100K (12.10 µg/sample ± 2.56) (**Figure 5.14** A) were subtracted from the tendon spheroids' collagen results at day 20 (25K = 27.12 µg/sample ± 2.16, 50K = 39.05 µg/sample ± 3.88, and 100K = 51.21 µg/sample ± 9.14) (**Figure 5.14** B) to ascertain accurate collagen production as a result of spheroid culture (N=3, n=4). Production of collagen after 20 days of culture was not significantly different between starting RTF numbers of 25K and 50K (p value = 0.23) nor between 50K and 100K (p value = 0.40), to form a tendon spheroid (**Figure 5.14** B). A significant difference was however detected between 25K and 100K (p value = 0.04) (**Figure 5.14** B) (N=3, n=4). Therefore, 50K of RTF cells was considered an appropriate number to conduct an experiment to assess the effect of co-culture on ECM formation.

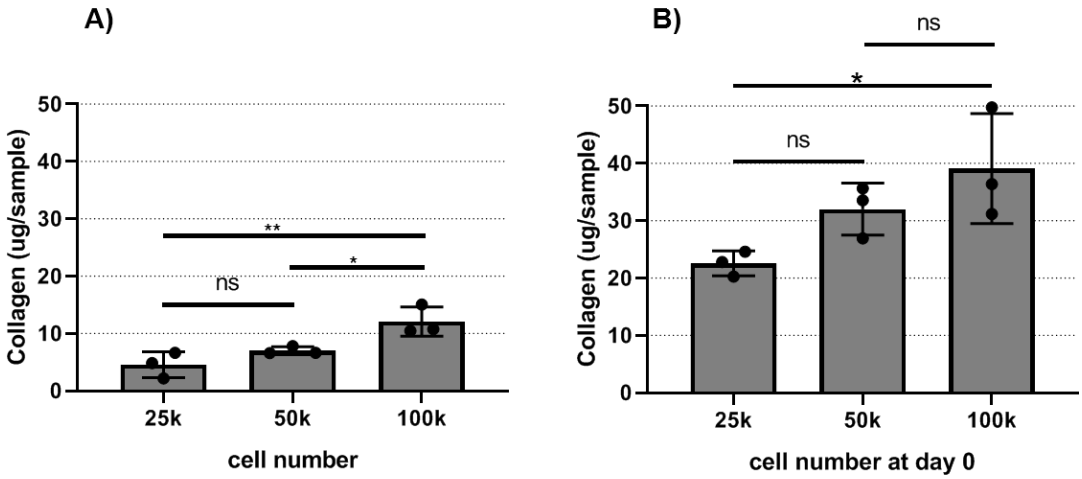

Figure 5.14: Comparison of collagen measurements for tendon spheroids at A) day 0 and B) day 20. *Use of 50K cells as a starting cell number for tendon spheroid formation was chosen based on the non-significant difference between the use of 25K or 100K. Furthermore, 25K produced a spheroid with significantly less collagen by day 20 compared to 100K. One-way ANOVA with Tukey's multiple comparison post-test was conducted with error bars showing the standard deviation (N=3, n=4).*

A similar experiment was performed for bone spheroids. Collagen measurements of dRObs for bone spheroid formation at day 0 were 4.12 µg/sample ± 0.79 for 25K, 8.43 µg/sample ± 0.61 for 50K, 13.36 µg/sample ± 1.21 for 100K, and 17.88 µg/sample ± 2.82 for 150K samples (**Figure 5.15** A), while at day 20 were 40.44 µg/sample ± 8.86 for 25K, 76.12 µg/sample ± 16.60 for 50K, 74.78 µg/sample ± 16.36 for 100K, and 86.94 µg/sample ± 21.15 for 150K (N=3, n=4) (**Figure 5.15** B). The measurements of collagen at day 0 were subtracted from the results at day 20 to disregard the collagen transferred from the 2D growth and expansion of cells before spheroid formation. The collagen measurements of different starting cell numbers at day 20 were significantly different between 25K starting cell number and all other cell numbers (i.e. 50K, 100K and 150K) (p value for 25K vs 50K = 0.038, 25K vs 100K = 0.044 and 25K vs 150K = 0.01) (N=3, n=4) (**Figure 5.15** B). However, no significant difference was found between collagen measurements after 20 days of culture of 50K, 100K and 150K of dRObs cells to form spheroids (N=3, n=4) (**Figure 5.15** B). Accordingly, 50K of dRObs cells were considered an appropriate number for further studies of co-culture effect on ECM formation. Consequently, 50K of RTF and 50K of dRObs cells were used to make a single co-culture spheroid to study the effect of 3D co-culture.

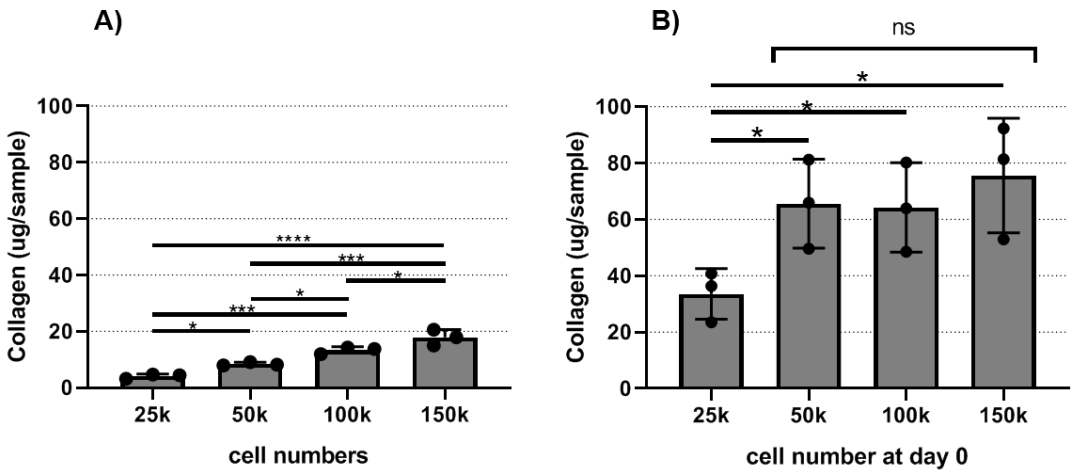

Figure 5.15: Comparison of collagen measurements for bone spheroids at A) day 0 and B) day 20. *Use of 50K cells as a starting number for tendon spheroid formation was chosen based on the non-significant difference between 100K or 150K. Furthermore, 25K produced a spheroid with significantly less collagen by day 20 compared to 50K, 100K and 150K. One-way ANOVA with Tukey's multiple comparison post-test was conducted with error bars showing the standard deviation (N=3, n=4).*

Accordingly, tendon-only, bone-only, mini-coculture and max-coculture spheroids were generated to assess ECM formation after 20 days of culture. The measurements of collagen in the ECM of all four groups (N=3, n=4 for each) between day 0 and day 20 were significantly different: for tendon-only, 10.54 µg/sample ± 0.83 (day 0) vs 34.46 µg/sample ± 3.89 (day 20, p = 0.0332); bone-only, 7.01 µg/sample ± 0.68 vs 68.28 µg/sample ± 9.1 (p = <0.0001); mini-coculture 15.81 µg/sample ± 1.85 vs 79.13 µg/sample ± 16.64 (p = <0.0001); and max-coculture 18.10 µg/sample ± 0.89 vs 75.58 µg/sample ± 2.57 (p = <0.0001) (**Figure 5.16**). These results proved that the culture of tendon-only, bone-only, mini-coculture and max-coculture for 20 days increased the collagen content of the ECM.

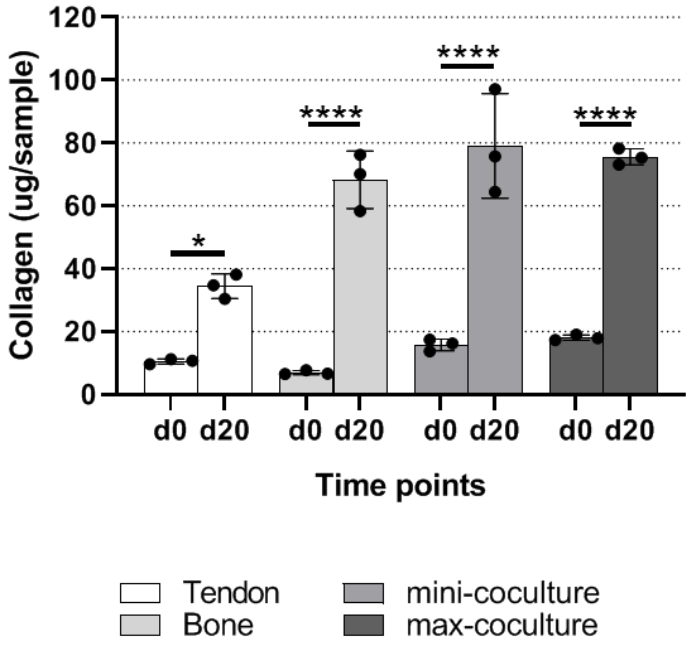

Figure 5.16: Collagen content was measured as an indicator of ECM formation in tendon-only, bone-only, mini-coculture and max-coculture*. All groups showed a significant increase in collagen content after 20 days of culture. Two-way ANOVA with Tukey's multiple comparison post-test was conducted with error bars showing the standard deviation (N=3, n=4).*

5.3.5.2 GAGs in the ECM

The measurements of GAGs in the ECM of all 4 groups (N=3, n=4 for each) between day 0 and day 20 were also significantly different: for tendon-only 4.229 µg/sample ± 0.76 (day 0) vs 7.31 µg/sample ± 1.05 (day 20, p = 0.0332); bone-only 1.41 µg/sample ± 1.21 vs 15.94 µg/sample ± 0.42 (p = <0.0001); mini-coculture 5.64 µg/sample ± 0.51 vs 15.09/sample ± 1.86 (p = <0.0001); and max-coculture 4.79 µg/sample ± 1.04 vs 14.87 µg/sample ± 1.03 (p = <0.0001) (**Figure 5.17**). These results prove that the

culture of tendon-only, bone-only, mini-coculture and max-coculture for 20 days increase GAGs content of the ECM.

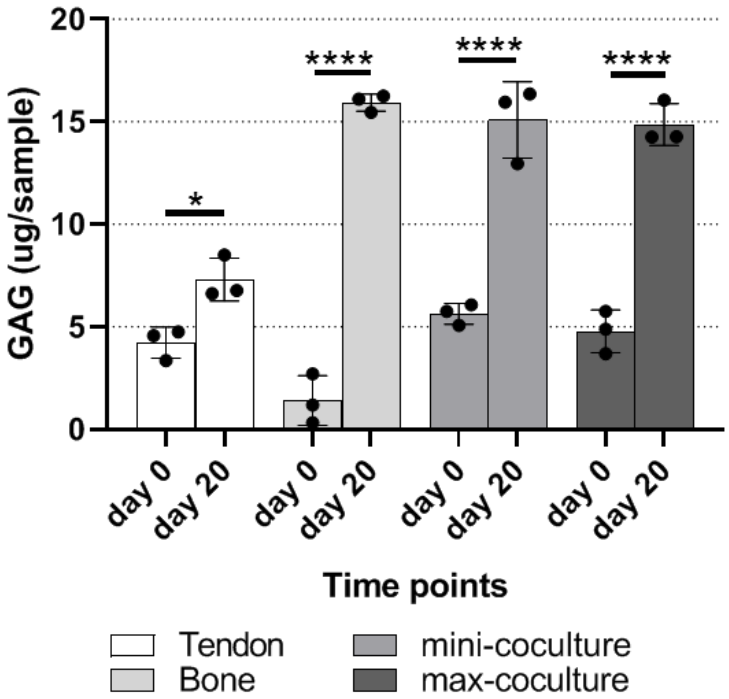

Figure 5.17: GAGs content was measured as an indicator of ECM formation in tendon-only, bone-only, mini-coculture and max-coculture. *All groups showed a significant increase of GAGs content after 20 days of culture. Two-way ANOVA with Tukey's multiple comparison post-test was conducted with error bars showing the standard deviation (N=3, n=4).*

5.3.6 Effect of co-culture on CSA, cell density, ECM formation and chondrogenic transformation

The aims of this experiment were to 1) assess the effect of co-culture by comparing the summation of tendon-only and bone-only spheroids cultured separately for 20 days to their co-culture, 2) determine the effect of various tendon/bone cell-cell contact by comparing mini-coculture to max-coculture, and 3) assess chondrogenic transformation by measuring ECM GAGs content.

The effect of co-culture on CSA was assessed by comparing the summation of tendon-only and bone-only spheroid measurements to mini-coculture and max-coculture after 20 days. This study showed a significant decrease in CSA caused by co-culture (**Figure 5.18**). The summation of tendon-only and bone-only CSA at day 20 was 116.10 µm² ± 8.10, which was significantly greater than the mini-coculture CSA (106.30 µm² ± 6.07) and the max-coculture (104.40 µm² ± 5.37) (p value of separate cultures vs: mini-coculture = 0.0188, max-coculture = 0.0053) (N= 8, n=3)

(**Figure 5.18**). However, there was no significant difference between mini-coculture and max-coculture CSA measurements (p value = 0.8434; N=8, n=3) (**Figure 5.18**). This implied that different tendon/bone cell-cell contact did not influence a change in CSA.

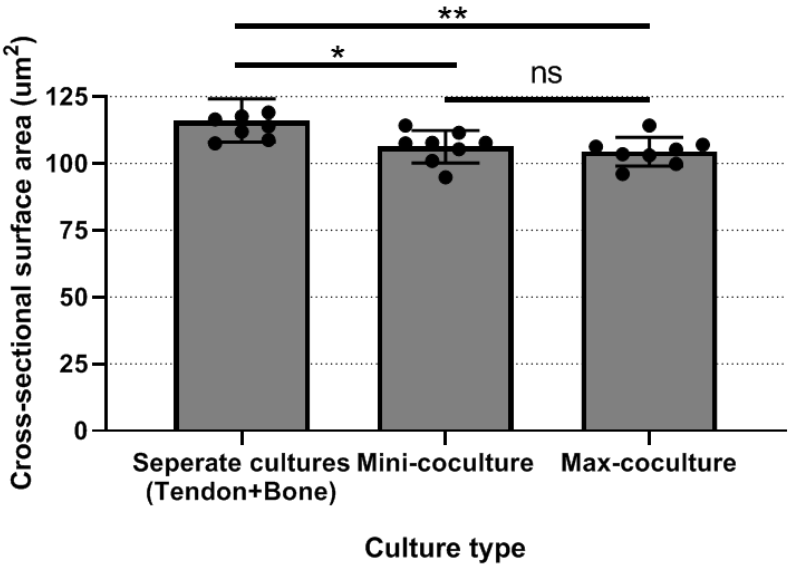

Figure 5.18: The summation of CSA of separate tendon and bone spheroid culture at day 20 was significantly more than mini-coculture and max-coculture*. This result showed an inhibitory effect of co-culture, resulting in smaller sized spheroids. One-way ANOVA with Tukey's multiple comparison post-test was conducted with error bars showing the standard deviation (N=8, n=3).*

Based on the previous result, two hypotheses were examined; that the cause of the decrease in CSA was due to a decrease in 1) cell density, or/and 2) ECM formation. Therefore, the cell density of the summation of separately cultured tendon-only and bone-only spheroids was compared to mini-coculture and max-coculture. This experiment showed no significant difference in cell density between the summation of separately cultured tendon-only and bone-only spheroids (379.50 ng/ml ± 3.88) compared to mini-coculture (308.80 ng/ml ± 42.43, p = 0.888; N=3, n=4) and max-coculture (340.00 ng/ml ± 38.54, p = 0.3733; N=3, n=4) (**Figure 5.19**). This result contradicts the hypothesis of decreased CSA being caused by a decrease in cell density. Moreover, there was no significant difference between mini-coculture and max-coculture cell density measurements (p = 0.5203; N=3, n=4) (**Figure 5.19**), which implied that different tendon/bone cell-cell contacts did not influence a change in cell density.

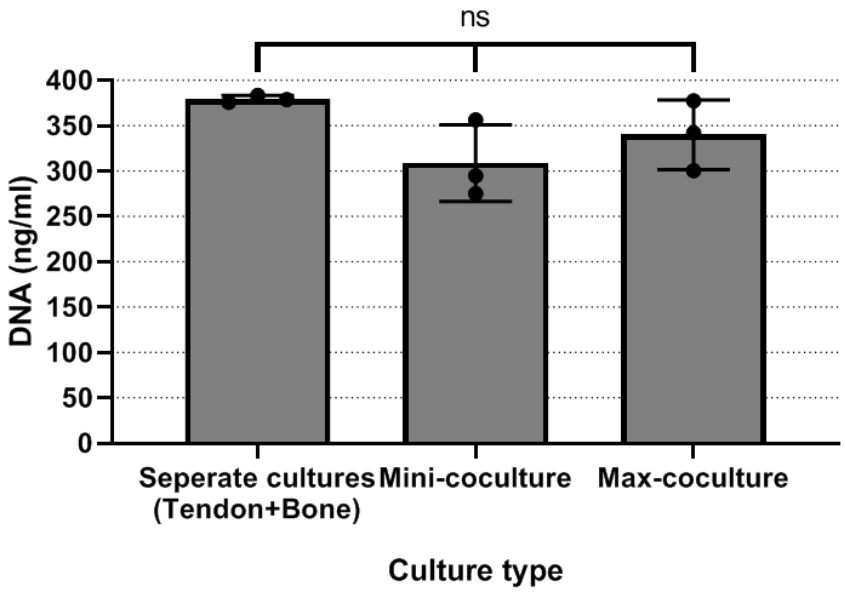

Figure 5.19: The summation of DNA content of separate tendon and bone spheroids culture at day 20 was not significantly different than mini-coculture and max-coculture. *This result showed no effect of co-culture on cell density. One-way ANOVA with Tukey's multiple comparison post-test was conducted with error bars showing the standard deviation (N=3, n=4).*

The summation of ECM collagen in bone-only and tendon-only spheroids after 20 days of culture was 98.02 µg/sample ± 11.63, significantly different from 74.45 ug/sample ± 3.08 in the max-coculture after 20 days (**Figure 5.20**) (p = 0.031, N=3, n=4). However, ECM collagen in mini-coculture after 20 days (77.10 µg/sample ± 14.19) was not significantly different from the summation of the separate tendon and bone spheroid culture (p = 0.05; N=3, n=4) (**Figure 5.20**). Similarly, ECM collagen in the mini-coculture (77.10 µg/sample ± 14.19) was not significantly different from max-coculture (74.45 ug/sample ± 3.08) (p = 0.94; N=3, n=4) (**Figure 5.20**). Therefore, the effect of 3D co-culture using RTF and dROb cells resulted in a reduction of ECM collagen content when using the max-coculture method (p = 0.05; N=3, n=4) (**Figure 5.20**), which supported the hypothesis that the decrease of CSA was caused by a decrease in ECM formation. However, the decrease of the ECM collagen content caused by the mini-coculture method was not significant (p value = 0.94; N=3, n=4) (**Figure 5.20**).

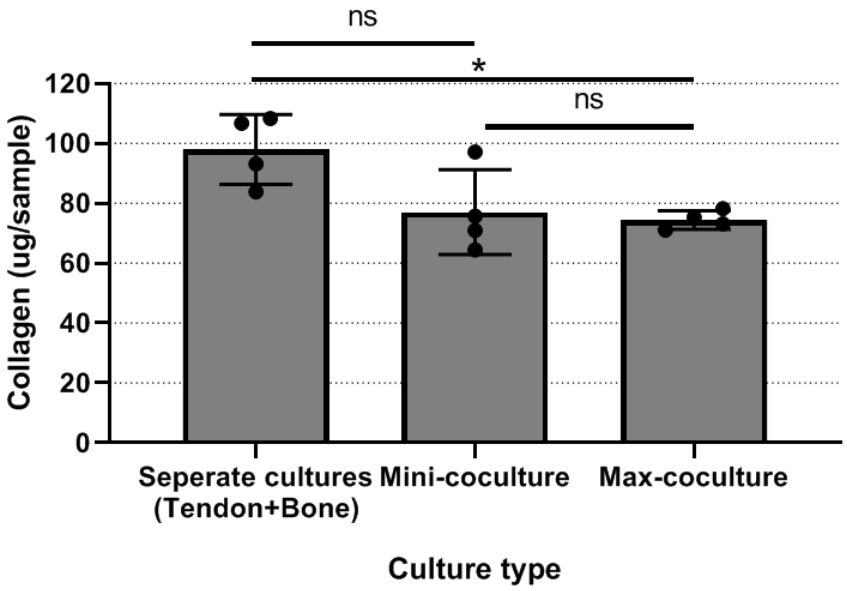

Figure 5.20: The summation of collagen content of separate tendon and bone spheroid cultures was not significantly different from mini-coculture after 20 days. *However, it was significantly different from max-coculture. This result showed a decrease in collagen content caused by max-coculture, and that an increased level of RTF-dROb cell-cell contact resulted in a further decrease in collagen content. One-way ANOVA with Tukey's multiple comparison post-test was conducted with error bars showing the standard deviation (N=4, n=4).*

The effect of co-culture on the ECM content of GAGs was used to determine chondrogenic transformation activity (Wang *et al.*, 2007). Accordingly, the ECM content of GAGs was compared between the sum of separately cultured tendon and bone spheroids with their co-culture. After 20 days of culture, the summation of ECM GAGs content from bone-only and tendon-only spheroids (23.24 µg/sample ± 1.23) was significantly more than mini-coculture and max-coculture (15.09 µg/sample ± 1.86 and 14.86 µg/sample ± 1.03) (p value of: separate culture vs mini-coculture = 0.001, separate culture vs max-coculture = 0.0009; N=3, n=4) (**Figure 5.21**). This result indicated that co-culture of RTF and dROb cells in 3D through spheroid culture inhibited their collective GAGs production in the ECM, further supporting the hypothesis that decreased CSA was caused by a decrease in ECM formation. Furthermore, the effect of different levels of RTF/dROb communications in the co-culture was assessed by comparing the ECM GAGs content of mini-coculture (15.09 µg/sample ± 1.86) and max-coculture (14.86 µg/sample ± 1.03), which showed no significant difference when the contact between RTF and dROb cells was increased in the max-coculture (p = 0.98; N=3, n=4)(**Figure 5.21**).

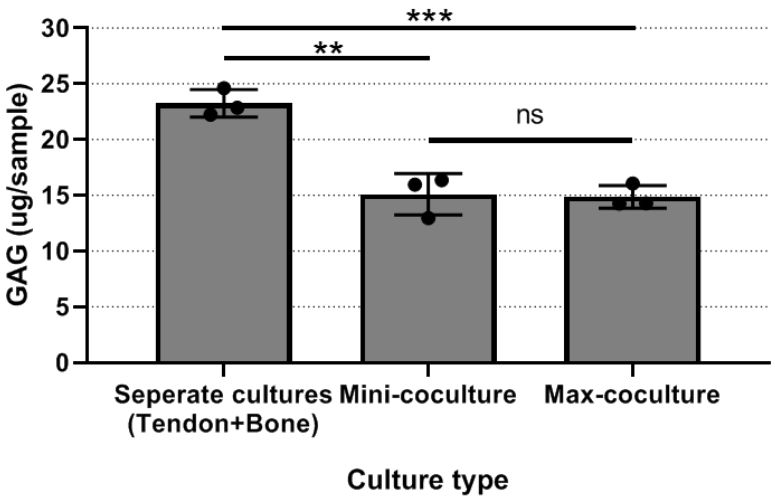

Figure 5.21: The summation of GAGs content of separate tendon and bone spheroids culture was significantly different from mini-coculture and max-coculture GAGs content after 20 days of culture. *Nonetheless, there was no significant difference between mini-coculture and max-coculture. One-way ANOVA with Tukey's multiple comparison post-test was conducted with error bars showing the standard deviation (N=3, n=4).*

5.3.1 Comparing 2D culture to the spheroid 3D culture

A comparison was conducted between of 50K RTF (tendon cells) and 50K dROb cells (bone cells) separately cultured in standard 2D 96-well plates to those cultured as spheroids. The comparison was to assess cell number and normalise ECM formation (i.e. collagen and GAGs measurements) to cell number at day 20.

The number of tendon cells after 20 days of culture in 2D (86.80K ± 34.15) was significantly more than when cultured as a spheroid (5.48K ± 1.01) ($p = 0.0146$; N=3, n=4) (**Figure 5.22** A). Similarly, the number of bone cells in 2D (182.7K ± 6.72) was significantly more than their spheroid 3D culture (143.9K ± 2.04) ($p = 0.0007$; N=3, n=4) (**Figure 5.22** B).

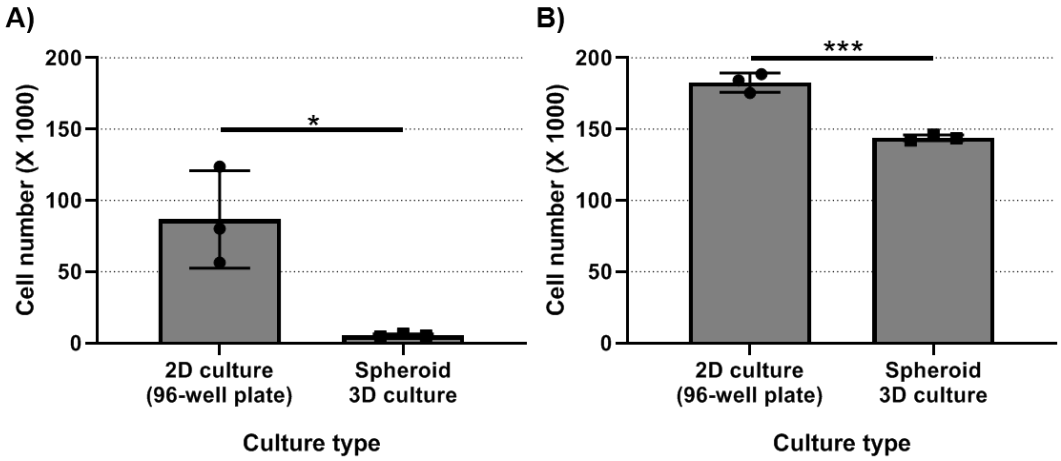

Figure 5.22: Cell numbers of A) tendon and B) bone cells in 2D culture vs spheroid 3D culture after 20 days in cultivation. *Unpaired, two-tailed t-tests were conducted with error bars showing the standard deviation (N=3, n=4)*

Collagen content of tendon cells' ECM after 20 days of culture in 2D was 0.42 ng/cell ± 0.13, which was not significantly different from 0.64 ng/cell ± 0.10 when assessed in spheroid 3D culture (p = 0.0886; N=3, n=4) (**Figure 5.23** A). Likewise, the collagen content of bone cells' ECM after 20 days of culture in 2D was 0.34 ng/cell ± 0.03, which was significantly more than 0.05 ng/cell ± 0.01, when measured in spheroid 3D culture (p = 0.000;, N=3, n=4) (**Figure 5.23** B).

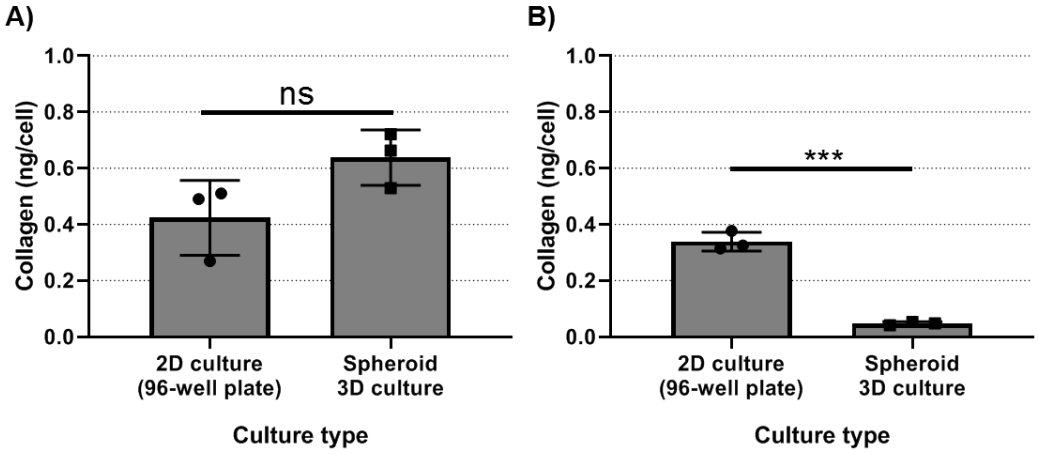

Figure 5.23: Collagen content measured in a standard 2D culture of A) RTF cells and B) dROb cells compared to their culture in 3D as spheroids. *The collagen content resulting from 2D culture was significantly more than 3D culture. Unpaired, two-tailed t-tests were performed on each group with error bars showing the standard deviation (N=3, n=4).*

Furthermore, GAGs content in the ECM of tendon and bone cell culture showed similar observations to collagen. GAGs content of tendon cells' ECM after 20 days of culture in 2D was 0.14 ng/cell ± 0.04, which was not significantly different from 0.14 ng/cell ± 0.03 in spheroid 3D culture (p = 0.9741; N=3, n=4) (**Figure 5.24** A). In contrast, GAGs content of bone cells' ECM after 20 days of culture in 2D was 0.07

ng/cell ± 0.01, significantly more than 0.01 ng/cell ± 0.01 in spheroid 3D culture (p = <0.0001; N=3, n=4) (**Figure 5.24** B).

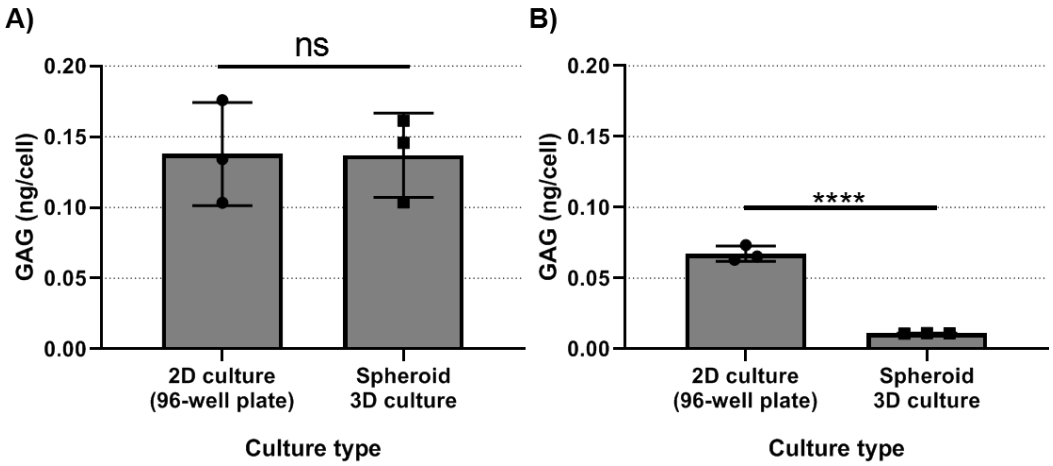

Figure 5.24: GAGs content measured in a standard 2D culture of A) RTF cells and B) dROb cells compared to their culture in 3D as spheroids. *The GAGs content resulting from 2D culture was significantly more than 3D culture. Unpaired, two-tailed t-tests were performed on each group with error bars showing the standard deviation (N=4, n=4).*

In summary, this study has qualitatively shown that monocultures of two tendon or bone spheroids fuse and make one spheroid over time (**Figures 5.5** and **5.7**). In contrast, their mini-coculture did not show visible signs of merging (**Figure 5.7**). Moreover, a max-coculture of tendon and bone cells showed a self-organising behaviour, as bone cells occupied the core of the spheroid and the tendon cells were pushed to the periphery (**Figure 5.8**). This was followed by characterisation of each spheroid group's CSA, cell density, collagen and GAGs at days 0 and 20. Tendon cells showed a decrease in CSA and cell density over time (**Figures 5.9** and **5.12**), while collagen and GAGs showed an increase (**Figures 5.16** and **5.17**), whereas, bone, mini-coculture and max-coculture spheroids showed an increase in CSA, cell density, collagen and GAGs (**Figures 5.9, 5.12, 5.16,** and **5.17**). The effect of spheroid 3D co-culture of bone and tendon cells was measured by comparing the summation of tendon and bone monoculture CSA, cell density, collagen and GAGs, to mini- and max-coculture results. The decrease in CSA, collagen and GAGs measurements were observed as an effect of 20 days of co-culture (**Figures 5.18, 5.20,** and **5.21**). No significant changes were detected in cell density.

Moreover, there was no significant effect in different levels of co-culture contact (mini-coculture vs max-coculture) on CSA, cell density, collagen or GAGs (**Figures 5.18, 5.20** and **5.21**), meaning the degree of contact between bone and tendon cells did not

have an effect on their co-culture. Finally, spheroid 3D monocultures were compared to 2D monocultures for cell proliferation, collagen, and GAGs contents. This experiment showed that spheroid 3D culture had significantly lower cell density and ECM formation compared to 2D culture. Consequently, an important research question should be addressed: do the results of 2D or 3D cell density and ECM formation better represent the natural cell behaviour in the native tissue?

5.4 Discussion

This chapter aimed to investigate the use of spheroid culture to create tendon and bone co-cultures and examine the effect of co-culture on spheroids' CSA, cell density and ECM formation. The changes in spheroid size (CSA), cell density and ECM formation over time were determined between tendon-only, bone-only, and their co-culture of in spheroids, which was combined with studying the effect of different levels of RTF/dROb cell-cell contact in the co-culture. Finally, the difference in ECM formation between 3D culture and 2D culture was assessed. The results of this study showed a contrast in response to spheroid culture between RTF and dROb cells. While bone spheroids showed an increase in size, cell density and ECM formation after 20 days of culture as a bone spheroid (**Figures 5.9** B, **5.12** B, **5.16**, and **5.17**), tendon spheroids showed a decrease in size and cell density, and a minimal increase in ECM formation (**Figures 5.9** A, **5.12** A, **5.16**, and **5.17**).

Use of spheroid culture to generate tendon and bone spheroids was achieved successfully (**Figure 5.4**). In this study, the non-adhesive culture ware surface method was used for the generation of spheroids, as it offered a highly reproducible and cost-effective method that was capable of generating spheroids from a high cell number (i.e. 50K of RTF or dRObs)). Other alternatives included use of the hanging-drop or microwells fabrication methods. However, the hanging-drop method had a limited number of cells for spheroid generation (i.e. a maximum of 5K) while the microwells fabrication required highly specialised materials and expertise with no notable advantage over non-adhesive culture ware surface for the purpose of this study. Formation of tendon and bone spheroids was confirmed qualitatively by CFM at day 1 (**Figure 5.4** A and B). These generated tendon and bone spheroids were also used for 3D co-culture (i.e. mini-coculture) (**Figure 5.4** C).

Furthermore, the same cell numbers of RTF and dROb cells were used to form a homogenised mixture of cells to generate a single spheroid (i.e. max-coculture) (**Figure 5.4** D). Use of mini-coculture and max-coculture was aimed to study the effect

of different levels of RTF/dROb contact in a spheroid co-culture. To the author's knowledge, this was a novel approach to studying the effect of tendon and bone cells in co-culture. Co-culture of tendon and bone has been researched previously in 2D (Wang *et al.*, 2007), in which they showed a chondrogenic transformation of cells in the co-culture, and they hypothesized that osteoblast-fibroblast interaction might eventually lead to enthesis formation. Consequently, an objective of this study was to use 3D culture in the form of spheroids to examine this hypothesis.

To study the effect of co-culture of tendon and bone spheroids on CSA, a study of monocultures of tendon and bone spheroids CSA was conducted (**Figure 5.9** A and B). This created a reference control which can be compared to the co-culture to study its effect. Firstly, CSA of tendon spheroids showed a decreasing pattern (**Figure 5.9** A) in which they retained one-eighth of their day 1 CSA after 20 days of culture. In contrast, CSA of bone spheroids doubled in size by day 20 (**Figure 5.9** B). A comparison of these results to mini-coculture and max-coculture spheroids was conducted to observe if co-culturing would cause an increase, decrease or no effect on CSA. The results indicated a decrease in CSA in both types of co-culture (**Figure 5.18**), which could be due to slowed cellular proliferation and subsequent reduction in cell density by day 20, or inhibition of ECM formation caused by co-culture. Accordingly, two hypotheses were constructed, either 1) co-culture of RTF (tendon) and dROb (bone) cells decreased cell proliferation and caused the CSA decrease, or/and 2) co-culture of RTF and dROb cells inhibited ECM formation and caused the decline in CSA. Therefore, separate experiments were designed to investigate the effect of co-culture on cell density and ECM formation.

Cell density determination for spheroids can be performed using several methods. DNA quantification as an indicator of cell density can be achieved by using proliferation assays such as Quanti-it™ PicoGreen™ dsDNA Assay Kit (Molecular Probes, Invitrogen, UK) (Chambers *et al.*, 2014) and CyQUANT™ Cell Proliferation Assay Kit (Molecular Probes, Invitrogen, UK). Moreover, metabolic-based assays can be used, such as CellTiter-Glo® 3D Cell Viability Assay (Promega, UK) (Lazzari *et al.*, 2018) and Culture 3D Spheroid Colorimetric Assay (R&D Systems Inc, USA) (Perotti *et al.*, 2019). For this study, cell density was determined by quantifying DNA using CyQUANT™ Cell Proliferation Assay Kit. This kit offered flexibility on conducting the experiment as it involved a storage step at -80°C. This step was used to collect and store samples of all groups from different time points to conduct the procedure in

one session, which should help reduce variability in assay technique. The results showed a parallel correlation between the decrease in tendon spheroids' CSA and cell density over time (**Figures 5.9** A and **5.11**). However, there was no correlation between bone spheroids' CSA and cell density in the first 7 days, as the CSA was decreasing while cell density was increasing (**Figures 5.9** A and **5.11**). This could be because the dROb cells forming the spheroids did not complete their spheroid formation and cell attachment until day 7, as they showed a decrease in CSA towards day 7 then the CSA started to increase (**Figure 5.9** B).

The mini-coculture and max-coculture showed a parallel decrease in cell density (**Figure 5.11**) until day 10, when cell density then started to increase and show a similar original starting cell density by day 20 (**Figure 5.12**). A possible explanation of this finding could be that while tendon cells lose their cell density from 165.80 ng/ml ± 37.49 at day 0 to 43.67 ng/ml ± 2.48 at day 20, bone cells increased their cell density from 123.9 ng/ml ± 2.68 at day 0 to 335.80 ng/ml ± 4.09 at day 20. Therefore, the initial high cell density at day 0 of mini-coculture and max-coculture was the result of the combination of day 0 readings of tendon and bone cells. As tendon cell density decreased, it caused the initial decrease in cell density of both mini-coculture and max-coculture until day 7. On the other hand, when the steep decline of tendon cell density was equalised by the increase of bone cell density at day 7, both the mini-coculture and max-coculture cell densities started to increase at day 10 (**Figure 5.11**). Moreover, comparing the summation of day 20 tendon and bone spheroids cell densities to mini-coculture and max-culture showed no significant difference. This indicated that the co-culture did not affect cell density (**Figure 5.19**). This finding was contrary to what has been reported in Wang *et al.*, 2007, as they have reported an inhibitory effect of tendon and bone cell co-culture. However, their experiments were conducted in a 2D environment while the experiments presented in this study were conducted in 3D.

ECM is an essential component of natural tissues. It provides a microenvironment for cell attachment, proliferation, communication, and migration. Moreover, its content gives tissues their mechanical properties (Frantz, Stewart and Weaver, 2010). Therefore, mimicking the natural ECM properties of a tissue is an essential goal for tissue engineering. Consequently, in this study, collagen and GAGs were measured as an indicator of ECM formation in spheroid culture. The ECM formation was measured to firstly determine normal ECM formation of tendon-only and bone-only

spheroids, then to assess the effect of their co-culture on ECM formation. In contrary to their CSA and cell density results, tendon spheroids had an increase in ECM collagen content by day 20 (39.05 µg/sample ± 3.88) (**Figure 5.16**). However, bone spheroids collagen content was 76.12 µg/sample ± 16.60 at day 20 (**Figure 5.14**). GAGs measurements showed a similar trend, with tendon spheroids' at 7.31 µg/sample ± 1.05 by day 20 (**Figure 5.17**) while bone spheroids was 15.94 µg/sample ± 0.42 (**Figure 5.17**). These ECM formation results of separate cultures of tendon and bone spheroids provided a reference control for comparison to their co-culture. Accordingly, the summation of separate tendon and bone ECM content of collagen and GAGs had a significantly higher result than their mini-coculture and max-coculture (**Figures 5.20** and **5.21**). This indicated an inhibitory effect of co-culture on ECM collagen content. Besides, mini-coculture and max-coculture did not have a significantly different collagen or GAGs content in their ECM. The cause of this inhibitory effect was firstly attributed to a decrease of cell density caused by co-culture, as a similar observation has been reported in the literature (Wang *et al.*, 2007). However, upon examination of cell density, the summation of separate monocultures' cell density was not significantly different from mini-coculture and max-coculture. This result eliminated a decrease in cell density as the reason for the reduction of ECM collagen and GAGs content, leaving a change in cell protein synthesis as another possible reason for the inhibitory result. Unfortunately, due to limited time, this was not investigated further.

GAGs are abundant in cartilage (Aspberg, 2012; Couchman and Pataki, 2012) and the enthesis has a fibrocartilage component in its unique structure (Benjamin *et al.*, 2006; Paxton *et al*. 2012). Furthermore, formation of the enthesis is believed to be triggered by direct contact of bone and tendon cells in foetal life (Lu and Thomopoulos, 2013). Based on this fact, Wang and colleagues showed a chondrogenic transformation of the cells in co-culture, and they hypothesised that osteoblast-fibroblast interaction might eventually lead to enthesis formation (Wang *et al.*, 2007). Accordingly, ECM GAGs measurements were used as a sign of chondrogenic transformation caused by co-culture. Thus, there was no significant indication of chondrogenic transformation triggered by co-culture of bone and tendon cells (**Figure 5.21**). The ECM content of GAGs decreased due to co-culture (**Figure 5.21**). However, the chondrogenic transformation could have started at a molecular level but not been significant enough to translate into produced GAGs proteins by the cells. This is one of the limitations of the study, which can be improved by studying gene

expression of chondrogenic markers in the same models, using reverse transcription polymerase chain reaction (RT-PCR), immunohistochemistry (as performed in Wang *et al.*, 2007; and Calejo *et al.*, 2018) or transcriptomics (as performed in Kuntz *et al.*, 2018). Moreover, various levels of RTF/dRObb cell-cell contact in co-culture did not show a significant difference in ECM GAGs content (**Figure 5.21**), indicating no difference between mini-coculture and max-coculture.

At the end of this project, the ECM formation of RTF and dRObb cells in 3D and 2D was compared. The comparison aimed to examine which culture method resulted in a higher ECM formation per cell. 50K of each cell type was seeded in a standard tissue culture 96-well plate (2D) and a U-bottomed, cell-repellent 96-well plate (3D spheroid culture) and cell number, collagen and GAGs measurements were collected. There was no significant difference in collagen or GAGs measurements of tendon cells between 2D and 3D spheroid culture (**Figures 5.23** A and **5.24** A). In contrast, collagen and GAGs measurements of bone cells were conducted that showed higher 2D readings than 3D spheroid culture (**Figures 5.23** B and **5.24** B).

The work done in this study aimed to study cell-cell interaction in a novel spheroid-based 3D co-culture model. However, these tendon and bone spheroid models could be further used in other applications of spheroid culture. Tissue engineering using the spheroid method has a promising future. The use of spheroids as building blocks for large tissue engineered constructs have been reported in the literature (Fennema *et al.*, 2013; Blakely *et al.*, 2015; Laschke and Menger, 2017). Moreover, an organ printing concept is not inconceivable using spheroids as building blocks, since vessel-forming spheroid co-cultures of bone and endothelial cells were reported in the literature. By using spheroids as units, an arrangement of pure bone spheroids with a network of vessel-forming spheroids might enable efficient nutrients and gas supply to a thick tissue engineered construct.

In conclusion, the work performed in this chapter has demonstrated the development of a 3D co-culture system using spheroid culture. It has also shown the use of CSA, collagen, GAGs and cell density assessments to detect the effect of 3D co-culture. The developed system was used to co-culture bone and tendon cells in two different cell-cell interaction levels: mini-coculture and max-coculture. CSA and cell density of tendon spheroids decreased over 20 days of culture. In contrast, they both increased in bone, mini-culture spheroids and max-coculture spheroids after 20 days. ECM formation increased after 20 days for tendon, bone, mini-coculture and max-coculture

spheroids. The co-culture of bone and tendon cells using spheroids resulted in a decrease of CSA and ECM formation compared to the summation of separately cultured tendon and bone cells in spheroids. However, there was no significant difference in cell density between the co-cultured tendon and bone cells compared to the summation of separately cultured tendon and bone cells. Moreover, different levels of RTF/dROb cell-cell interaction did not have a difference in their co-culture effect.

Chapter 6. General Discussion

6.1 The novel 3D co-culture systems

The three main aims of this study were to 1) design and develop 3D co-culture systems that allow two distinct cell type populations to have an interface, 2) assess and characterise system suitability for cell integration, and 3) use the developed system to investigate the effect of co-culturing tendon and bone in 3D. These aims were used to investigate the main hypothesis, which was '*3D co-culture of tendon and bone cells results in a change in GAGs as a sign of chondrogenic transformation in the ECM in addition to a change in cell density and collagen content when compared to the summation of 3D monocultures of the same cell types'*. To test this hypothesis, the use of tissue engineering and co-culture techniques to model the enthesis in 3D were employed.

As demonstrated in the previous chapters, two 3D co-culture models were designed and developed. These two co-culture models can be used to study the cellular interaction between the cell types of the enthesis. They also can be used to study other tissue interfaces in the body, such as nerve to muscle, muscle to tendon, or cartilage to bone. Furthermore, the developed system could be used in other fields such as cancer migration studies, drug development, immune cell responses and many other cell-cell interaction-based studies.

Following the development of the two 3D co-culture models, 3D optimised assessments were described. These assessments helped determine the suitability of the systems for cellular integration and demonstrate the use of cell density and ECM formation to detect the effect of 3D co-culture on cellular behaviour.

6.1.1 Design of 3D co-culture models

As hypothesised in chapter 1 of this thesis, a better understanding of natural enthesis development could lead to discovering better management options after enthesis injury. However, studying the development of the enthesis requires a standardised model that can be used to conduct reproducible studies. Accordingly, Wang *et al.* (2007) described the first attempt to develop a 2D co-culture system of primary tendon and bone cells to model the enthesis. Their developed system was used to culture primary fibroblasts and osteoblasts with direct contact. They reported that direct contact between tendon and bone cells resulted in an increased expression of enthesis interface gene markers such as type II collagen, aggrecan and cartilage oligomeric matrix protein (COMP). Accordingly, they hypothesised that direct contact of tendon and bone cells in the co-culture can lead to chondrogenic transformation.

Similar findings were also reported in the literature using human tendon and bone cells (Calejo *et al.*, 2018). However, these studies were conducted in standard 2D culture, in which the cells are significantly different in their proliferation, gene expression, protein production and interactions compared to 3D culture (Tibbitt and Anseth, 2012; Lee *et al.*, 2013; Luca *et al.*, 2013). The difference between 2D and 3D culture has been discussed in detail in **section 1.2.2.1**. Therefore, the design and development of reproducible 3D co-culture systems was the first aim of this study.

Attempts to multi-culture distinct populations in 3D have been previously reported in the literature, including a scaffold of four zones mimicking the zones of the enthesis with incorporation of chondrocytes, fibroblasts and osteoblasts (Kim *et al.*, 2014). Li *et al.* (2016) described the development of a scaffold that mimics the tendon-cartilage-bone arrangement of the enthesis. Moreover, an implantable biphasic cartilage-bone scaffold has also been reported (Radhakrishnan *et al.*, 2018). Liu *et al.* (2017) reported the use of decellularised tendons with collagen fibres disrupted at the edges to mimic the disorganised collagen fibres of the enthesis, for use as a bone-tendon-bone attachment. Although these studies provide excellent models for enthesis reconstruction and surgical replacement, they are not suitable to study the natural development of the enthesis and the effect of co-culture on cells. All the scaffolds presented in these studies have ECM structure and components manipulated and prepared artificially to resemble the four zones of the enthesis. Although this has helped mimic the normal enthesis, it has also added more factors that may affect cellular interaction and gene expression, which are sensitive to the different mechanical characteristics of the scaffold (Urrutia, 2017). Other similar studies that have described the use of co-cultures to produce a surgical repair option have been listed in (**Table 6.1**). All of these studies aimed to generate a transplantable scaffold for use in orthopaedic surgeries. Both 3D co-culture systems presented in this thesis aimed to study the cell-cell interaction between two distinct cell populations in 3D co-culture. Accordingly, the two developed 3D co-culture systems aimed to produce results that could be confidently attributed to the effect of 3D co-culture on cells.

In both 3D co-coculture systems developed in this study, the formation of a 3D interface between the two distinct cell populations in the hydrogel-based and spheroid 3D co-culture systems was confirmed by CFM dataset z-axis projection images. The study of CFM dataset Z-axis projections showed a clear demarcation of distinctively and fluorescently labelled tendon and bone cells (**Figure 3.20**) in both systems.

However, in the hydrogel-based method, it did not show in which level of the Z-axis range the cells were residing, i.e., were the cells distributed evenly across the depth of the scaffold or aggregated at the bottom of the scaffold? Therefore, 3D digital simulations were used, which verified the distribution of the co-cultured cells throughout the thickness of the hydrogel construct (**Figure 3.21**). This was not required for the spheroid 3D co-culture as the cells were compacted in a minimal structure compared to the large-scale hydrogel-based method.

To the author's knowledge, the use of spheroid culture to study the effect of tendon and bone cells in co-culture has not been reported in the literature. However, spheroid culture is a popular technique to study cell-cell interactions in the broader field of tissue engineering, including examples like co-culture of islet cells and bone marrow stem cells (Wittig *et al.*, 2013; Shin *et al.*, 2015), and bone spheroid neovascularisation when osteoblasts are co-cultured with endothelial cells (Beger *et al.*, 1998; Road, 2003; Alajati *et al.*, 2008; Walser *et al.*, 2013). Therefore, the possibilities for exploring the effects of co-culture on different cell type combinations are endless.

Table 6.1: Reported scaffold-dependent co-culture for surgical reconstruction of enthesis in various

Type of study	Cell source and types	Co-culture system design	Main outcomes	reference
In-vitro cell culture, construct development, and testing	Human fibroblasts, chondrocytes, and osteoblasts	Four collagen layers separately engineered and mineralised to mimic natural enthesis layers	A Multilayer scaffold. Provided physical, chemical, and mechanical environment mimicking natural layers of the enthesis. Supported adhesion and proliferation of all cell types in the study	(Kim et al., 2014)
In-vitro cell culture and construct development followed by in-vivo testing	Rabbit bone marrow stromal cells (BMSCs)	physically modified tendon extracellular matrix (ECM) into a Random-Aligned-Random composite using ultrasound treatment	Enhanced expression of chondrogenic and osteogenic transformation genes (Sox9, Runx2, Col2a1) compared to unmodified tendon ECM. The modified tendon ECM enhanced bone and fibrocartilage formation at the interface	(Liu et al., 2017)
In-vitro cell culture and construct development followed by in-vivo testing	Rabbit BMSCs, osteoblasts, and chondrocytes	Triphasic silk-based graft in which three regions respectively referring to ligament, cartilage and bone layers of interface were designed	High proliferation and differentiation ability into relevant cell lineage. Enhancement of osseointegration confirmed by robust pull-out force. Formation of three-layered structure (micro-CT and histological analysis)	(Li et al., 2016)
In-vitro cell culture and construct development followed by in-vivo testing	Rat osteoblasts and Caprine chondrocytes	Gradient biphasic hydrogel construct with chondroitin sulfate nanoparticles (ChS-NPs) and nanohydroxyapatite (nHA) (~30-90 nm) in chondral and subchondral hydrogel zones respectively	Higher osteoblasts proliferation. Co-culture showed layer-specific retention of cells and cell-cell interaction In-vivo experiment showed complete closure of defect after 8 weeks of culture compared to non-closure of defect observed in control, higher bone mineral density, better biomechanical compression endurance.	(Radhakrishnan et al., 2018)
In-vitro cell culture, construct development, and testing	Rabbit fibroblasts, chondrocytes, and osteoblasts	Decellularized rabbit Achilles tendons fabricated as stratified scaffold containing three biofunctional regions supporting fibrogenesis, chondrogenesis, and osteogenesis	Improved bio-physio-chemical properties of the scaffold. Up-regulated expression of cartilage- and bone-relevant markers. Confirmation of tissue-specific ECM formation	(Wang et al., 2015)
In-vitro cell culture, construct development, and testing	Mouse myoblasts (C2C12) and fibroblasts (NIH3T3)	Triphasic scaffold made from either Poly(ε-caprolactone) / collagen or poly(ʟ-lactide) / collagen co-electrospinning a scaffold with 3 regions	Regional variation in mechanical properties reported in different layers of the triphasic scaffold. Cell attachment and myotube formation were observed.	(Ladd et al., 2011)
In-vitro cell culture, construct development, and testing	BMSCs	Self-organised Bone-ligament-bone construct	Structural and functional properties mimics native ACL. Grafts achieved better vascular and neural development than current golden standard therapeutic options.	(Ma *et al.*, 2012)
In-vitro cell culture, construct development, and testing	Myogenic precursor cells including primary satellite and rat tendon fibroblasts	Self-organised muscle-tendon construct	Increase in the expression and localisation of paxillin and present of relevant structural feature resembling native muscle-tendon junction	(Larkin *et al.*, 2006)

6.1.2 Two novel systems, two possible different applications?

Upon wider review of the enthesis literature, two main fields are apparent: 1) research aiming to produce clinically relevant enthesis constructs (i.e. surgical implants), and 2) research aiming to understand the development and healing process of the enthesis. The scaffold-dependent 3D co-culture system is more suitable for further development into a surgical implant. Whereas, the spheroid 3D co-culture is more suitable to study cell-cell interactions, signalling and the molecular events of enthesis development in a rapid and straightforward system.

6.1.2.1 Development of a 3D model that has the potential for use as an enthesis construct.

The work presented in chapter 3 and chapter 4 of this thesis showed the design and development of a 3D scaffold-dependent co-culture system to model the interface between tendon and bone cells. The system depended on using a half-well plug to block half of a well of a 24-well plate, allowing casting of a single cell-encapsulated hydrogel. After the gel set, the half-well plug was removed to expose the other half of the well (**Figure 3.3** C). An encapsulated hydrogel with another distinct cell population was cast on the exposed half-well to allow a side-to-side culture in a single well (**Figure 3.3** E). To the author's knowledge, a similar technique using encapsulated hydrogels to co-culture two distinct cell populations has not been reported.

Other techniques in the literature aiming to test the same aim of cellular include the use of a commercially available poly-L-lactic acid (PLA) woven fabric scaffold (Kim *et al.*, 2014). This study cultured bone and tendon cells on opposing sides of the scaffold with a 10 mm cell-free gap between them. They reported no migration of cells into the gap; hence, no direct cell-cell contact was established. Therefore, the co-culture effect observed and reported in that study was most likely due to the cell types sharing the same environment and culture media, which resulted in a paracrine effect of co-culture. In contrast, the hydrogel-based scaffold-dependent 3D co-culture model reported in this thesis offered a direct cell-cell contact for the study of co-culture. Another study showed the use of silk scaffolds to co-culture fibroblasts, bone marrow stem cells (BMSCs) and osteoblasts, to evaluate the co-culture effect on the differentiation of BMSCs (He *et al.*, 2012). The study reported a chondrogenic transformation of BMSCs caused by co-culturing them between fibroblasts and osteoblasts. Cell-cell contact was not confirmed in this study. Nonetheless, the experimental design was excellent for the purpose of the study, in which they

experimented on five sample groups: 1) fibroblasts, 2)fibroblasts/BMSCs, 3) BMSCs, 4) Osteoblasts/BMSCs, 5) Osteoblasts (**Figure 6.1**). This combination of sample groups offered two monoculture controls (fibroblasts and osteoblasts) and three test groups (fibroblasts/BMSCs, osteoblasts/BMSCs, and BMSCs). In this thesis, the quantitative production of GAGs was used as an indication of chondrogenic transformation, as fibrochondrocytes produce much more GAGs than fibroblasts and osteoblasts (Koob and Vogel, 1987; Vogel *et al.*, 1993, 1994). In contrast, they investigated the effect of co-culture via assessment of the gene expression of chondrogenic markers using reverse RT-PCR and immunohistochemistry, which is a more accurate analysis of chondrogenic transformation. A similar RT-PCR analysis was planned and designed for this project, however, due to lack of time and previous experience performing RT-PCR, this experiment was not carried out despite sample collection. Future efforts to uncover the effects of using the developed 3D co-culture systems on gene expression and signalling pathways are vital for the progression of this work.

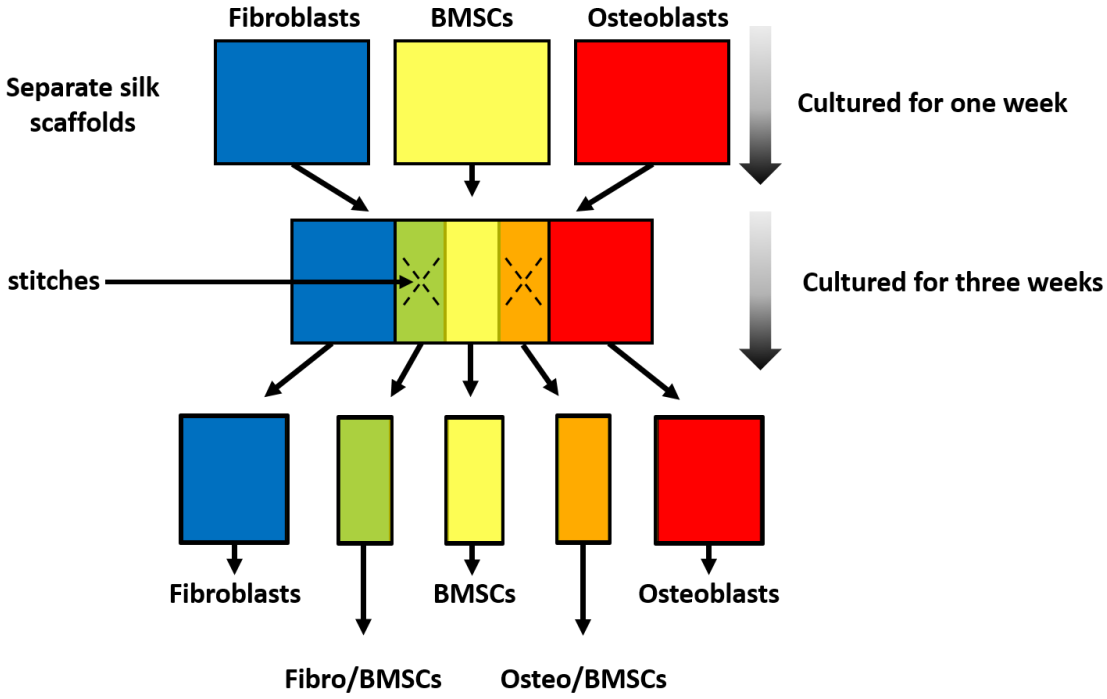

Figure 6.1: A self-drawn diagram depicting the experimental design adopted from He et al. *(2012) for their co-culture model, investigating the effect of fibroblast, BMSC and osteoblast co-culture on chondrogenic transformation.*

Following the confirmation of 3D interface formation in **chapter 3**, hydrogel suitability for the long-term experiment was assessed in **section 4.4.1** of **chapter 4**. Based on support for cell attachment, cell viability and hydrogel structural integrity, fibrin hydrogel was chosen for further investigations of the effect of co-culture on cell density and ECM formation. Fibrin hydrogel has been well documented and researched over the past seven decades when it was first isolated as a hydrogel (Wagreich and Tarlov, 1945; Ferry and Morrison, 1947). It has also been used as a fibrin glue in various applications in the past, including as a cerebrospinal fluid sealant (Sierra, Nissen and Welch, 1990), or in repair of parenchymal kidney injuries (Braun *et al.*, 1977) or a ruptured calcaneal tendon (Rupp and Stemberger, 1978). Current uses of fibrin glue include improving neurodegeneration in a rat model of acute spinal injury (E. Garcia *et al.*, 2019), skin regeneration (Miller *et al.*, 2019) and vocal cord wound closure (Chen *et al.*, 2019). It was also used in drug and cell delivery applications (Chotitumnavee *et al.*, 2019; J. P. Garcia *et al.*, 2019; Krug *et al.*, 2019; Masgutov *et al.*, 2019; Musto *et al.*, 2019; Rowley *et al.*, 2019; Rubalskii *et al.*, 2019; Zhao *et al.*, 2019). Due to cell attachment proteins being naturally present in fibrin hydrogel, it has become popular in cell culture applications. Bone marrow stem cells were seeded on top of fibrin hydrogel for culture almost five decades ago (Hahn and van Kersen-Bax, 1971). This progressed into tissue engineering uses, including encapsulation of cells in fibrin hydrogel. An early report of this use included the work of Idahl *et al. (*1980), when they encapsulated insulin producing beta-cells in fibrin hydrogel. Despite recent advances in biomaterials and the increasing number of cell-encapsulation-friendly materials, fibrin hydrogel is still a popular choice for tissue engineering and cell encapsulation (Bou Assaf *et al.*, 2019; Musto *et al.*, 2019; Schnabel-Lubovsky *et al.*, 2019). Moreover, even though fibrin hydrogel has weak mechanical properties, it is still used in musculoskeletal tissue engineering (Paxton *et al.* 2010; Lebled *et al.* 2014; Khodabukus *et al.*, 2007; Paxton *et al.*, 2012).

Investigating the effect of co-culture required the use of a suitable control. For this purpose, monocultures of hydrogel-encapsulated bone and tendon cells were cultivated at the same time as co-cultures (see **section 4.3.5**), resulting in three groups of cell-encapsulated fibrin hydrogels: 1) tendon-only, 2) bone-only, and 3) their co-culture. To test the effect of co-culture after 20 days of cultivation, cell density and ECM content of collagen and GAGs were measured. Cell density was evaluated to assess if co-culture affected cell proliferation. Also, to determine the co-culture effect, collagen and GAGs were evaluated to assess how much ECM was produced in the

scaffold. This was an essential indicator of the ability of cells to produce their own ECM for replacement of the biodegradable fibrin hydrogel.

The effect of co-culture was evaluated by comparing the summation of the results of the monocultures of tendon-only and bone-only cell-encapsulated fibrin hydrogels to their co-culture. This showed no significant difference in ECM collagen and GAGs content caused by their co-culture (**Figures 4.14** and **4.16**), which was not as hypothesised at the beginning of this study. Surprisingly, to the author's knowledge, only one article in the literature has compared quantified collagen and GAGs measurements for assessment of ECM formation to study the effect of co-culture of bone and tendon cells (Cooper *et al.*, 2014). They also reported no significant effect of co-culture on ECM collagen and GAGs contents after 28 days of culture (Cooper *et al.*, 2014). Other studies in the literature have assessed the effect of co-culture by studying gene expression of osteogenic (e.g. Runx2 and Osteonectin), tenogenic (e.g. TNMD and Scleraxis), and chondrogenic (e.g. aggrecan, Col2a1 and COMP) phenotypes. In these studies, the effect of co-culture was determined by showing an increase in chondrogenic gene expression markers (Wang *et al.*, 2007; He *et al.*, 2012; Calejo *et al.*, 2018). These markers are indicators of the effect of co-culturing bone and tendon cells with direct contact on their phenotypic change and behaviour.

The scaffold-dependent 3D co-culture and its assessment methods described in this thesis offer a reproducible system to explore the effect of direct cell-cell interaction in a 3D scaffold-dependent co-culture. Other hydrogel models to assess co-culture effect have been reported (Chen *et al.,* 2008; Chwalek *et al.*, 2014; Zehnder e*t al.,* 2017). In the Chen et al. study (2008), the system developed a 3D co-culture using hydrogels, although the two distinct cell types did not have direct cell-cell contact. The method presented in the Chwalek *et al.* (2014) publication offered a hydrogel-based co-culture system that has the two distinct cell types distributed through the hydrogel in a homogenised state.

In contrast, the system developed in this study offers a single 3D interface between the two distinct cell populations, allowing only the cells of the interface to have direct cell-cell communication. In the hydrogel-based co-culture system described in Zehnder *et al.* (2017), the cells were layered on top of the hydrogel and cultured in a homogenised mixture. In contrast, the cells in this study were encapsulated in hydrogels.

Moreover, assessment methods of suitability for cell integration were presented after the development of the co-culture system. These assessments methods could be used in combination with the scaffold-dependent 3D co-culture system for other applications beyond tendon and bone cell co-culture. Other tissue interface combinations could be used, such as muscle-tendon, cartilage-bone or nerve-muscle. It could also be used for other concepts, such as migratory studies of immune cells, cancer cell invasion, or reinnervations. The practicality of the co-culture system also offers an option to use two types of hydrogels in the system, depending on hydrogel-cell combination suitability. For example, osteoblasts could be encapsulated in a stiffer hydrogel while tendon fibroblasts could be encapsulated in a softer hydrogel, representing the normal stiffness of the natural ECM of each tissue.

A key limitation of this study was lack of a mechanical testing component. As already established in the literature, mechanical stimulation has an integral role in enthesis development (see **section 1.1.3.2**). Other limitations of using the scaffold-dependent system to study the effect of co-culture included the labour-intensive, time- and resource-consuming process of 3D co-culture. For example, to run a single experiment to study the effect of co-culture on one factor (i.e., cell density, collagen or GAGs), three groups consisting of tendon-only, bone-only and their co-culture cell-encapsulated hydrogels had to be prepared in the same day. This included making one cell type suspension and encapsulation in fibrin hydrogel, then waiting for the fibrin hydrogel to set, followed by making the other cell type suspension in the same way, before adding growth media. Moreover, the duration of the study was originally 28 days; this was adjusted to 20 days as repeats needed to be increased to complete a full set of cell density, collagen and GAGs experiments with their independent repeats. This had a significant impact on the number of independent experiments conducted. Furthermore, fibrin biodegradation and contraction over time were important limitations for the duration of the study. The aim of using fibrin hydrogel was for eventual replacement by the cells' own ECM, which requires matching fibrin degradation rate with ECM formation rate. The use of fibrin hydrogel provided excellent biocompatibility for the cells; however, it lacked the desired mechanical properties of natural tendon and bone tissues. Another limitation of this system was the inability to attribute the changes observed in cell density, collagen or GAGs content to a distinct cell population.

6.1.2.2 Development of a 3D model suitable for studying cellular interaction, signalling and molecular events in enthesis development

In **chapter 5** of this thesis, the spheroid co-culture of rat tendon and bone cells was described. Four groups of spheroids, including two monocultures and two co-cultures (tendon-only, bone-only, mini-coculture and max-coculture), were used to test the main hypothesis.. The cross-sectional surface area (CSA), cell density, collagen and GAGs content for each group of spheroids was assessed.

These investigations revealed a parallel decrease in CSA and cell density of tendon spheroids (**Figures 5.8** and **5.11**), which was surprisingly accompanied by an increase in ECM collagen and GAGs content. Similar observations in fibroblast spheroids were reported by Hoyer *et al.* (2015) but with contradicting results of decreased GAGs measurements. They, however, measured GAGs soluble in the growth medium, whereas in this study the GAGs content in the ECM of the spheroids was assessed. On the other hand, the bone spheroids showed an increase in CSA, cell density, collagen and GAGs content of the ECM (**Figures 5.8, 5.11, 5.15**, and **5.16**). The summation of these monoculture results was compared as controls to the two types of co-cultures, which revealed a significant difference in CSA, collagen and GAGs measurements caused by the co-culture, when compared to the control summation of monocultures (**Figures 5.17, 5.19,** and **5.20**). This is in support of the literature where co-culture of chondrocyte and osteoblast spheroids result in a decrease in GAGs caused by the co-culture (Jiang, Nicoll and Lu, 2005).

In contrast, co-culture can trigger an increase in GAGs measurements, as observed when synovial membrane stem cells were co-cultured with osteoblasts (Xie *et al.*, 2018), indicating that different combinations of distinct cells in spheroid co-culture can produce contrasting results. However, no significant difference in cell density due to co-culture was observed (**Figure 5.18**), which is also in support to findings reported by Jiang, Nicoll and Lu (2005) using chondrocytes and osteoblasts, and Xie *et al.* (2018) using synovial membrane stem cell and osteoblast spheroid co-cultures. The effect of different degrees of cell-cell contact was also examined by comparing the two groups of co-cultures (i.e. the mini-coculture and max-coculture). This revealed no significant difference between co-culturing tendon and bone cells with minimum contact or maximum contact (**Figures 5.17, 5.19, 5.18** and **5.20**). However, further analysis of the difference between mini-coculture and max-coculture regarding gene expression and signalling pathways can be further studied.

These results showed that cell-cell contact between tendon and bone cells in spheroid co-culture caused a decrease in ECM formation within the spheroid. This supports part of the main hypothesis of this thesis, that 3D co-culture of tendon and bone cells results in a change in cell density, collagen content and GAGs as a sign of chondrogenic transformation in the ECM, when compared to the summation of same cell monocultures. In contrast, the scaffold-dependent and hydrogel-based system did not show a similar result. This could be attributed to the immediate and large-scale cell-cell contact observed in spheroid co-culture, compared to the low-scale and interface-limited contact in the scaffold-dependent system. Moreover, the distinct populations of cells in the scaffold-dependent system had more space between them, which, in turn, could delay the effect of direct cell-cell contact.

The spheroid co-culture system offered a simple and easy technique to study cell-cell interactions. The use of mini-coculture and max-coculture variants of co-culture offered potential insight on the role of scale of cell-cell contact. To the author's knowledge, most spheroid co-cultures have been performed as a max-coculture variant of co-culture. Another variant of cell-cell contact co-culture that could be introduced is the use of separately cultured spheroids that have a common growth medium exchange. This level of cell-cell contact will assess the paracrine effect of two distinct spheroids. A proposed technique would be to microfabricate U-bottom moulds for 96-well plates on an agarose layer. This re-engineered hydrophobic agarose surface with U-bottoms would help form spheroid cultures. Upon the formation of spheroids on these microfabricated well moulds, the walls made from agarose could be lowered between adjacent spheroids by manually cutting the agarose. This would allow two adjacently placed spheroids to share the same growth medium, resulting in a non-direct co-culture. The results of such a system could be compared to max-coculture to investigate the role of direct cell-cell contact on co-culture. Studies focusing on the effect of co-culture on protein synthesis, gene expression, cell signalling, and proteomics are ideal for the use of this array of different levels of cell-cell contact.

The work performed in chapter 5 of this thesis aimed to study cell-cell interaction in a novel spheroid-based 3D co-culture model. However, these tendon and bone spheroid models could be further used in other applications of spheroid culture. The tendon-only and bone-only spheroid data presented in chapter 5 could be beneficial to the field of bone, tendon and ligament tissue engineering. The use of bone

spheroids for filling defects of bones has been reported (Yanagihara *et al.*, 2018), as well as for tendons and ligament tissue engineering (Hoyer *et al.*, 2015; Kraus *et al.*, 2018). Tissue engineering using the spheroid method has a promising future. The use of spheroids as building blocks for large tissue engineered constructs has been reported (Fennema *et al.*, 2013; Blakely *et al.*, 2015; Laschke and Menger, 2017). Moreover, an organ printing concept is not inconceivable, using spheroids as building blocks when vessel-forming spheroid co-culture of bone and endothelial cells, as reported by Mironov *et al.*, (2009) and Walser *et al.*, (2013). By using spheroids as units, for example as an arrangement of pure bone spheroids with a network of vessel-forming spheroids, this might enable adequate nutrient and gas supply to a thick tissue engineered construct.

Finally, the limitations of spheroid culture use include the small-scale nature of spheroid culture, which presents logistical challenges. These challenges include finding suitable high-throughput spheroid generation methods, applying mechanical stimulations, and difficulty in quantification of ECM components due to the assay range sensitivities not detecting the small ECM component quantities produced. Moreover, cells have different intra-cellular adherence strengths. Therefore, some cells may not be suitable for spheroid formation with standard methods.

6.2 Use of external stimuli on the developed 3D co-culture systems to advance enthesis research in the future

All previous work performed on the 3D co-culture systems was to assess the basic constituent of the co-culture: cell interaction. The work aimed to understand the fundamental responses of static, unstimulated cells in co-culture to characterise their cellular interaction behaviour. Accordingly, these were the first steps towards creating a model to research the enthesis. This should also include further characterisation of gene expression and signalling pathways.

Following complete characterisation of static 3D co-culture, external stimuli should be investigated. Stimuli can include mechanical and chemical factors. However, it is important to recapitulate the complexity of the enthesis' ECM mechanical environment, different cell populations, and the effect of mechanical stimulation on development and maturity as discussed in **sections 1.1.2** and **1.1.3.2** (**Table 6.1**). Accordingly, an attempt to incorporate a third and/or fourth cell type to the developed systems can be proposed for future studies. In the scaffold-dependent 3D co-culture, a modification of the system can be applied that would enable the addition of a third

compartment as a transitional layer between the tendon and bone. This could be achieved by changing the splitting of the well plugs described in **section 3.3.2.2.2** from two parts into three parts. This transitional compartment can be used to add a third cell type and convert the co-culture into a tri-culture. Candidate cell types for this third layer could be chondrocytes, fibrochondrocytes or fibroblasts overexpressing chondrogenic genes. Moreover, it would be exciting to add MSCs to all cell-encapsulated hydrogel groups (tendon-only, bone-only and their co-culture) and characterise their differentiation when cultured in monocultures compared to co-cultures.

Moreover, spheroid 3D co-culture can be further expanded into a tri-culture of tendon, bone and cartilage cells. This would allow the exploration of various cellular interactions between different types of cells. For example, using tendon, bone and cartilage cells, monocultures of each cell type could be compared to the others. This could be followed by characterisation of different combinations for co-culture (tendon-bone, bone-cartilage and cartilage-tendon), ultimately ending in the assessment of their tri-culture.

6.2.1 Incorporating mechanical stimuli in enthesis research

The mechanical stimuli during enthesis development after birth dictate its maturation (Benjamin and Ralphs, 1998; Benjamin *et al.*, 2002; Schwartz *et al.*, 2013). Schwartz *et al.* (2013) used neonatal mouse experimental models to paralyse the rotator cuff muscles in one side and preserve the contralateral side as controls. The paralysis stopped muscle loading on the enthesis and denied its natural mechanical stimuli. As a result, the authors reported defects in the fibrocartilage formation in the enthesis and a decrease in its pull-resistance before failure in the paralysed side compared to the normal side. Accordingly, mechanical stimulation has an integral role in the maturation of the mechanical properties and functional efficiency of the enthesis ECM.

Incorporating mechanical stimuli in tissue engineered products has been reported heavily in the field of musculoskeletal research. However, the enthesis has complex mechanical properties that transitionally change across the multilayer structure of the enthesis, further complicated by the role of active mechanical stimuli exerted by muscle movements. Therefore, it is crucial to first classify the types of mechanical stimulants. These are of two general types: 1) passive stimulants, and 2) active stimulants. Both these types of mechanical stimulants affect the enthesis and, therefore, an ideal *in vitro* model should be exposed to both types.

Suitable mechanical properties of the ECM (i.e. passive stimulation) that mimic the natural enthesis and mechanical stimulation (i.e. active stimulation) of a tissue engineered construct are an important factor for enthesis regeneration research (Locke, Abraham and Killian, 2017). All cell populations in the enthesis are mechanoresponsive; therefore, it is essential to optimise a tissue engineered product that mimics the mechanical environment of the enthesis (Lu and Thomopoulos, 2013).

Evaluating the effect of mechanical stimulation should first uncover the effect of passive mechanical stimuli on cells (i.e. mechanical properties of scaffolds). This can be followed by incorporating active mechanical stimuli.

6.2.1.1 Incorporating mechanical stimuli in the two developed 3D co-culture systems reported in this thesis

6.2.1.1.1 The scaffold-dependent 3D co-culture system

To further develop the 3D co-culture systems reported in this thesis, active mechanical stimulation needs to be introduced to the systems. In the hydrogel-based system, a bioreactor similar to that used in Testa *et al.*, (2017) can be used to exercise the constructs. Bioreactors are devices that support an *in vitro* biologically relevant environment, helping to mimic the natural tissue. Moreover, commercially available silicone cell culture chambers (e.g. flexiPERM, SARSTEDT, Germany) provide an excellent application for the scaffold-dependent 3D co-culture system described in this thesis. These silicone chambers are flexible and can be attached to a bioreactor motor that can exert stretching load. However, a more versatile mechanical stimulation that involves compression in addition to stretching is of equal importance. This is because tendons require stretching stimulation to develop, while cartilages need compressive loading, and both tissues are part of the transitional layers of the enthesis (Benjamin and Ralphs, 2001; Benjamin *et al.*, 2006; Font Tellado, Balmayor and Van Griensven, 2015). Accordingly, an ideal bioreactor for enthesis research should provide both stretching and compressive loading.

It is important to consider the transitional mechanical properties of the enthesis starting from the hard, weight-bearing bone layer, through the compressive resistant fibrocartilage layer, to the tensile tendon layer. Moreover, the transition in mineralisation and cellular populations should be considered. These factors will dictate the choice of suitable hydrogel (or hydrogels) that can demonstrate these unique mechanical properties of the enthesis.

6.2.1.1.2 Spheroid 3D co-culture system

Deploying mechanical stimulation on spheroid 3D co-culture has different challenges from the scaffold-dependent system. The fact that spheroids are measured in the micrometre scale make it more difficult to subject them to mechanical stimuli and measure the change caused by it. There are many methods in the literature that describe a protocol to apply compression forces and measure their effectiveness.

Methods for applying mechanical forces include embedding spheroids to study spheroid tumour growth in hydrogels of different stiffnesses (Helmlinger *et al.*, 1997; Cheng *et al.*, 2009; Mills *et al.*, 2014), using osmotic pressure on spheroids contained in a film (Montel *et al.*, 2011), or using controlled microtweezers (Montel *et al.*, 2011). Other possible methods to exert mechanical stimulation on spheroids could be the use of low-speed centrifugation or a plunger-based increase in hydrostatic pressure on spheroid culture, which would require designing a suitable bioreactor.

6.2.1.2 Studying the effect of mechanical stimuli

Mechanical stimulation effect on cellular signalling pathways:

Upon applying the mechanical stimulant for the duration of a proposed experiment, cell viability, cell density, ECM formation, gene expression and signalling pathways could be investigated, comparing mechanically stimulated samples to static controls. Moreover, stiffness of spheroids could also be assessed by the use of micro-cantilevers, as described by Montel *et al.*, (2011).

Mechanical stimulation of an *in vitro* developed construct seeded with fibroblasts caused significantly different signalling activity changes to the ECM molecules, intra-cellular molecules and cytoskeleton proteins when compared to static constructs. These various signalling activities included an upregulated expression of collagen molecules such as type VI collagen alpha-3, type I collagen alpha-2 and 1 (Smith *et al.*, 2012; Fang and Eglen, 2017). Moreover, Li *et al.* (2006) reported that compressive mechanical load on MSC-encapsulated hydrogel facilitated the expression of Sox9, a chondrogenic transcription factor. Other studies of MSCs under compressive stimuli showed increased cartilage-specific collagens and GAGs (Huang *et al.*, 2004; Mauck *et al.*, 2007; Erickson *et al.*, 2009). Accordingly, studying the effect of 3D co-culture combined with mechanical stimulation might elucidate key cellular interactions and signalling pathways that are crucial for enthesis development.

These findings could also be explored by using the spheroid 3D culture presented in this thesis. The system provides an easy method to create various groups of

spheroids, such as tendon, bone and potentially cartilage spheroids. The effect of mechanical stimulation using methods discussed previously in **section 6.2.1.1.2** could be explored, in addition to co-culturing groups of them to combine mechanical stimulation and co-culture.

Mechanical stimulation effect on ECM structure and mechanical properties:

Mechanical stimulation has been shown to improve the mechanical properties of tissue engineered products in the literature. Xu *et al.* (2014) have described how uniaxial mechanical stimulation of a poly(L-lactide-co ε-caprolactone)/collagen (P(LLA-CL)/Col) scaffold seeded with tendon-derived stem cells has triggered tendon regeneration and improved mechanical properties in a rabbit patellar tendon defect model. Additionally, Deng *et al.* (2009) reported the use of static stretching stress on a polyglycolic acid scaffold seeded with human fibroblasts, which resulted in improved mechanical properties with organised collagen fibres. Moreover, an improvement in mechanical properties and tensile strength in an enthesis model made from a decellularised bone scaffold and highly dense type I collagen seeded with fibrocartilage cells was reported by McCorry *et al.* (2017). These studies have demonstrated the feasibility of applying mechanical stimuli to improve the structural mechanical properties of tissue engineered products. This concept could be adopted for the developed scaffold-dependent co-culture system for further improvement of enthesis modelling.

6.2.2 Incorporating chemical stimuli in enthesis research

Growth factors associated with tendon and bone healing have been researched in the field as a treatment option to stimulate enthesis repair and formation (Paxton *et al*., 2012). Ectopic endochondral ossification can be induced in *in vivo* models by local application of bone morphogenetic proteins (BMP) (Saito *et al.*, 2001). Hashimoto *et al.* (2007) hypothesised that local application of BMP-2 might provide suitable stimulation for enthesis formation in a rabbit model based on the Saito *et al.* (2001) findings. It has also been shown that healing at the enthesis was accelerated by incorporating BMP-2 into fibrin or collagen and hyaluronic sponges (Kim *et al.*, 2007; Seeherman *et al.*, 2008).

Moreover, inceased formation of the fibrocartilagenous and bone layers of the enthesis, accompanied by elevated gene expression of cartilaginous tissue and improved mechanical properties, were reported when BMP-2 incorporated into polyethylene glycol hydrogels with progenitor cells were compared to controls (Chen

et al., 2011). The use of other growth factors to assess formation of a fibrocartilaginous layer in the enthesis has also been reported. Granulocyte colony-stimulating factor (G-CSF) has been incorporated within a gelatin hydrogel that has been shown to increase the ultimate tensile strength at the enthesis, accompanied by upregulation of osteogenic markers (Sasaki *et al.*, 2008). The use of trasforming growth factor beta (TGF-ß) has also been tested as an enhancer for enthesis healing using sustained application of TGF- ß3, which showed an increase in interface strength in the tested group compared to controls (Manning *et al.*, 2011).

Accordingly, the use of chemical stimuli can aid the mechanical properties of scaffolds incorporated with cells. Furthermore, studying gene expression and signalling pathways affected by these chemical stimuli will help elucidate the various factors affecting enthesis development and maturation.

Chapter 7. Conclusion

The work presented in this thesis describes the successes and challenges in developing novel 3D co-culture systems to model the enthesis *in vitro* using tissue engineering techniques. It has been highlighted that repair of the damaged enthesis in patients suffering from musculoskeletal trauma or spondyloarthropathies is impaired and that current gold standard therapy has high failure and re-injury rates. To explore other possible therapeutic options, the knowledge gap surrounding the natural development and healing processes of the enthesis must be investigated. One way to achieve this is to produce a 3D co-culture system that allows cells to be cultured together at an artificial interface.

Two contrasting methodologies were conceived, designed and produced to co-culture bone and tendon cells in 3D with a direct interface between the two cell types. These two novel designs were shown to successfully result in direct cell-cell contact and both have not been reported previously in the literature.

The development and characterisation of the two 3D co-culture methods presented here will allow for a wide array of further research focused on the healing and/or development of the enthesis *in vitro*. Furthermore, these *in vitro* systems offer a suitable platform for investigating the effect of mechanical and/or chemical stimuli to study resulting mechanical properties, gene expression, signalling pathways and protein synthesis of co-cultured cells, thereby facilitating future exciting research on enthesis biology, engineering and therapy. The systems themselves could also be adapted for use in other related research fields, and as such may become important research tools in musculoskeletal tissue interface regeneration.

The hydrogel-based 3D design was accompanied by a series of tests to facilitate appropriate hydrogel choice. These tests included cell attachment, cell viability, cell density and hydrogel structural integrity. Accordingly, fibrin hydrogel was chosen over agarose, gellan and collagen hydrogels as the most suitable choice for the purpose of this study. The effect of direct contact between the two distinct cell types was evaluated via measuring cell density and ECM formation (collagen and GAGs). The hydrogel-based method showed no significant effect of co-culture on cell density or ECM formation.

The spheroid-based 3D methodology resulted in a simple and rapid system for providing a fast and cost-effective option to test the effects of cellular co-cultures in 3D. Cellular contact was observed, and spheroid size of distinct cells was characterised. Direct contact between tendon and bone cells in 3D using spheroid

culture resulted in an inhibitory effect on cell proliferation and ECM formation. This finding proved that the use of the 3D co-culture system had an effect on cells' behaviour, and therefore, it can be an important tool to study the effect of cell-cell contact between distinct populations of cells.

Bibliography

Abbott, A. (2003) ‘Cell culture: biology’s new dimension.’, Nature. England, pp. 870–872. doi: 10.1038/424870a.

Adamczyk, C. et al. (2008) ‘An immunohistochemical study of the extracellular matrix of entheses associated with the human pisiform bone’, Journal of anatomy. Blackwell Science Inc, 212(5), pp. 645–653.

Agrawal, C. M. and Ray, R. B. (2001) ‘Biodegradable polymeric scaffolds for musculoskeletal tissue engineering’, Journal of Biomedical Materials Research: An Official Journal of The Society for Biomaterials, The Japanese Society for Biomaterials, and The Australian Society for Biomaterials and the Korean Society for Biomaterials. Wiley Online Library, 55(2), pp. 141–150.

Ahearne, M. (2014) ‘Introduction to cell-hydrogel mechanosensing.’, Interface focus, 4, p. 20130038.

Ahmad Khalili, A. and Ahmad, M. R. (2015) ‘A Review of Cell Adhesion Studies for Biomedical and Biological Applications’, International Journal of Molecular Sciences. Edited by F.-G. Tseng, pp. 18149–18184. doi: 10.3390/ijms160818149.

Ahmed, T. et al. (2010) ‘Polyhydroxybutyrate and its copolymer with polyhydroxyvalerate as biomaterials: influence on progression of stem cell cycle.’, Biomacromolecules. United States, 11(10), pp. 2707–2715.

Akiyama, M. et al. (2006) ‘Periosteal cell pellet culture system: a new technique for bone engineering.’, Cell transplantation. United States, 15(6), pp. 521–532.

Alain, K. and Querellou, J. (2009) ‘Cultivating the uncultured: limits, advances and future challenges’, Extremophiles. Springer, 13(4), pp. 583–594.

Alajati, A. et al. (2008) ‘Spheroid-based engineering of a human vasculature in mice.’, Nature methods. United States, 5(5), pp. 439–445.

Alberts, B. et al. (1994) ‘Molecular Biology of the Cell (Third Edition) Biochemistry for the Medical Sciences’, 22(3), p. 1994.

Albrecht, D. R. et al. (2006) ‘Probing the role of multicellular organization in three-dimensional microenvironments’, Nature Methods. Nature Publishing Group, 3, p. 369.

Alsaykhan, H. M. and Fogg, Q. A. (2014) ‘Making a 3D model of Entheses using HREM technology, method review and potentials’, master’s degree thesis.

Anderson, J. C. et al. (2006) ‘Environmentally controlled invasion of cancer cells by engineered bacteria’, Journal of molecular biology. Elsevier, 355(4), pp. 619–627.

Angeline, M. E. and Rodeo, S. A. (2012) ‘Biologics in the management of rotator cuff surgery.’, Clinics in sports medicine. United States, 31(4), pp. 645–663.

Anton, D. et al. (2015) ‘Three-dimensional cell culture: A breakthrough in vivo’, International Journal of Molecular Sciences, 16(3), pp. 5517–5527.

Aoki, M. et al. (2001a) ‘Fibrous connection to bone after immediate repair of the canine infraspinatus: The most effective bony surface for tendon attachment’, Journal of Shoulder and Elbow Surgery. Mosby, 10(2), pp. 123–128.

Aoki, M. et al. (2001b) ‘Fibrous connection to bone after immediate repair of the canine infraspinatus: The most effective bony surface for tendon attachment’, Journal of Shoulder and Elbow Surgery. Mosby, 10(2), pp. 123–128.

Apostolakos, J. et al. (2014a) ‘The enthesis: a review of the tendon-to-bone insertion.’, Muscles, ligaments and tendons journal, 4(3), pp. 333–42.

Apostolakos, J. et al. (2014b) ‘The enthesis: a review of the tendon-to-bone insertion’, Muscles, ligaments and tendons journal. CIC Edizioni Internazionali, 4(3), pp. 333–342.

Ashworth, A. et al. (2008) ‘Opportunities and challenges in ovarian cancer research, a perspective from the 11th Ovarian cancer action/HHMT Forum, Lake Como, March 2007’, Gynecologic Oncology, 108, pp. 652–657.

Aspberg, A. (2012) ‘The Different Roles of Aggrecan Interaction Domains’, Journal of Histochemistry & Cytochemistry. Journal of Histochemistry & Cytochemistry, 60(12), pp. 987–996.

AU - Maritan, S. M., AU - Lian, E. Y. and AU - Mulligan, L. M. (2017) ‘An Efficient and Flexible Cell Aggregation Method for 3D Spheroid Production’, JoVE. MyJoVE Corp, (121), p. e55544.

Aufderheide, Adam C and Athanasiou, K. A. (2005) ‘Comparison of scaffolds and culture conditions for tissue engineering of the knee meniscus.’, Tissue engineering. United States, 11(7–8), pp. 1095–1104.

Aufderheide, Adam C. and Athanasiou, K. A. (2005) ‘Comparison of Scaffolds and Culture Conditions for Tissue Engineering of the Knee Meniscus’, Tissue Engineering, 11(7–8), pp. 1095–1104.

Bacchus, W. et al. (2012) ‘Synthetic two-way communication between mammalian cells.’, Nature biotechnology. United States, 30(10), pp. 991–996.

Badylak, S. F. (2004) ‘Xenogeneic extracellular matrix as a scaffold for tissue reconstruction.’, Transplant immunology. Netherlands, 12(3–4), pp. 367–377.

Baker, B. M. and Chen, C. S. (2012) ‘Deconstructing the third dimension - how 3D culture microenvironments alter cellular cues’, Journal of Cell Science, 125(13), pp. 3015–3024.

Baker, Brendon M and Chen, C. S. (2012) ‘Deconstructing the third dimension – how 3D culture microenvironments alter cellular cues’, Journal of Cell Science, 125(13), pp. 3015 LP – 3024.

Balagadde, F. K. et al. (2008) ‘A synthetic Escherichia coli predator-prey ecosystem.’, Molecular systems biology. England, 4, p. 187.

Batorsky, A. et al. (2005) ‘Encapsulation of adult human mesenchymal stem cells within collagen-agarose microenvironments.’, Biotechnology and bioengineering, 92(4), pp. 492–500.

Bayrak, E. and Yilgor Huri, P. (2018) ‘Engineering Musculoskeletal Tissue Interfaces ’, Frontiers in Materials , p. 24.

Beger, C. et al. (1998) ‘Vascularization of purified pancreatic islet-like cell aggregates (pseudoislets) after syngeneic transplantation.’, Diabetes. United States, 47(4), pp. 559–565.

Beitzel, K. et al. (2013) ‘The future role of mesenchymal stem cells in the management of shoulder disorders’, Arthroscopy - Journal of Arthroscopic and Related Surgery. Arthroscopy Association of North America, 29(10), pp. 1702–1711.

Beloqui, A. et al. (2008) ‘Recent trends in industrial microbiology’, Current opinion in microbiology. Elsevier, 11(3), pp. 240–248.

Benjamin, M. et al. (2002) ‘The skeletal attachment of tendons--tendon “entheses”.’, Comparative biochemistry and physiology. Part A, Molecular & integrative physiology, 133(4), pp. 931–945.

Benjamin, M. et al. (2006) ‘Where tendons and ligaments meet bone: attachment sites ('entheses’) in relation to exercise and/or mechanical load.’, Journal of anatomy. England, 208(4), pp. 471–490.

Benjamin, M. and McGonagle, D. (2001) ‘The anatomical basis for disease localisation in seronegative spondyloarthropathy at entheses and related sites.’, Journal of anatomy. England, 199(Pt 5), pp. 503–526.

Benjamin, M. and McGonagle, D. (2009) ‘Entheses: Tendon and ligament attachment sites’, Scandinavian Journal of Medicine and Science in Sports, 19(4), pp. 520–527.

Benjamin, M. and Ralphs, J. R. (1998) ‘Fibrocartilage in tendons and ligaments--an adaptation to compressive load.’, Journal of anatomy. England, 193 (Pt 4, pp. 481–494.

Benjamin, M. and Ralphs, J. R. (2001) ‘Entheses--the bony attachments of tendons and ligaments.’, Italian journal of anatomy and embryology = Archivio italiano di anatomia ed embriologia. Italy, 106(2 Suppl 1), pp. 151–157.

Bermúdez-Humarán, L. G. et al. (2011) ‘Lactococci and lactobacilli as mucosal delivery vectors for therapeutic proteins and DNA vaccines’, in Microbial cell factories. BioMed Central, p. S4.

Blakely, A. M. et al. (2015) ‘Bio-Pick, Place, and Perfuse: A New Instrument for Three-Dimensional Tissue Engineering.’, Tissue engineering. Part C, Methods. United States, 21(7), pp. 737–746.

Blickenstaff, K. R., Grana, W. A. and Egle, D. (1997) ‘Analysis of a semitendinosus autograft in a rabbit model.’, The American journal of sports medicine. United States, 25(4), pp. 554–559.

Bogdanowicz, D. R. and Lu, H. H. (2013) ‘Studying cell-cell communication in co-culture’, Biotechnology journal, 8(4), pp. 395–396.

Borschel, G. H. et al. (2005) ‘Tissue engineering of recellularized small-diameter vascular grafts.’, Tissue engineering. United States, 11(5–6), pp. 778–786.

Bou Assaf, R. et al. (2019) ‘Evaluation of the Osteogenic Potential of Different Scaffolds Embedded with Human Stem Cells Originated from Schneiderian

Membrane: An In Vitro Study.', BioMed research international. United States, 2019, p. 2868673.

Braun, F. et al. (1977) '[Experiences with a biological adhesive system (fibrin) in the dressing of kidney parenchymal wounds (animal experiment and 1st clinical experiences)].', Zentralblatt fur Chirurgie. Germany, 102(20), pp. 1235–1246.

Brenner, K., You, L. and Arnold, F. H. (2009) 'Response to Goldman and Brown: Making sense of microbial consortia using ecology and evolution', Trends in Biotechnology, 27(1), p. 4.

Brent, A. E., Schweitzer, R. and Tabin, C. J. (2003) 'A somitic compartment of tendon progenitors', Cell. Elsevier, 113(2), pp. 235–248.

Breslin, S. and O'Driscoll, L. (2013) 'Three-dimensional cell culture: The missing link in drug discovery', Drug Discovery Today. Elsevier Ltd, 18(5–6), pp. 240–249.

Bruchez, M. et al. (1998) 'Semiconductor nanocrystals as fluorescent biological labels', science. American Association for the Advancement of Science, 281(5385), pp. 2013–2016.

Burg, K. J., Porter, S. and Kellam, J. F. (2000) 'Biomaterial developments for bone tissue engineering.', Biomaterials, 21(23), pp. 2347–2359.

Byun, C. K. et al. (2013) 'Productive chemical interaction between a bacterial microcolony couple is enhanced by periodic relocation.', Journal of the American Chemical Society. United States, 135(6), pp. 2242–2247.

Calejo, I. et al. (2018) 'Bi-directional modulation of cellular interactions in an in vitro co-culture model of tendon-to-bone interface', Cell Proliferation, 51(6), p. e12493.

Caliari, S. R. and Burdick, J. A. (2016) 'A practical guide to hydrogels for cell culture', Nature methods, 13(5), pp. 405–414.

Campbell, J. J. et al. (2011) 'A multifunctional 3D co-culture system for studies of mammary tissue morphogenesis and stem cell biology.', PloS one. United States, 6(9), p. e25661.

Carletti, E. et al. (2011) 'Microfabrication of PDLLA scaffolds.', Journal of tissue engineering and regenerative medicine. England, 5(7), pp. 569–577.

Carrion, B. et al. (2014) ‘A safe and efficient method to retrieve mesenchymal stem cells from three-dimensional fibrin gels.’, Tissue engineering. Part C, Methods. United States, 20(3), pp. 252–263.

Cascone, M. G. et al. (2001) ‘Bioartificial polymeric materials based on polysaccharides.’, Journal of biomaterials science. Polymer edition, 12(3), pp. 267–281.

Chambers, K. F. et al. (2014) ‘3D Cultures of Prostate Cancer Cells Cultured in a Novel High-Throughput Culture Platform Are More Resistant to Chemotherapeutics Compared to Cells Cultured in Monolayer’, PLOS ONE. Public Library of Science, 9(11), p. e111029.

Chan, B. P. and Leong, K. W. (2008) ‘Scaffolding in tissue engineering: General approaches and tissue-specific considerations’, European Spine Journal, 17(SUPPL. 4).

Chang, P.-C. et al. (2007) ‘Bone tissue engineering with novel rhBMP2-PLLA composite scaffolds.’, Journal of biomedical materials research. Part A. United States, 81(4), pp. 771–780.

Chen, C.-H. et al. (2011) ‘Enhancement of rotator cuff tendon-bone healing with injectable periosteum progenitor cells-BMP-2 hydrogel in vivo.’, Knee surgery, sports traumatology, arthroscopy: official journal of the ESSKA. Germany, 19(9), pp. 1597–1607.

Chen, L. X. et al. (2019) ‘Investigation of Surgical Adhesives for Vocal Fold Wound Closure.’, The Laryngoscope. United States.

Chen, M. C. W., Gupta, M. and Cheung, K. C. (2008) ‘Hydrogel-based microfluidic systems for co-culture of cells.’, Conference proceedings: ... Annual International Conference of the IEEE Engineering in Medicine and Biology Society. IEEE Engineering in Medicine and Biology Society. Annual Conference. United States, 2008, pp. 4848–4851.

Cheng, G. et al. (2009) ‘Micro-Environmental Mechanical Stress Controls Tumor Spheroid Size and Morphology by Suppressing Proliferation and Inducing Apoptosis in Cancer Cells’, PLOS ONE. Public Library of Science, 4(2), p. e4632.

Chimenti, I. et al. (2011) ‘Human cardiosphere-seeded gelatin and collagen scaffolds as cardiogenic engineered bioconstructs.’, Biomaterials. Netherlands, 32(35), pp. 9271–9281.

Chitcholtan, K., Sykes, P. H. and Evans, J. J. (2012) ‘The resistance of intracellular mediators to doxorubicin and cisplatin are distinct in 3D and 2D endometrial cancer’, Journal of translational medicine. BioMed Central, 10(1), p. 38.

Chotitumnavee, J. et al. (2019) ‘In vitro evaluation of local antibiotic delivery via fibrin hydrogel.’, Journal of dental sciences. Netherlands, 14(1), pp. 7–14.

Chuang, J. S., Rivoire, O. and Leibler, S. (2010) ‘Cooperation and Hamilton’s rule in a simple synthetic microbial system.’, Molecular systems biology. England, 6, p. 398.

Chun, S.-I. et al. (2015) ‘Cytotoxicity of TSP in 3D Agarose Gel Cultured Cell’, PLOS ONE. Edited by M.-H. Wu. Inje University Industry-Academic Cooperation Foundation, 10(6), p. e0128739.

Chung, S. et al. (2009) ‘Cell migration into scaffolds under co-culture conditions in a microfluidic platform.’, Lab on a chip. England, 9(2), pp. 269–275.

Chwalek, K. et al. (2014) ‘Glycosaminoglycan-based hydrogels to modulate heterocellular communication in in vitro angiogenesis models.’, Scientific reports. England, 4, p. 4414.

Cooper, J. O. et al. (2014) ‘Co-cultured tissue-specific scaffolds for tendon/bone interface engineering’, Journal of tissue engineering. SAGE Publications, 5, pp. 2041731414542294–2041731414542294.

Couchman, J. R. and Pataki, C. A. (2012) ‘An introduction to proteoglycans and their localization.’, The journal of histochemistry and cytochemistry: official journal of the Histochemistry Society. United States, 60(12), pp. 885–897.

Cserjesi, P. et al. (1995) ‘Scleraxis: a basic helix-loop-helix protein that prefigures skeletal formation during mouse embryogenesis’, Development. The Company of Biologists Ltd, 121(4), pp. 1099–1110.

Curcio, E. et al. (2007) ‘Mass transfer and metabolic reactions in hepatocyte spheroids cultured in rotating wall gas-permeable membrane system.’, Biomaterials. Netherlands, 28(36), pp. 5487–5497.

‘Current Applications of Tissue Engineering in Biomedicine’ (2013) Journal of Biochips & Tissue Chips. OMICS International., pp. 1–14. doi: 10.4172/2153-0777.S2-004.

Dean, D. M. et al. (2007) ‘Rods, tori, and honeycombs: the directed self-assembly of microtissues with prescribed microscale geometries.’, FASEB journal: official publication of the Federation of American Societies for Experimental Biology. United States, 21(14), pp. 4005–4012.

Deng, D. et al. (2009) ‘Engineering human neo-tendon tissue in vitro with human dermal fibroblasts under static mechanical strain’, Biomaterials, 30(35), pp. 6724–6730.

Derwin, K. A. et al. (2018) ‘Enthesis Repair: Challenges and Opportunities for Effective Tendon-to-Bone Healing.’, The Journal of bone and joint surgery. American volume. United States, 100(16), p. e109.

Desoize, B., Gimonet, D. and Jardiller, J. C. (1998) ‘Cell culture as spheroids: an approach to multicellular resistance.’, Anticancer research. Greece, 18(6A), pp. 4147–4158.

Dhandayuthapani, B. et al. (2011) ‘Polymeric Scaffolds in Tissue Engineering Application: A Review’, 2011(ii).

Dilley, R. J. and Morrison, W. A. (2014) ‘Vascularisation to improve translational potential of tissue engineering systems for cardiac repair’, The international journal of biochemistry & cell biology. Elsevier, 56, pp. 38–46.

Dingle, A. M. et al. (2018) ‘Abstract 129: The Osseointegrated Neural Interface (ONI): A Rabbit Model for Chronic Peripheral Nerve Interfacing in Bone with Percutaneous Osseointegrated Connectors’, Plastic and Reconstructive Surgery Global Open. Wolters Kluwer Health, 6(4 Suppl), pp. 101–102.

Dragoo, J. L. et al. (2007) ‘Healing full-thickness cartilage defects using adipose-derived stem cells.’, Tissue engineering. United States, 13(7), pp. 1615–1621.

Drury, J. L. and Mooney, D. J. (2003) ‘Hydrogels for tissue engineering: scaffold design variables and applications’, 24, pp. 4337–4351.

Du, Y. et al. (2007) ‘Identification and characterization of a novel prespheroid 3-dimensional hepatocyte monolayer on galactosylated substratum.’, Tissue engineering. United States, 13(7), pp. 1455–1468.

Dubessy, C. et al. (2000) ‘Spheroids in radiobiology and photodynamic therapy.’, Critical reviews in oncology/hematology. Netherlands, 36(2–3), pp. 179–192.

Durand, R. E. and Olive, P. L. (1982) ‘Cytotoxicity, Mutagenicity and DNA damage by Hoechst 33342.’, Journal of Histochemistry & Cytochemistry. SAGE Publications Sage CA: Los Angeles, CA, 30(2), pp. 111–116.

Ede, D. et al. (2018) ‘Microfluidic Flow Cell Array for Controlled Cell Deposition in Engineered Musculoskeletal Tissues’, Tissue Engineering Part C: Methods. Mary Ann Liebert, Inc., publishers, 24(9), pp. 546–556.

Edmondson, R. et al. (2014) ‘Three-dimensional cell culture systems and their applications in drug discovery and cell-based biosensors.’, Assay and drug development technologies, 12(4), pp. 207–18.

Edmondson, R., Adcock, A. F. and Yang, L. (2016) ‘Influence of Matrices on 3D-Cultured Prostate Cancer Cells’ Drug Response and Expression of Drug-Action Associated Proteins’, PLOS ONE. Public Library of Science, 11(6), p. e0158116.

El-Ali, J., Sorger, P. K. and Jensen, K. F. (2006) ‘Cells on chips.’, Nature. England, 442(7101), pp. 403–411.

Elema, H. et al. (1990) ‘Use of porous biodegradable polymer implants in meniscus reconstruction. 2) Biological evaluation of porous biodegradable polymer implants in menisci’, Colloid and polymer science. Springer, 268(12), pp. 1082–1088.

Engler, C. et al. (2009) ‘Assessment of attachment factors for primary cultured human corneal endothelial cells.’, Cornea. United States, 28(9), pp. 1050–1054.

Erggelet, C. et al. (2007) ‘Regeneration of ovine articular cartilage defects by cell-free polymer-based implants.’, Biomaterials. Netherlands, 28(36), pp. 5570–5580.

Erickson, I. E. et al. (2009) ‘Differential maturation and structure-function relationships in mesenchymal stem cell- and chondrocyte-seeded hydrogels.’, Tissue engineering. Part A. United States, 15(5), pp. 1041–1052.

Eriksson, K., Kindblom, L. G. and Wredmark, T. (2000) ‘Semitendinosus tendon graft ingrowth in tibial tunnel following ACL reconstruction: a histological study of 2

patients with different types of early graft failure.', Acta orthopaedica Scandinavica. England, 71(3), pp. 275–279.

Fallica, B. et al. (2012) 'Alteration of cellular behavior and response to PI3K pathway inhibition by culture in 3D collagen gels', PloS one. Public Library of Science, 7(10), p. e48024.

Fang, Y. and Eglen, R. M. (2017) 'Three-Dimensional Cell Cultures in Drug Discovery and Development', SLAS discovery: advancing life sciences R & D. 2017/05/18. SAGE Publications, 22(5), pp. 456–472.

Felton, E. J. et al. (2012) 'Heterotypic cell pair co-culturing on patterned microarrays.', Lab on a chip. England, 12(17), pp. 3117–3126.

Fennema, E. et al. (2013) 'Spheroid culture as a tool for creating 3D complex tissues.', Trends in biotechnology. England, 31(2), pp. 108–115.

Fenwick, S. A et al. (2001) 'Expression of transforming growth factor-beta isoforms and their receptors in chronic tendinosis.', Journal of anatomy, 199(Pt 3), pp. 231–240.

Ferris, C. J. et al. (2013) 'Modified gellan gum hydrogels for tissue engineering applications', Soft Matter. The Royal Society of Chemistry, 9(14), pp. 3705–3711.

Ferry, J. D. and Morrison, P. R. (1947) 'Preparation and properties of serum and plasma proteins. VIII. The conversion of human fibrinogen to fibrin under various conditions1, 2', Journal of the American Chemical Society. ACS Publications, 69(2), pp. 388–400.

Font Tellado, S., Balmayor, Elizabeth R and Van Griensven, M. (2015) 'Strategies to engineer tendon/ligament-to-bone interface: Biomaterials, cells and growth factors.', Advanced drug delivery reviews. Netherlands, 94, pp. 126–140.

Font Tellado, S., Balmayor, Elizabeth R. and Van Griensven, M. (2015) 'Strategies to engineer tendon/ligament-to-bone interface: Biomaterials, cells and growth factors', Advanced Drug Delivery Reviews. Elsevier, 94, pp. 126–140.

Francois, S. et al. (2009) 'A poly(L-lactic acid) nanofibre mesh scaffold for endothelial cells on vascular prostheses.', Acta biomaterialia. England, 5(7), pp. 2418–2428.

Frantz, C., Stewart, K. M. and Weaver, V. M. (2010) ‘The extracellular matrix at a glance’, Journal of Cell Science, 123(24), pp. 4195 LP – 4200.

Freed, L. E. et al. (1994) ‘Biodegradable polymer scaffolds for tissue engineering’, Bio/technology. Nature Publishing Group, 12(7), p. 689.

Friedman, M. J. et al. (1985) ‘Autogeneic Anterior Cruciate Ligament (ACL) Anterior Reconstruction of the Knee A Review.’, Clinical Orthopaedics and Related Research, 196.

Frimat, J.-P. et al. (2011) ‘A microfluidic array with cellular valving for single cell co-culture’, Lab on a Chip. The Royal Society of Chemistry, 11(2), pp. 231–237.

Fujioka, H. et al. (1997) ‘Changes in the expression of type-X collagen in the fibrocartilage of rat Achilles tendon attachment during development’, Journal of orthopaedic research. Wiley Online Library, 15(5), pp. 675–681.

Fujioka, H. et al. (1998) ‘Comparison of surgically attached and non-attached repair of the rat Achilles tendon-bone interface. Cellular organization and type X collagen expression.’, Connective tissue research. England, 37(3–4), pp. 205–218.

Fukuda, J. et al. (2006) ‘Micropatterned cell co-cultures using layer-by-layer deposition of extracellular matrix components.’, Biomaterials. Netherlands, 27(8), pp. 1479–1486.

Furukawa, K. S. et al. (2001) ‘Formation of human fibroblast aggregates (spheroids) by rotational culture.’, Cell transplantation. United States, 10(4–5), pp. 441–445.

Garcia, E. et al. (2019) ‘Use of a combination strategy to improve neuroprotection and neuroregeneration in a rat model of acute spinal cord injury.’, Neural regeneration research. India, 14(6), pp. 1060–1068.

Garcia, J. P. et al. (2019) ‘Fibrin-hyaluronic acid hydrogel-based delivery of antisense oligonucleotides for ADAMTS5 inhibition in co-delivered and resident joint cells in osteoarthritis.’, Journal of controlled release: official journal of the Controlled Release Society. Netherlands, 294, pp. 247–258.

Gdynia, G. et al. (2007) ‘Basal caspase activity promotes migration and invasiveness in glioblastoma cells.’, Molecular cancer research: MCR. United States, 5(12), pp. 1232–1240.

Gehin, A. et al. (1996) ‘Studies of Clostridium cellulolyticum ATCC 35319 under dialysis and co-culture conditions.’, Letters in applied microbiology. England, 23(4), pp. 208–212.

Gianotti, S. M. et al. (2009) ‘Incidence of anterior cruciate ligament injury and other knee ligament injuries: a national population-based study.’, Journal of science and medicine in sport. Australia, 12(6), pp. 622–627.

Gilbert, T. W., Sellaro, T. L. and Badylak, S. F. (2006) ‘Decellularization of tissues and organs.’, Biomaterials. Netherlands, 27(19), pp. 3675–3683.

Goers, L., Freemont, P. and Polizzi, K. M. (2014) ‘Co-culture systems and technologies: taking synthetic biology to the next level’, Journal of The Royal Society Interface, 11(96).

Gondi, C. S. et al. (2007) ‘Intraperitoneal injection of a hairpin RNA-expressing plasmid targeting urokinase-type plasminogen activator (uPA) receptor and uPA retards angiogenesis and inhibits intracranial tumor growth in nude mice.’, Clinical cancer research : an official journal of the American Association for Cancer Research. United States, 13(14), pp. 4051–4060.

Greco, K. V et al. (2011) ‘High density micromass cultures of a human chondrocyte cell line: a reliable assay system to reveal the modulatory functions of pharmacological agents.’, Biochemical pharmacology. England, 82(12), pp. 1919–1929.

Griffith, L. G. and Swartz, M. A. (2006) ‘Capturing complex 3D tissue physiology in vitro.’, Nature reviews. Molecular cell biology. England, 7(3), pp. 211–224.

Grigolo, B. et al. (2009) ‘Osteoarthritis treated with mesenchymal stem cells on hyaluronan-based scaffold in rabbit.’, Tissue engineering. Part C, Methods. United States, 15(4), pp. 647–658.

Guarino, V. and Ambrosio, L. (2008) ‘The synergic effect of polylactide fiber and calcium phosphate particle reinforcement in poly epsilon-caprolactone-based composite scaffolds.’, Acta biomaterialia. England, 4(6), pp. 1778–1787.

Gurski, L. A. et al. (2010) ‘3D Matrices for Anti-Cancer Drug Testing and Development’, Oncology Issues. Taylor & Francis, 25(1), pp. 20–25.

Haga, T. et al. (2008) ‘Role of E-cadherin in the induction of apoptosis of HPV16-positive CaSki cervical cancer cells during multicellular tumor spheroid formation.’, Apoptosis: an international journal on programmed cell death. Netherlands, 13(1), pp. 97–108.

Hahn, G. M. and van Kersen-Bax, I. (1971) ‘[The growth of bone marrow cells on fibrin].’, Comptes rendus hebdomadaires des seances de l’Academie des sciences. Serie D: Sciences naturelles. France, 272(18), pp. 2338–2341.

Hall, S. (1997) ‘Axonal regeneration through acellular muscle grafts.’, Journal of anatomy. England, 190 (Pt 1, pp. 57–71.

Hamilton, G. A., Westmorel, C. and George, A. E. (2001) ‘Effects of medium composition on the morphology and function of rat hepatocytes cultured as spheroids and monolayers.’, In vitro cellular & developmental biology. Animal. Germany, 37(10), pp. 656–667.

Hamilton, S. K. et al. (2013) ‘Development of 3D hydrogel culture systems with on-demand cell separation’, Biotechnology Journal. John Wiley & Sons, Ltd, 8(4), pp. 485–495.

Harcombe, W. (2010) ‘Novel cooperation experimentally evolved between species’, Evolution: International Journal of Organic Evolution. Wiley Online Library, 64(7), pp. 2166–2172.

Hasegawa, S. et al. (2007) ‘In vivo evaluation of a porous hydroxyapatite/poly-DL-lactide composite for bone tissue engineering.’, Journal of biomedical materials research. Part A. United States, 81(4), pp. 930–938.

Hashimoto, Y. et al. (2007) ‘Generation of tendon-to-bone interface “enthesis” with use of recombinant BMP-2 in a rabbit model.’, Journal of orthopaedic research: official publication of the Orthopaedic Research Society. United States, 25(11), pp. 1415–1424.

Hatherell, K. et al. (2011) ‘Development of a three-dimensional, all-human in vitro model of the blood-brain barrier using mono-, co-, and tri-cultivation Transwell models.’, Journal of neuroscience methods. Netherlands, 199(2), pp. 223–229.

He, P. et al. (2012) ‘In vitro ligament-bone interface regeneration using a trilineage coculture system on a hybrid silk scaffold.’, Biomacromolecules. United States, 13(9), pp. 2692–2703.

Helmlinger, G. et al. (1997) ‘Solid stress inhibits the growth of multicellular tumor spheroids.’, Nature biotechnology. United States, 15(8), pp. 778–783.

Hems, T. and Tillmann, B. (2000) ‘Tendon entheses of the human masticatory muscles’, *Anatomy and Embryology*. Springer, 202(3), pp. 201–208.

Hesselman, M. C. et al. (2012) ‘A multi-platform flow device for microbial (co-) cultivation and microscopic analysis’, PLoS One. Public Library of Science, 7(5), p. e36982.

Holtfreter, J. (1943) ‘A study of the mechanics of gastrulation. Part I’, Journal of Experimental Zoology. John Wiley & Sons, Ltd, 94(3), pp. 261–318.

Hong, J. W., Song, S. and Shin, J. H. (2013) ‘A novel microfluidic co-culture system for investigation of bacterial cancer targeting’, Lab on a chip. Royal Society of Chemistry, 13(15), pp. 3033–3040.

Hongisto, V., Jernström, S., Fey, V., Mpindi, J. P., et al. (2013) ‘High-Throughput 3D Screening Reveals Differences in Drug Sensitivities between Culture Models of JIMT1 Breast Cancer Cells’, PLoS ONE.

Hongisto, V., Jernström, S., Fey, V., Mpindi, J.-P., et al. (2013) ‘High-Throughput 3D Screening Reveals Differences in Drug Sensitivities between Culture Models of JIMT1 Breast Cancer Cells’, PLoS ONE. Edited by M. A. Deli. Public Library of Science, 8(10), p. e77232.

Hoyer, M. et al. (2015) ‘In vitro characterization of self-assembled anterior cruciate ligament cell spheroids for ligament tissue engineering.’, Histochemistry and cell biology. Germany, 143(3), pp. 289–300.

Hsu, S.-H. and Tseng, H.-J. (2004) ‘In vitro biocompatibility of PTMO-based polyurethanes and those containing PDMS blocks’, Journal of biomaterials applications. SAGE Publications, 19(2), pp. 135–146.

Hu, G. and Li, D. (2007) ‘Three-dimensional modeling of transport of nutrients for multicellular tumor spheroid culture in a microchannel.’, Biomedical microdevices. United States, 9(3), pp. 315–323.

Huang, C.-Y. C. et al. (2004) ‘Effects of cyclic compressive loading on chondrogenesis of rabbit bone-marrow derived mesenchymal stem cells.’, Stem cells (Dayton, Ohio). United States, 22(3), pp. 313–323.

Huang, C. P. et al. (2009) ‘Engineering microscale cellular niches for three-dimensional multicellular co-cultures.’, Lab on a chip. England, 9(12), pp. 1740–1748.

Huang, G. S. et al. (2013) ‘Solid freeform-fabricated scaffolds designed to carry multicellular mesenchymal stem cell spheroids for cartilage regeneration.’, European cells & materials. Switzerland, 26, pp. 179–94; discussion 194.

Huang, H. et al. (2013) ‘Peptide Hydrogelation and Cell Encapsulation for 3D Culture of MCF-7 Breast Cancer Cells’, PLoS ONE.

Hutmacher, D. W. (2000) ‘Scaffolds in tissue engineering bone and cartilage.’, Biomaterials. Netherlands, 21(24), pp. 2529–2543.

Idahl, L. A. et al. (1980) ‘Initial uptake and insulin releasing action of chloromercuribenzene-p-sulphonic acid (CMBS) in suspensions of pancreatic islet cells.’, Medical biology. Finland, 58(2), pp. 101–108.

Ingram, J. H. et al. (2007) ‘The use of ultrasonication to aid recellularization of acellular natural tissue scaffolds for use in anterior cruciate ligament reconstruction.’, Tissue engineering. United States, 13(7), pp. 1561–1572.

Ingram, M. et al. (1997) ‘Three-dimensional growth patterns of various human tumor cell lines in simulated microgravity of a NASA bioreactor.’, In vitro cellular & developmental biology. Animal. Germany, 33(6), pp. 459–466.

Ino, K., Ito, A. and Honda, H. (2007) ‘Cell patterning using magnetite nanoparticles and magnetic force.’, Biotechnology and bioengineering. United States, 97(5), pp. 1309–1317.

Inui, A. et al. (2010) ‘Potency of double-layered poly L-lactic acid scaffold in tissue engineering of tendon tissue.’, International orthopaedics. Germany, 34(8), pp. 1327–1332.

Javaherian, S., O’Donnell, K. A. and McGuigan, A. P. (2011) ‘A fast and accessible methodology for micro-patterning cells on standard culture substrates using Parafilm inserts.’, PloS one. United States, 6(6), p. e20909.

Jessup, C. M. et al. (2004) ‘Big questions, small worlds: microbial model systems in ecology.’, Trends in ecology & evolution. England, 19(4), pp. 189–197.

Jiang, J., Nicoll, S. B. and Lu, H. H. (2005) ‘Co-culture of osteoblasts and chondrocytes modulates cellular differentiation in vitro’, Biochemical and Biophysical Research Communications, 338(2), pp. 762–770.

Jiang, Y. et al. (2005) ‘A multiscale model for avascular tumor growth.’, Biophysical journal. United States, 89(6), pp. 3884–3894.

Jockenhoevel, S. et al. (2001) ‘Fibrin gel – advantages of a new scaffold in cardiovascular tissue engineering’, European Journal of Cardio-Thoracic Surgery, 19(4), pp. 424–430.

Ju, Y. M. et al. (2008) ‘Beneficial effect of hydrophilized porous polymer scaffolds in tissue-engineered cartilage formation.’, Journal of biomedical materials research. Part B Applied biomaterials. United States, 85(1), pp. 252–260.

Juneja, S. C. and Veillette, C. (2013) ‘Defects in tendon, ligament, and enthesis in response to genetic alterations in key proteoglycans and glycoproteins: a review.’, Arthritis. United States, 2013, p. 154812.

Karande, T. S., Ong, J. L. and Agrawal, C. M. (2004) ‘Diffusion in musculoskeletal tissue engineering scaffolds: design issues related to porosity, permeability, architecture, and nutrient mixing’, Annals of biomedical engineering. Springer, 32(12), pp. 1728–1743.

Khodabukus, A. et al. (2007) ‘Engineered Muscle: A Tool for Studying Muscle Physiology and Function’, Exercise and Sport Sciences Reviews, 35(4).

Kim, B., Baez, C. E. and Atala, A. (2000) ‘Biomaterials for tissue engineering’, pp. 2–9.

Kim, B. S. et al. (2014) ‘Human collagen-based multilayer scaffolds for tendon-to-bone interface tissue engineering’, Journal of Biomedical Materials Research - Part A. Department of Chemical Engineering, Hanyang University, Hanyangdaehak-ro 55, Ansan, Kyeonggi-do, 426-791, South Korea: John Wiley and Sons Inc., 102(11), pp. 4044–4054.

Kim, H.-J. et al. (2007) ‘The role of transforming growth factor-beta and bone morphogenetic protein with fibrin glue in healing of bone-tendon junction injury.’, Connective tissue research. England, 48(6), pp. 309–315.

Kim, H. J. et al. (2008) ‘Defined spatial structure stabilizes a synthetic multispecies bacterial community’, Proceedings of the National Academy of Sciences, 105(47), pp. 18188 LP – 18193.

Kim, J. Bin (2005) ‘Three-dimensional tissue culture models in cancer biology.’, Seminars in cancer biology. England, 15(5), pp. 365–377.

Kinney, M. A. et al. (2014) ‘Engineering Three-Dimensional Stem Cell Morphogenesis for the Development of Tissue Models and Scalable Regenerative Therapeutics’, Annals of Biomedical Engineering, 42(2), pp. 352–367.

Klopp, A. H. et al. (2010) ‘Mesenchymal Stem Cells Promote Mammosphere Formation and Decrease E-Cadherin in Normal and Malignant Breast Cells’, PLoS ONE. Edited by C. Creighton. Public Library of Science, 5(8), p. e12180.

Knecht, S. et al. (2007) ‘Mechanical testing of fixation techniques for scaffold-based tissue-engineered grafts.’, Journal of biomedical materials research. Part B Applied biomaterials. United States, 83(1), pp. 50–57.

Knight, R. L. et al. (2008) ‘The use of acellular matrices for the tissue engineering of cardiac valves.’, Proceedings of the Institution of Mechanical Engineers. Part H, Journal of engineering in medicine. England, 222(1), pp. 129–143.

Koob, T. J. and Vogel, K. G. (1987) ‘Site-related variations in glycosaminoglycan content and swelling properties of bovine flexor tendon.’, Journal of orthopaedic research: official publication of the Orthopaedic Research Society. United States, 5(3), pp. 414–424.

Kramschuster, A. and Turng, L.-S. (2013) ‘Fabrication of Tissue Engineering Scaffolds’, Handbook of Biopolymers and Biodegradable Plastics. William Andrew Publishing, pp. 427–446.

Kraus, A. et al. (2018) ‘Spheroid formation and modulation of tenocyte-specific gene expression under simulated microgravity’, Muscles, ligaments and tendons journal. CIC Edizioni Internazionali, 7(3), pp. 411–417.

Kronenberg, H. M. (2003) ‘Developmental regulation of the growth plate’, Nature. Nature Publishing Group, 423(6937), p. 332.

Krug, C. et al. (2019) ‘Fibrin glue displays promising in vitro characteristics as a potential carrier of adipose progenitor cells for tissue regeneration.’, Journal of tissue engineering and regenerative medicine. England, 13(3), pp. 359–368.

Kumar, a and Dek, M. (2010) ‘Nanofiber Reinforced Composite Polymer Electrolyte Membranes’, (February).

Kuntz, L. A. et al. (2018) ‘Biomarkers for tissue engineering of the tendon-bone interface’, PloS one. Public Library of Science, 13(1), pp. e0189668–e0189668.

Kunz-Schughart, L. A. et al. (2004) ‘The use of 3-D cultures for high-throughput screening: the multicellular spheroid model.’, Journal of biomolecular screening. United States, 9(4), pp. 273–285.

Kuo, C. K. and Tuan, R. S. (2008) ‘Mechanoactive tenogenic differentiation of human mesenchymal stem cells.’, Tissue engineering. Part A. United States, 14(10), pp. 1615–1627.

Kurane, A., Simionescu, D. T. and Vyavahare, N. R. (2007) ‘In vivo cellular repopulation of tubular elastin scaffolds mediated by basic fibroblast growth factor.’, Biomaterials. Netherlands, 28(18), pp. 2830–2838.

Lafosse, L. et al. (2008) ‘The outcome and structural integrity of arthroscopic rotator cuff repair with use of the double-row suture anchor technique. Surgical technique.’, The Journal of bone and joint surgery. American volume. United States, 90 Suppl 2, pp. 275–286.

Laiho, M., Weis, M. B. and Massague, J. (1990) ‘Concomitant loss of transforming growth factor (TGF)-beta receptor types I and II in TGF-beta-resistant cell mutants implicates both receptor types in signal transduction.’, The Journal of biological chemistry. United States, 265(30), pp. 18518–18524.

Landry, J. et al. (1985) ‘Spheroidal aggregate culture of rat liver cells: histotypic reorganization, biomatrix deposition, and maintenance of functional activities.’, The Journal of cell biology. United States, 101(3), pp. 914–923.

Langer, R. (1993) ‘VacantiJP’, Tissue engineering. Science, 260(5110), pp. 920–926.

Lanza, R. (2013) ‘Principles of tissue engineering /’, Principles of tissue engineering /. Third edit. Burlington, Mass.:

Laschke, M. W. and Menger, M. D. (2017) ‘Life is 3D: Boosting Spheroid Function for Tissue Engineering.’, Trends in biotechnology. England, 35(2), pp. 133–144.

Laternser, S. et al. (2018) ‘A Novel Microplate 3D Bioprinting Platform for the Engineering of Muscle and Tendon Tissues’, SLAS technology. 2018/06/12. SAGE Publications, 23(6), pp. 599–613.

Lazzari, G. et al. (2018) ‘Multicellular spheroid based on a triple co-culture: A novel 3D model to mimic pancreatic tumor complexity’, Acta Biomaterialia. Elsevier, 78, pp. 296–307.

Lebled, C., Grover, L. M. and Paxton, J. Z. (2014) ‘Combined decellularisation and dehydration improves the mechanical properties of tissue-engineered sinews’, Journal of Tissue Engineering. SAGE Publications Ltd STM, 5, p. 2041731414536720.

Leddy, H. A., Awad, H. A. and Guilak, F. (2004) ‘Molecular diffusion in tissue-engineered cartilage constructs: effects of scaffold material, time, and culture conditions.’, Journal of biomedical materials research. Part B Applied biomaterials. United States, 70(2), pp. 397–406.

Lee, J. M. et al. (2013) ‘A three-dimensional microenvironment alters protein expression and chemosensitivity of epithelial ovarian cancer cells in vitro.’, Laboratory investigation; a journal of technical methods and pathology, 93(5), pp. 528–42.

Leonhardt, H. et al. (2000) ‘Dynamics of DNA replication factories in living cells’, The Journal of cell biology. Rockefeller University Press, 149(2), pp. 271–280.

Li, H. et al. (2016) ‘Functional regeneration of ligament-bone interface using a triphasic silk-based graft’, Biomaterials, 106, pp. 180–192.

Li, J. et al. (2006) ‘Growth and metabolism of human hepatocytes on biomodified collagen poly(lactic-co-glycolic acid) three-dimensional scaffold.’, ASAIO journal (American Society for Artificial Internal Organs: 1992). United States, 52(3), pp. 321–327.

Li, K. W. et al. (2006) ‘Gene regulation ex vivo within a wrap-around tendon.’, Tissue engineering. United States, 12(9), pp. 2611–2618.

Liang, Y. et al. (2011) ‘An in situ formed biodegradable hydrogel for reconstruction of the corneal endothelium.’, Colloids and surfaces. B, Biointerfaces. Netherlands, 82(1), pp. 1–7.

Lim, J. J. and Temenoff, J. S. (2009) ‘Tendon and Ligament Tissue Engineering: Restoring Tendon/Ligament and Its Interfaces’, in Meyer, U. et al. (eds) Fundamentals of Tissue Engineering and Regenerative Medicine. Berlin, Heidelberg: Springer Berlin Heidelberg, pp. 255–269.

Lin, R.-Z. and Chang, H.-Y. (2008) ‘Recent advances in three-dimensional multicellular spheroid culture for biomedical research.’, Biotechnology journal. Germany, 3(9–10), pp. 1172–1184.

Linden, S. K., Driessen, K. M. and McGuckin, M. A. (2007) ‘Improved in vitro model systems for gastrointestinal infection by choice of cell line, pH, microaerobic conditions, and optimization of culture conditions.’, Helicobacter. England, 12(4), pp. 341–353.

Liu, H. et al. (2017) ‘Biomimetic tendon extracellular matrix composite gradient scaffold enhances ligament-to-bone junction reconstruction’, Acta Biomaterialia, 56, pp. 129–140.

Liu, J. et al. (2007) ‘Functional three-dimensional HepG2 aggregate cultures generated from an ultrasound trap: comparison with HepG2 spheroids.’, Journal of cellular biochemistry. United States, 102(5), pp. 1180–1189.

Liu, J. et al. (2010) ‘PHBV and predifferentiated human adipose-derived stem cells for cartilage tissue engineering.’, Journal of biomedical materials research. Part A. United States, 94(2), pp. 603–610.

Liu, X. Y. et al. (2010) ‘Biocompatibility investigation of polyethylene glycol and alginate-poly-L-lysine for islet encapsulation.’, ASAIO journal (American Society for Artificial Internal Organs : 1992). United States, 56(3), pp. 241–245.

Locke, R. C., Abraham, A. C. and Killian, M. L. (2017) ‘Orthopedic Interface Repair Strategies Based on Native Structural and Mechanical Features of the Multiscale

Enthesis', ACS Biomaterials Science & Engineering. American Chemical Society, 3(11), pp. 2633–2643.

Longati, P. et al. (2013) '3D pancreatic carcinoma spheroids induce a matrix-rich, chemoresistant phenotype offering a better model for drug testing.', BMC cancer, 13, p. 95.

Lu, H.-F. et al. (2003) 'Galactosylated PVDF membrane promotes hepatocyte attachment and functional maintenance.', Biomaterials. Netherlands, 24(27), pp. 4893–4903.

Lu, H. H. et al. (2010) 'Tissue engineering strategies for the regeneration of orthopedic interfaces', Annals of Biomedical Engineering, 38(6), pp. 2142–2154.

Lu, H. H. and Thomopoulos, S. (2013) 'Functional Attachment of Soft Tissues to Bone: Development, Healing, and Tissue Engineering', Annual review of biomedical engineering, 15, pp. 201–226.

Luca, Anna C et al. (2013) 'Impact of the 3D microenvironment on phenotype, gene expression, and EGFR inhibition of colorectal cancer cell lines', PloS one. Public Library of Science, 8(3), p. e59689.

Luca, Anna C. et al. (2013) 'Impact of the 3D Microenvironment on Phenotype, Gene Expression, and EGFR Inhibition of Colorectal Cancer Cell Lines', PLoS ONE, 8(3).

Lv, D. et al. (2017) 'Three-dimensional cell culture: A powerful tool in tumor research and drug discovery', Oncology letters. 2017/10/03. D.A. Spandidos, 14(6), pp. 6999–7010.

Maffulli, N. (1998) 'Overuse tendon conditions: Time to change a confusing terminology', Arthroscopy: The Journal of Arthroscopic & Related Surgery, 14(8), pp. 840–843.

Manning, C. N. et al. (2011) 'Sustained delivery of transforming growth factor beta three enhances tendon-to-bone healing in a rat model.', Journal of orthopaedic research: official publication of the Orthopaedic Research Society. United States, 29(7), pp. 1099–1105.

Maria, O. M. et al. (2011) ‘Matrigel improves functional properties of human submandibular salivary gland cell line’, The international journal of biochemistry & cell biology. Elsevier, 43(4), pp. 622–631.

Markham, D. C., Simpson, M. J. and Baker, R. E. (2015) ‘Choosing an Appropriate Modelling Framework for Analysing Multispecies Co-culture Cell Biology Experiments.’, Bulletin of mathematical biology. United States, 77(4), pp. 713–734.

Martin, R. M., Leonhardt, H. and Cardoso, M. C. (2005) ‘DNA labeling in living cells.’, Cytometry. Part A: the journal of the International Society for Analytical Cytology. United States, 67(1), pp. 45–52.

Masgutov, R. et al. (2019) ‘Adipose-Derived Mesenchymal Stem Cells Applied in Fibrin Glue Stimulate Peripheral Nerve Regeneration.’, Frontiers in medicine. Switzerland, 6, p. 68.

Mauck, R. L. et al. (2007) ‘Regulation of cartilaginous ECM gene transcription by chondrocytes and MSCs in 3D culture in response to dynamic loading.’, Biomechanics and modeling in mechanobiology. Germany, 6(1–2), pp. 113–125.

McCorry, M. C. et al. (2017) ‘A model system for developing a tissue engineered meniscal enthesis.’, Acta biomaterialia. England, 56, pp. 110–117.

vanVan der Meer, A. D. et al. (2013) ‘Three-dimensional co-cultures of human endothelial cells and embryonic stem cell-derived pericytes inside a microfluidic device.’, Lab on a chip. England, 13(18), pp. 3562–3568.

Meng, W. and Takeichi, M. (2009) ‘Adherens junction: molecular architecture and regulation.’, Cold Spring Harbor perspectives in biology. United States, 1(6), p. a002899.

Merten, O.-W. (2015a) ‘Advances in cell culture: anchorage dependence.’, Philosophical transactions of the Royal Society of London. Series B, Biological sciences, 370(1661), p. 20140040.

Merten, O.-W. (2015b) ‘Advances in cell culture: anchorage dependence’, Philosophical transactions of the Royal Society of London. Series B, Biological sciences. The Royal Society, 370(1661), p. 20140040.

Miki, Y. et al. (2012) ‘The advantages of co-culture over mono cell culture in simulating in vivo environment.’, The Journal of steroid biochemistry and molecular biology. England, 131(3–5), pp. 68–75.

Miller, R. et al. (2019) ‘Systematic review of fibrin glue in burn wound reconstruction.’, The British journal of surgery. England, 106(3), pp. 165–173.

Mills, K. L. et al. (2014) ‘Elastic Free Energy Drives the Shape of Prevascular Solid Tumors’, PLOS ONE. Public Library of Science, 9(7), p. e103245.

Mimura, T. et al. (2008) ‘A novel exogenous concentration-gradient collagen scaffold augments full-thickness articular cartilage repair.’, Osteoarthritis and cartilage. England, 16(9), pp. 1083–1091.

Mironov, V. et al. (2009) ‘Organ printing: tissue spheroids as building blocks.’, Biomaterials. Netherlands, 30(12), pp. 2164–2174.

Montel, F. et al. (2011) ‘Stress Clamp Experiments on Multicellular Tumor Spheroids’, Physical Review Letters. American Physical Society, 107(18), p. 188102.

Moraes, C. et al. (2012) ‘Organs-on-a-chip: a focus on compartmentalized microdevices’, Annals of biomedical engineering. Springer, 40(6), pp. 1211–1227.

MOSCONAMoscona, A. (1961) ‘Rotation-mediated histogenetic aggregation of dissociated cells. A quantifiable approach to cell interactions in vitro.’, Experimental cell research. United States, 22, pp. 455–475.

MOSCONAMoscona, A. and MOSCONAMoscona, H. (1952) ‘The dissociation and aggregation of cells from organ rudiments of the early chick embryo’, Journal of anatomy, 86(3), pp. 287–301.

Mothersill, C. et al. (2007) ‘Role of Osteoblast–Fibroblast Interactions in the Formation of the Ligament-to-Bone Interface’, Anticancer Research, 11(4), pp. 1609–1621.

Mountziaris, P. M., Tzouanas, S. N. and Mikos, A. G. (2010) ‘Dose effect of tumor necrosis factor-alpha on in vitro osteogenic differentiation of mesenchymal stem cells on biodegradable polymeric microfiber scaffolds.’, Biomaterials. Netherlands, 31(7), pp. 1666–1675.

Musto, M. et al. (2019) ‘3D Organotypic Spinal Cultures: Exploring Neuron and Neuroglia Responses Upon Prolonged Exposure to Graphene Oxide.’, Frontiers in systems neuroscience. Switzerland, 13, p. 1.

Nagai, Y. et al. (2012) ‘The mechanical stimulation of cells in 3D culture within a self-assembling peptide hydrogel’, Biomaterials, 33(4), pp. 1044–1051.

Nam, Y. S. and Park, T. G. (1999) ‘Biodegradable polymeric microcellular foams by modified thermally induced phase separation method.’, Biomaterials, 20(19), pp. 1783–1790.

Napolitano, A. P. et al. (2007) ‘Dynamics of the self-assembly of complex cellular aggregates on micromolded nonadhesive hydrogels.’, Tissue engineering. United States, 13(8), pp. 2087–2094.

O’Brien, F. J. (2011) ‘Biomaterials & scaffolds for tissue engineering’, Materials Today. Elsevier Ltd, 14(3), pp. 88–95.

O’Connell, G., Garcia, J. and Amir, J. (2017) ‘3D Bioprinting: New Directions in Articular Cartilage Tissue Engineering’, ACS Biomaterials Science & Engineering. American Chemical Society, 3(11), pp. 2657–2668.

Oegema, T. R. J. et al. (1997) ‘The interaction of the zone of calcified cartilage and subchondral bone in osteoarthritis.’, Microscopy research and technique. United States, 37(4), pp. 324–332.

Ohara, T. et al. (2010) ‘Evaluation of scaffold materials for tooth tissue engineering.’, Journal of biomedical materials research. Part A. United States, 94(3), pp. 800–805.

Okano, T. et al. (2006) ‘Mechanism of cell detachment from temperature-modulated, hydrophilic-hydrophobic polymer surfaces1’, The Biomaterials: Silver Jubilee Compendium, 16(4), pp. 109–115.

Ozbolat, I. T. (2015) ‘Scaffold-Based or Scaffold-Free Bioprinting: Competing or Complementing Approaches?’, Journal of Nanotechnology in Engineering and Medicine. ASME, 6(2), pp. 24701–24706.

Padulo, J. et al. (2016) ‘Muscles, Ligaments and Tendons Journal - Basic principles and recommendations in clinical and field Science Research: 2016 Update.’, Muscles, ligaments and tendons journal. Italy, 6(1), pp. 1–5.

Pampaloni, F., Reynaud, E. G. and Stelzer, E. H. K. (2007) ‘The third dimension bridges the gap between cell culture and live tissue.’, Nature reviews. Molecular cell biology. England, 8(10), pp. 839–845.

Pankajakshan, D. et al. (2008) ‘Development of a fibrin composite-coated poly(epsilon-caprolactone) scaffold for potential vascular tissue engineering applications.’, Journal of biomedical materials research. Part B, Applied biomaterials. United States, 87(2), pp. 570–579.

Park, S. H. et al. (2018) ‘Three-Dimensional Bio-Printed Scaffold Sleeves With Mesenchymal Stem Cells for Enhancement of Tendon-to-Bone Healing in Anterior Cruciate Ligament Reconstruction Using Soft-Tissue Tendon Graft’, Arthroscopy. Elsevier, 34(1), pp. 166–179.

Parvizi, J. and Kim, G. K. (2010) ‘Chapter 39 - Cartilage’, in Parvizi, J. and Kim, G. K. B. T.-H. Y. O. (eds). Philadelphia: W.B. Saunders, pp. 80–81.

Paxton, J. Z. et al. (2012) ‘Monitoring sinew contraction during formation of tissue-engineered fibrin-based ligament constructs.’, Tissue engineering. Part A. United States, 18(15–16), pp. 1596–1607.

Paxton, J. Z., Baar, K. and Grover, L. M. (2012) ‘Current Progress in Enthesis Repair: Strategies for Interfacial Tissue Engineering’, Orthopedic & Muscular System: Current Research. OMICS International.,. doi: 10.4172/2161-0533.S1-003.

Paxton, J. Z., Grover, L. M. and Baar, K. (2010) ‘Engineering an in vitro model of a functional ligament from bone to bone.’, Tissue engineering. Part A. United States, 16(11), pp. 3515–3525.

Payne, S., Smith, R. P. and You, L. (2012) ‘Quantitative analysis of the spatiotemporal dynamics of a synthetic predator-prey ecosystem.’, Methods in molecular biology (Clifton, N.J.). United States, 813, pp. 315–330.

Perotti, V. et al. (2019) ‘An actionable axis linking NFATc2 to EZH2 controls the EMT-like program of melanoma cells’, Oncogene.

Pierschbacher, M. D. and Ruoslahti, E. (1984) ‘Cell attachment activity of fibronectin can be duplicated by small synthetic fragments of the molecule’, Nature, 309(5963), pp. 30–33.

Pihlajamaki, H. et al. (2007) ‘The impact of polyglycolide membrane on a tendon after surgical rejoining. A histological and histomorphometric analysis in rabbits.’, Journal of biomedical materials research. Part A. United States, 81(4), pp. 987–993.

Prasad Nayak, B. et al. (2010) ‘In vitro study of stem cell communication via gap junctions for fibrocartilage regeneration at entheses’, Regenerative Medicine. Future Medicine, 5(2), pp. 221–229.

Qi, X., Ye, J. and Wang, Y. (2009) ‘Alginate/poly (lactic-co-glycolic acid)/calcium phosphate cement scaffold with oriented pore structure for bone tissue engineering.’, Journal of biomedical materials research. Part A. United States, 89(4), pp. 980–987.

R Edwards, J. et al. (2008) Lymphatics and bone, Human pathology.

Radhakrishnan, J. et al. (2018) ‘Gradient nano-engineered in situ forming composite hydrogel for osteochondral regeneration’, Biomaterials, 162, pp. 82–98.

Rajabi, S. et al. (2018) ‘Human embryonic stem cell-derived cardiovascular progenitor cells efficiently colonize in bFGF-tethered natural matrix to construct contracting humanized rat hearts.’, Biomaterials. Netherlands, 154, pp. 99–112.

Ramakrishna, S. et al. (2001) ‘Biomedical applications of polymer-composite materials: A review’, Composites Science and Technology, 61(9), pp. 1189–1224.

Rathbone, S. et al. (2010) ‘Biocompatibility of polyhydroxyalkanoate as a potential material for ligament and tendon scaffold material.’, Journal of biomedical materials research. Part A. United States, 93(4), pp. 1391–1403.

Ratner, B. D. and Bryant, S. J. (2004) ‘BIOMATERIALS: Where We Have Been and Where We Are Going’, (1), pp. 41–75.

Ravialy et al. (2015) ‘3D Cell Culture Systems: Advantages and Applications’, Journal of Cellular Physiology VO - 230. Wiley Subscription Services, Inc., (1), p. 16.

Rivron, N. C. et al. (2009) ‘Tissue assembly and organization: developmental mechanisms in microfabricated tissues.’, Biomaterials. Netherlands, 30(28), pp. 4851–4858.

Rivron, N. C. et al. (2012) ‘Sonic Hedgehog-activated engineered blood vessels enhance bone tissue formation.’, Proceedings of the National Academy of Sciences of the United States of America. United States, 109(12), pp. 4413–4418.

Robertson, D. B., Daniel, D. M. and Biden, E. (1986) ‘Soft tissue fixation to bone.’, The American journal of sports medicine. United States, 14(5), pp. 398–403.

Rodeo, S. A. et al. (1993) ‘Tendon-healing in a bone tunnel. A biomechanical and histological study in the dog.’, The Journal of bone and joint surgery. American volume. The American Orthopedic Association, 75(12), pp. 1795795–803.

Rossetti, L. et al. (2017) ‘The microstructure and micromechanics of the tendon-bone insertion.’, Nature materials. England, 16(6), pp. 664–670.

Rowley, A. T. et al. (2019) ‘Extracellular Matrix-Based Strategies for Immunomodulatory Biomaterials Engineering.’, Advanced healthcare materials. Germany, 8(8), p. e1801578.

Rubalskii, E. et al. (2019) ‘Fibrin glue as a local drug-delivery system for bacteriophage PA5.’, Scientific reports. England, 9(1), p. 2091.

Ruoslahti, E., Hayman, E. G. and Pierschbacher, M. D. (1985) ‘Extracellular matrices and cell adhesion.’, Arteriosclerosis (Dallas, Tex.). United States, 5(6), pp. 581–594.

Ruoslahti, E. and Reed, J. C. (1994) ‘Anchorage dependence, integrins, and apoptosis.’, Cell. United States, 77(4), pp. 477–478.

Rupp, G. and Stemberger, A. (1978) ‘[Treatment of fresh ruptures of the Achilles tendon with resorbable suture materials and a fibrin adhesive].’, Die Medizinische Welt. Germany, 29(19), pp. 796–798.

Sachlos, E. and Czernuszka, J. T. (2003) ‘Making tissue engineering scaffolds work. Review: the application of solid freeform fabrication technology to the production of tissue engineering scaffolds.’, European cells & materials. Switzerland, 5, pp. 29–40.

Saeidi, N. et al. (2011) ‘Engineering microbes to sense and eradicate Pseudomonas aeruginosa, a human pathogen’, Molecular systems biology. EMBO Press, 7(1), p. 521.

Sahoo, S. et al. (2011) ‘Interface tissue engineering: next phase in musculoskeletal tissue repair.’, Annals of the Academy of Medicine, Singapore, 40(5), pp. 245–247.

Sahoo, S., Toh, S. L. and Goh, J. C. H. (2010) ‘A bFGF-releasing silk/PLGA-based biohybrid scaffold for ligament/tendon tissue engineering using mesenchymal progenitor cells’, Biomaterials. Elsevier, 31(11), pp. 2990–2998.

Saito, N. et al. (2001) ‘A biodegradable polymer as a cytokine delivery system for inducing bone formation.’, Nature biotechnology. United States, 19(4), pp. 332–335.

Sansone, P. et al. (2007) ‘IL-6 triggers malignant features in mammospheres from human ductal breast carcinoma and normal mammary gland.’, The Journal of clinical investigation. United States, 117(12), pp. 3988–4002.

Sasaki, K. et al. (2008) ‘Enhancement of tendon-bone osteointegration of anterior cruciate ligament graft using granulocyte colony-stimulating factor.’, The American journal of sports medicine. United States, 36(8), pp. 1519–1527.

Schindelin, J. et al. (2012) ‘Fiji: an open-source platform for biological-image analysis’, Nature Methods. Nature Publishing Group, a division of Macmillan Publishers Limited. All Rights Reserved., 9, p. 676.

Schleich, A. (1967) ‘Studies on aggregation of human ascites tumor cells.’, European journal of cancer. England, 3(4), pp. 243–246.

Schnabel-Lubovsky, M. et al. (2019) ‘Visualizing cell-laden fibrin-based hydrogels using cryogenic scanning electron microscopy and confocal microscopy.’, Journal of tissue engineering and regenerative medicine. England, 13(4), pp. 587–598.

Schwartz, a. G. et al. (2013) ‘Muscle loading is necessary for the formation of a functional tendon enthesis’, Bone. Elsevier B.V., 55(1), pp. 44–51.

Schweitzer, R. et al. (2001) ‘Analysis of the tendon cell fate using Scleraxis, a specific marker for tendons and ligaments.’, Development (Cambridge, England). England, 128(19), pp. 3855–3866.

Scott, A. et al. (2007) ‘Tenocyte responses to mechanical loading in vivo: a role for local insulin-like growth factor 1 signaling in early tendinosis in rats.’, Arthritis and rheumatism. United States, 56(3), pp. 871–881.

Screen, H. R. C. et al. (2015) ‘Tendon functional extracellular matrix’, Journal of orthopaedic research: official publication of the Orthopaedic Research Society, 33(6), pp. 793–799.

Seeherman, H. J. et al. (2008) ‘rhBMP-12 accelerates healing of rotator cuff repairs in a sheep model.’, The Journal of bone and joint surgery. American volume. United States, 90(10), pp. 2206–2219.

Shafiee, A. and Atala, A. (2017) ‘Tissue Engineering: Toward a New Era of Medicine.’, Annual review of medicine. United States, 68, pp. 29–40.

Shao, X. X. et al. (2006) ‘Evaluation of a hybrid scaffold/cell construct in repair of high-load-bearing osteochondral defects in rabbits’, Biomaterials. Elsevier, 27(7), pp. 1071–1080.

Shaw, H. M. and Benjamin, M. (2007) ‘Structure–function relationships of entheses in relation to mechanical load and exercise’, Scandinavian journal of medicine & science in sports. Wiley Online Library, 17(4), pp. 303–315.

Sherwood, J. K. et al. (2002) ‘A three-dimensional osteochondral composite scaffold for articular cartilage repair’, Biomaterials. Elsevier, 23(24), pp. 4739–4751.

Shin, J.-Y. et al. (2015) ‘Transplantation of heterospheroids of islet cells and mesenchymal stem cells for effective angiogenesis and antiapoptosis.’, Tissue engineering. Part A. United States, 21(5–6), pp. 1024–1035.

Shou, W., Ram, S. and Vilar, J. M. G. (2007) ‘Synthetic cooperation in engineered yeast populations.’, Proceedings of the National Academy of Sciences of the United States of America. United States, 104(6), pp. 1877–1882.

Sierra, D. H., Nissen, A. J. and Welch, J. (1990) ‘The use of fibrin glue in intracranial procedures: preliminary results.’, The Laryngoscope. United States, 100(4), pp. 360–363.

Silva-Correia, J., Oliveira, J. M. and Reis, R. L. (2016) ‘Gellan Gum-based Hydrogels for Tissue Engineering Applications’, Biomaterials from Nature for Advanced Devices and Therapies. (Wiley Online Books). doi: doi:10.1002/9781119126218.ch19.

daDa Silva, L. P. et al. (2018) ‘Gellan Gum Hydrogels with Enzyme-Sensitive Biodegradation and Endothelial Cell Biorecognition Sites.’, Advanced healthcare materials. Germany, 7(5).

Slater, C. R. (2017) ‘The Structure of Human Neuromuscular Junctions: Some Unanswered Molecular Questions’, International journal of molecular sciences. MDPI, 18(10), p. 2183.

Slater, S. C. et al. (2011) ‘An in vitro model of the glomerular capillary wall using electrospun collagen nanofibres in a bioartificial composite basement membrane.’, PloS one. United States, 6(6), p. e20802.

Smietana, M. J. et al. (2017) ‘Tissue-Engineered Tendon for Enthesis Regeneration in a Rat Rotator Cuff Model.’, BioResearch open access. United States, 6(1), pp. 47–57.

Smith, L. et al. (2012) ‘Tissue-Engineering Strategies for the Tendon/Ligament-to-Bone Insertion’, Connective Tissue Research, 53(2), pp. 95–105.

Song, H. et al. (2004) ‘Spatial composition of prostate cancer spheroids in mixed and static cultures.’, Tissue engineering. United States, 10(7–8), pp. 1266–1276.

Spalazzi, J. P. et al. (2008) ‘Mechanoactive scaffold induces tendon remodeling and expression of fibrocartilage markers.’, Clinical orthopaedics and related research. United States, 466(8), pp. 1938–1948.

Stevens, L. R. et al. (2016) ‘Tissue engineering with gellan gum’, Biomaterials Science. The Royal Society of Chemistry, 4(9), pp. 1276–1290.

Sugimoto, Y. et al. (2013) ‘Scx+/Sox9+ progenitors contribute to the establishment of the junction between cartilage and tendon/ligament’, Development. Oxford University Press for The Company of Biologists Limited, 140(11), pp. 2280–2288.

Suzawa, Y. et al. (2010) ‘Regenerative behavior of biomineral/agarose composite gels as bone grafting materials in rat cranial defects.’, Journal of biomedical materials research. Part A. United States, 93(3), pp. 965–975.

Szot, C. S. et al. (2011) ‘3D in vitro bioengineered tumors based on collagen I hydrogels.’, Biomaterials. Netherlands, 32(31), pp. 7905–7912.

Takahashi, K. et al. (2007) ‘Induction of pluripotent stem cells from adult human fibroblasts by defined factors.’, Cell, 131(5), pp. 861–72.

Takeichi, M. (1988) ‘The cadherins: cell-cell adhesion molecules controlling animal morphogenesis.’, Development (Cambridge, England). England, 102(4), pp. 639–655.

Takezawa, T. et al. (1993) ‘Characterization of morphology and cellular metabolism during the spheroid formation by fibroblasts.’, Experimental cell research. United States, 208(2), pp. 430–441.

Takezawa, T., Mori, Y. and Yoshizato, K. (1990) ‘Cell culture on a thermo-responsive polymer surface.’, Bio/technology (Nature Publishing Company). United States, 8(9), pp. 854–856.

Tanaka, Y. et al. (2010) ‘The optimization of porous polymeric scaffolds for chondrocyte/atelocollagen based tissue-engineered cartilage.’, Biomaterials. Netherlands, 31(16), pp. 4506–4516.

Temiz, A. et al. (2010) ‘Esterified hyaluronic acid improves cartilage viability in experimental tracheal reconstruction with an auricular graft.’, Otolaryngology--head and neck surgery : official journal of American Academy of Otolaryngology-Head and Neck Surgery. England, 143(6), pp. 772–778.

Testa, S. et al. (2017) ‘Combination of biochemical and mechanical cues for tendon tissue engineering’, Journal of cellular and molecular medicine. 2017/05/04. John Wiley and Sons Inc., 21(11), pp. 2711–2719.

Tetsumura, S. et al. (2006) ‘Biomechanical comparison of different fixation methods on the tibial side in anterior cruciate ligament reconstruction: a biomechanical study in porcine tibial bone’, Journal of Orthopaedic Science, 11(3), pp. 278–282.

Thomopoulos, S. et al. (2003) ‘Variation of biomechanical, structural, and compositional properties along the tendon to bone insertion site’, Journal of orthopaedic research. Wiley Online Library, 21(3), pp. 413–419.

Thomopoulos, S. et al. (2007) ‘Decreased muscle loading delays maturation of the tendon enthesis during postnatal development.’, Journal of orthopaedic research: official publication of the Orthopaedic Research Society. United States, 25(9), pp. 1154–1163.

Thomopoulos, S., Genin, G. M. and Galatz, L. M. (2010) ‘The development and morphogenesis of the tendon-to-bone insertion - what development can teach us about healing -.’, Journal of musculoskeletal & neuronal interactions. Greece, 10(1), pp. 35–45.

Tibbitt, M. W. and Anseth, K. S. (2009) ‘Hydrogels as extracellular matrix mimics for 3D cell culture.’, Biotechnology and bioengineering. United States, 103(4), pp. 655–663.

Tibbitt, M. W. and Anseth, K. S. (2012) ‘Dynamic microenvironments: the fourth dimension.’, Science translational medicine, 4(160), p. 160ps24.

Tredan, O. et al. (2007) ‘Drug resistance and the solid tumor microenvironment.’, Journal of the National Cancer Institute. United States, 99(19), pp. 1441–1454.

Tseng, P., Di Carlo, D. and Judy, J. W. (2009) ‘Rapid and dynamic intracellular patterning of cell-internalized magnetic fluorescent nanoparticles.’, Nano letters. United States, 9(8), pp. 3053–3059.

Tung, Y.-C. et al. (2011) ‘High-throughput 3D spheroid culture and drug testing using a 384-hanging drop array’, Analyst. The Royal Society of Chemistry, 136(3), pp. 473–478.

Tzanakakis, E. S., Hansen, L. K. and Hu, W. S. (2001) ‘The role of actin filaments and microtubules in hepatocyte spheroid self-assembly.’, Cell motility and the cytoskeleton. United States, 48(3), pp. 175–189.

Ueno, K. et al. (1992) ‘Formation of multicellular spheroids composed of rat hepatocytes.’, Research communications in chemical pathology and pharmacology. United States, 77(1), pp. 107–120.

Unsworth, B. R. and Lelkes, P. I. (1998) ‘Growing tissues in microgravity.’, Nature medicine. United States, 4(8), pp. 901–907.

Urrutia, C. O. (2017) ‘Mechanical Stimulation of Cells Through Scaffold Design for Tissue Engineering’, in Dominguez-García, M. V. (ed.). Rijeka: IntechOpen, p. Ch. 7.

Vaquette, C. et al. (2010) ‘Aligned poly(L-lactic-co-e-caprolactone) electrospun microfibers and knitted structure: a novel composite scaffold for ligament tissue engineering.’, Journal of biomedical materials research. Part A. United States, 94(4), pp. 1270–1282.

Vogel, K. G. et al. (1993) ‘Proteoglycans in the compressed region of human tibialis posterior tendon and in ligaments.’, Journal of orthopaedic research : official publication of the Orthopaedic Research Society. United States, 11(1), pp. 68–77.

Vogel, K. G. et al. (1994) ‘Aggrecan in bovine tendon.’, Matrix biology: journal of the International Society for Matrix Biology. Netherlands, 14(2), pp. 171–179.

Waggett, A. D. et al. (1998) ‘Characterization of collagens and proteoglycans at the insertion of the human Achilles tendon.’, Matrix biology: journal of the International Society for Matrix Biology. Netherlands, 16(8), pp. 457–470.

Wagreich, H. and Tarlov, I. M. (1945) ‘Studies on the strength of fibrinogen-thrombin clots’, ARCHIVES OF BIOCHEMISTRY. ACADEMIC PRESS INC 525 B ST, STE 1900, SAN DIEGO, CA 92101-4495, 7(2), pp. 345–352.

van der Wal, B. C. et al. (1997) ‘Paracrine interactions between mesothelial and colon-carcinoma cells in a rat model.’, International journal of cancer. United States, 73(6), pp. 885–890.

Walser, R. et al. (2013) ‘Generation of co-culture spheroids as vascularisation units for bone tissue engineering.’, European cells & materials. Switzerland, 26, pp. 222–233.

Wang, I.-N. E. et al. (2007) ‘Role of osteoblast–fibroblast interactions in the formation of the ligament-to-bone interface’, Journal of Orthopaedic Research. John Wiley & Sons, Ltd, 25(12), pp. 1609–1620.

Wang, I. E. et al. (2006) ‘Age-dependent changes in matrix composition and organization at the ligament-to-bone insertion’, Journal of Orthopaedic Research. Wiley Online Library, 24(8), pp. 1745–1755.

Wang, I. N. E. and Lu, H. H. (2006) ‘Role of cell-cell interactions on the regeneration of soft tissue-to-bone interface’, Annual International Conference of the IEEE Engineering in Medicine and Biology - Proceedings, pp. 783–786.

Weber, W., Daoud-El Baba, M. and Fussenegger, M. (2007) ‘Synthetic ecosystems based on airborne inter- and intrakingdom communication.’, Proceedings of the National Academy of Sciences of the United States of America. United States, 104(25), pp. 10435–10440.

West, E. R. et al. (2007) ‘Physical properties of alginate hydrogels and their effects on in vitro follicle development.’, Biomaterials. Netherlands, 28(30), pp. 4439–4448.

Whang, K. et al. (1999) ‘Engineering bone regeneration with bioabsorbable scaffolds with novel microarchitecture’, Tissue engineering. Mary Ann Liebert, Inc. 2 Madison Avenue Larchmont, NY 10538 USA, 5(1), pp. 35–51.

Williams, C. and Wick, T. M. (2005) ‘Endothelial cell-smooth muscle cell co-culture in a perfusion bioreactor system.’, Annals of biomedical engineering. United States, 33(7), pp. 920–928.

Wilson, R. et al. (2010) ‘Comprehensive profiling of cartilage extracellular matrix formation and maturation using sequential extraction and label-free quantitative proteomics’, Molecular & cellular proteomics: MCP. 2010/02/26. The American Society for Biochemistry and Molecular Biology, 9(6), pp. 1296–1313.

van de Witte, P. et al. (1996) ‘Phase separation processes in polymer solutions in relation to membrane formation’, Journal of Membrane Science, 117(1–2), pp. 1–31.

Wittig, C. et al. (2013) ‘Incorporation of bone marrow cells in pancreatic pseudoislets improves posttransplant vascularization and endocrine function.’, PloS one. United States, 8(7), p. e69975.

Wolf, F. et al. (2008) ‘A low percentage of autologous serum can replace bovine serum to engineer human nasal cartilage.’, European cells & materials. Switzerland, 15, pp. 1–10.

Woo, S. L. Y. et al. (2006) ‘Biomechanics of knee ligaments: Injury, healing, and repair’, Journal of Biomechanics, pp. 1–20. doi: 10.1016/j.jbiomech.2004.10.025.

van der Worp, H. B. et al. (2010) ‘Can Animal Models of Disease Reliably Inform Human Studies?’, PLoS Medicine. Public Library of Science, 7(3), pp. 1–8.

Wrana, J. L. et al. (1994) ‘Mechanism of activation of the TGF-beta receptor.’, Nature. England, 370(6488), pp. 341–347.

Wu, L., Lin, L. and Qin, Y.-X. (2015) ‘Enhancement of cell ingrowth, proliferation, and early differentiation in a three-dimensional silicon carbide scaffold using low-intensity pulsed ultrasound’, Tissue engineering. Part A. 2014/07/23. Mary Ann Liebert, Inc., 21(1–2), pp. 53–61.

Wu, L. Y., Di Carlo, D. and Lee, L. P. (2008) ‘Microfluidic self-assembly of tumor spheroids for anticancer drug discovery.’, Biomedical microdevices. United States, 10(2), pp. 197–202.

Wu, M.-H., Huang, S.-B. and Lee, G.-B. (2010) ‘Microfluidic cell culture systems for drug research’, Lab on a Chip. Royal Society of Chemistry, 10(8), pp. 939–956.

Wu, X. et al. (2003) ‘Immunofluorescent labeling of cancer marker Her2 and other cellular targets with semiconductor quantum dots’, Nature biotechnology. Nature Publishing Group, 21(1), p. 41.

Xie, X. et al. (2018) ‘A co-culture system of rat synovial stem cells and meniscus cells promotes cell proliferation and differentiation as compared to mono-culture’, Scientific reports. Nature Publishing Group UK, 8(1), p. 7693.

Xu, K. et al. (2017) ‘Efficient decellularization for tissue engineering of the tendon-bone interface with preservation of biomechanics.’, PloS one. United States, 12(2), p. e0171577.

Xu, X. et al. (2012) ‘Recreating the tumor microenvironment in a bilayer, hyaluronic acid hydrogel construct for the growth of prostate cancer spheroids’, Biomaterials. Elsevier, 33(35), pp. 9049–9060.

Xu, Y. et al. (2014) ‘The effect of mechanical stimulation on the maturation of TDSCs-poly(L-lactide-co-e-caprolactone)/collagen scaffold constructs for tendon tissue engineering’, Biomaterials, 35(9), pp. 2760–2772.

Yanagihara, K. et al. (2018) ‘Treatment of Bone Defects by Transplantation of Genetically Modified Mesenchymal Stem Cell Spheroids’, Molecular Therapy - Methods & Clinical Development. Elsevier, 9, pp. 358–366.

Yang, L. (2015) ‘Self-assembled nanostructures for bone tissue engineering’, Nanotechnology-Enhanced Orthopedic Materials, pp. 121–139.

Yang, P.-L. and Marek-Sadowska, M. (2018) ‘High-Performance Architecture Using Fast Dynamic Reconfigurable Accelerators’, IEEE Transactions on Very Large Scale Integration (VLSI) Systems. IEEE, 26(7), pp. 1209–1222.

Yang, P. J. and Temenoff, J. S. (2009) ‘Engineering orthopedic tissue interfaces.’, Tissue engineering. Part B, Reviews. United States, 15(2), pp. 127–141.

Yang, S. et al. (2001) ‘The design of scaffolds for use in tissue engineering. Part I. Traditional factors’, Tissue engineering. Mary Ann Liebert, Inc., 7(6), pp. 679–689.

Yeh, C.-H. et al. (2011) ‘Using a co-culture microsystem for cell migration under fluid shear stress.’, Lab on a chip. England, 11(15), pp. 2583–2590.

Yip, D. and Cho, C. H. (2013) ‘A multicellular 3D heterospheroid model of liver tumor and stromal cells in collagen gel for anti-cancer drug testing’, Biochemical and Biophysical Research Communications. Academic Press, 433(3), pp. 327–332.

Yoshimoto, H. et al. (2003) ‘A biodegradable nanofiber scaffold by electrospinning and its potential for bone tissue engineering’, Biomaterials, pp. 2077–2082. doi: 10.1016/S0142-9612(02)00635-X.

Yoshiya, S. et al. (2000) ‘Graft healing in the bone tunnel in anterior cruciate ligament reconstruction.’, Clinical orthopaedics and related research. United States, (376), pp. 278–286.

Young, M. F. (2003) ‘Bone matrix proteins: their function, regulation, and relationship to osteoporosis.’, Osteoporosis international: a journal established as result of cooperation between the European Foundation for Osteoporosis and the National Osteoporosis Foundation of the USA. England, 14 Suppl 3, pp. S35-42.

Yu, N. Y. C. et al. (2010) ‘In vivo local co-delivery of recombinant human bone morphogenetic protein-7 and pamidronate via poly-D, L-lactic acid.’, European cells & materials. Switzerland, 20, pp. 431–432.

Yu, X., Dillon, G. P. and Bellamkonda, R. B. (1999) ‘A laminin and nerve growth factor-laden three-dimensional scaffold for enhanced neurite extension.’, Tissue engineering. United States, 5(4), pp. 291–304.

Yuhas, J. M. et al. (1977) ‘A simplified method for production and growth of multicellular tumor spheroids.’, Cancer research. United States, 37(10), pp. 3639–3643.

Z. Paxton, J. (2013) ‘Current Progress in Enthesis Repair: Strategies for Interfacial Tissue Engineering’, Orthopedic & Muscular System, 01(S1), pp. 1–13.

Zehnder, T., Boccaccini, A. R. and Detsch, R. (2017) ‘Biofabrication of a co-culture system in an osteoid-like hydrogel matrix’, Biofabrication, 9(2), p. 025016.

Zeidan, A. A., Radstrom, P. and van Niel, E. W. J. (2010) ‘Stable coexistence of two Caldicellulosiruptor species in a de novo constructed hydrogen-producing co-culture.’, Microbial cell factories. England, 9, p. 102.

Zelzer, E. and Blitz, E. (2010) ‘Bone ridge patterning during musculoskeletal assembly is mediated through SCX regulation of Bmp4 at the tendon-skeleton junction’, Bone, (46), p. S59.

Zengler, K. et al. (2002) ‘Cultivating the uncultured’, Proceedings of the National Academy of Sciences. National Acad Sciences, 99(24), pp. 15681–15686.

Zeugolis, D. I., Paul, G. R. and Attenburrow, G. (2009) ‘Cross-linking of extruded collagen fibers--a biomimetic three-dimensional scaffold for tissue engineering applications.’, Journal of biomedical materials research. Part A. United States, 89(4), pp. 895–908.

Zhang, R. and Ma, P. X. (1998) ‘Porous poly (L -lactic acid)/ apatite composites created by biomimetic process’.

Zhao, N. et al. (2019) ‘Dual Aptamer-Functionalized in Situ Injectable Fibrin Hydrogel for Promotion of Angiogenesis via Codelivery of Vascular Endothelial Growth Factor and Platelet-Derived Growth Factor-BB.’, ACS applied materials & interfaces. United States.

Appendix

Promulgation of data

1) Published abstracts

- Alsaykhan, H. and Paxton, J. Z. (2016) 'DEVELOPING A NOVEL 3-DIMENSIONAL (3D) CO-CULTURE SYSTEM TO GENERATE A TENDON-BONE TISSUE INTERFACE: EVALUATION OF HYDROGELS', *Orthopaedic Proceedings*. The British Editorial Society of Bone & Joint Surgery, 98-B(SUPP_16), p. 14. doi: 10.1302/1358-992X.98BSUPP_16.BORS2016-014.
- Alsaykhan, H. and Paxton, J. Z. (2018) 'Using 3D cell spheroids to investigate musculoskeletal interface formation' *Oxford Abstracts.* 8th World Congress of Biomechanics. P.4-5
- J. W. Mortimer, H. M. Alsaykhan, P. A Rust, J. Z. Paxton (2019) 'Designing clinically-relevant tissue-engineered models of the tendon-bone interface', *Transl Sports Med*. 2018; 1(Supp.1):13. DOI: 10.1002/tsm2.17 (Abstract; Tendon UK: Emerging Themes in Translational Tendon Science, Oxford, 2018)

Abstract

Free Access

DEVELOPING A NOVEL 3-DIMENSIONAL (3D) CO-CULTURE SYSTEM TO GENERATE A TENDON-BONE TISSUE INTERFACE: EVALUATION OF HYDROGELS

H. Alsaykhan, J.Z. Paxton

Published Online: 21 Feb 2018

Tools Share

Entheses are the anchorage sites of tendons to bones in the musculoskeletal system. They have a unique microanatomy that allow smooth transfer of mechanical load through tendon to bone. However, entheses are prone to injury due to their small surface area[1,2]. The overall success rate of the current gold standard treatment (directly attaching the tendon to bone) is small[3,4]. Consequently, the aim of this study was to evaluate different hydrogels and their suitability for developing an *in-vitro* co-culture system to manufacture 3D tissue interfaces.

To create a 3D *in-vitro* tissue interface, half-well plugs were created by pouring silicone in wells of a 24-well plate. When set, it was cut into halves to be used as half-well plugs, blocking one side of a culture well. A tendon-cell-encapsulated hydrogel was poured into the exposed half and, when set, the plug was removed and a bone-cell-encapsulated gel was added. Cells were fluorescently labelled to enable identification of cell types under fluorescent microscopy (Tendon – green, bone – red). The suitability of different hydrogels to form an *in vitro* tissue interface was evaluated: fibrin, agarose and gellan.

This study demonstrates that 3D co-cultures can be manufactured *in-vitro*. The novel system enabled the culture of two cell types (bone/tendon) in direct contact, creating an *in-vitro* interface. In addition, this study shows that fibrin gel supports cell morphology, while both cell types failed to show normal morphology in agarose and gellan. Further studies evaluating cell viability in these hydrogels are currently underway.

O0286 Using 3D cell spheroids to investigate musculoskeletal interface formation

Hamad Alsaykhan, Jennifer Paxton
University of Edinburgh, Edinburgh, United Kingdom

Abstract

Introduction

Musculoskeletal interfaces such as the bone-tendon, bone-cartilage and muscle-tendon transitions are unique in both structure and function [1]. There is a current lack of understanding about the cellular processes governing how these tissue interfaces form and repair following injury. Here, we describe the formation of spheroid-based 3D co-culture systems to study cell-cell interaction at the bone-tendon interface (enthesis) *in vitro*.

Methods

As a proof of concept, 3D cell spheroids were formed from mouse osteoblasts (MC3T3), temporarily stained with red CellTracker™ and GFP-tagged chick tendon fibroblasts using 25K per cell type in 96-well plates. Individual bone and tendon spheroids were then combined into a single well and confocal fluorescent microscopy confirmed that a composite structure was formed after 48 hrs of co-culture (Figure 1A). To investigate musculoskeletal interface formation in a species-matched system, individual tendon cell spheroids (TS) were manufactured using 25K or 50K rat tendon fibroblasts and bone cell spheroids (BS) using 25K or 50K rat osteoblasts in individual wells of a cell-repellent 96-well plate. Following 24 hrs of incubation in standard growth medium (S-DMEM) and culture conditions, 25K TS and 25K BS were combined in a single well to form a bone-tendon spheroid (BTS) which was then cultured for 14 days. BS and TS alone (50K) were also cultured in identical conditions. BTS were observed to ascertain whether BS and TS would unite into a composite structure with an interfacial region using light microscopy. Surface areas of BS, TS and BTS were measured using digital imaging software (ImageJ, NIH, USA) to obtain spheroid size observations.

Results

BS and TS form within 24hrs of plating and form a BTS within 24hrs of combination in culture (Figure 1B). Surface area measurements of BS and TS show that BS are significantly larger than TS at day 1 (75.1 ± 1.5 μm^2 vs. 47.7 ± 4.2 μm^2, $p<0.05$; Figure 1C). BS increase in size over the 14 day culture period to 90.7 ± 8.2 μm^2 ($p<0.05$; Figure 1C) whereas TS decrease in size to 8.1 ± 1.3 μm^2 ($p<0.05$; Figure 1C) over the 14 days. Combination of 25K BS and TS (BTS) show an increase in size over the culture period from 61.4 ±1.1 μm^2 on day 1 to 94.9 ± 4.4 μm^2 on day 14 ($P<0.05$; Figure 1C).

Discussion

This data suggests that a simple spheroid culture may be used to investigate musculoskeletal interface formation *in vitro*. Current studies are focused on the effect of co-culture on BTS, examining cell viability, protein production (eg. collagen, glycosaminoglycans) and the expression of bone-tendon interface relevant markers (eg. Fibrocartilage) for model validation.

References

1. Yang, P.J. & Temenoff, J.S. (2009) Tissue Eng Part B Rev. 2009 Jun;15(2)

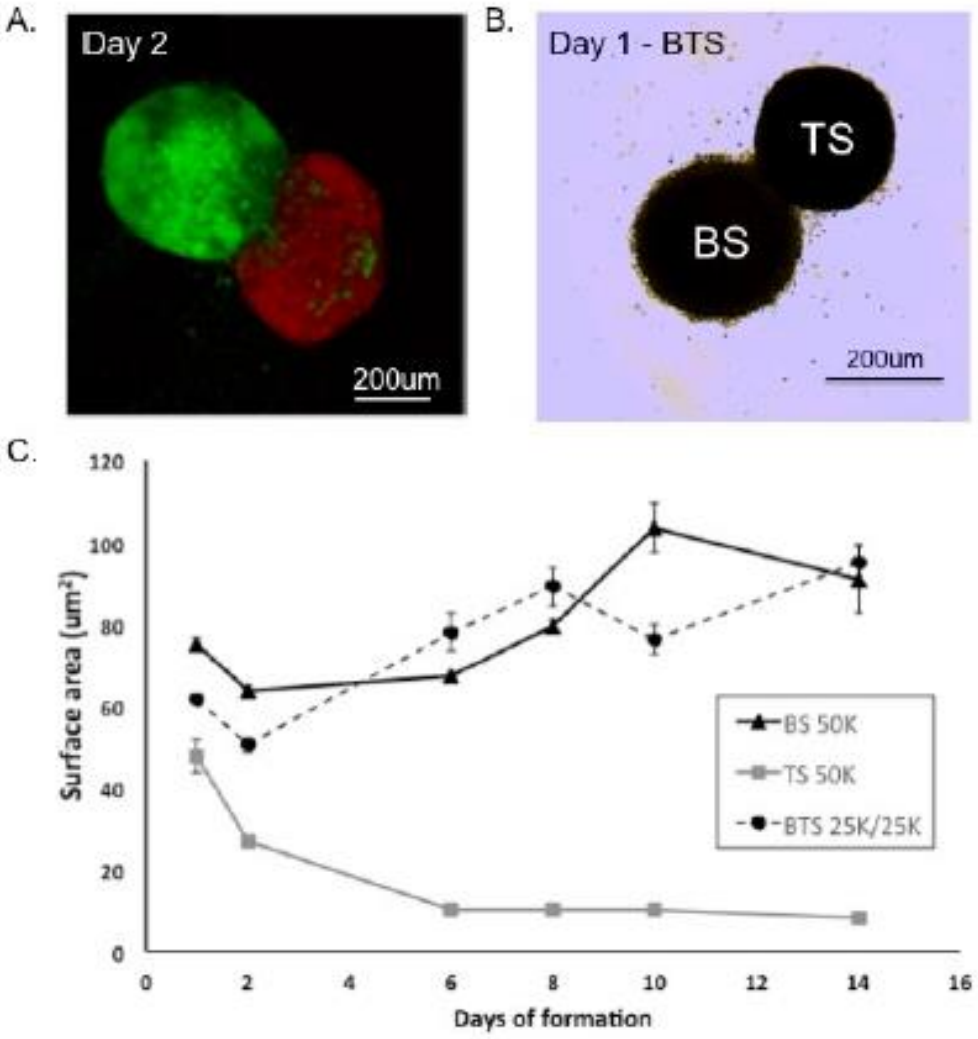

Figure 1. A) Bone-tendon spheroid (BTS) made from bone (MC3T3; red) and tendon (green) cells. **B)** BTS made from rat osteoblast spheroid (BS) and rat tendon fibroblast spheroid (TS). **C)** Surface area measurements of BS, TS and BTS over the course of 14 days in culture.

Designing clinically-relevant tissue-engineered models of the tendon-bone interface

J. W. Mortimer[1]; H. M. Alsaykhan[1]; P. A. Rust[2]; J. Z. Paxton[1]

[1]*Deanery of Biomedical Sciences, University of Edinburgh, Edinburgh, UK;*

[2]*Department of Plastic Surgery, St. John's Hospital, Livingston, UK*

The enthesis is the specialised transitional region between tendon/ligament and bone, often across a fibrocartilagenous zone, allowing uniform transmission of force. Injury and repair of the enthesis, however, such as in tendon/ligament avulsion, leads to poorly-organised fibrovascular tissue, vulnerable to failure [Smith, 2012]. The Paxton laboratory adopts interfacial tissue engineering to generate and investigate the enthesis in 3-dimensions (3-D), and manufacture whole multi-tissue constructs for potential implantation in traumatised or diseased areas. Building upon 2-D co-culture [Wang, 2007], we are investigating 3-D osteoblast-fibroblast co-cultures in both scaffold-dependent (cells embedded in hydrogels) and scaffold-independent (spheroid-cultured cells) designs, with fluorescence tracking showing cell migration across the interface. Evaluation of functional cellular outcomes measuring collagen and glycosaminoglycan production and fibrocartilage-relevant marker expression is currently underway. Clinical applicability of our models remains a core principle, and we are enhancing a multi-tissue bone anchor-fibrin scaffold construct [Paxton, 2010] into an osteoblast-fibroblast co-culture model specific for flexor tendon avulsion injury. Analysis of human morphometrics through dissection and histology has led to the design of multiple model/enthesis sizes, acknowledging an important biomechanical feature and clinical practicality. We will shortly be investigating 3-D bioprinting for co-culture creation, aiming to integrate this into our translational models.

References: 1. Paxton *et al*, Tissue Eng Part A, 16 (11):3515–25, 2010.

2. Smith *et al*, Connect Tissue Res, 53(2):95–105, 2012.

3. Wang *et al*, J Orthop Res, 25(12):1609–20, 2007.

2) Oral presentations

- 6th of September 2016, developing a novel 3-Dimensional (3D) co-culture system to generate a tendon-bone interface: evaluation of hydrogels. *British Orthopaedic Research Society conference*, University of Glasgow, Scotland.
- 9th of July 2018, using 3D cell spheroids to investigate musculoskeletal interface formation. *8th World Congress of Biomechanics,* Dublin, Republic of Ireland.

3) Poster presentations

- 19th-21st of July 2015, Development of a novel culture system to investigate cellular interactions at engineered tissue interfaces. *Tissue and Cell Engineering Society.* Southampton, UK.
- 31st of May 2016, developing a novel 3-Dimensional (3D) co-culture system to investigate tissue interfaces. *TransMed* conference, University of Edinburgh, Scotland.
- 27th of April 2017, developing a novel 3-dimentsion (3D) co-culture system to generate a tissue interface model. *Edinburgh Musculoskeletal Group*. University of Edinburgh, Scotland.
- 4th of December 2018. Evaluating a novel 3-dimensional spheroid co-culture to model tissue interfaces. *Edinburgh Musculoskeletal Group*. University of Edinburgh, Scotland.

4) Accepted abstracts for conference presentation:

- 11th-13th of June 2019, *Joint conference of the Tissue and Cell Engineering Society and the UK Society for Biomaterials:*
    a. 3D co-culture of tendon and bone cell-encapsulated scaffolds: system development and assessing the effect of co-culture.
    b. Investigating the use of cell spheroids for producing *in vitro* co-culture models of interface formation.
- 9th-11th of August 2019, *The 19th Congress of The International Federation of Associations of Anatomists:*
    a. Studying the effect of 3D co-culture on tendon and bone cells using a novel 3D spheroid system.
    b. Design and development of a novel 3D model to investigate cell-cell interaction at musculoskeletal interfaces